CHEMICAL AND ISOTOPIC VARIATIONS IN PLAGIOCLASE ACROSS THE TRANSITION BETWEEN THE MAIN AND UPPER ZONES, WESTERN BUSHVELD COMPLEX.

BY

PELELE BERNARD LEHLOENYA

Dissertation submitted in the fulfillment of the requirements for the degree of

MASTER OF SCIENCE

IN

GEOLOGY

Faculty of Natural and Agricultural Sciences

University of the Free State

Bloemfontein, South Africa

UNIVERSITY OF THE FREE STATE
UNIVERSITEIT VAN DIE VRYSTAAT
YUNIVESITHI YA FREISTATA

UFS·UV
NATURAL AND AGRICULTURAL SCIENCES
NATUUR- EN LANDBOUWETENSKAPPE
GEOLOGY
GEOLOGIE

Declaration

I, Pelele Bernard Lehloenya, declare this dissertation to be my own, unaided work. It is submitted in fulfilment for the qualification of Master of Science degree in Geology, in the faculty of Natural and Agricultural Sciences, Department of Geology, University of the Free State. It has not been submitted before for any degree or examination at any other University or tertiary institution. I also declare that all sources cited or quoted are indicated and acknowledged in a list of references. I further concede copyright of the dissertation in favour of the University of the Free State.

Pelele Bernard Lehloenya

26th Day of April 2017

Dedication

To my parents, Letsoela and Mapelele. The whole family-Pelaelo, Matete, Mahao, Mabolaeng, Mpinane, Lesaoana, Liteboho, Sakinah and Didimalang. Lastly my younger sisters Mojatsohle, Takatso and Mamotena (late).

Acknowledgements

Firstly, I would like to express my sincere gratitude to Dr. Frederick Roelofse for suggesting and supervising this project and for his advice on the preparation and completion of this dissertation. I greatly applaud him for the awesome academic guidance he gave me throughout the entire duration of this study. I do appreciate the experience and knowledge he shared with me concerning isotopic variation of the Bushveld Complex and other layered mafic intrusions.

I would like to thank Messrs Radikgomo and Choane for preparing all resources used in this study (thin sections, epoxy-embedded thick sections, pressed pellets and fusion discs, respectively), Megan Purchase for calibration of the XRF. Prof Tredoux for the inspiration she gave me throughout my study. I also thank the entire staff of the geology department in the University of the Free State (i.e. Mrs Rina Immelman & Andries Felix). Prof Steve Prevec and his intern, Thapelo Moloto, are thanked for their assistance with the use of the Jeol JXA 8230 Superprobe, instrument sponsored by NRF/NEP grant 40113 (UID 74464), housed at the Department of Geology, Rhodes University, and for making me feel welcome at Grahamstown. Christel Tinguely of the Department of Geological Sciences, University of Cape Town is acknowledged for her assistance in Laser Ablation work for trace element determination conducted at the department. Richard Carlson and Timothy Mock of the Carnegie Institution for Science are thanked for their help with Laser Ablation work conducted at their institution, and for the unforgettable visit in Washington DC. Ann Hawkins for accommodating me in her house while in Washington DC.

I do acknowledge, with gratefulness, the funds granted to me by the National Research Foundation (NRF) under a Thuthuka grant to my supervisor (TKK13053018360), which made it possible to this study.

I would like to thank my family for the support it has shown me throughout the time of my studying. I would also like to recognise my friends who really supported me in all facets in time of need, and are Seelane Motsomi, Khoase Shata, Mpandlana Qhola, Mawala Masilo and Tankiso Bobore.

In Deo speravi, maximus.

Abstract

The *in situ* compositional (major element, trace element and Sr-isotopic) and petrographic results of plagioclase as obtained from the gabbroic cumulates across the boundary between the Main and Upper Zones of the western Bushveld Complex, as studied from the 1119.13 m, BK-2 drill core are reported. The data are compared with similar dataset on this petrogenetically important stratigraphic sequence and a model that better explains the petrogenesis of the Pyroxenite Marker interval is proposed.

There is a significant variation within and between coexisting plagioclase crystals across the studied stratigraphic interval, which is not a new phenomenon in the Bushveld Complex and other layered intrusions. *In situ* major element compositions recorded a continuous upward trend of increasing plagioclase anorthite (i.e. a reversed differentiation trend) content from ~ 342 m below the Pyroxenite Marker. The REE abundances of plagioclase show LREE enrichment and slight depletion of HREEs relative to chondrites.

The initial $^{87}Sr/^{86}Sr$ ratios of plagioclase averaged 0.7086 in the lower Main Zone and 0.7078 in the Upper Zone, showing an isotopic ratio decrease up the stratigraphy of BK-2. The Sr-isotopic composition of plagioclase in the Upper Zone was relatively constant with stratigraphic position, and this is coupled with a normal differentiation trend as exemplified by the anorthite (An%) content of plagioclase.

The disappearance of inverted pigeonite in the vicinity below the Pyroxenite Marker, coupled with a reversal in mineral compositions and an inflection in initial $^{87}Sr/^{86}Sr$ ratios, mark a zone of prolonged magma mixing, culminating in the Pyroxenite Marker.

The proposed model for petrogenesis of the Pyroxenite Marker is suggestive that the interval may have formed due to; stabilization of pyroxene at the expense of plagioclase because of rapid homogenization of two stratified magma layers that might have caused a minor shift in phase equilibria, perhaps as a result of a transient fluctuation in pressure within the chamber.

The isotopically heterogeneous integration stage of the BK-2 (i.e. the lower parts of the Main Zone below the Pyroxenite Marker) was caused by several influxes of magma of distinct composition, and the isotopically homogeneous differentiation stage (i.e. that part of the Main Zone above the Pyroxenite Marker and the overlying Upper Zone) was manifested by magma evolution that was dominated by fractional crystallization processes without strong evidence to suggest further large-scale magma influxes.

Isotopic variations at the mineral scale are of great use in the monitoring of magma evolution, processes and timescales, together with core-rim variations that are good tracers of magma mixing.

Table of contents

List of figures

List of tables

1. INTRODUCTION

Research on layered igneous intrusions has yielded critical information on the differentiation of magmas and the interaction between mantle-derived magmas and the crust that they intrude. A lot of early work was done on mineral chemistry, and most of the geochemical work done on layered intrusions and the world's largest layered intrusion, the Bushveld Complex, in particular, focused on whole-rock geochemical and isotopic variations from a stratigraphic perspective. However, in more recent years, much of the focus has shifted towards gaining a better understanding of chemical and isotopic variations between and within constituent minerals in layered intrusions (e.g. Prevec *et al.* 2005; Roelofse & Ashwal, 2012; Roelofse *et al.* 2015; Mangwegape *et al.* 2016), with resultant advances in our understanding on the petrogenesis of these intrusions. The present study will focus on compositional (major element, trace element and Sr-isotopic) variations between and within plagioclase across the boundary between the Main and Upper zones in the Western Limb of the Bushveld Complex as intersected by the Bierkraal (BK-2) drill hole. It is the intention of this study to:

- ✓ Obtain data in order compare and contrast it with similar datasets on this petrogenetically important stratigraphic interval.
- ✓ Propose a model for the petrogenesis of the Pyroxenite Marker interval.

1.2.1 Geological background and stratigraphy of the Bushveld Complex

The Bushveld Complex, which covers an area of approximately 66 000 km^2 (Willemse, 1969; Van der Merwe, 1978), is the largest preserved layered mafic intrusion known on Earth (Tegner *et al.* 2006) (Figure 1) and hosts some of the world's largest and richest orthomagmatic metal deposits (Lee, 1996; Cawthorn *et al.* 2005).

According to Kinnaird (2005), the Bushveld igneous province comprises of;

i) A suite of mafic sills, which intruded Transvaal Supergroup floor rocks.

ii) The bimodal volcanic Rooiberg group.

iii) The Rustenburg Layered Suite, which is the largest and oldest mafic-layered complex.

iv) The Lebowa Granite Suite and the Rashoop Granophyre Suite, the latter that developed at the contact between granites and the Rustenburg Layered Suite. The Rashoop Suite is comprised of metamorphosed sediments and intrusive acidic rocks.

v) Various satellite intrusions of similar age; e.g. Molopo farms and Nkomati-Uitkomst.

The above-mentioned components of the Bushveld Complex were emplaced within a very short space of time as presented in Table 1.

The layered mafic to ultramafic cumulates of the Rustenburg Layered Suite of the Bushveld Complex form a lopolith (Eales & Cawthorn, 1996; Kruger, 2005), which was intruded into Palaeoproterozoic (2.5-2.06 Ga) supracrustal rocks of the Transvaal

Supergroup (Ashwal *et al.* 2005) at ~2055 Ma (2054.4 ± 1.3 Ma according to Scoates and Friedman (2008) and 2054.89 ± 0.37 Ma according to Zeh *et al.* (2015)).

1.2.2 The Rustenburg Layered Suite (RLS)

The RLS is presumed to be broadly "dish" shaped and about 350 km across, with the layered cumulates constituting a stratigraphic sequence of ~ 7- 9 km thick (Eales & Cawthorn, 1996; Kruger, 2005).

The RLS consists of five limbs or lobes; four exposed segments—the Eastern limb, the Northern limb, the far Western limb and the Western limb, with a fifth limb, the Southeastern (or Bethal) limb, concealed by younger sediments (Kinnaird *et al.* 2005) (Figure 1).

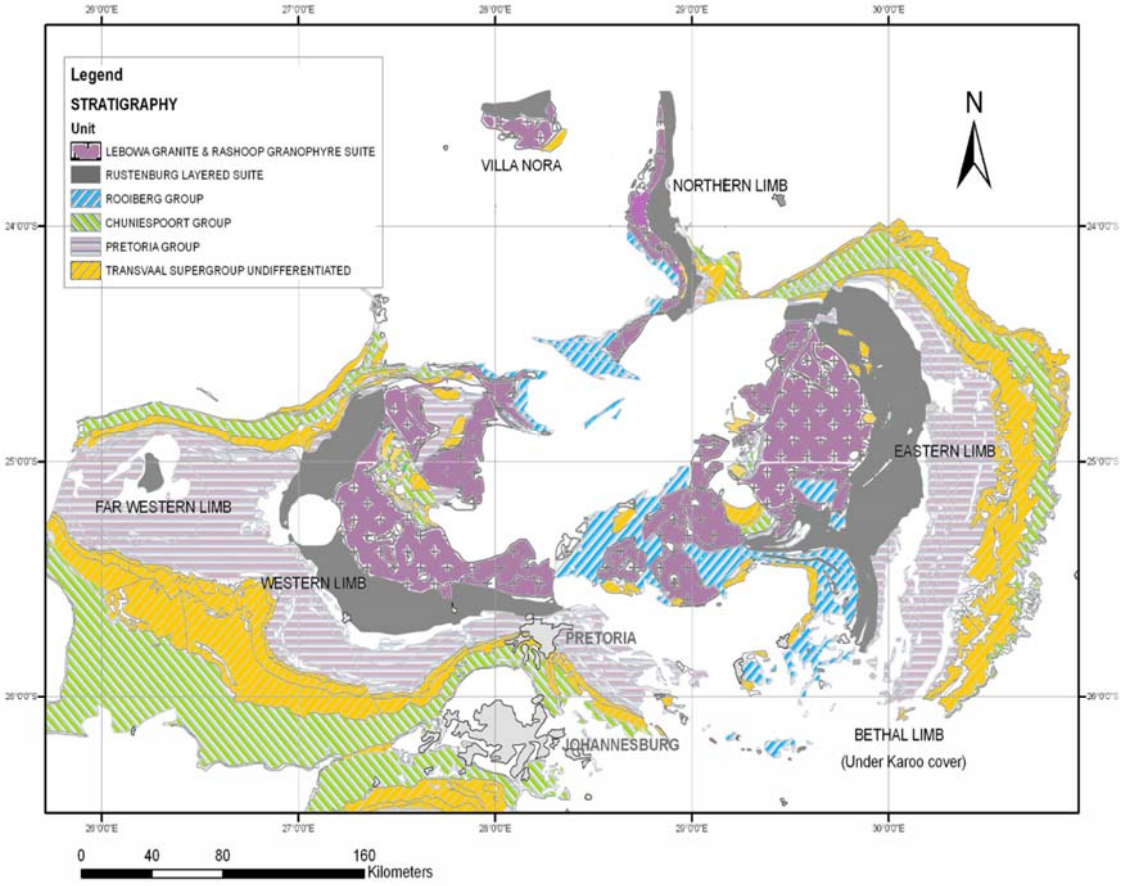

Figure 1: Geological map of the Bushveld Complex, modified after Roelofse (2010).

Table 1: Age dates of the various components of the larger Bushveld magmatic province. Ages were acquired from different authors: [1]Harmer & Armstrong (2000); [2]Kruger (1989); [3]Mapeo *et al*. (2004); [4]de Waal *et al.* (2001), and [5]Zeh *et al*. (2015).

Lithostratigraphic unit		**Age (Ma ± 95%)**
Loskop Formation	Rhyolite	2057.2 ± 3.8[1]
Lebowa Granite Suite	Makhutso Granite	2053.4 ± 3.9[1]
	Nebo Granite	2054.2 ± 2.8[1]
	Steelpoort park Granite	2057.5 ± 4.2[1]
Rustenburg Layered Suite	Critical Zone (SHRIMP)	2054.4 ± 2.8[1]
	Critical Zone (IDTIMS)	2054.5 ± 1.5[1]
	Centre of RLS (CA-ID-TIMS)	2054.89 ± 0.37[5]
Rashoop Granophyre Suite	Rooikoppies Porphyry	2061.8 ± 5.5[1]
Rooiberg Group	Kwaggasnek Formation	2057.3 ± 2.8[1]
Satellite intrusions	Molopo Farms	2044 ± 24[2]
	Mashaneng Complex	2054 ± 2[3]
	Uitkomst Complex	2044± 8[4]
		(2055 ± 45/-17)[4]

The Eastern Limb occurs as a 200 km, westerly dipping bow-shaped body stretching from Chuniespoort in the north to Stoffberg in the south (Roelofse, 2010). The Bethal Limb has been identified based on a gravity high and is known from borehole core only (Buchanan, 1975).

The Northern Limb is well-defined by a north south-oriented winding outcrop (Kinnaird *et al.* 2005) which is partly covered by younger rocks, with outcrops limited to its eastern edge and near Villa Nora (Roelofse and Ashwal, 2012).

The Far Western Limb stretches from the west of the Pilanesberg Complex towards the Botswana border in the west (Roelofse, 2010). The limb consists of two zones underlain by substantial thickness of Bushveld rocks, the first immediately west of the Pilanesberg Complex and the second about 60 km further to the west (Biesheuvel, 1970).

The Western Limb (Figure 2), part of which forms the focus of this study, occurs as a 200 km long bow-shaped body with an easterly dip extending from Thabazimbi in the north to north of Pretoria in the south (Roelofse, 2010).

The stratified mafic-ultramafic rocks of the Bushveld Complex range from dunite to diorite in composition (Kinnaird *et al.* 2005), (Figures 2 and 3).

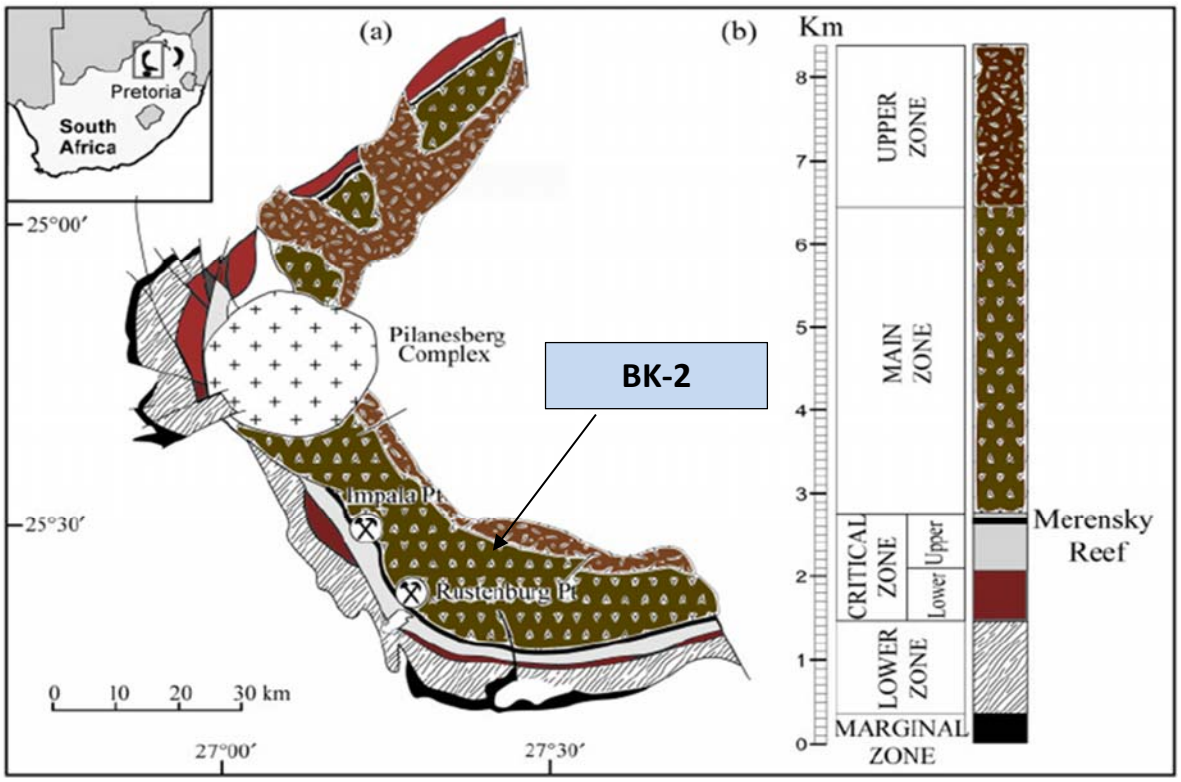

Figure 2: Details of the geology of the Western lobe of the Bushveld Complex, South Africa. (a) Simplified geological map, modified after Von Gruenewaldt (1986, 1989). (b) Generalized stratigraphy of the Bushveld Complex modified after Eales & Cawthorn (1996).

The Rustenburg Layered Suite is informally divided into five major zones (Figures 2 & 3), the exact boundaries of which have been extensively debated (e.g. Kruger, 1990). From bottom to top, these zones are; the Marginal, Lower, Critical, Main, and Upper zones (Chutas *et al.* 2012). The magmatic pseudo-stratigraphic units in the Rustenburg Layered Suite are typically identified based on modal mineralogy and isotopic signatures, specifically initial strontium ratios (e.g. Kruger, 2005).

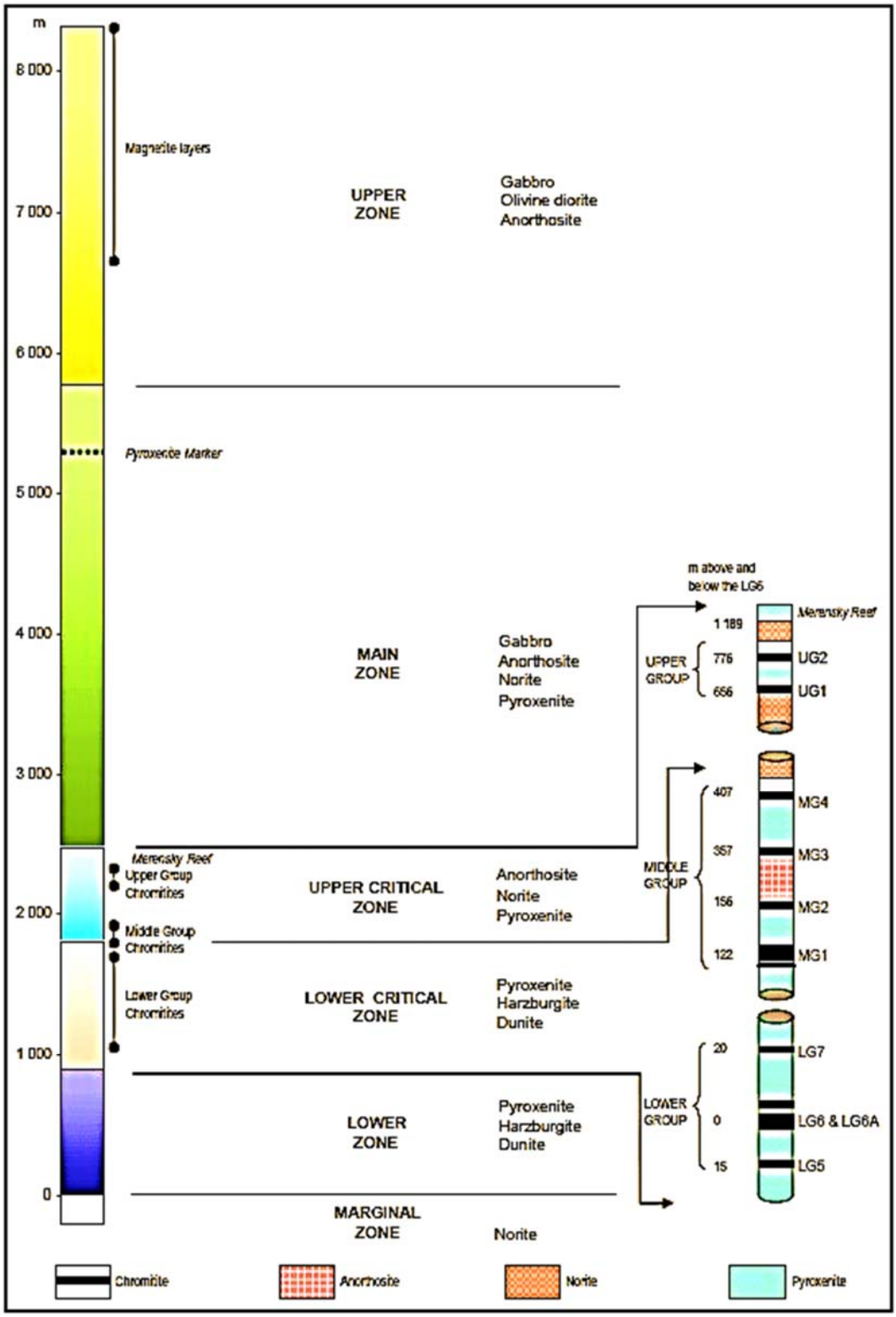

Figure 3: Generalised stratigraphic column of the Rustenburg Layered Suite, Bushveld Complex (Viljoen &Schürmann, 1998).

1.2.3 Lithostratigraphic units of the Rustenburg Layered Suite

1.2.3.1 Marginal Zone

The Marginal Zone is not always present in the Eastern and Western lobes of the Bushveld Complex (Kinnaird *et al.* 2005). Where it occurs, it consists of heterogeneous noritic rocks of up to 880 m thick, which may represent composite sills, or the distal facies of evolved magmas (Cawthorn *et al.* 1981). The latter rocks show varying quantities of accessory clinopyroxene, quartz, biotite and hornblende that mirror varying degrees of contamination from the underlying sediments (Kinnaird, 2005).

1.2.3.2 Lower Zone

The ultramafic Lower Zone has the most limited lateral extent (Kinnaird, *et al.* 2005), with the maximum thickness of about 1 300 m where it occurs. The zone is dominated by bronzitites and olivine-bearing rocks (Willemse, 1964), with varying amounts of intercumulus plagioclase, clinopyroxene, biotite and chromite (Eales & Cawthorn, 1996). The absence of chromitites is a distinguishing feature (Roelofse, 2010), except for the Northern Limb (Hulbert, 1983).

1.2.3.3 Critical Zone

The Critical Zone is sub-divided into two compositionally different subzones, namely the upper and lower Critical Zones. It has an approximate thickness of about 1.2 km, with two economically important PGE-bearing layers (the Merensky Reef and the UG2 chromitite) and 13 major chromitite layers (Cameron, 1980, 1982).

The lower Critical Zone according to Kinnaird *et al*. (2005) is distinguished by a thick succession of orthopyroxenitic cumulates, whereas the upper Critical Zone according to Eales *et al*. (1986) is characterized by a number of cyclic units sequentially composed of ultramafic cumulates, chromitite, harzburgite and/or pyroxenite, norite and anorthosite from their bases upwards. The transition between the lower and upper Critical Zones is characterised by the first appearance of cumulus plagioclase (Roelofse, 2010).

1.2.3.4 Main Zone

The Main Zone, which is the thickest of the zones (Kinnaird *et al.* 2005) is ca. 3 km thick and is composed mainly of norite in the basal and uppermost portions, but gabbronorite is dominant in the central portion, while olivine and chromite are lacking and anorthosites are rare (Mitchell, 1990). The Main Zone does not show the same degree of modal layering as the Critical Zone, although it shows distinct cryptic layering (Molyneux 1974; Mitchell 1990; Nex *et al.* 1998).

The Main Zone contains plagioclase, clinopyroxene, and low-Ca pyroxene as the dominant cumulus phases (Wager & Brown, 1968). In this zone, there is a prominent orthopyroxenite layer, the so-called “Pyroxenite Marker”, which occurs near the top of this sequence (Kruger *et al.* 1987), and is present in both the Eastern (von Gruenewaldt, 1970) and Western limbs (Cawthorn *et al.* 1991). It is in the Main Zone that Maier *et al.* (2001) hypothesized that the Pyroxenite Marker formed in response to localized super cooling and the suppression of plagioclase crystallization.

Cawthorn and Walraven (1998) observed a dramatic increase in anorthite (An%) content in plagioclase and Mg-number in orthopyroxene from below up to the Pyroxenite Marker and also a decrease in initial $^{87}Sr/^{86}Sr$ ratio (0.708-0.707) at this level, which was interpreted to reflect major addition of a different magma composition.

1.2.3.5 Upper Zone

The Upper Zone is about 2 - 3 km thick, and characterised by approximately 25 magnetitite layers in four groups (Kinnaird *et al.* 2005), with its base having been conventionally defined by the appearance of cumulus magnetite (Kruger 1990; Nex *et al*. 1998).

However, the position of the boundary between the Main Zone and the Upper Zone remains controversial (Manyeruke, 2007), with some authors preferring to place the boundary at the level of the Pyroxenite Marker (e.g. Kruger, 1990).

Based on the reversal in initial strontium (Sr_i) isotopic ratio towards less radiogenic compositions (Figure 4) and the trend of iron enrichment (Von Gruenewaldt, 1973; Klemm *et al.* 1985), Kruger (1990) placed the boundary between the Main and Upper zones at the level of the Pyroxenite Marker (Manyeruke, 2007).

Three subzones have been proposed for the Upper Zone based on the appearance of cumulus magnetite (UZa), olivine (UZb) and apatite (UZc), respectively (SACS, 1980, Mitchell, 1990) (Figure 5).

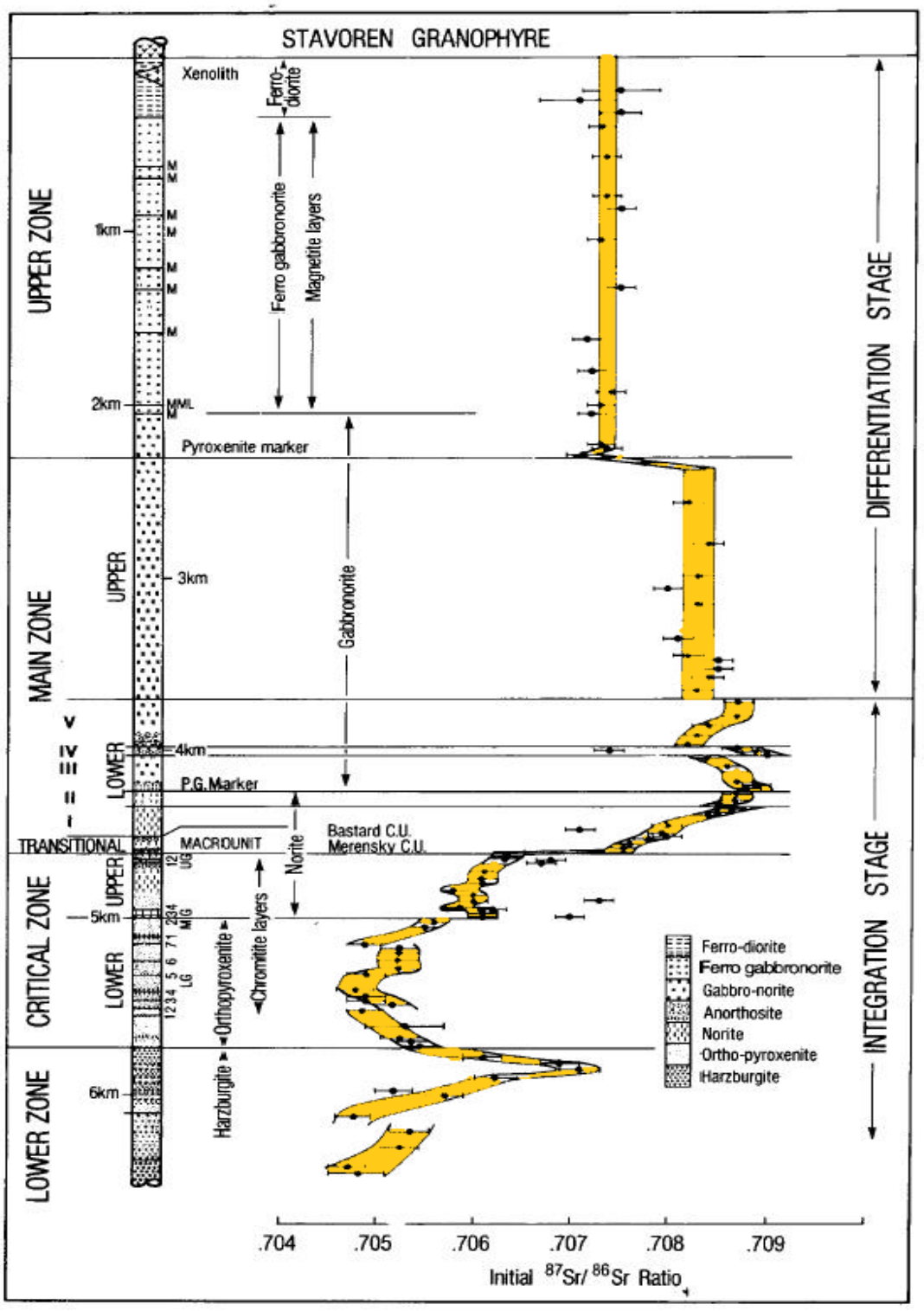

Figure 4: Composite stratigraphic diagram of the western Bushveld Complex indicating the mineralogy and thickness as well as the Sr-isotopic profile, modified after (Kruger, 1994).

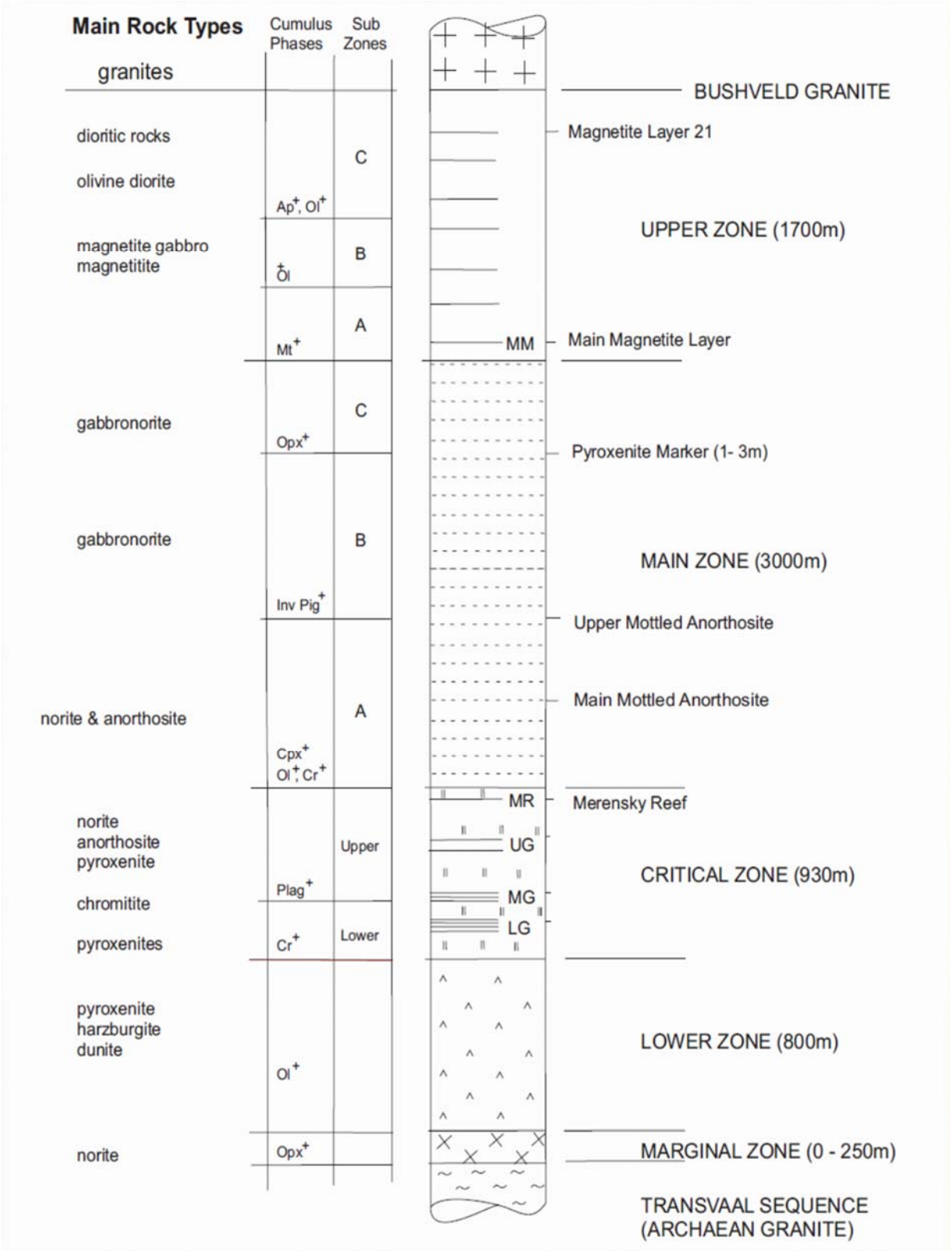

Figure 5: Stratigraphy of the Rustenburg Layered Suite of the Western Bushveld Complex (Mitchell, 1990).

1.3 The Bierkraal drill core (BK-2): Geology

The 1119.13 m long BK-2 drill core was drilled on the farm Bierkraal, which is situated northeast of Rustenburg in the Western Bushveld Complex (Figures 1, 2 & 6) (Tegner *et al.* 2006). The average dip of the Rustenburg Layered Suite in the Bierkraal area is approximately 24^{o} NNE (Walraven & Wolmarans, 1979). The borehole BK-2 was sited near the base of the magnetite-bearing Upper Zone, intersected the Pyroxenite Marker at 484 m, and penetrated about 600 m of the underlying Main Zone (Cawthorn *et al.* 1991).

Two complementary boreholes were also drilled on the farm. BK-1 was collared in the Bushveld granite that overlies the layered mafic rocks, the uppermost of which was intersected at a depth of 380 m (Cawthorn and Walsh, 2001). BK-3 was drilled to overlap the lowest section of BK-1, and due to the lack of reliable marker horizons, the extent of overlap was estimated to be 600 m (Cawthorn and Walsh, 2001).

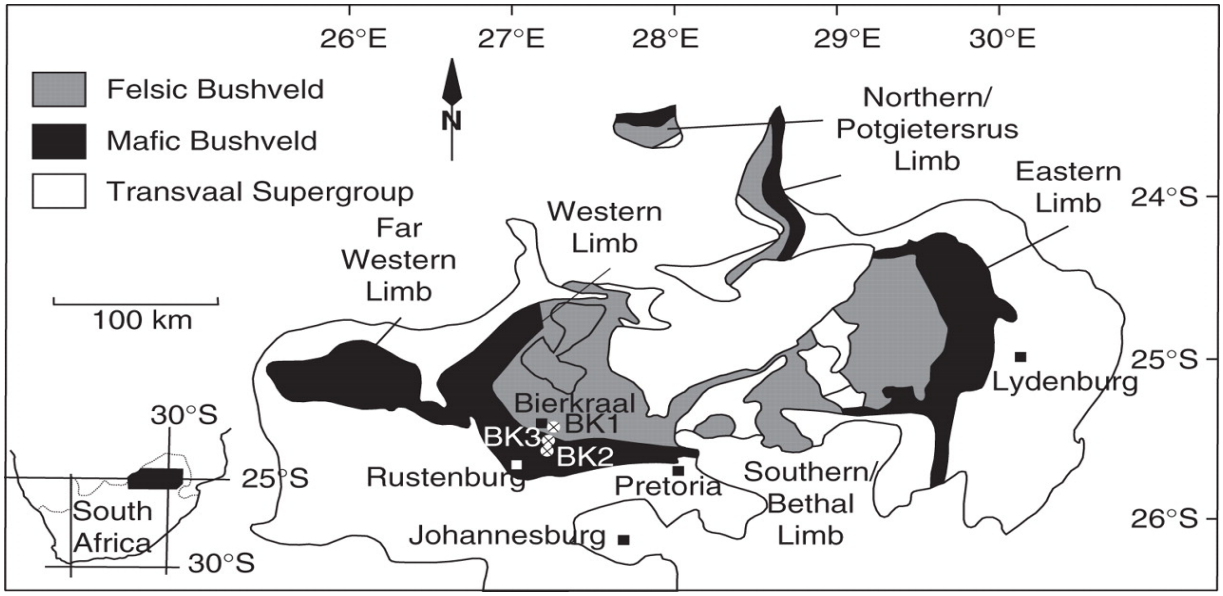

Figure 6: Map of the Bushveld Complex showing the location of the Bierkraal drill holes, BK1, BK2 and BK3 modified after Lundgaard *et al*. (2006).

2. Methodology

2.1 BK-2 Sampling

The 1119.13 m long, BK-2 drill core was sampled at the National Core Library of the Council for Geoscience. A total of 46 samples (each ~ 10 cm long by 2.5 cm radius = ~196.35 cm^3) were collected from the core (that was laid out in 156 trays) at an average sampling interval of about 24 m.

The first sample was taken from a depth of 1117.68 m, whereas the last was taken from a depth of 67.84 m and the entire sample set was labelled PL-001 to PL-046. During sampling the Main Magnetitite layer was encountered at a depth of 172.02 m, while Kruger *et al.* (1987) and Tegner *et al.* (2006), placed the base of it at a depth of 171 m. The sampled drill core covered the stratigraphy of parts of the Main and Upper Zones of the Rustenburg Layered Suite. No attempts were made to re-log the core as the core has

been logged in detail by Cawthorn & McCarthy (1985), Reynolds (1985b), Merkle & von Gruenewaldt (1986), Kruger *et al*. (1987), Cawthorn & Walsh (1988) and von Gruenewaldt (1993).

2.2 Petrography

Forty-five polished thin sections (Figure 7) were prepared out of the collected samples of BK-2, and then studied using transmitted light on an Olympus BX51 petrographic microscope, equipped with an Olympus SC 30 camera and Analysis imager software. In addition, a similar number of epoxy-embedded polished thick sections were also prepared and studied using reflected light on the same microscope. Polished thin sections were studied in order to describe the textural relationships between constituent minerals and to determine the modal mineralogy by visually estimating, whereas polished thick sections were investigated in order to identify apparently cumulus plagioclase crystals, the compositions of which could be determined using electron microprobe analysis and laser ablation (MC)-ICP-MS.

Throughout this document, rocks are classified according to the guidelines proposed by the Commission on the Systematics of Igneous Rocks of the International Union of Geological Sciences (IUGS) (Le Maitre *et al.* 1989) (Figure 8).

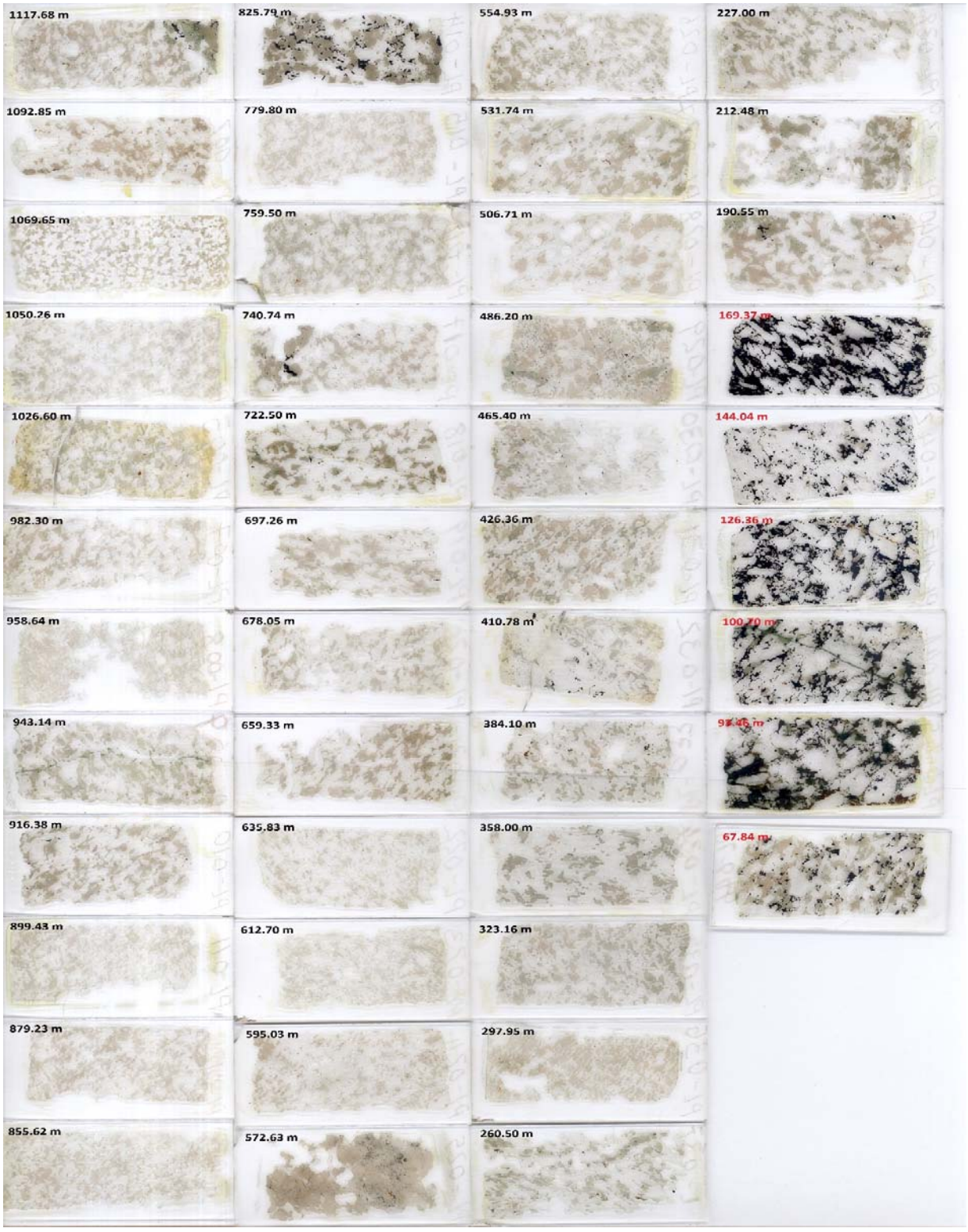

Figure 7: 45 thin sections prepared from samples obtained from the Bierkraal drill core (BK-2) in stratigraphic sequence.

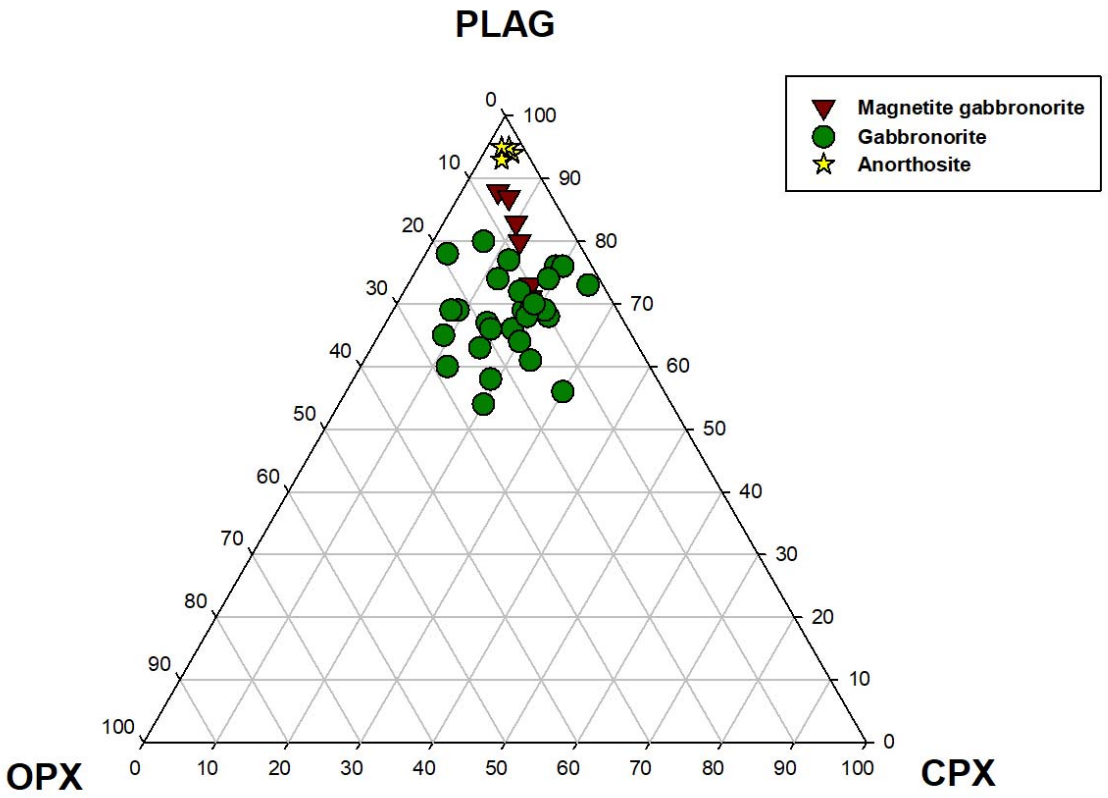

Figure 8: The classification scheme for gabbroic rocks without taking into account olivine and feldspathoids. Plag is plagioclase, cpx is clinopyroxene, opx is orthopyroxene (Le Maitre, 2005).

2.3 Whole-rock major and trace element geochemistry

For the determination of the whole rock major and trace element geochemistry, a PANalytical Axios Wavelength Dispersive X-ray fluorescence spectrometer was used. The said XRF spectrometer, housed in the Department of Geology at the University of the Free State, is equipped with a Rh end window tube, with 4 kW anode (consisting of Rh) and a W cathode (filament).

The maximum voltage that the tube can produce is 60 kV, with the current altering in order to maintain 4 kW. It is equipped with modern software (Super Q V.4) for qualitative and quantitative analysis.

The analysis of major and trace elements in geological materials by X-ray fluorescence is made possible by the atoms' behaviour during interaction with radiation. When materials are excited with high-energy, short wavelength radiation (i.e. X-rays), they can become ionized. If the energy of the radiation is sufficient to dislodge a tightly held inner electron, the atom becomes unstable and an outer electron replaces the missing inner electron. When this happens, energy is released due to the decreased binding energy of the inner electron orbital compared with an outer one. The emitted radiation is of lower energy than the primary incident X-rays and is termed fluorescent radiation. The energy of the emitted photon is characteristic of a transition between specific electron orbitals in a particular element. The intensity of the secondary X-rays is used to determine the concentrations of the elements present by reference to calibration standards (see Tables 2 & 3) with appropriate corrections being made for instrumental errors and the effects the composition of the sample has on its X-ray emission intensities (Rollinson, 1993).

Table 2: Certified and measured values (oxides) of standard reference materials of Mintek and University of the Free State, respectively.

	Certified Values		**Measured values**	
Oxides	NIM-N (Mintek)	NIM-P (Mintek)	NIM-N (UFS)	NIM-P (UFS)
SiO_2	52.64	51.10	52.68	51.70
TiO_2	0.20	0.20	0.18	0.19
Al_2O_3	16.50	4.18	16.28	3.88
Fe_2O_3	8.97	12.70	9.07	12.68
MgO	7.50	25.33	7.41	24.92
MnO	0.18	0.22	0.19	0.23
CaO	11.50	2.66	11.70	2.64
Na_2O	2.46	0.37	0.34	0.13
K_2O	0.25	0.09	0.19	0.03
P_2O_5	0.03	0.02	0.02	0.02
NiO	0.02	0.07	0.02	0.07

Table 3: Certified and measured values (traces) of standard reference materials of Mintek and University of the Free State, respectively.

	Certified values		**Measured values**	
Traces	NIM-N (Mintek)	NIM-P (Mintek)	NIM-N (UFS)	NIM-P (UFS)
Sc	38	29	33.89	24.72
V	220	230	169.29	241.17
Cr	30	24000	34.31	24997.16
Co	58	110	51.35	93.63
Ni	120	555	113.26	547.60
Cu	14	18	32.95	88.01
Zn	68	100	56.07	98.56
As	-	-	6.14	2.37
Br	-	-	9.49	4.60
Rb	6	5	2.39	1.52
Sr	260	32	251.98	30.20
Y	7	5	5.26	1.97
Zr	23	30	9.38	8.97
Nb	-	-	< 0.01	< 0.01
Mo	-	-	< 0.01	< 0.01
Ag	-	-	< 0.01	< 0.01
Cd	-	-	< 0.01	3.24
Ba	100	46	167.78	170.85
Pb	7	6	3.16	1.28
U	0.6	0.4	< 0.01	< 0.01

2.3.1 Sample Preparation for XRF analysis

Part of every sample of the 46 collected during the study was crushed and milled using a jaw-crusher and swing mill, respectively.

For major element determinations, 10 g of sample powder was heated to 110°C overnight, to dry the sample and then to 1000°C for 4 hours, to gravimetrically determine the loss on ignition (LOI).

A flux consisting of 0.2445 g La_2O_3, 0.705 g $Li_2B_4O_7$, 0.5505 g Li_2CO_3 and 0.02 g $NaNO_3$ was added to 0.28 g of sample. The mixture was then heated to 1000°C for approximately 5 min until a melt was formed within a Pt crucible. The melt was then poured into a mould and pressed to form a fusion disc for subsequent analysis.

For the determination of trace elements and Na_2O, 8 g of sample was added to 3 g of Hoechst wax ($C_6H_8O_3N_2$). This was mixed for 10-20 minutes in a Turbula mixer to ensure that the sample was mixed into a homogeneous state. The mixture was then pressed using a hydraulic press to form a pressed pellet for subsequent analysis.

2.4 *In situ* major-element geochemistry of plagioclase

An electron probe micro-analyzer (EPMA) is a microbeam instrument used mainly for the *in situ*, non-destructive chemical analysis of microscopic solid samples (Reed, 2005).

The primary importance of an EPMA is the ability to acquire precise, quantitative elemental analyses at very small "spot" sizes (as little as 1-2 microns), primarily by wavelength-dispersive spectrometry.

Xiang and Xuan (2010) maintain that the spatial scale of analysis, combined with the ability to create detailed images of the sample, makes it possible to analyze geological materials *in situ* and to resolve complex chemical variation within single phases (in geology, mostly glasses and minerals).

Electron Probe Micro Analyzer data acquisition was performed at the Department of Geology (Rhodes University), on a Jeol JXA 8230 Superprobe, using four WD spectrometers. Analytical conditions employed for quantitative analyses were: 15 kV for the accelerating voltage, beam current of 20 nA, a spot beam size of >1 micron, and counting times of 10 seconds on peak and 5 seconds on background with the exception of potassium (30 seconds on peak, 15 seconds on background). Natural and synthetic standards were used for quantifying the characteristic X-rays as displayed in Table 4 below.

Table 4: Measurement conditions and crystals used for each element.

WDS elements			
Element	**X-ray**	**Crystal**	**Peak Pos.**
Si	Kα	TAP	77.635
Al	Kα	TAP	90.734
Ca	Kα	PETJ	107.463
Mg	Kα	TAP	107.511
Fe	Kα	LIF	134.463
Ti	Kα	LIF	190.944
Mn	Kα	LIFL	146.115
Ba	Kα	PETL	88.815
Sr	Kα	PETL	219.586
Na	Kα	TAPL	129.406
K	Kα	PETL	119.364

Elements were measured using large diffracting crystals for higher sensitivity as shown in Table 4. Plagioclase–An_{65} (Si, Al, Ca, and Na), orthoclase (K), periclase (Mg), almandine (Fe), barite (Ba), rhodonite (Mn), rutile (Ti), and celestite (Sr) were used as standards and the ZAF matrix correction method was employed for quantification as shown in Table 5.

Table 5: Standards used and ZAF (atomic, absorption and fluorescence) matrix correction.

Element	Standard name	Mass (%)	ZAF Fac.	Z	A	F
SiO_2	Plag-An65_SPI	54.2100	3.0527	4.4064	0.6925	1.0004
Al_2O_3	Plag-An65_SPI	28.5300	4.1586	5.8530	0.7029	1.0109
CaO	Plag-An65_SPI	11.8000	0.8570	0.9355	0.9160	1.0001
MgO	Periclase_SPI	100.0039	5.3788	7.8316	0.6868	1.0000
FeO	Almandine_SPI	23.2700	0.1990	0.2024	0.9832	1.0000
TiO_2	Rutile_SPI	99.9834	0.5913	0.6060	0.9757	1.0000
MnO	Rhodonite_SPI	42.3000	0.2678	0.2737	0.9787	1.0000
BaO	Barite_SPI	65.8300	0.5360	0.5750	0.9322	1.0000
SrO	Celestite_SPI	56.2000	3.4782	4.3528	0.7955	1.0045
Na_2O	Plag-An65_SPI	4.3500	5.1358	10.7639	0.4753	1.0039
K_2O	Orthoclase_SPI	15.9600	1.0718	1.2041	0.8899	1.0002

Forty-four polished thick sections examined using reflected light microscopy to determine the positions of euhedral to subhedral (and therefore presumably cumulus) plagioclase crystals were selected for *in situ* major element determinations using EPMA. Plagioclase crystals that showed no or very little alteration were circled using a diamond pen on the epoxy embedded thick sections (Figures 10) to aid in finding the crystals during EPMA and LA-ICPMS analyses (for trace elements and Sr-isotopes). Representative back-scattered electron (BSE) images showing spots that were analysed are shown in Figure 9.

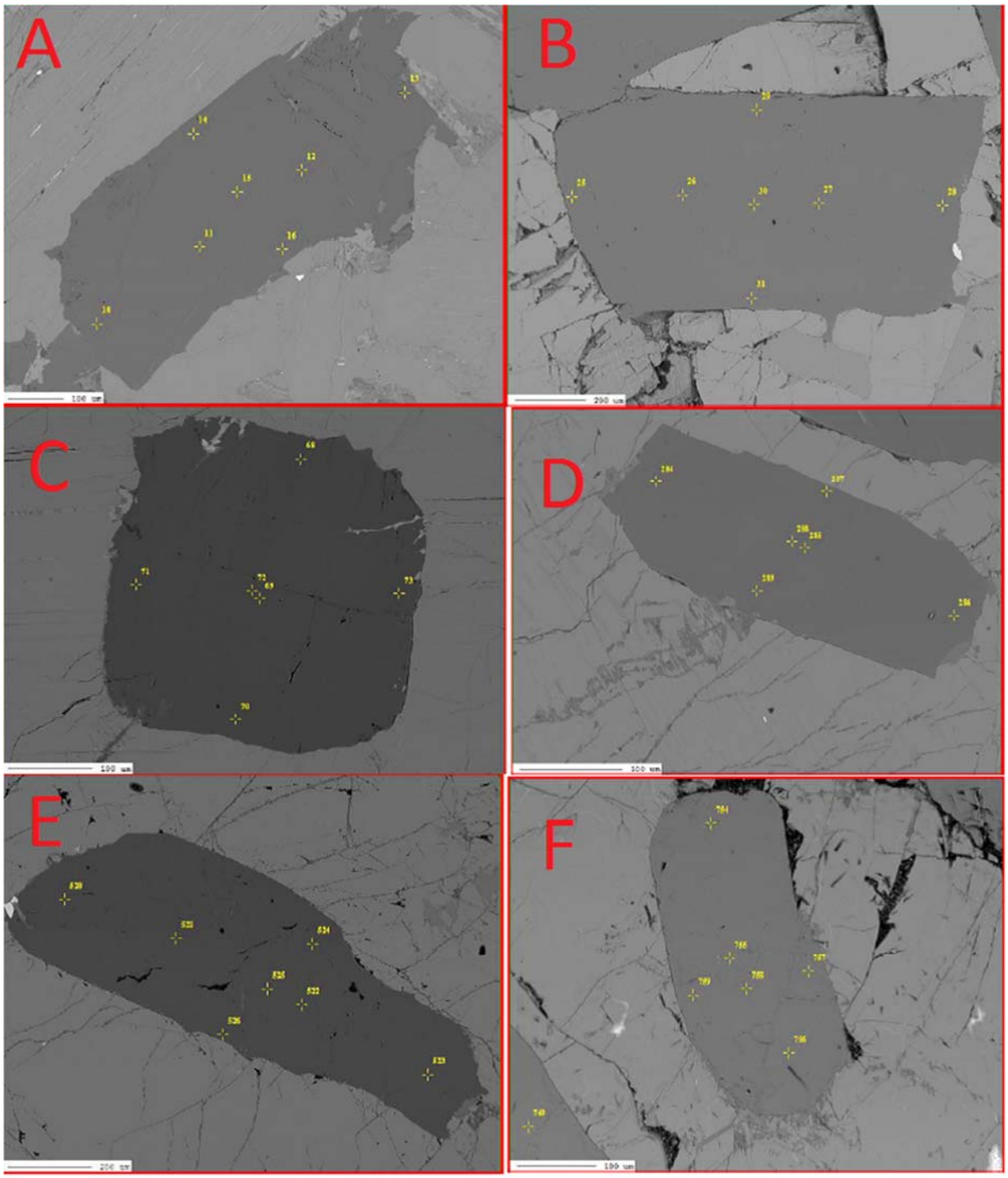

Figure 9: Back Scattered Electron (BSE) images of: (A-F) selected images of unaltered plagioclase crystals that were analysed for *in situ* major element chemistry, with yellow representing positions of spots that were analysed by EPMA.

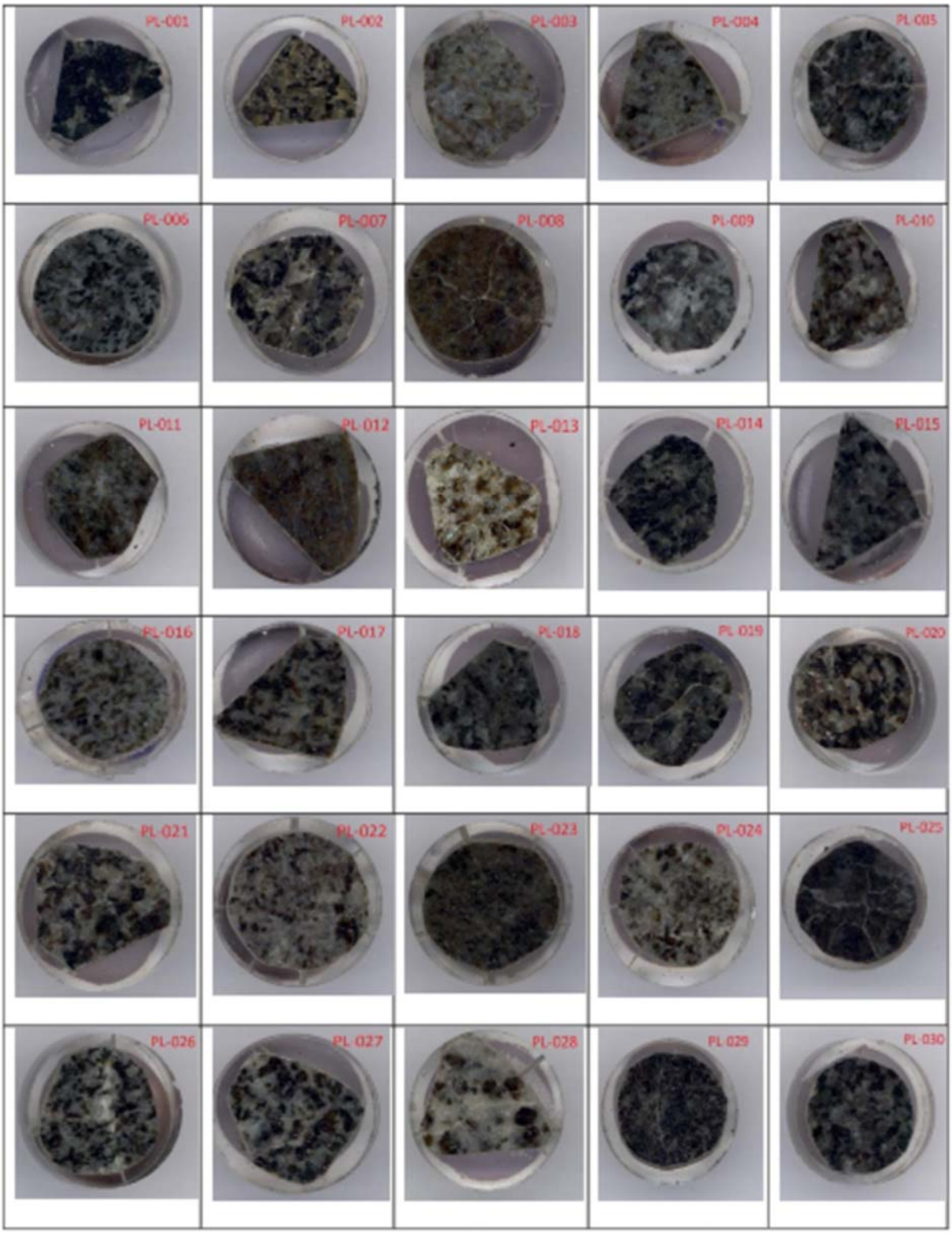

Figure 10: Epoxy-embedded polished thick sections (25.4 mm diameter) covering BK-2 stratigraphy.

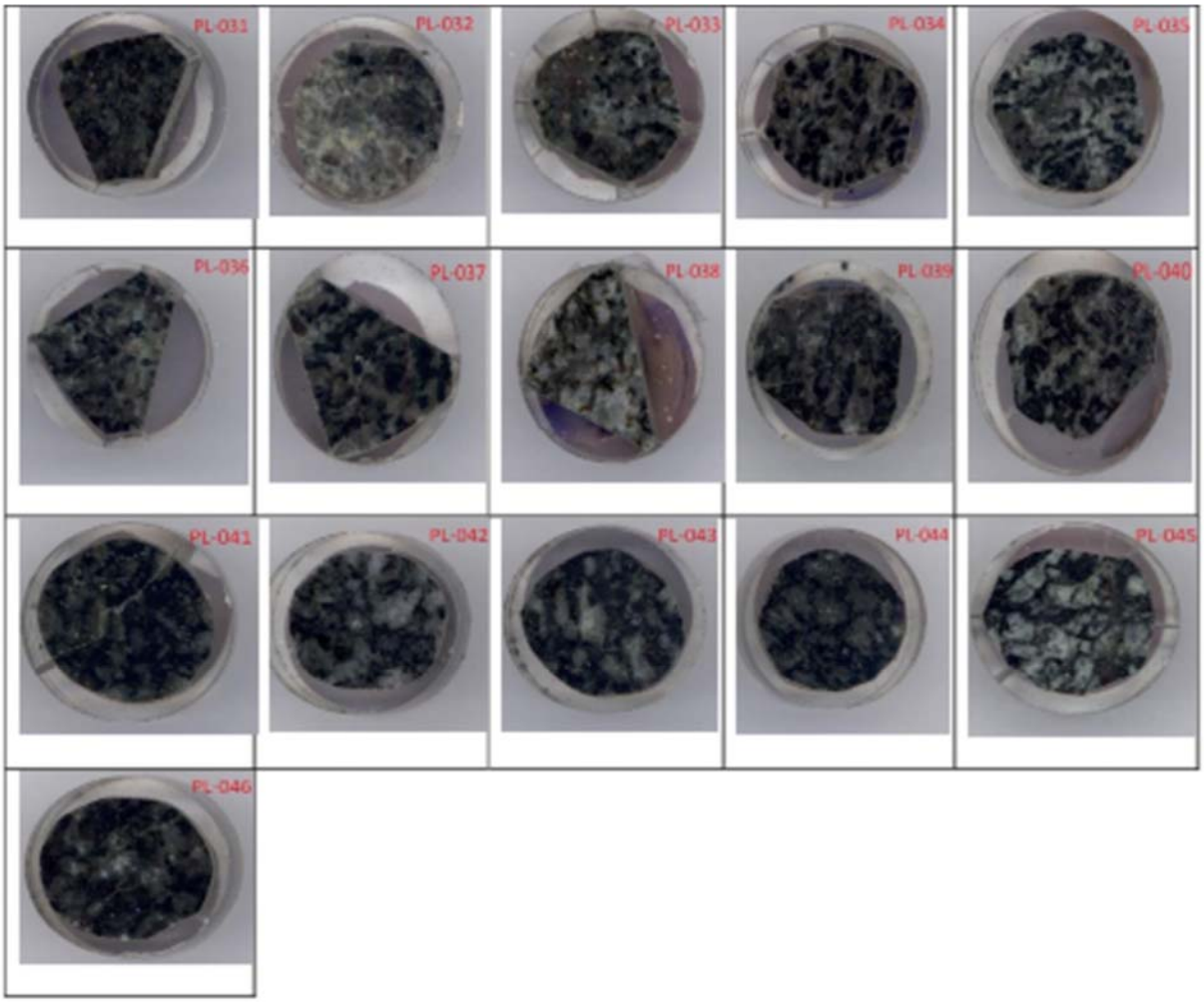

Figure 10: (Continued).

2.5 *In situ* trace-element geochemistry of plagioclase

The forty-four samples that were subjected to EPMA analysis, excluding PL-016 and PL-045, were cleaned with alcohol to remove the carbon coating. The selected plagioclase grains were analysed *in situ* for trace elements. Analyses were performed using the Thermo-Fisher X-Series II Quadrupole Laser Ablation-Inductively Coupled Plasma-Mass Spectrometer (LA-ICP-MS), equipped with a New Wave UP213 solid-state laser ablation system at the Department of Geological Sciences (University of Cape Town). The spot

size of the laser can be set to various diameters between 10 and 300 microns, but in this study, laser analytical parameters were as follows:

- Pulse frequency 10 Hz
- Spot diameter 110 µm

Laser analyses of silicate minerals and glasses are calibrated using well-characterized, homogeneous solid standards (NIST 610 and 612 glasses, Table 6 below). Either samples for laser ablation analysis are typically polished thick sections or polished 25 mm diameter disc mounts. The analytical parameters remained constant throughout measurement of both the samples and standards.

Table 6: Certified values of standard reference materials (Nist 610 & 612) for trace elements (Pearce *et al*. 1997) and measured values from the University of Cape Town, respectively.

	Certified values		**Measured values**	
	NIST-610	NIST-612	NIST-610 (UCT)	NIST-612 (UCT)
Rb	425.7	31.4	444.23	32.47
Sr	515.5	78.4	517.03	69.94
Y	-	-	476.07	34.28
Zr	-	-	438.40	33.70
Ba	453	38.6	438.80	36.43
La	-	-	484.57	34.93
Ce	-	39	468.43	35.05
Pr	-	-	455.37	33.88
Nd	-	36	458.83	35.46
Sm	-	39	466.20	36.40
Eu	-	36	482.47	35.04
Tb	-	-	465.33	36.08
Gd	-	39	572.70	54.73
Dy	-	35	446.70	34.50
Ho	-	-	469.03	36.97
Er	-	39	380.10	34.73
Tm	-	-	434.97	34.66
Yb	-	42	476.30	38.31
Lu	-	-	454.43	36.02

	Certified values		Measured values	
Pb	426	38.57	439.60	37.87
Th	457.2	37.79	473.97	36.17
U	461.5	37.38	472.17	35.66

2.6 *In situ* strontium isotopic determination

Forty-one polished thick sections that were prepared from the BK-2 drill core and used in the laser ablation analyses conducted at the University of Cape Town to determine the trace elements on the selected plagioclase grains, were used for *in situ* strontium isotopic determination on the very same plagioclase grains by ablating new spots next to the ones created earlier for trace element analysis (see Figure 24).

A minimum of two to three plagioclase grains were chosen in each sample, to ablate two or three spots per sample, in order to test for both inter-and intracrystalline Sr-isotopic variations.

The Sr-isotopic ratios of plagioclase were determined by using the New Generation (Nu Plasma II) HR MC-ICP-MS fixed to an Atlex SI laser system using a 193 nm excimer laser sampler, at the Department of Terrestrial Magnetism, Carnegie Institution for Science, Washington DC, USA.

The selected plagioclase crystals were ablated in He gas using a continuous fire mode, pulse rate of 10 Hz, and a spot diameter of 95 μm. The isotopic ratios after being measured were then corrected for the instrument fractionation factors, and analytical error (Ridley & Lichte, 1998), and following an exponential law and $^{86}Sr/^{88}Sr$ value of 0.1194 (Banner and Kaufman, 1994).

Krypton exists as an impurity in argon, the carrier gas used in the LA-MC-ICP-MS analyses (*e.g.,* Paton *et al.* 2007). The correction for the isobaric interference of ^{86}Kr on ^{86}Sr was attained by the subsequent subtraction of the blank analyses from the unknown signals and on "on-peak-zero" measurements (OPZ) which are based on background contribution (Davidson *et al.* 2001, Bizzarro *et al.* 2003, Schmidberger *et al.* 2003, Ramos *et al.* 2004, Paton *et al.* 2007). The BHVO-2 glass was analysed before and after every 9th spot and the $^{87}Sr/^{86}Sr$ ratio for each spot was corrected for the isobaric interference of ^{87}Rb on ^{87}Sr through monitoring of the ^{85}Rb ion signal by assigning a value to the $^{87}Rb/^{85}Rb$ ratio so that BHVO-2 gave $^{87}Sr/^{86}Sr = 0.703469 \pm 0.000014$ after Elburg *et al.*(2005).

Initial $^{87}Sr/^{86}Sr$ ratios were calculated using an age of 2054.4 Ma (Scoates and Friedman, 2008), using a decay constant of 1.393×10^{-11} y^{-1} (Nebel *et al.* 2011) and the corrected $^{87}Rb/^{86}Sr$ ratio as obtained from the LA-MC-ICPMS analyses. The error on the $^{87}Rb/^{86}Sr$ ratio was not propogated in the calculation of the initial $^{87}Sr/^{86}Sr$ ratio. The error on the $^{87}Rb/^{86}Sr$ ratio was generally of a similar order of magnitude to the error on the measured $^{87}Sr/^{86}Sr$ ratios, such that the error on the initial $^{87}Sr/^{86}Sr$ ratios too were generally of a similar order of magnitude.

The accuracy of the laser ablation protocol was assessed throughout the time of analysis by repeatedly analysing a sample of Steens Mountain Plagioclase. The $^{87}Sr/^{86}Sr$ average value of Steens Mountain plagioclase obtained during analysis was 0.70385 ± 0.00025 (2σ, n = 43), that is within error of the ratio obtained using TIMS (0.703657 ± 0.00001).

Figure 11: Nu (Plasma II) HR MC-ICP-MS fixed to an Atlex SI laser system using a 193 nm excimer laser sampler at the Department of Terrestrial Magnetism, Carnegie Institution for Science, Washington DC.

3. Results

3.1 Petrography

The observations of the forty-six studied samples covering 1117.68 m of the BK-2 stratigraphic succession were made, inclusive of the modal mineralogy, grain size and textures as provided in Electronic Appendix 1. Out of 44-studied rock samples, gabbronorites accounted for 50%, leucogabbronorites for 25%, magnetite gabbronorite for 14%, anorthosite for 9%, pegmatitic gabbronorite for 2% of all the studied Main Zone and Upper Zone samples collectively.

Intergranular texture was encountered in 51% of the studied samples, whereas subophitic texture was seen in ~ 26% of the studied samples. The latter was observed mainly in the upper Main Zone and Upper Zone, and then again lower in the Main Zone at a depth of between ~700 m to 980 m. Subophitic texture was observed mainly in gabbronorites and to a lesser extent in gabbros.

Ophitic texture was observed in about 14% of the studied samples, and is common in the plagioclase-rich rocks such as anorthosites. Poikilitic texture was observed in approximately 9% of all the studied samples. It occurs mainly within the lower parts of the Main Zone in leucogabbronorite, gabbronorite and gabbro.

Plagioclase is a ubiquitous phase in all of the rock samples studied. It exhibits mostly polysynthetic twinning.

Plagioclase occurs as euhedral to subhedral, tabular and elongated laths. Plagioclase laths show well developed preferential orientation in the anorthosite samples (Figures 14-C and 16-D) taken at depths of 506.71 m and 410.78 m, respectively, which may signify lamination possibly as a result of compaction during solidification.

Plagioclase altered to sericite was observed in pegmatitic gabbronorite and gabbronorite (Figure 13-C & D) taken from depths of 93.46 m and 100.70 m, respectively. Sericite is not widespread in the studied samples. Von Gruenewaldt (1971) attributed wedge-shaped and bent plagioclase twin lamellae, as in leucogabbronorite and gabbronorite (Figures 15-B & 16-C) samples taken at depths of 678.05 m and 465.40 m respectively, to deformation after deposition. This feature was observed in about 30% of the studied samples.

Clinopyroxene in the studied rock samples, occurs as subhedral to anhedral crystals which occasionally show an amoeboidal shape as in the magnetite gabbro (Figure 13-B) taken at a depth of 67.84 m in the Upper Zone. The relatively thick exsolution lamellae of orthopyroxene is characteristic of most clinopyroxene crystals, and twinning, although uncommon, was observed in some samples like the gabbronorite (Figure 14-B) taken at a depth of 486.20 m, approximately 2 m below the Pyroxenite Marker. Clinopyroxene in some instances occurs as chadacrysts enclosed within orthopyroxene oikocrysts (see Figure 14 – B).

In the studied rock samples, orthopyroxene shows a subhedral to anhedral habit. It characteristically shows thin and closely spaced clinopyroxene exsolution lamellae.

Orthopyroxene locally occurs as oikocrysts that enclose plagioclase laths (Figure 14-E) and rarely clinopyroxene.

Poldervaart and Hess (1951) ascribed the presence of thick augite exsolution lamellae in orthopyroxene as suggestive of inverted pigeonite as in the leucogabbronorite (Figure 14-D) taken at a depth of 635.83 m. Inverted pigeonite is prevalent throughout the lower reaches of the Main Zone sampled by BK-2 and vanishes at about 100 m below the Pyroxenite Marker in the upper part of the Lower Main Zone. Olivine occurs intermittently in the studied samples. It reveals anhedral to subhedral shapes and occurs in a very small proportion in the upper part of the Upper Zone sampled by BK-2.

In the studied rock samples, magnetite is virtually always anhedral (Figure 13,A-E), and is found only in the Upper Zone, while biotite is less abundant and was observed in only two Upper Zone samples (Figure 13-A & C). Biotite was encountered in the magnetite gabbro and pegmatitic gabbro taken at depths of 67.84 m and 93.46 m, respectively.

Quartz was a minor constituent of some samples. The BSE image of magnetite gabbronorite (Figure 12) taken at a depth of 100.70 m exhibits a myrmekitic texture, consisting of vermicular intergrowths of quartz in plagioclase. Opaque minerals modally contribute only a small percentage in samples of the Main Zone where magnetite is not present, and occurs within interstitial spaces or as inclusions within silicates.

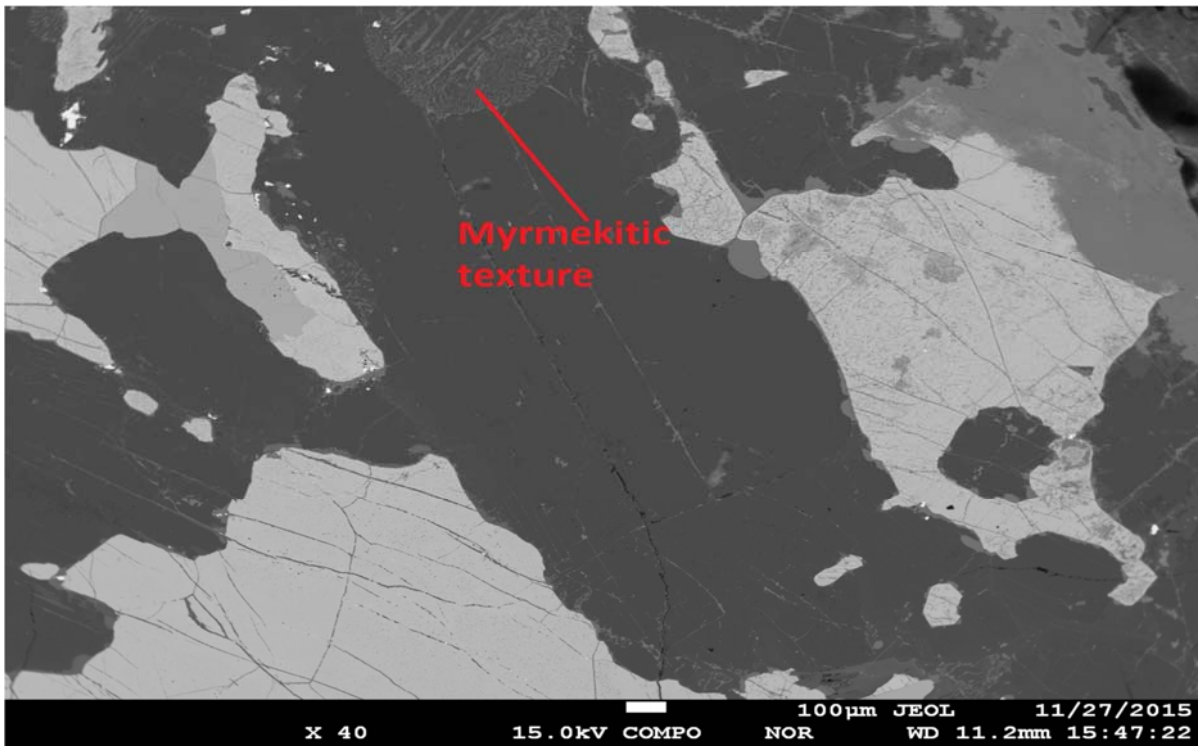

Figure 12: Back-scattered electron image of plagioclase (PL-044_plag1) showing myrmerkitic texture.

The variation in mineral mode across the entire length of the BK-2 drill core is shown in Figure 17 as a summary of the petrographic observations.

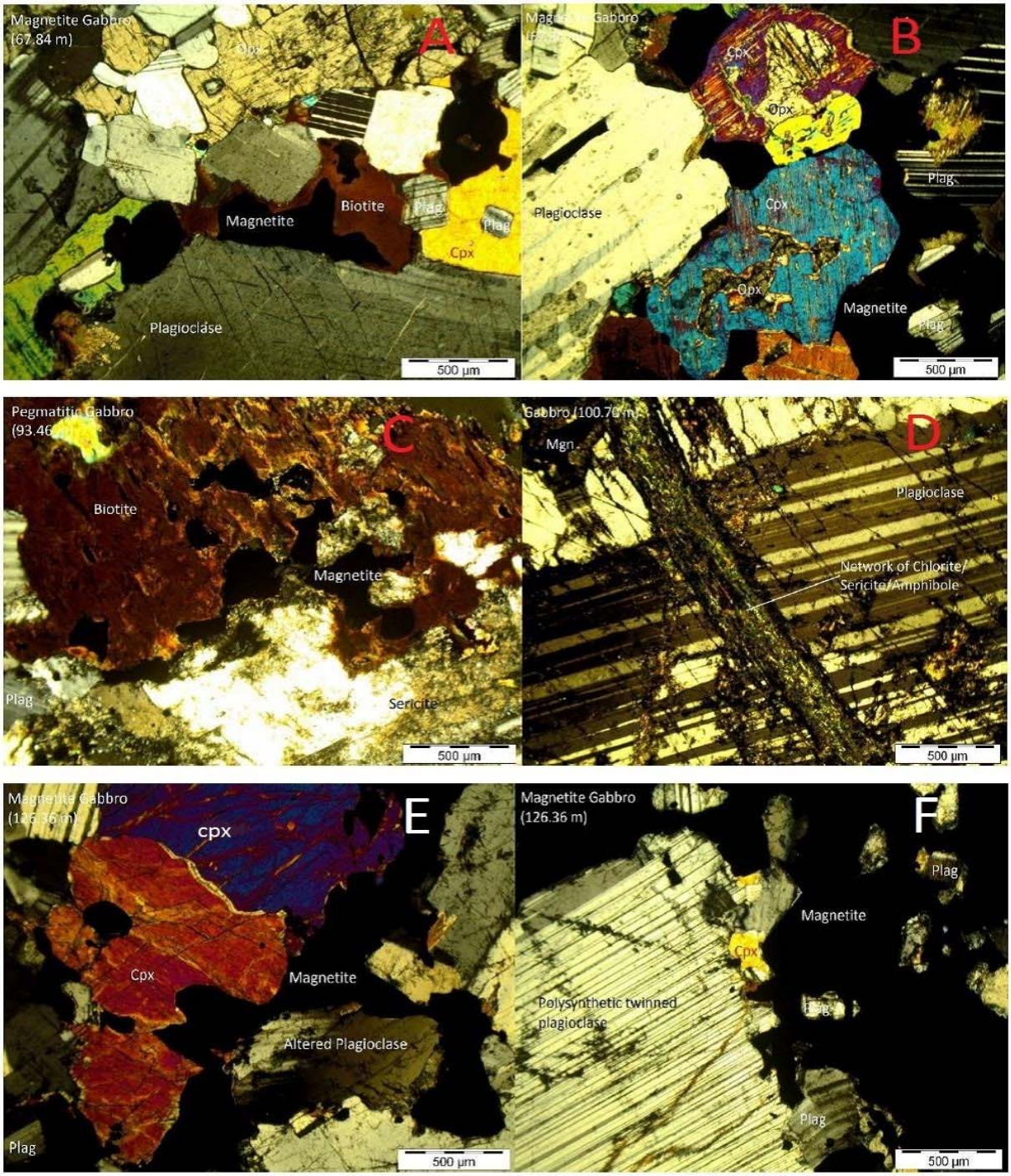

Figure 13: Cross-polarized, transmitted light photomicrographs of: (A) Clinopyroxene oikocryst enclosing plagioclase crystals and anhedral interstitial biotite occurring in association with magnetite. (B) Plagioclase with interstitial magnetite and clinopyroxene oikocryst with orthopyroxene exsolution lamellae. (C) Sericitization of plagioclase and highly altered biotite, both hosting interstitial magnetite. (D) Polysynthetic twinned plagioclase cut across by a network of chlorite/sericite/amphibole. (E) Magnetite occupied interstitial spaces between altered plagioclase. (F) Polysynthetic twinned plagioclase with magnetite enclosing altered plagioclase crystals.

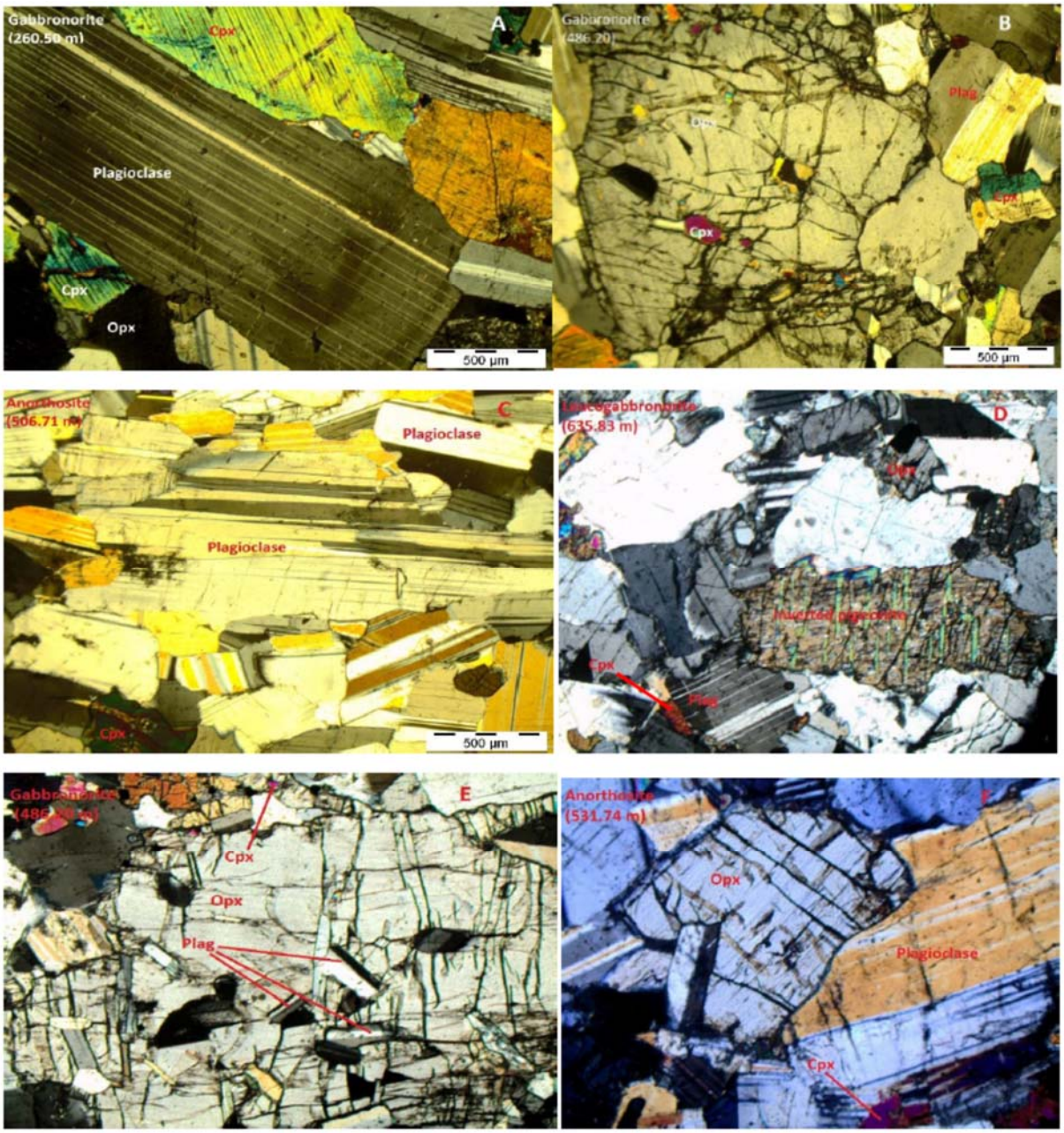

Figure 14: Cross-polarized light photomicrographs of: (A) Euhedral plagioclase laths and intergranular clinopyroxene. (B) Clinopyroxene and plagioclase crystals enclosed by orthopyroxene oikocryst. (C) Well to moderate preferentially orientated plagioclase laths in anorthosite. (D) Inverted pigeonite crystal containing thick clinopyroxene exsolution lamellae. (E) Orthopyroxene oikocryst enclosing plagioclase chadacrysts (~2 m above the Pyroxenite Marker). (F) Polysynthetic twinned plagioclase crystals partially engulfing orthopyroxene crystal.

Figure 15: Cross-polarized light photomicrographs of: (A) Clinopyroxene occupying interstitial spaces between twinned plagioclase crystals. (B) Plagioclase lath with bent and wedge-shaped twin lamellae with intergranular clinopyroxene and orthopyroxene. (C) Orthopyroxene oikocryst enclosing a small clinopyroxene chadacryst, with polysynthetic twinned plagioclase. (D)Orthopyroxene oikocryst enclosing clinopyroxene chadacrysts, and the orthopyroxene oikocryst surrounded by plagioclase crystals. (E) Clinopyroxene chadacrysts enclosed by orthopyroxene oikocryst. (F) Polysynthetic twinned plagioclase, with orthopyroxene oikocrysts enclosing clinopyroxene chadacrysts.

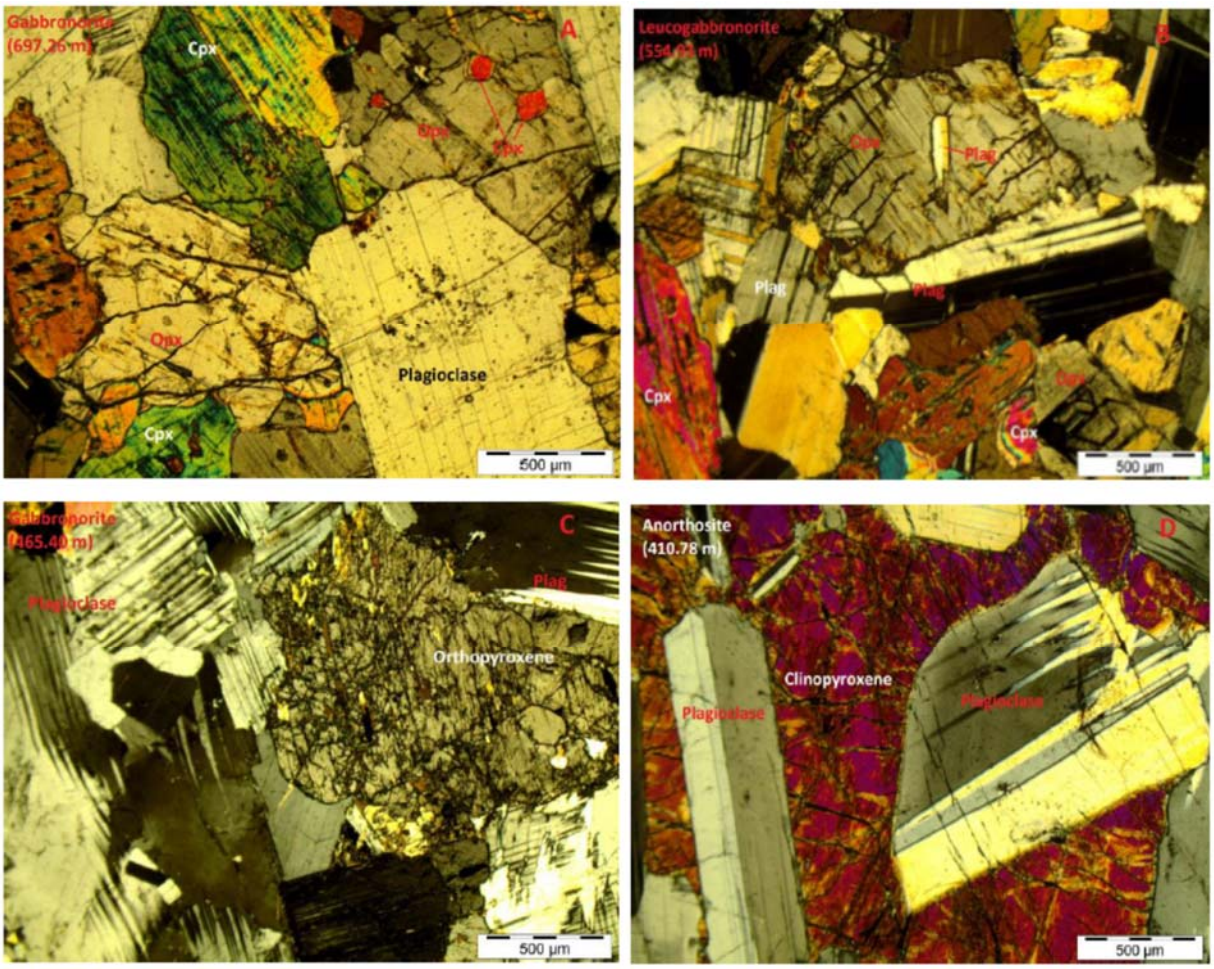

Figure 16: Cross-polarized light photomicrographs of: (A) Typical example of intergranular texture. (B) Plagioclase chadacryst ophitically enclosed by orthopyroxene oikocryst. (C) Bent and wedge-shaped twinned plagioclase occurring in association with orthopyroxene. (D) Twinned plagioclase laths ophitically enclosed by clinopyroxene crystal.

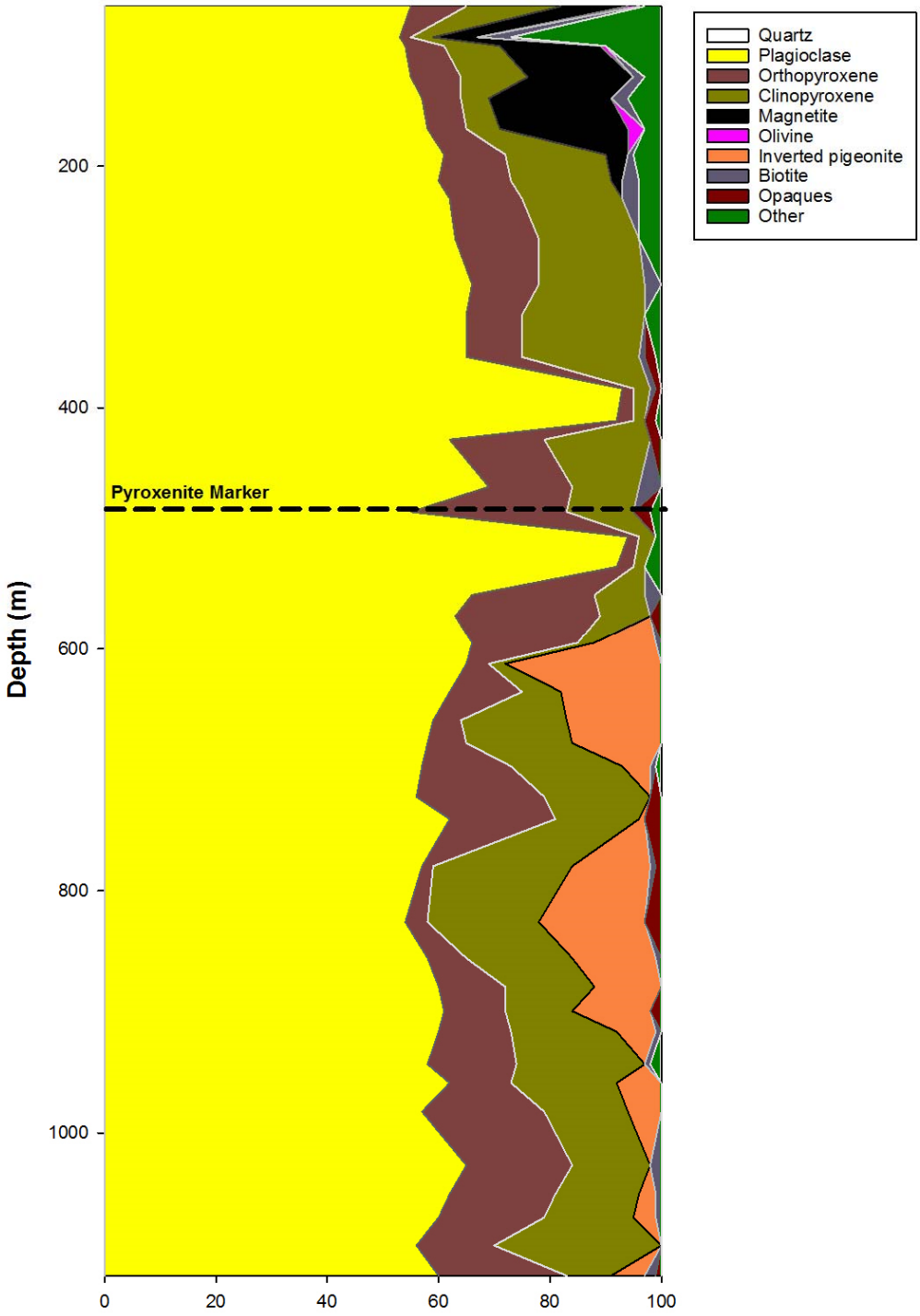

Figure 17: Depth vs. modal mineralogy graph showing plagioclase, ortho- and clinopyroxene as ubiquitous phases in the studied stratigraphic profile, Inverted pigeonite occurs in the lower Main Zone and magnetite in the Upper Zone. Quartz, olivine and biotite are minor phases.

3.2 Whole-rock major and trace element geochemistry

Major and trace element data for all studied rock samples are presented in Electronic Appendix 2. All analysed samples were relatively "fresh" and yielded an average loss on ignition (LOI) of 0.27 wt %. The major elements are extremely variable in the studied samples as reflected by the binary variation diagrams shown below (Figure 19). The binary variation diagrams of both whole rock major and trace elements show high varying modal proportions in the lower Main Zone and upper Main Zone, whereas the Upper Zone exhibits a less variable modal proportion.

3.2.1 Whole-rock major element geochemistry

The SiO_2 content of the studied samples averages 51.60 wt %. A significantly lower SiO_2 content of 22.32 wt % was found for the magnetite gabbronorite from a depth of 169.37 m, reflecting the high oxide relative to silicate content. The highest SiO_2 content (56.27 wt %) was observed in a sample of pegmatite gabbronorite from a depth of 943.14 m.

TiO_2 averaged 0.83 wt % in the studied samples, and P_2O_5 was generally low at less than ~0.1 wt %, the latter being a reflection of the lack / very low content of cumulus apatite in the samples. The TiO_2 content in samples from the Upper Zone is significantly higher than those from the Main Zone, a fact that can likely be ascribed to the presence of titaniferous magnetite in the Upper Zone.

Al_2O_3 (4.24 - 26.45 wt %), CaO (3.44 – 14.43 wt %), Na_2O (0.14 – 0.48 wt %) and K_2O (average of 0.21 wt %) show a negative correlation with MgO in the whole-rock analyses, which for the most part can be ascribed to variations in the mode of plagioclase versus

mafic silicates. NiO shows a positive correlation with MgO that is the results of K_d's >1 for the mafic silicates.

Fe_2O_3 (4.84 – 54.24 wt %) and MnO (0.07 – 0.38 wt %) similarly show a positive correlation with MgO as shown in the binary variation diagrams below (Figure 18). The maximum value of Fe_2O_3 was found in the magnetite gabbronorite (from a depth of 169.37 m), while the lowest value was measured in an anorthosite from a depth of 410.78 m. Most samples contain variable proportions of plagioclase and pyroxene and the five red diamonds represent plagioclase and magnetite in the Upper Zone.

The rocks composition is largely controlled by plagioclase, magnetite and pyroxene as they mostly plot within the field of latter minerals and Figure 18 below shows this. The correlation coefficients of oxides against MgO are; SiO_2 =0.5492, TiO_2=-0.6057, Al_2O_3=-0.5108, Fe_2O_3=-0.3924, MnO=0.6584, Na_2O=-0.6012, K_2O=-0.4802, P_2O_5=0.0326, NiO=0.4904.

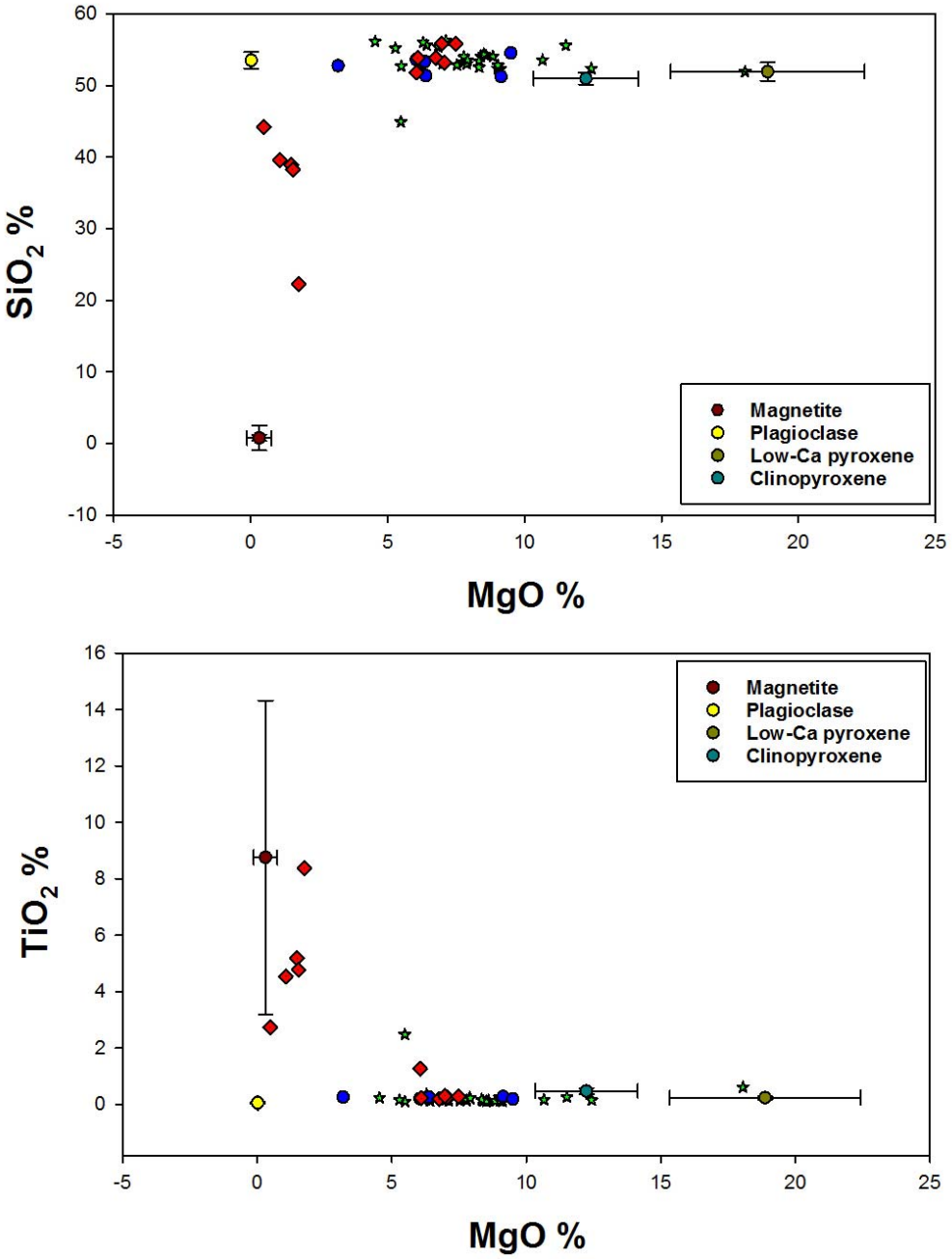

Figure 18: Binary variation diagrams of selected whole-rock major elements versus MgO (green stars represent lower Main Zone samples, blue circles upper Main Zone & red diamonds represent Upper Zone samples) with mineral compositions, see legend, (plagioclase from this study, magnetite, low-Ca pyroxene & clinopyroxene from Bellevue drillcore by Ashwal *et al*. 2005 (0 – 1900 m)), with error bars representing mean and standard deviation.

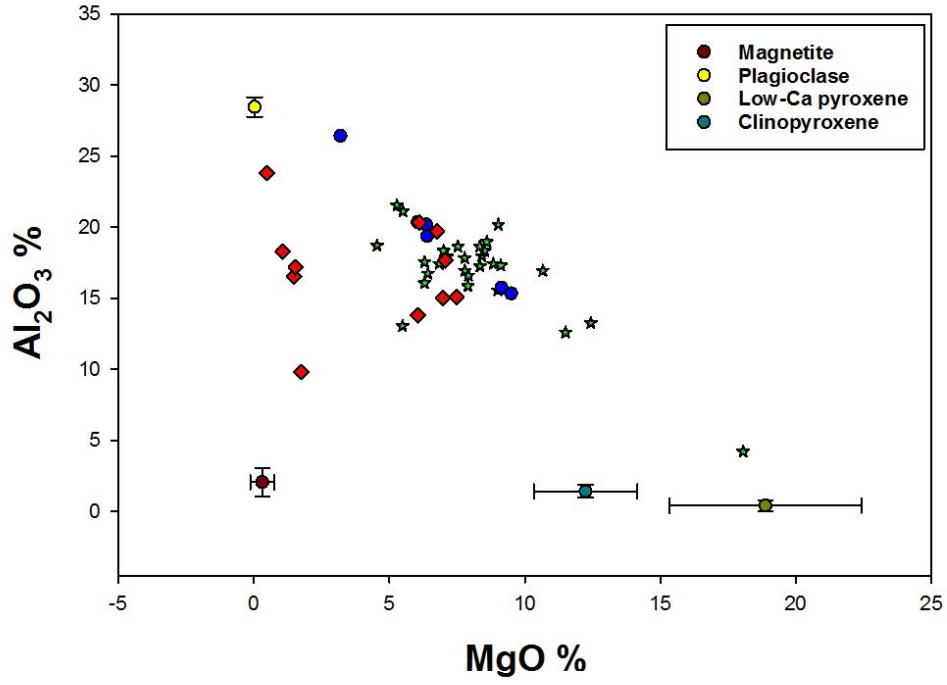

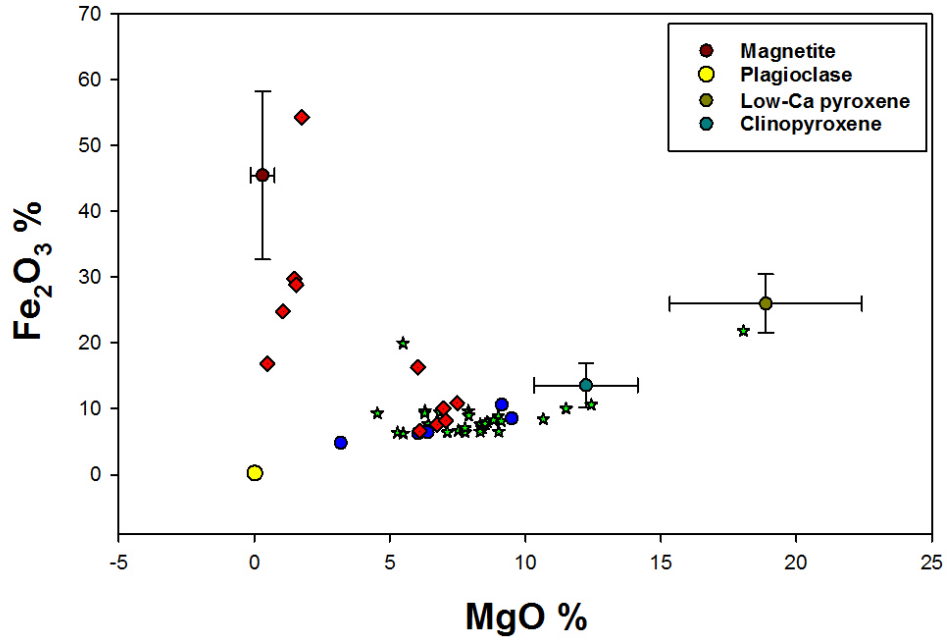

Figure 18: (Continued)

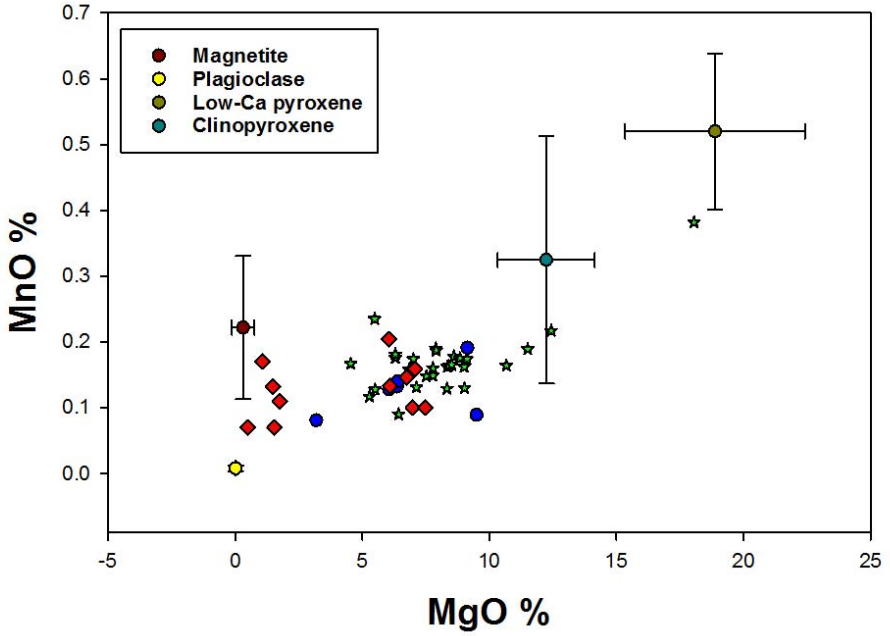

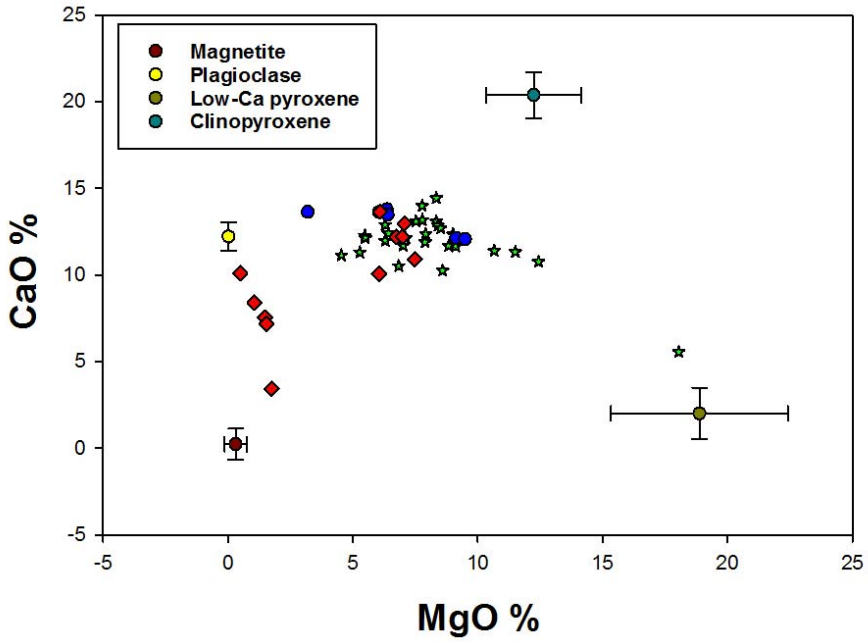

Figure 18: (Continued)

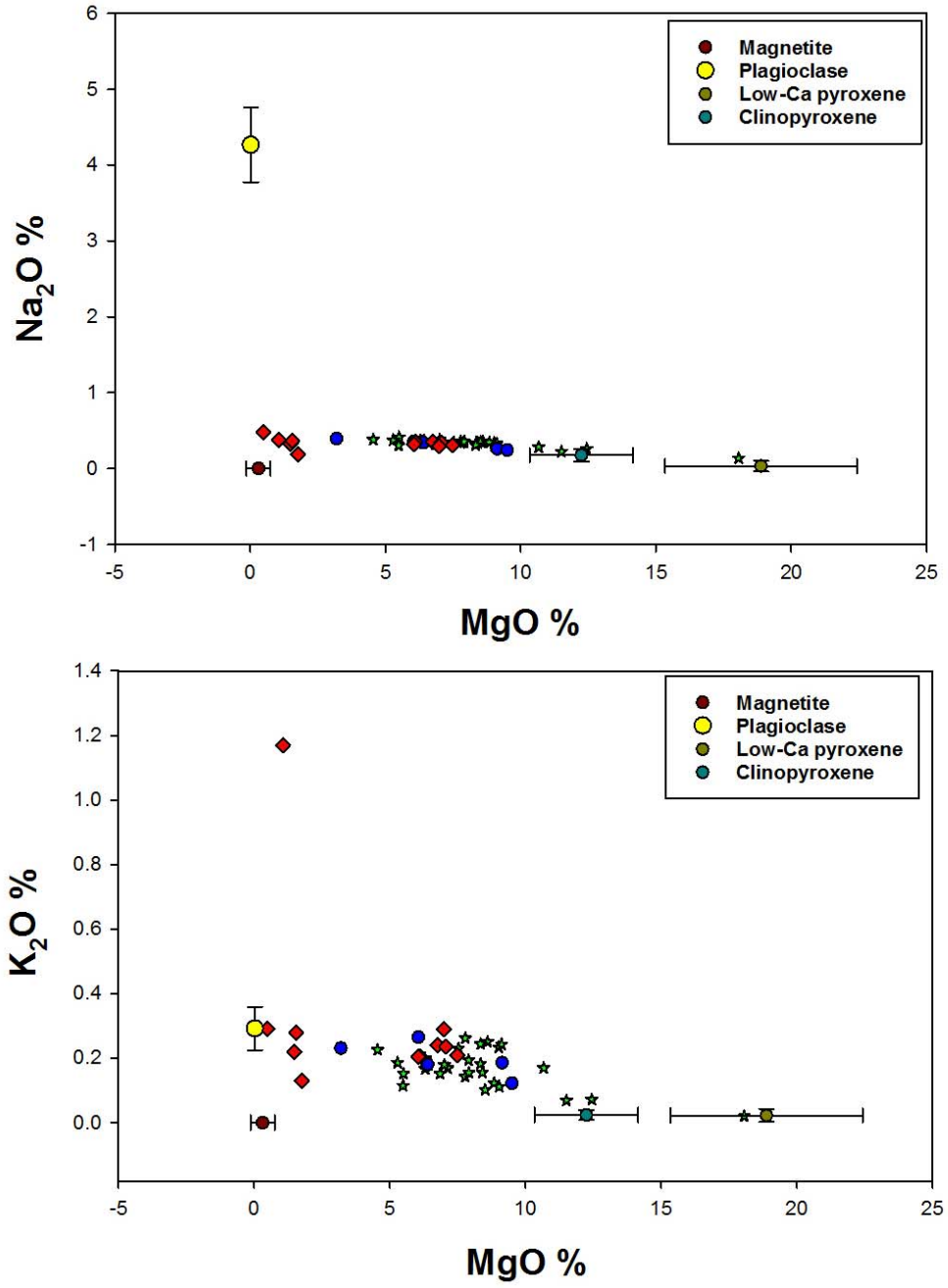

Figure 18: (Continued)

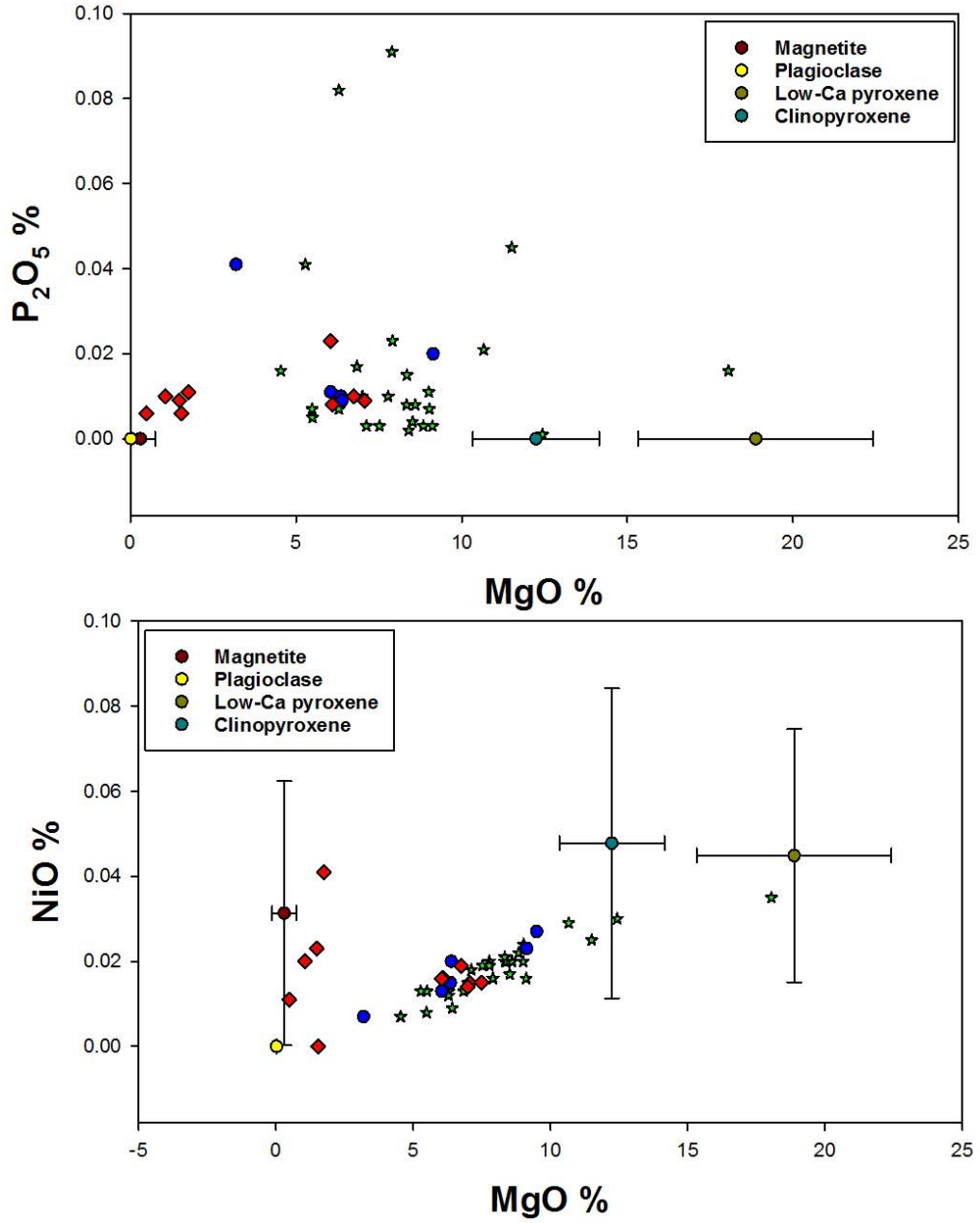

Figure 18: (Continued)

3.2.2 Whole-rock trace element geochemistry

Binary variation diagrams for the trace elements analysed as part of this study are shown in Figure 19 and their variation with depth in Figure 20. Sc shows a positive correlation with MgO with contents covering the range 5.18 – 43.65 ppm, with the lowest value being obtained from the magnetite gabbronorite at a depth of 144.04 m in the Upper Zone, and the highest value from the gabbronorite at a depth of 825.79 m in the Main Zone. The positive correlation between Sc and MgO is a reflection of K_d's > 1 for Sc in clinopyroxene and low-Ca pyroxene. The average Sc content was found to be 24.40 ppm.

Co, like Sc, shows a positive correlation with MgO with values covering the range 18.27 – 166.67 ppm. It is more enriched in the Upper Zone as compared to the Main Zone, which may in part be due to the element's preferential incorporation into magnetite (Lemarchand *et al.* 1987). The lower value was obtained from an anorthosite at a depth of 410.78 m in the upper Main Zone, and the higher value in the magnetite gabbronorite at a depth of 169.37 m of the Upper Zone.

Sr shows a negative correlation with MgO and it measured between 57.29 – 380.97 ppm, with an average of 246.04 ppm. The lower value was measured from a gabbronorite at a depth of 572.63 m in the Main Zone, while the highest value was obtained from a magnetite gabbronorite at a depth of 144.04 m in the Upper Zone. The behaviour of Sr is a reflection of the preferential incorporation of this element into plagioclase rather than into any of the mafic silicates. Ba displayed no distinct trend against MgO and recorded an average value of 180.29 ppm in the Upper Zone and 155.48 ppm in the Main Zone.

V shows very limited variation with MgO for most of the studied samples, but is enriched in many of the Upper Zone samples, reflecting the presence of magnetite. Concentrations for V range between 54.59 – 4618.95 ppm, with the lowest value being obtained from the leucogabbronorite at a depth of 595.95 m in the Main Zone, and the highest value from the magnetite gabbronorite at a depth of 169.37 m in the Upper Zone. The average V content for all studied samples was found to be 461.75 ppm.

Cr does not show clear trends with MgO, with a recorded average value of 124.93 ppm. It measured between 5.42 – 735.78 ppm, with the lowest value obtained from a gabbronorite at a depth of 144.04 m in the Upper Zone and highest from a gabbronorite at a depth of 486.20 m in the upper Main Zone.

Ni displays a strong positive correlation with MgO, with an average value of 141.51 ppm. It ranges between 52.65 – 506.85 ppm, with the lowest value obtained from an anorthosite at a depth of 410.78 m in the upper Main Zone and the highest value from magnetite gabbro at a depth of 169.37 m in the Upper Zone. This correlation is likely related to the presence of mafic silicates, into which Ni is preferentially incorporated relative to plagioclase.

Cu does not show clear trends with MgO, with a recorded average of 33.88 ppm. It measured within the range of 9.96 – 134.19 ppm, with a lower value obtained from a pegmatitic gabbronorite at a depth of 943.14 m in the lower Main Zone and the highest value being obtained from a magnetite gabbronorite from a depth of 169.37 in the Upper Zone. Interestingly, some Upper Zone samples returned fairly high Cu values that may be indicative of the presence of magmatic sulphides.

Zn shows a very weak positive correlation with MgO content for most of the samples, ranging in concentration between 29.42 – 248.74 ppm. The lowest value was obtained from an anorthosite at a depth of 410.78 m in the upper Main Zone and the highest value from a magnetite gabbronorite at a depth of 169.37 m in the Upper Zone. An average value of 62.47 ppm was recorded. High values recorded in some of the Upper Zone samples are attributed to the presence of magnetite, into which Zn is known to partition preferentially.

Rb shows no correlation with MgO, reflecting its incompatible behaviour with respect to the cumulus mineralogy of the rocks investigated. It ranges between 0.67 – 30.59 ppm, with a lower value obtained in a magnetite gabbronorite at a depth of 169.37 m in the Upper Zone and a higher value from a magnetite gabbronorite at a depth of 93.46 m in the Upper Zone. An average of 3.40 ppm was recorded.

Y shows a weak positive correlation with MgO, with an average value of 5.42 ppm. The lower value measured below 0.6 ppm and higher value at 10.29 ppm. The higher value was obtained from a gabbronorite from a depth of 212.48 m in the Upper Zone.

Zr does not show correlation with MgO, except high variability in both the Upper and Main zones. It measured an average value of 11.08 ppm, with a range of 2.85 – 30.91 ppm. The lower value was obtained from a leucogabbronorite at a depth of 899.43 m in the Main Zone and a higher value from a magnetite gabbronorite at a depth of 169.37 m in the Upper Zone. The lack of correlation is a reflection of the incompatible behaviour of Zr with respect to the main cumulus minerals.

The binary variation diagrams of the following whole-rock trace elements are not plotted as many samples returned values below detection as shown in Electronic Appendix 2. As measured a maximum value of 80.46 ppm, and was obtained from magnetite gabbronorite at a depth of 93.46 m in the Upper Zone and the lowest value measured below detection limit of 5 ppm. Br measured a highest value of 1.44 ppm, and was obtained from a gabbronorite at a depth of 465.40 m in the upper Main Zone, while the lowest value measured below detection limit of 1 ppm.

Nb and Mo both measured below detection limits of 0.6 and 07 ppm, respectively, with no high values measured above the limits. Ag measured a maximum value of 14.43 ppm, and was obtained from a gabbronorite at a depth 825.79 m in the Main Zone, while the lower value measured below detection limit of 7 ppm.

Cd measured a highest value of 11.87 ppm, and was acquired from a gabbronorite at a depth of 126. 36 m in the Upper Zone, while the lower value measured below detection limit of 5 ppm. Pb measured a highest value of 13.50 ppm, and was obtained from leucogabbronorite at a depth of 1002.82 m in the Main Zone, with the lower value that measured below detection limit of 2 ppm. U measured a maximum value of 2.74 ppm, and was acquired from magnetite gabbro at a depth 100.70 m in the Upper Zone, and the lower value measured below detection limit of 2 ppm.

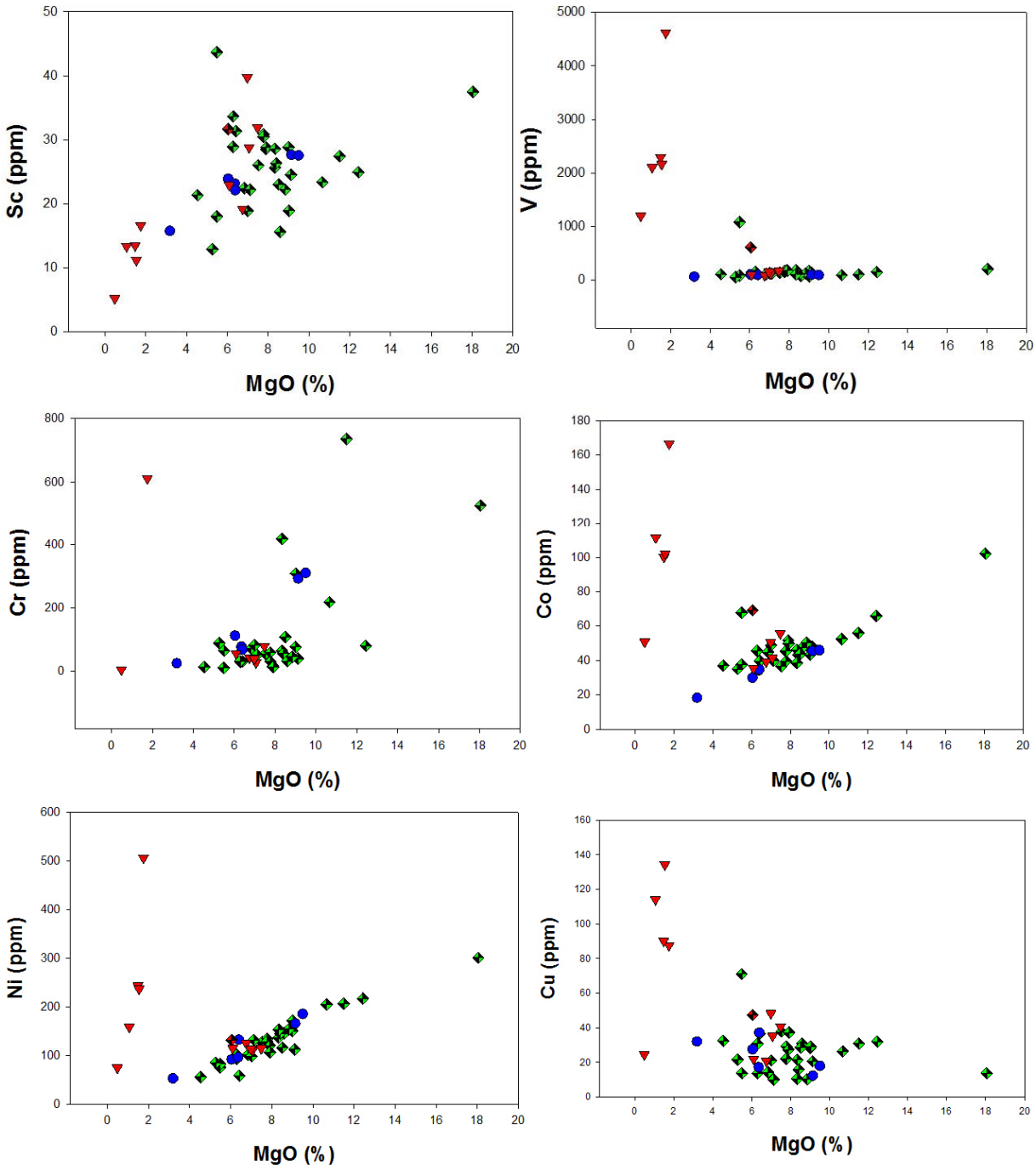

Figure 19: Binary variation diagrams of selected whole-rock trace elements versus MgO (red triangles represent Upper Zone and green diamonds for lower Main Zone samples & blue circles for upper Main Zone).

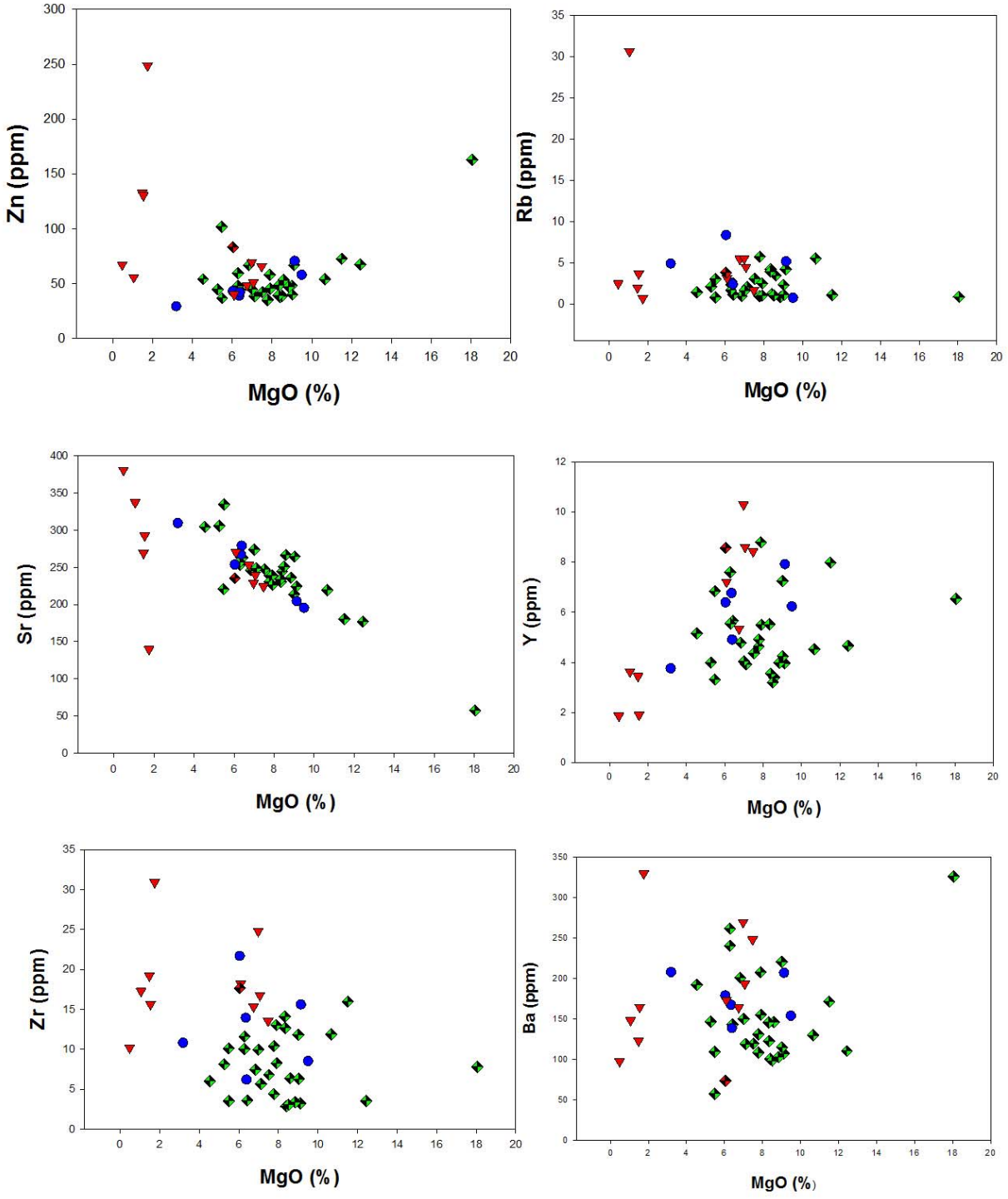

Figure 19: (Continued)

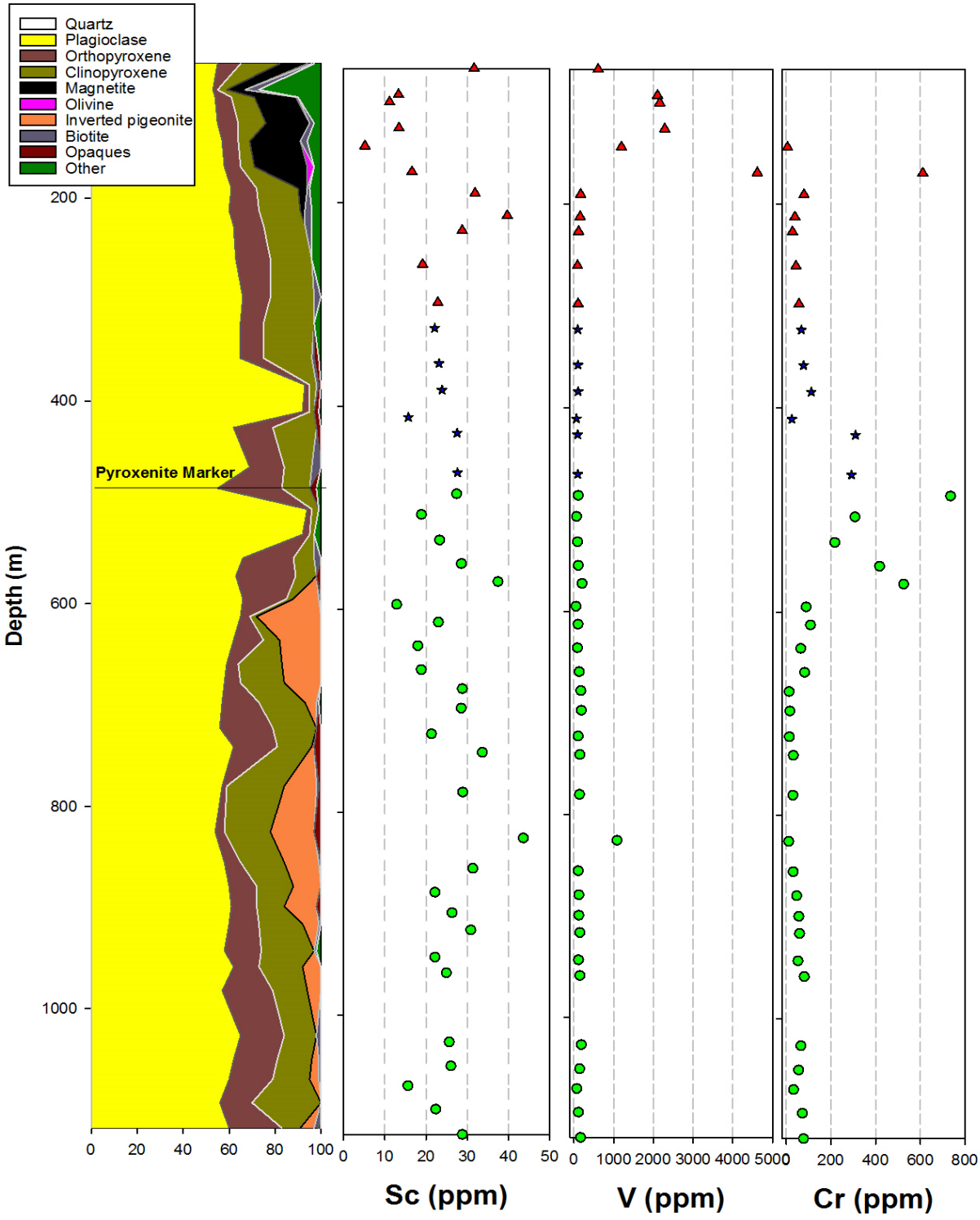

Figure 20: Whole-rock trace elements (ppm) vs depth (m) with modal mineralogy for comparison in all studied samples of BK-2 (green circles represent lower Main Zone samples, blue stars upper Main Zone samples & red triangles represent Upper Zone samples).

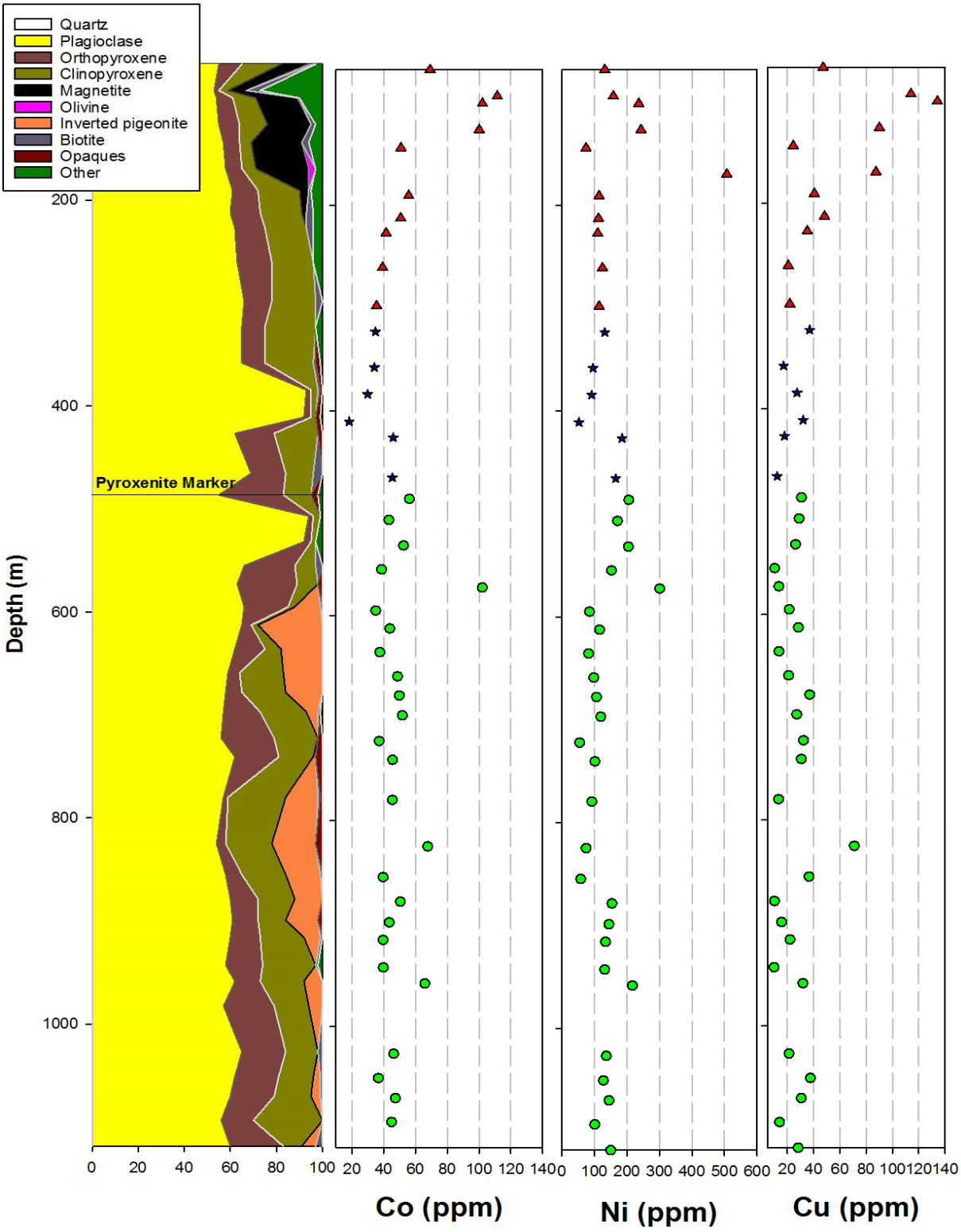

Figure 20: (Continued)

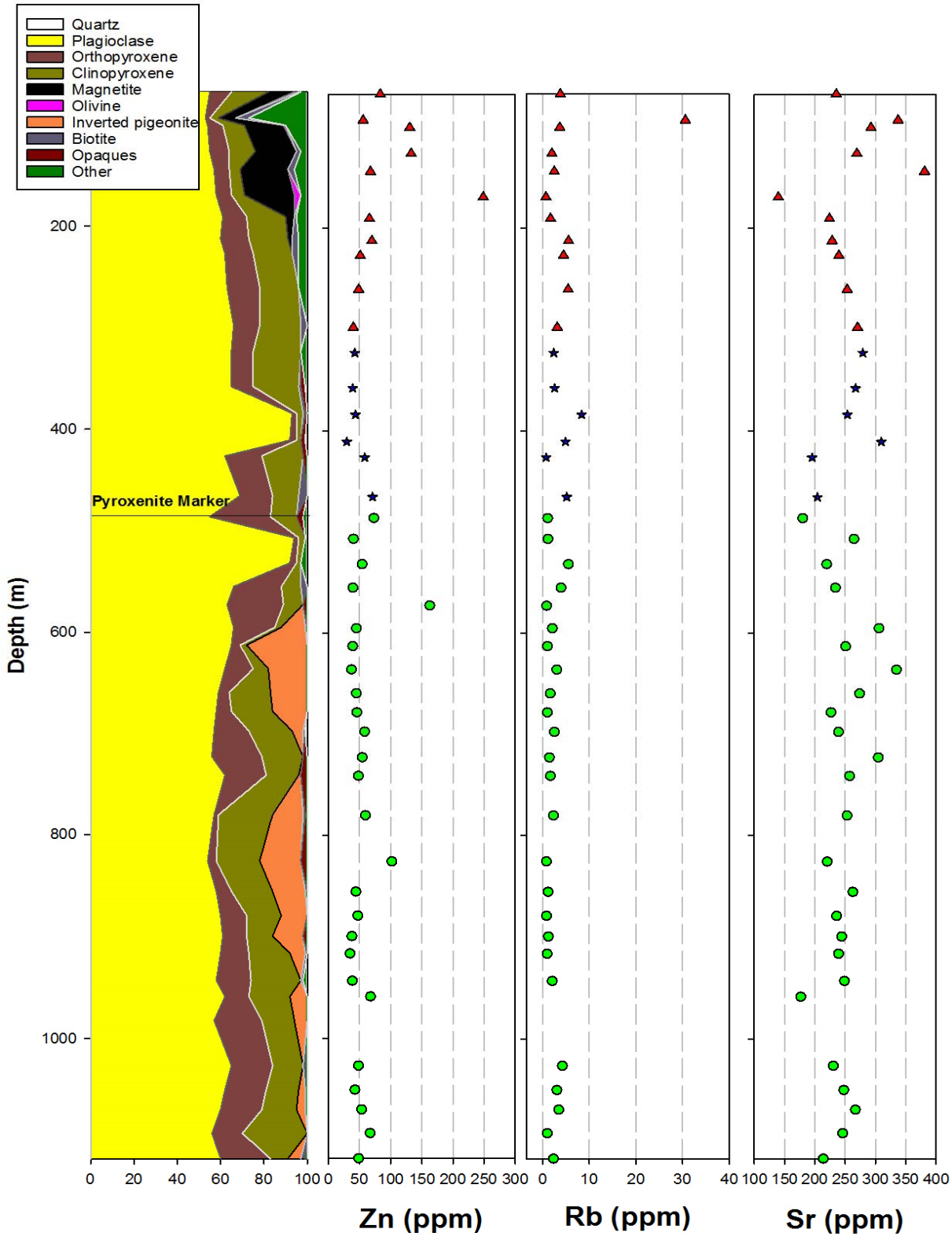

Figure 20: (Continued)

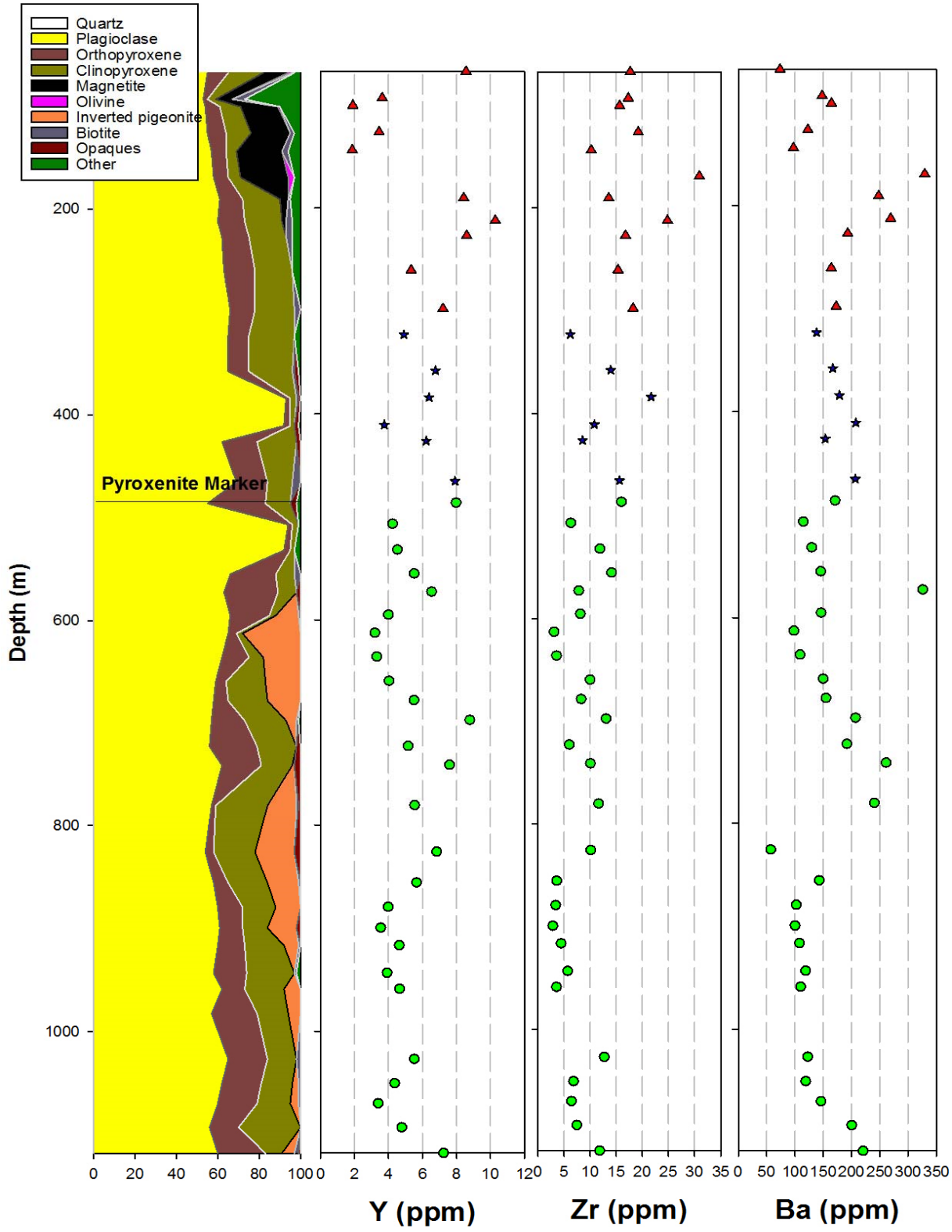

Figure 20: (Continued)

The whole-rock trace element plots against depth show variability across the entire stratigraphy of the BK-2. Sc is highly variable with a dispersed lithophile behaviour and is preferentially incorporated in ferromagnesian minerals. In the upper reaches of the lower Main Zone, very close to the Pyroxenite Marker, Sc concentrations decrease with a decrease of ferromagnesian minerals mode while plagioclase increased. Sc seems to lack affinity for magnetite as its concentrations decreased in the presence of magnetite.

V does not vary significantly throughout the Main Zone up to the Upper Zone at a depth of about 200 m. V concentrations increase dramatically in the presence of signifying its preferential incorporation into magnetite. Cr does not vary much in the lower Main Zone, but in the upper reaches of the lower Main Zone below the Pyroxenite Marker, Cr concentrations increase distinctly and remain increased in several samples occurring above the Pyroxenite Marker.

Co, Ni, Cu and Zn concentrations remain fairly constant throughout the Main Zone, with generally higher concentrations associated with magnetite-rich layers of the Upper Zone. An increase of concentrations in the Upper Zone for the above-mentioned trace elements may indicate the presence of magmatic sulphides as earlier indicated. Rb concentrations do not vary significantly over the entire interval sampled.

Generally, Sr concentrations are high as compared to other measured trace elements; the fact is because Sr is excluded from most common minerals, due to its incompatibility, except in plagioclase, which is a dominant mineral mode. Y, Zr and Ba (highly concentrated like Sr) are highly variable in the lower Main Zone, but towards the Pyroxenite Marker, their concentrations decrease and sharply increase very close to

Pyroxenite Marker. In the upper reaches of the Upper Zone, Y and Ba concentrations decrease and this being indicative of lack of affinity for magnetite, which is present, while Zr concentration in the Upper Zone shows an increase.

3.3 *In situ* major element mineral geochemistry of plagioclase

The *in situ* major element geochemical data of the selected plagioclase crystals are presented in Appendix A; together with cation proportions so that the quality of the analysis can be assessed (see Electronic Appendix 4). The anorthite content (An%) variation of plagioclase varies considerably over the studied stratigraphic interval, with an average of 60.9 ± 4.8%, and minima and maxima of 50.4% and 72.4%, respectively. Figures 23 and 24 show plots of plagioclase anorthite content (An%) against depth (m) with the modal mineralogy shown for comparison. The analyses was done on a minima of 3 grains and maxima of 5 grains per sample. For the Main Zone, anorthite content of plagioclase was on average 62.0 ± 4.7%, varying between 50.4% and 72.4%.

The anorthite content of plagioclase in the Upper Zone ranges between 51.2% and 67.7% respectively, with an average of 57.9 ± 3.6%. The rock samples seem to be more anorthositic as are shown in the feldspar ternary diagram (Figure 21).

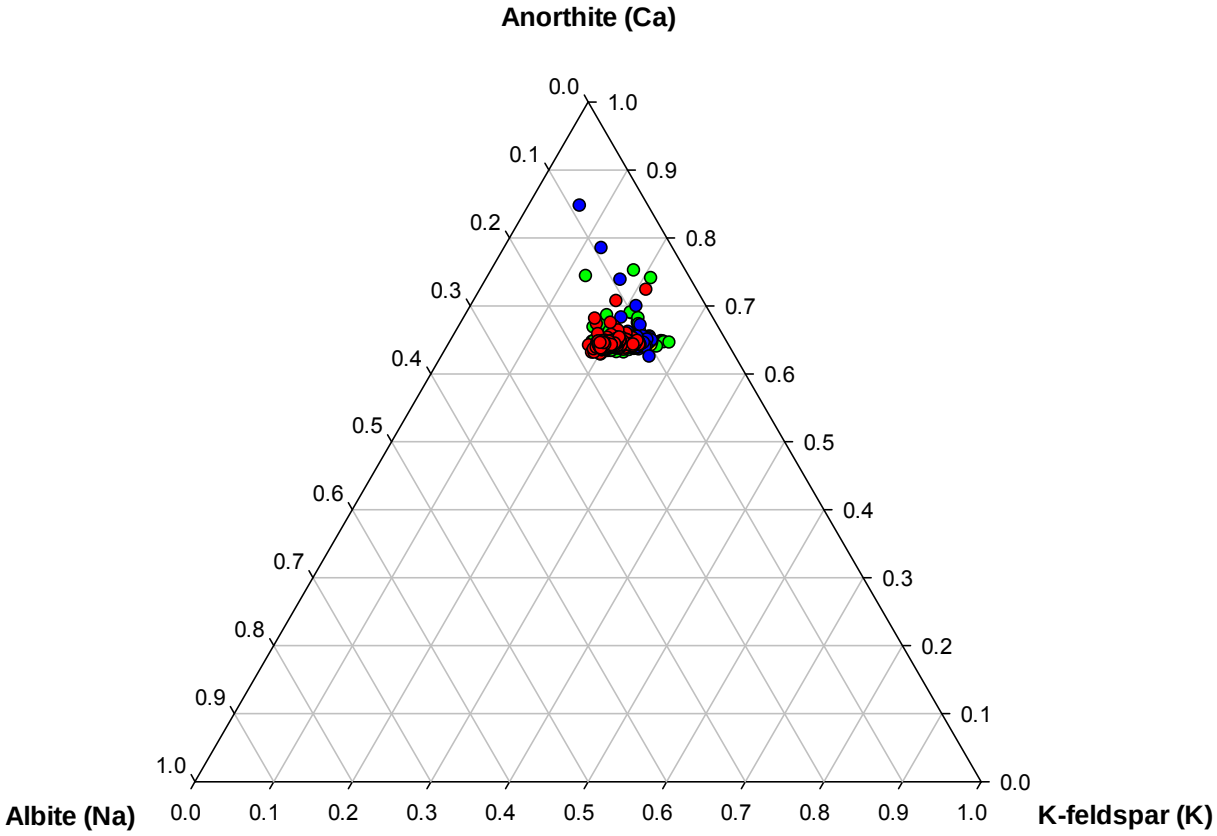

Figure 21: Feldspar ternary diagram of all analysed spots showing An%, green circles representing lower Main Zone, blue circles representing upper Main Zone and red circles representing Upper Zone.

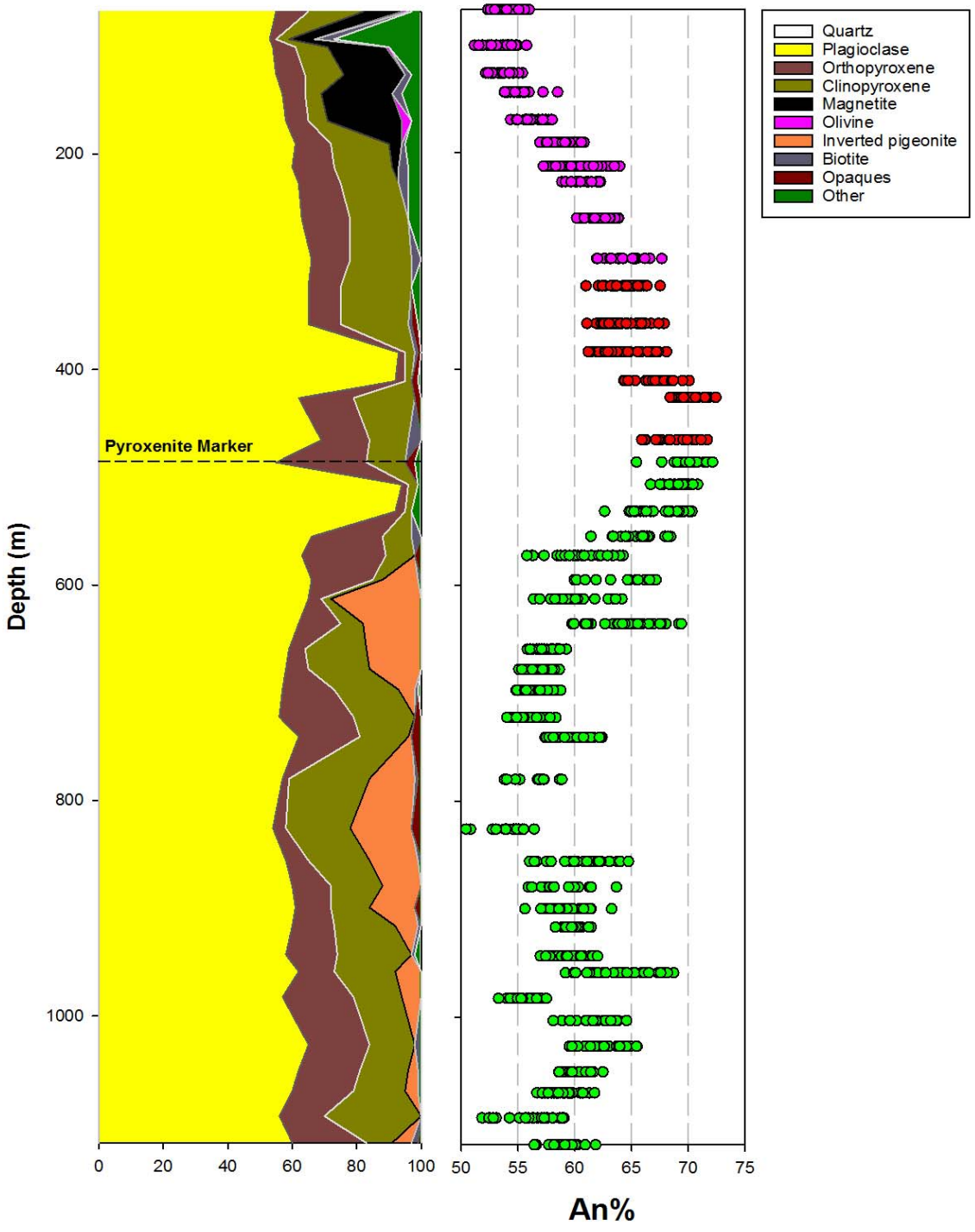

Figure 22: The plagioclase anorthite content (An %) per analysed spot plotted against depth, with modal mineralogy showing variation across the stratigraphic profile of BK-2 (An % plot; green circles = lower Main Zone, red = upper Main Zone and pink = Upper Zone).

A decrease of anorthite (An%) content is encountered from the lower reaches of the Main Zone, from a depth of 1117.68 m to 1092.85 m, with an average value of 56.7%. This is followed by a reversed differentiation trend from a depth of 1092.85 m up to 1026.60 m, from a low of 56.7% up to 64.7% at 1026.60 m. Another decrease of anorthite content is encountered from a depth of 1026.60 m to 982.30 m, with an average value of 57.3%. From the latter depth up to 958.60 m, anorthite content increased up to an average value of 63.5%, followed by a small decrease to an average value of 60.5% at a depth of 943.14 m.

From a depth of 943.14 m up to 855.62 m, anorthite content remains relatively constant with a measured average value of 61.1%. At a depth of 825.79 m, a sharp decrease of anorthite content that recorded an average value of 54.3% was observed. Again, anorthite content increase was measured from a depth of 825.79 m up to 740.40 m, with an average value of 57.6%. A slight decrease of anorthite content was recorded at a depth of 722.50 m with an average value of 56.6%. From a depth of 697.26 m up to 506.71 m, which is below the Pyroxenite Marker described by Cawthorn *et al* (1990), anorthite content increase was observed with a minimum average value of 57.3% and maximum average value of 70.3%, respectively. It was earlier mentioned that the analyses was done on a minima of 3 grains and maxima of 5 grains per sample.

Above the Pyroxenite Marker, at depths of 465.40 m and 426.36 m, anorthite content recorded nearly constant values of 70.0% and 70.7%, respectively, with an average value of 70.3%. There is another decrease of anorthite content (i.e. normal differentiation) from a depth of 426.36 m up to 384.10 m, with an average value of 65.9%. From a depth of 384.10 up to 292.95 m, anorthite recorded nearly constant/slightly increasing values, with

a minimum average value of 64.4% and 65.9%, respectively. Anorthite content decreased from a depth of 260.50 m up to 67.84 m, with a total average value of 58.4%.

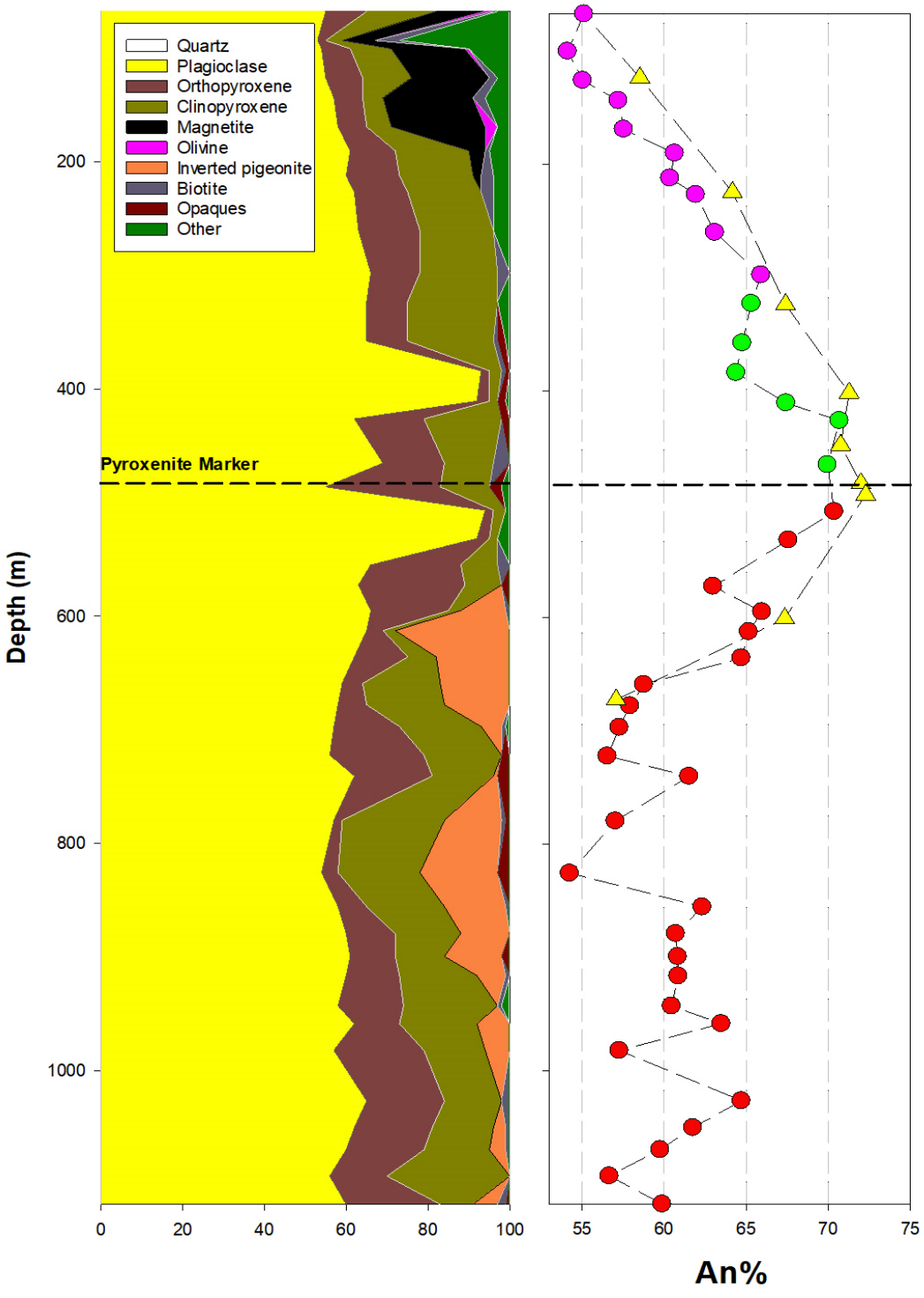

Figure 23: *In situ* An% average of samples vs. depth with modal mineralogy for comparison (pink circle = Upper Zone, green circle = upper Main Zone and red circle = lower Main Zone) and yellow triangles represent BK-2 bulk rock samples by Tegner *et al*. 2006.

3.4 *In situ* trace element geochemistry of plagioclase

The *in situ* trace element composition of plagioclase was determined as described above in section 2.5 and is presented in Appendix B. Twenty-two individual trace elements, in Table 7 below, were analysed for on approximately 266 spots in the 44 selected rock samples. The spot size diameter of the holes made during ablation was 110 µm (Figure 24).

The average concentrations of Rb, Sr, Ba, La, Ce, Pr, Nd, Sm, Gd, Tb, Dy Pb, Th and U in plagioclase are higher in the Upper Zone as compared to the Main Zone, while the concentrations of Y, Zr, Eu and Yb in plagioclase are higher in the Main Zone than in the Upper Zone. Ho and Er in the Upper and Main Zones both measured similar values of 0.01 and 0.03 ppm, respectively. Lastly, Tm and Lu both measured < 0.01 ppm in the Upper and Main zones (see Table 7).

Table 7: Average concentrations, standard deviations, minimum (Min) and maximum (Max) values (in ppm) of the *in situ* trace elements Rb, Sr, Y, Zr, Ba, La, Ce, Pr, Nd,Sm, Eu, Gd, ,Dy, Ho, Er, Tm, Yb, Lu, Pb, Th, & U in plagioclase.[1]

		Rb	Sr	Y	Zr	Ba	La	Ce	Pr	Nd	Sm	Eu
Upper Zone	***Average***	5.07	418.37	0.28	0.10	153.85	4.15	6.59	0.58	2.04	0.25	0.73
	Std.Dev	6.55	37.97	0.14	0.24	35.32	1.14	1.44	0.12	0.45	0.08	0.10
	Min	1.47	269.87	0.12	< 0.01	72.73	2.35	3.72	0.39	1.35	0.15	0.54
	Max	49.27	489.30	0.72	1.43	340.95	7.76	10.05	0.87	3.21	0.45	0.97
Main Zone	***Average***	3.80	383.02	0.29	0.37	123.31	3.44	5.29	0.43	1.49	0.17	0.75
	Std.Dev	3.02	58.95	1.29	3.65	33.71	0.99	1.53	0.15	0.70	0.20	0.24
	Min	< 0.01	39.11	0.06	< 0.01	9.77	0.95	1.63	0.09	0.56	0.06	0.06
	Max	30.62	547.63	17.94	51.75	228.90	5.83	9.12	1.51	8.81	2.83	1.48
		Gd	**Tb**	**Dy**	**Ho**	**Er**	**Tm**	**Yb**	**Lu**	**Pb**	**Th**	**U**
Upper Zone	***Average***	0.16	0.02	0.07	0.01	0.03	< 0.01	0.01	< 0.01	4.05	0.03	0.02
	Std.Dev	0.07	0.01	0.04	0.01	0.03	< 0.01	0.01	< 0.01	2.51	0.08	0.05
	Min	0.05	< 0.01	0.03	< 0.01	0.01	< 0.01	< 0.01	< 0.01	1.99	< 0.01	< 0.01
	Max	0.33	0.04	0.22	0.03	0.13	0.01	0.07	0.01	13.37	0.55	0.37
Main Zone	***Average***	0.13	0.01	0.06	0.01	0.03	< 0.01	0.03	< 0.01	1.98	0.01	< 0.01
	Std.Dev	0.42	0.04	0.27	0.05	0.15	0.02	0.15	0.02	0.54	0.03	0.01
	Min	0.03	< 0.01	0.01	< 0.01	< 0.01	< 0.01	< 0.01	< 0.01	0.25	< 0.01	< 0.01
	Max	5.97	0.57	3.74	0.71	1.97	0.27	1.91	0.27	3.39	0.28	0.11

[1] A list of analysed isotopes given in Appendix B.

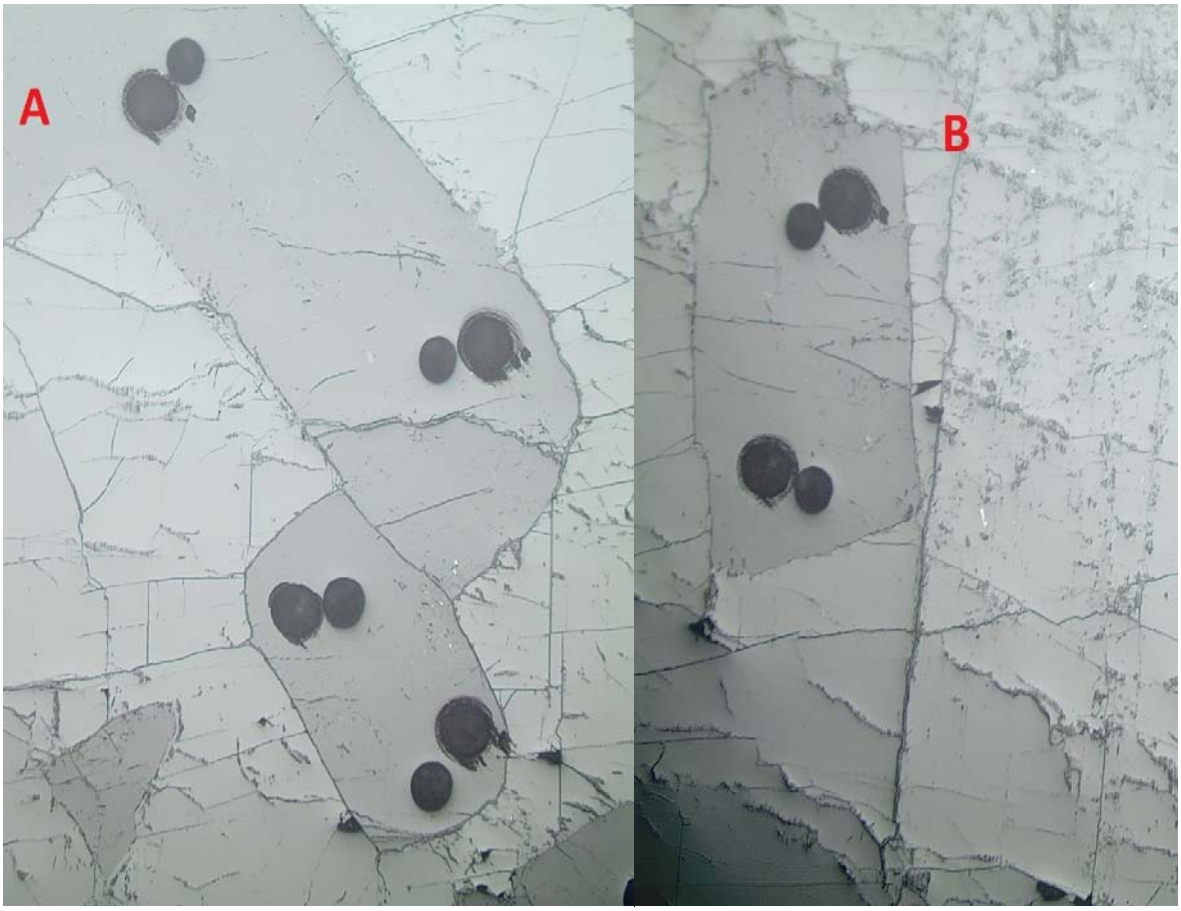

Figure 24: (A) and (B) Reflected light photomicrograph of plagioclase from depth of 190.55 m, showing larger diameter holes (generated during isotopic analyses) and smaller diameter holes (generated during trace elemental analyses) caused by laser during ablation.

Plots showing trace element concentrations in plagioclase versus depth in the BK-2 drill core are shown in Figure 25 with error bars representing standard deviation, and those without errors bars is due to relative standard deviation (%RSD) which was not measured during analysis. The standard deviation was calculated using ((mean*%RSD)/100).

The concentration of Rb in plagioclase in general is ranging between 0.02 ppm – 49.27 ppm and does not show significant variation over the length of the BK-2 drill core. Sr in plagioclase shows a fair amount of scatter across the length of the BK-2 drill core and on average, appears to be higher in most of the Upper Zone samples compared to the Main Zone samples (see also Table 7 above).

The concentration of most of the other elements analysed for, including REE, is consistently low and does not show significant variation across the length of the BK-2 core. The concentration of Pb in plagioclase is typically lower than ~4 ppm for the Main Zone, with higher concentrations being typical for Upper Zone plagioclase. Th and U concentrations are similarly low for most of the Main Zone plagioclase spots analysed, with higher values confined to spots from Upper Zone plagioclase.

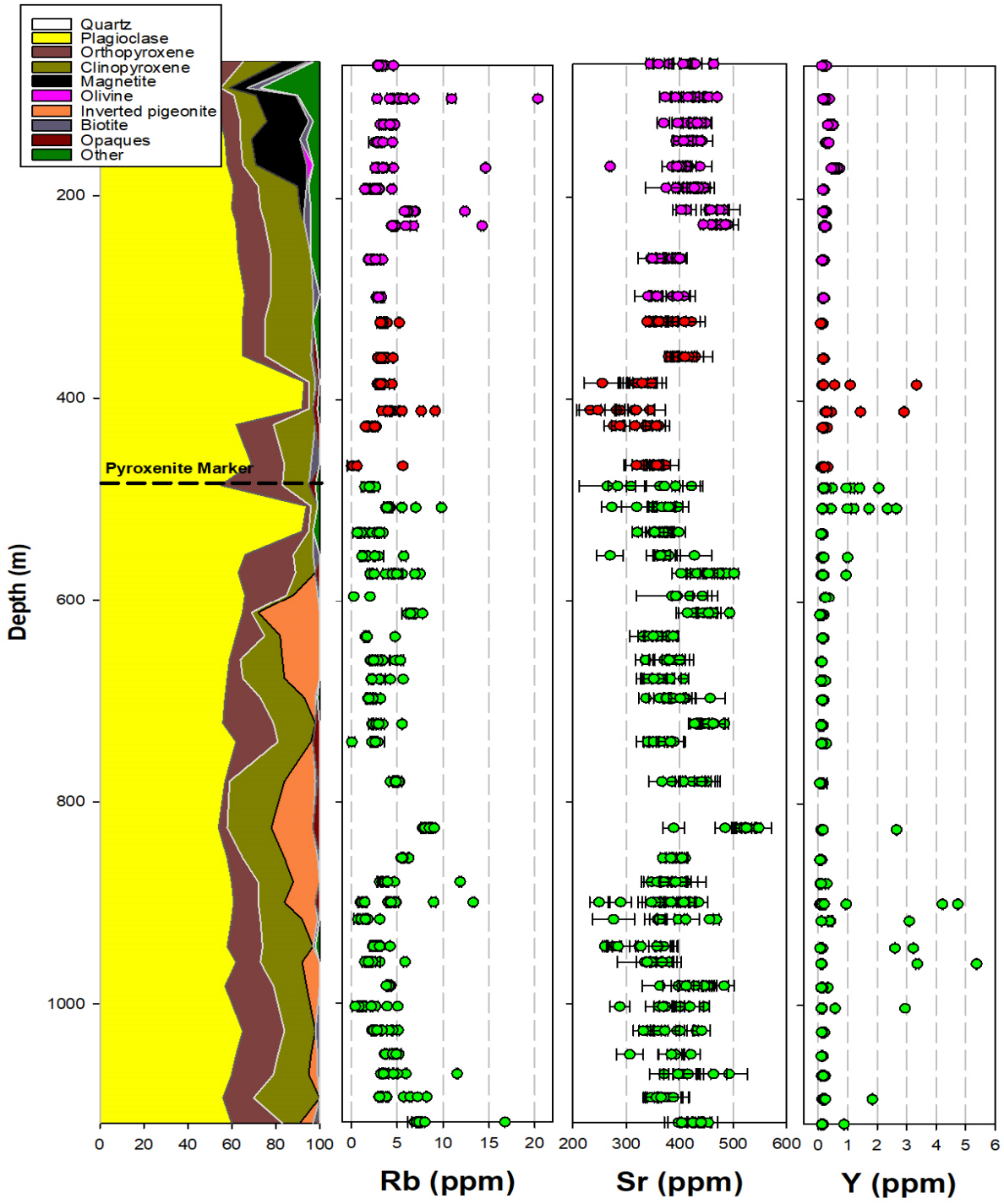

Figure 25: Plots of in situ trace elements (ppm) against depth (m), with green circles representing lower Main Zone samples, red circles upper Main Zone samples and pink circles Upper Zone samples, with error bars indicating standard deviations.

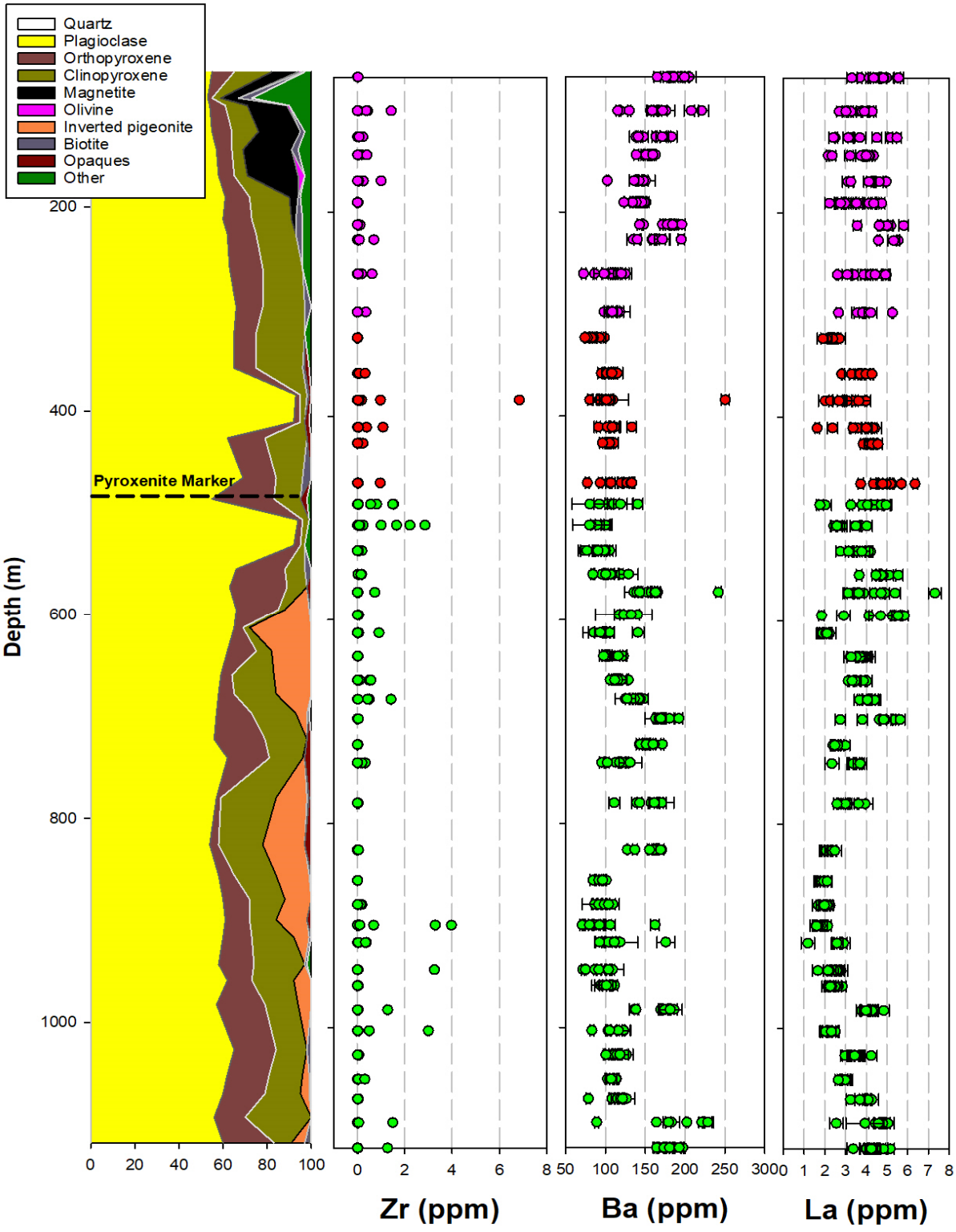

Figure 25: (Continued)

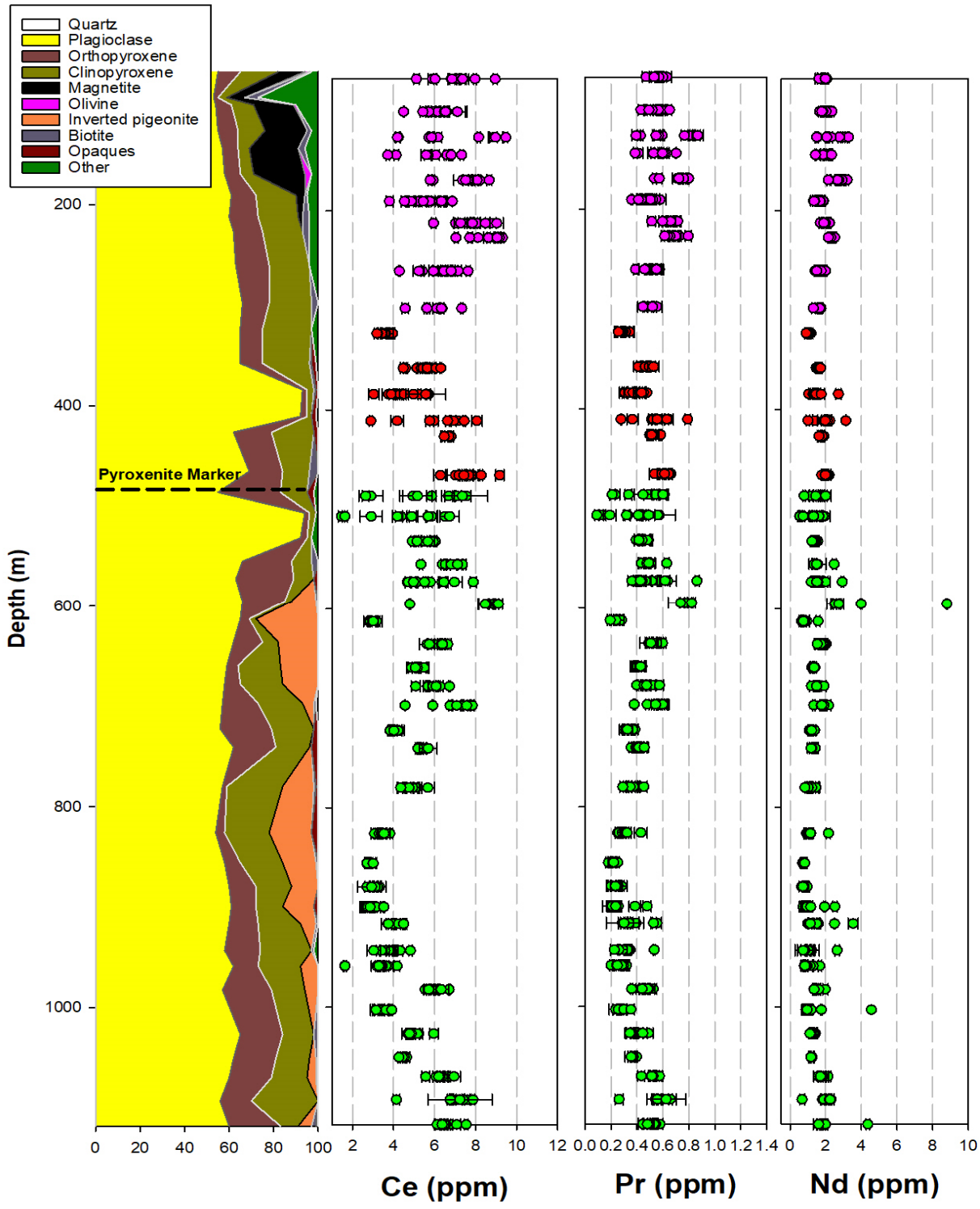

Figure 25: (Continued)

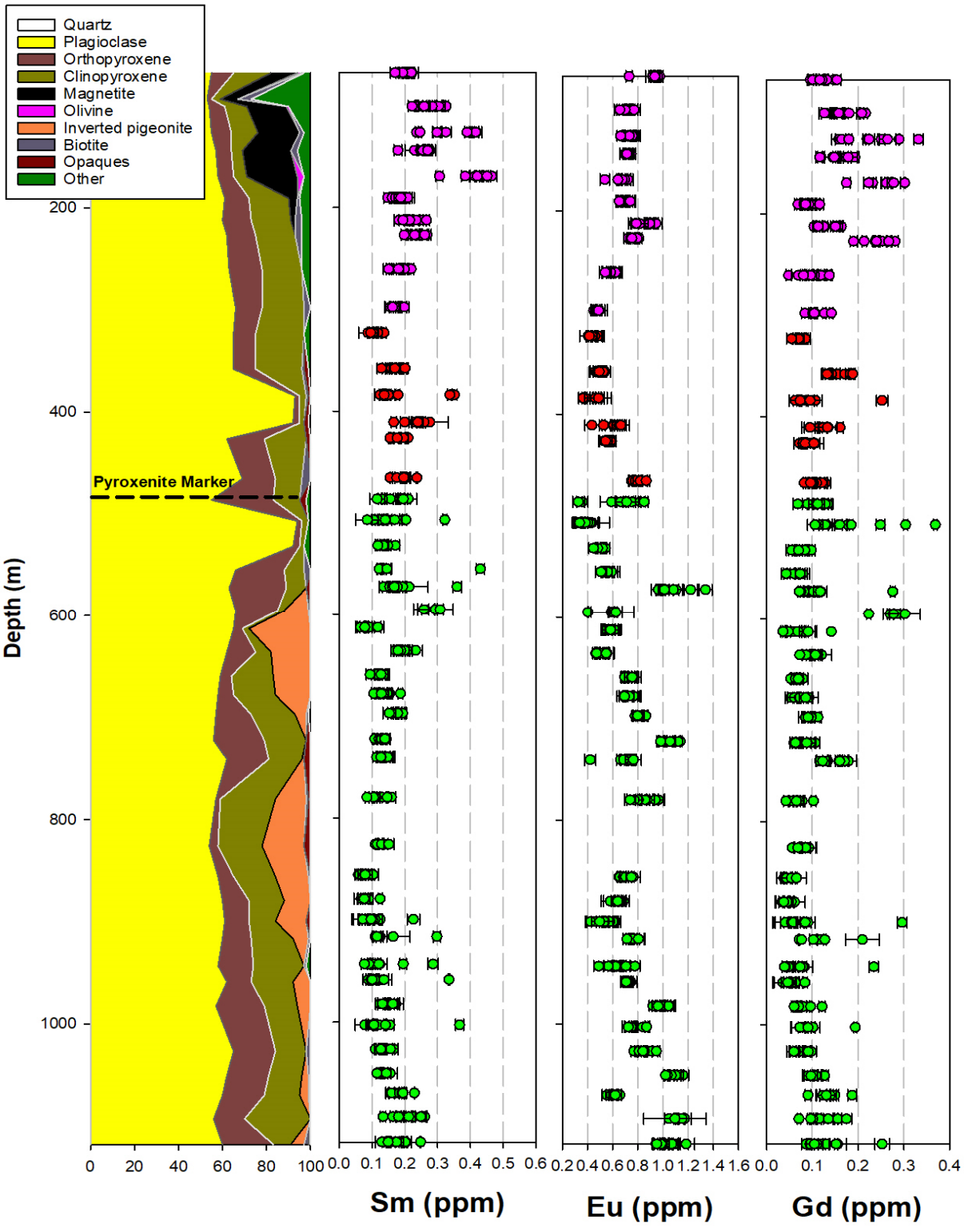

Figure 25: (Continued)

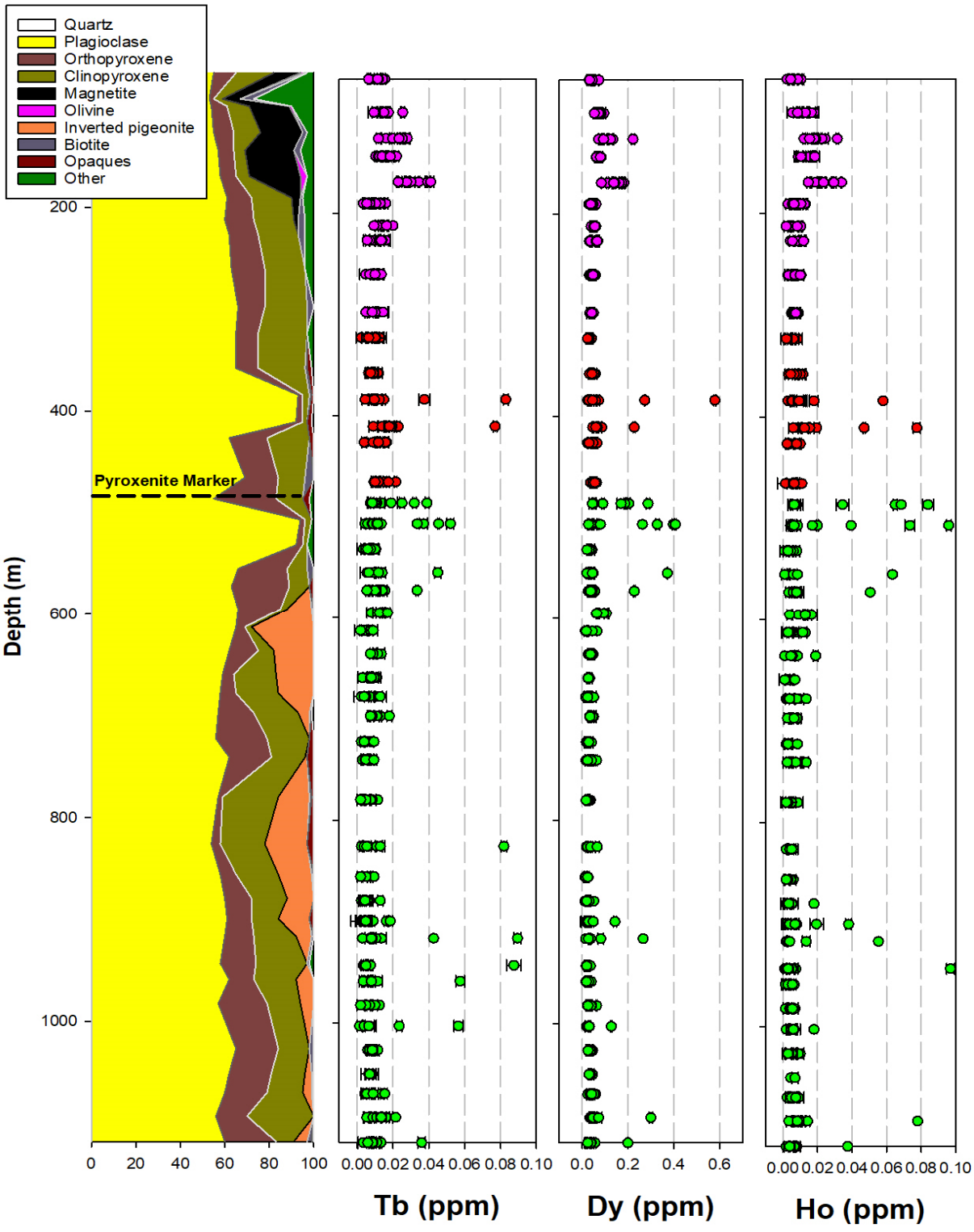

Figure 25: (Continued)

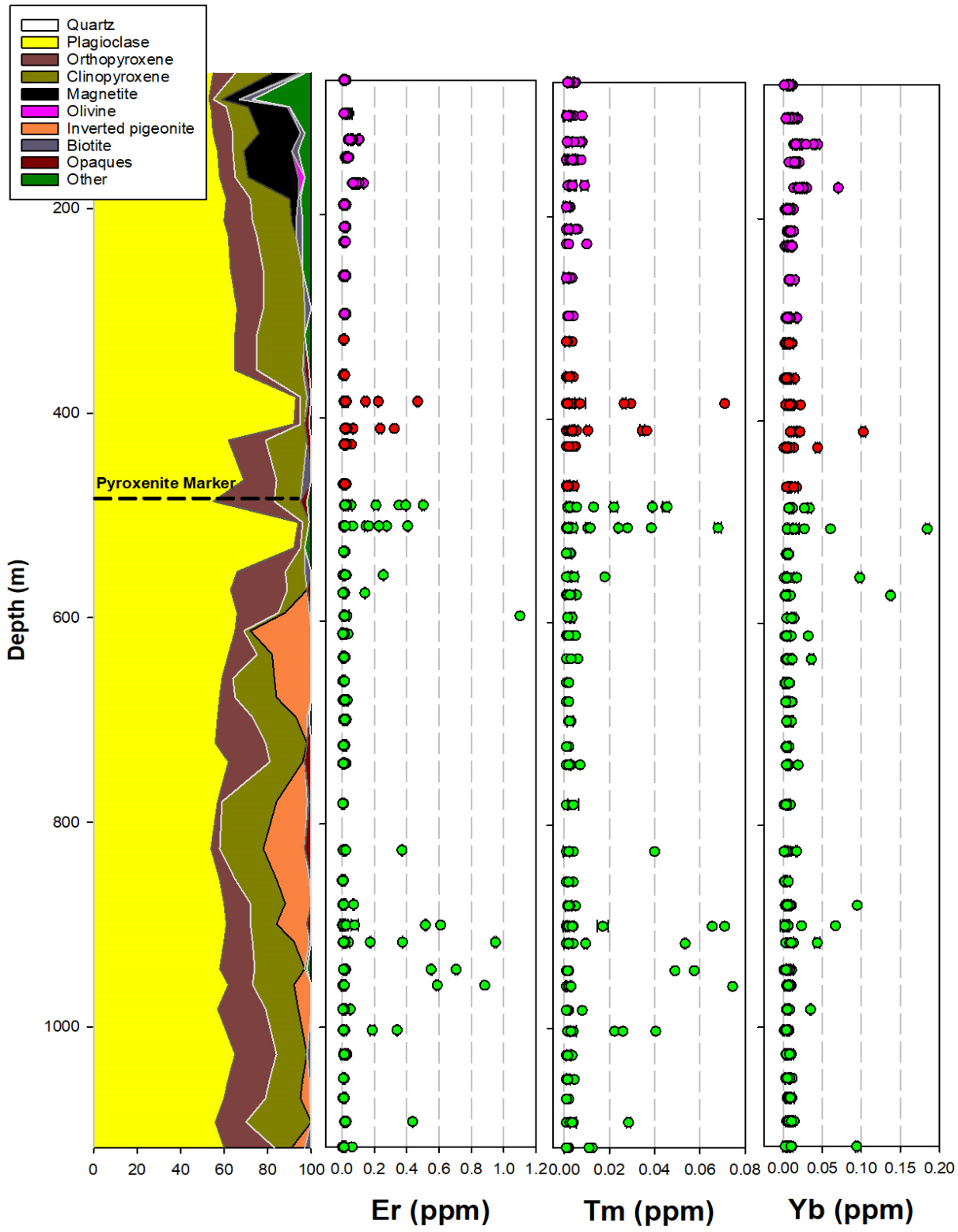

Figure 25: (Continued)

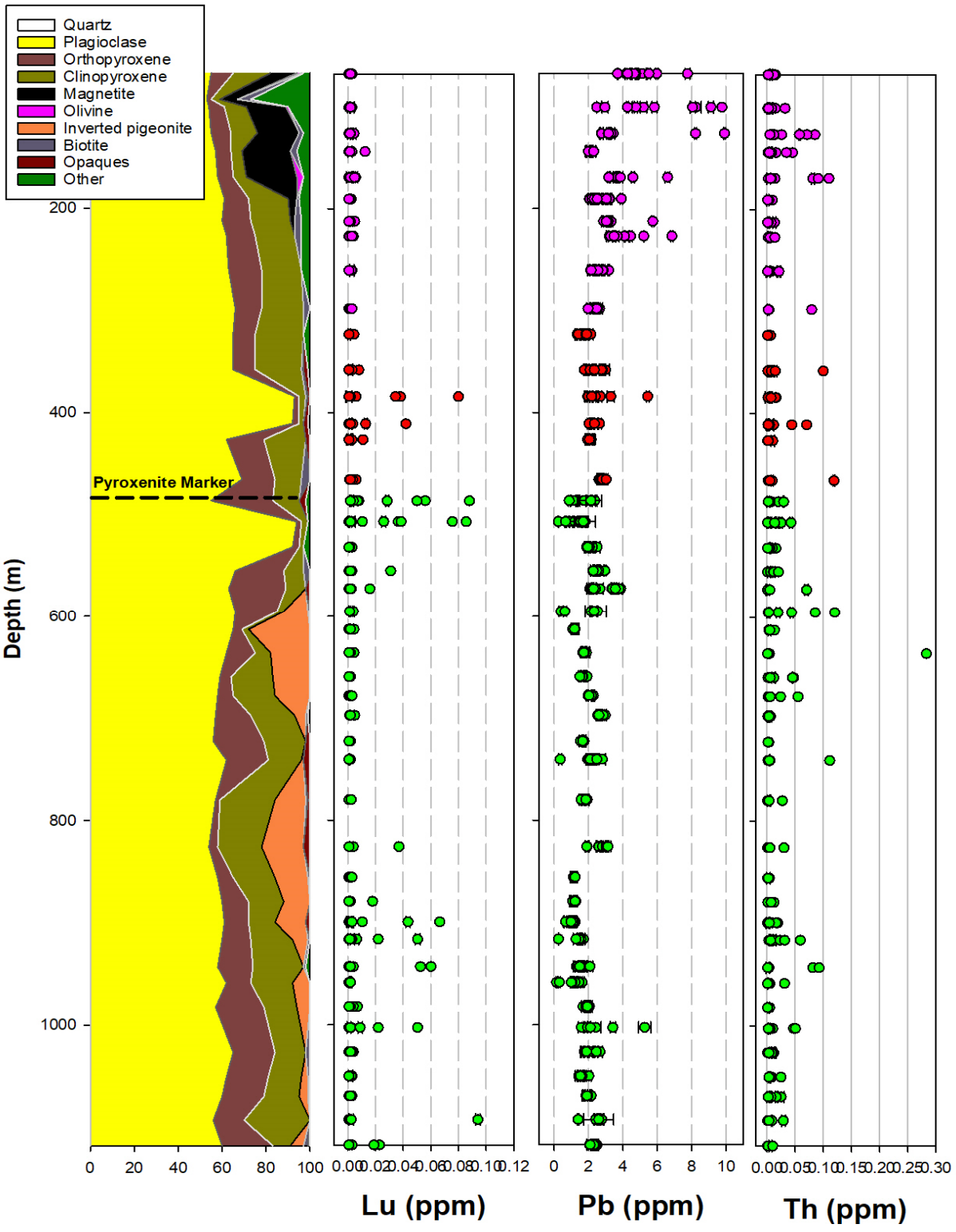

Figure 25: (Continued)

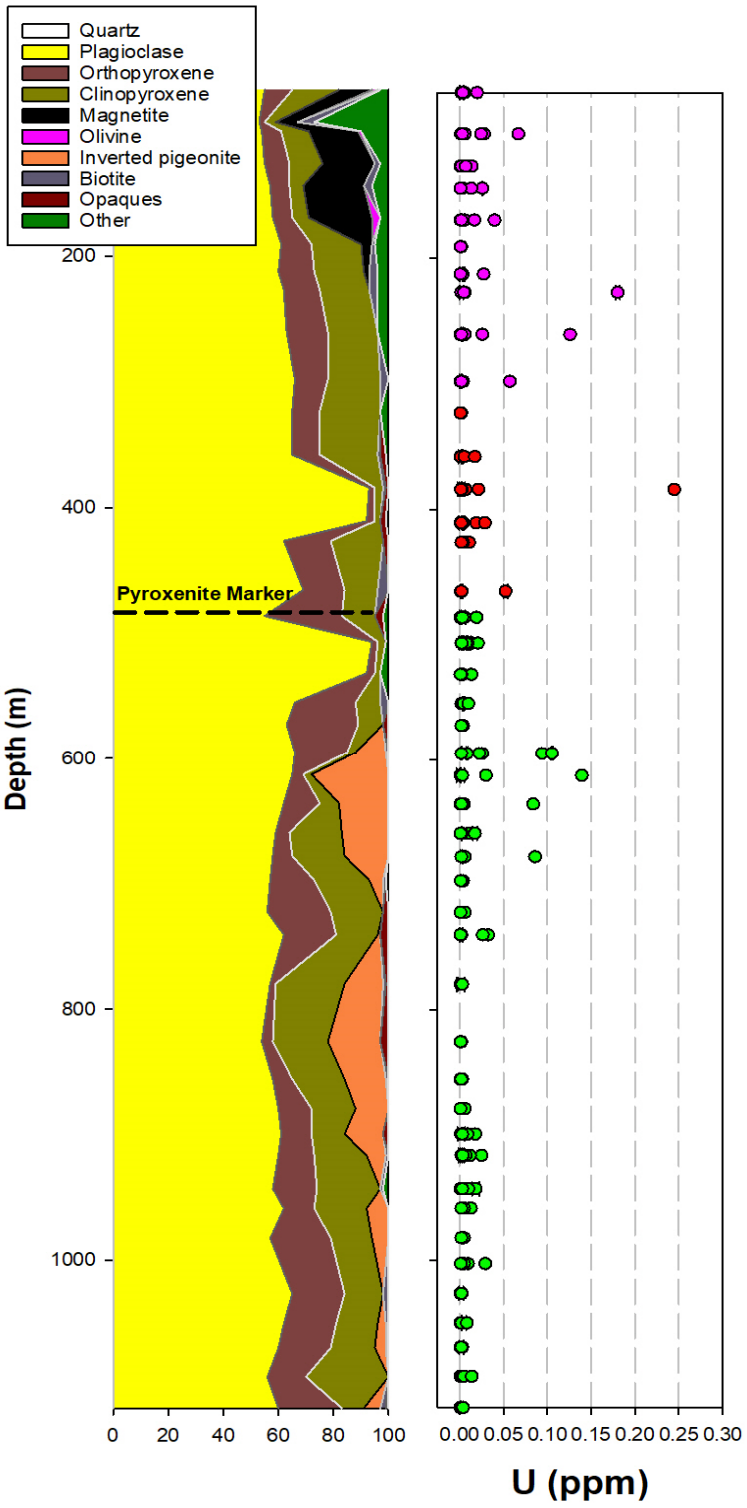

Figure 25: (Continued)

Plagioclase of the lower Main Zone has La concentration that is covering the range 4-10 times chondrites (using the chondrite values of Anders & Grevesse (1989)) and Lu is covering < 0.01 - 3 times chondrites, with analysed samples showing distinct fractionation of the LREEs and limited fractionation of the HREEs. $(Ce/Sm)_N$ ratios average at 5.38 and $(Tb/Yb)_N$ ratios at 1.26, excluding sample PL-024 which has a bit higher REE concentrations than the other samples analysed. Most lower Main Zone plagioclase samples show a positive Eu anomaly, with an average Eu/Eu* ratio of 10.21, where Eu= measured europium and Eu*= $((Sm+Gd)_N/2)$. One sample (PL-024) from the lower Main Zone (the leucogabbronorite from a depth of 595.03 m) shows anomalous REE values that are, with the exception of La, higher than any of the other lower Main Zone samples. This sample shows less pronounced fractionation of the LREEs ($(Ce/Sm)_N$ = 1.44) and slightly more pronounced fractionation of the HREEs ($(Tb/Yb)_N$ = 1.32). The sample shows a negative Eu anomaly in plagioclase, with Eu/Eu* ratio of 0.74 (Figure 26), coupled with a positive Gd anomaly.

The upper Main Zone has La concentrations covering the range of 5-11 times chondrites and Lu covering the range of < 0.01-0.3 times chondrites, with samples showing distinct fractionation of the LREEs ($(Ce/Sm)_N$ = 6.92) and lesser fractionation of the HREEs ($(Tb/Yb)_N$ = 1.44). The analysed samples show a positive Eu anomaly in plagioclase, with average Eu/Eu* ratio of 10.71 (Figure 27). The negative and zero values are not plotted in the log charts, rather only positive values are interpreted on a logarithmic scale.

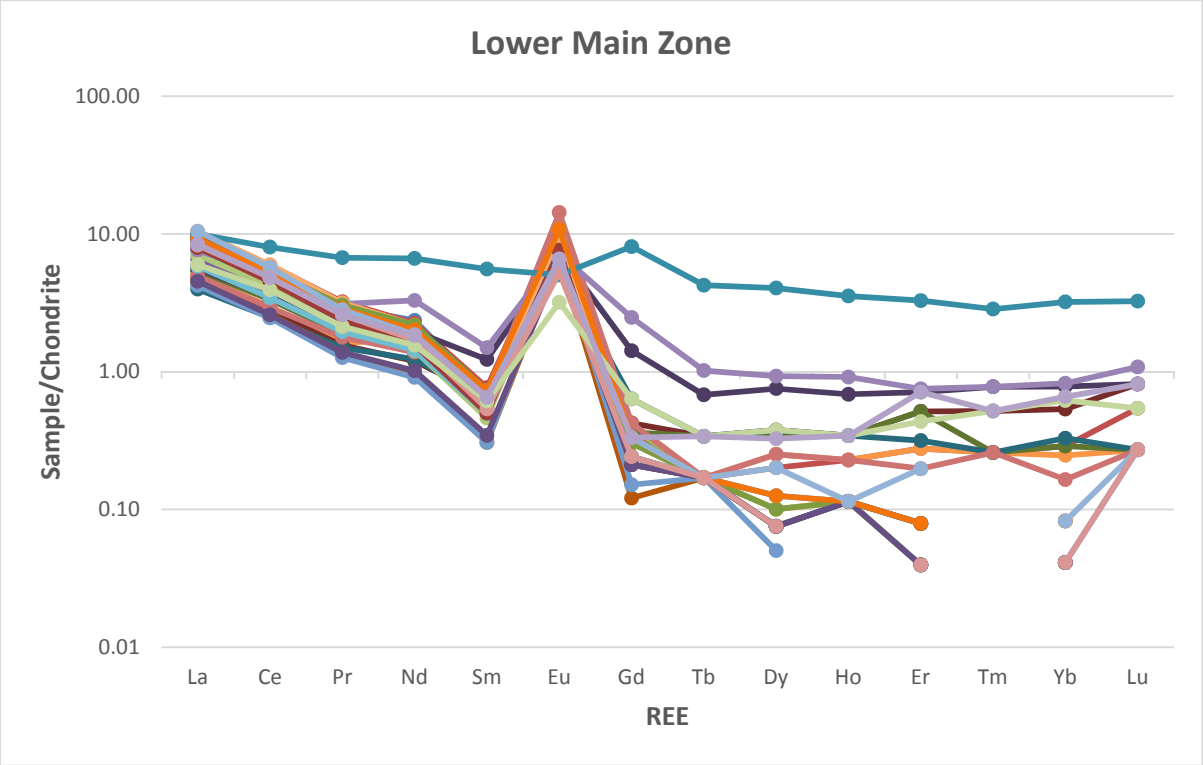

Figure 26: Chondrite-normalised REE abundances in plagioclase from the lower Main Zone of the BK-2 drill core.

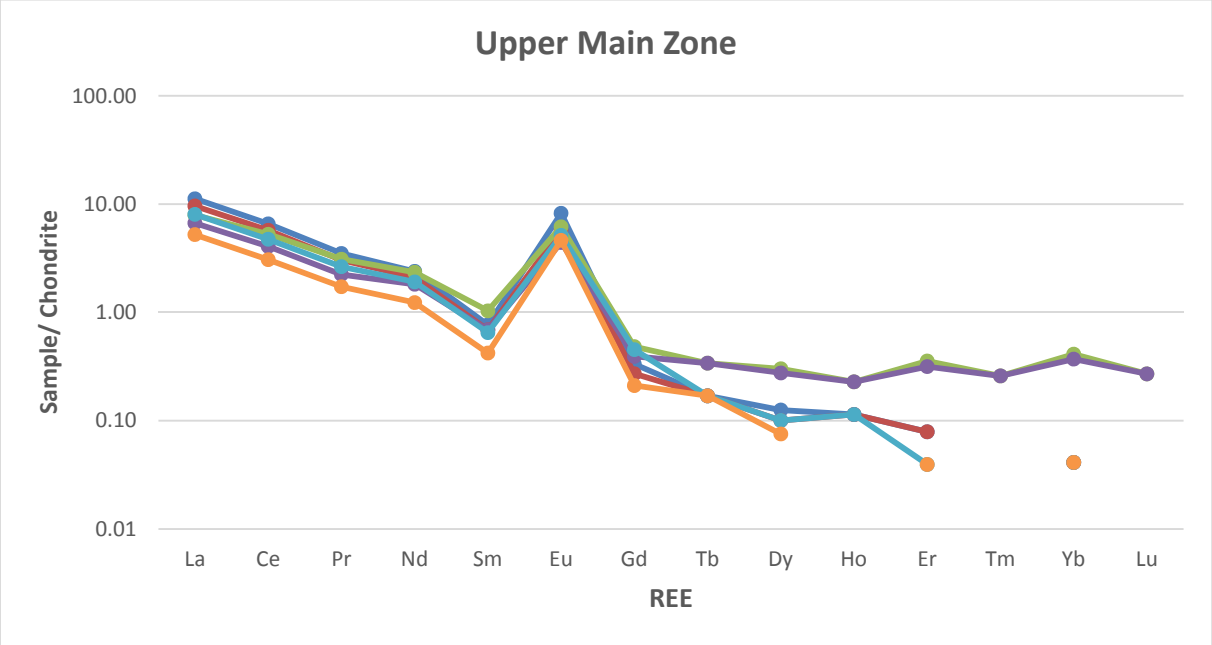

Figure 27: Chondrite-normalised REE abundances in plagioclase from the upper Main Zone of the BK-2 drill core.

The Upper Zone has La concentrations covering the range of 8-14 times chondrites and Lu measuring below detection limit of < 0.01, with LREEs strongly fractionated ($(Ce/Sm)_N$ = 6.14) and with $(Tb/Yb)_N$ having an average value of 5.0. The analysed samples show a positive Eu anomaly in plagioclase, with Eu/Eu* average ratio of 10.26 (Figure 28).

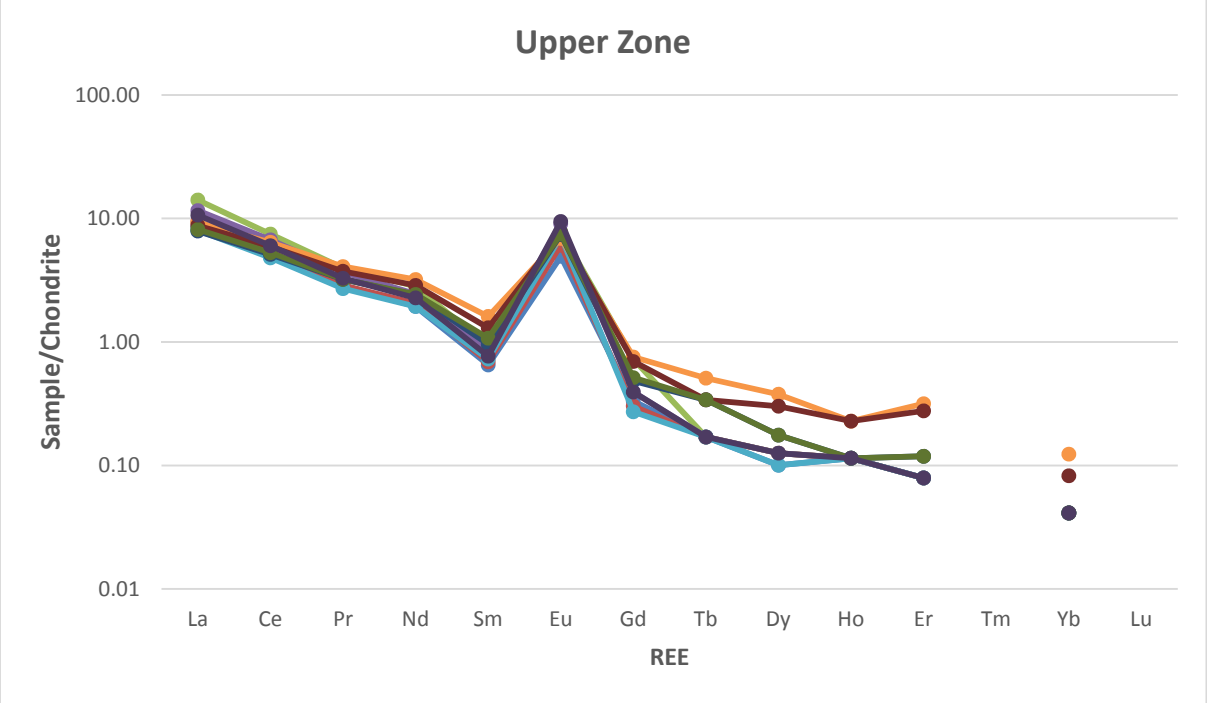

Figure 28: Chondrite-normalised REE abundances in plagioclase from the Upper Zone of the BK-2 drill core.

3.5 *In situ* strontium isotopic geochemistry of plagioclase

Strontium isotopic ($^{87}Sr/^{86}Sr$) data for plagioclase in the studied rock samples are presented in Appendix C. Figures 29 and 30 show the variation of initial $^{87}Sr/^{86}Sr$ compositions of all analysed spots plotted against depth, with spot size of diameter 95 μm (Figure 24), and modal mineralogy shown for comparison.

The radioactive parent isotope (^{87}Rb) decays to the radiogenic daughter isotope (^{87}Sr) by beta decay, $^{87}Rb - \beta \rightarrow ^{87}Sr$. Since the mass spectrometer lacks the capability to measure absolute concentrations of individual isotope species, the abundance of both parent and daughter isotopes are expressed relative to an isotope whose natural abundance does not change with time, such as ^{86}Sr. In age calculations, two isotopic ratios, R = parent/stable ($^{87}Rb/^{86}Sr$) and I = daughter/stable ($^{87}Sr/^{86}Sr$) are required. However, the $^{87}Sr/^{86}Sr$ ratio is measured directly on the mass spectrometer with corrections applied as per the methodology section above; $^{87}Rb/^{86}Sr$ is calculated by monitoring the 85/88 signal and multiplying that by ((87Rb/85Rb)/0.1194).

Calculating initial ratio of known ages, 2054.4 Ma (Scoates & Friedman, 2008) in this study, fundamental equation of radioactive decay is used (e.g. Faure, 1986): $I = R(e^{\lambda t} - 1)$, where λ is a decay constant, t = time : $^{\lambda}Rb = 1.39 \times 10^{-11}$ y^{-1} (Nebel *et al.* 2011) in this study.

The initial $^{87}Sr/^{86}Sr$ ratios of plagioclase averages 0.7086 in the lower Main Zone, 0.7081 in the upper Main Zone and 0.7078 in the Upper Zone. More isotopic variation is observed from the base of the studied succession and decreases up the stratigraphy of BK-2.

The initial strontium (Sr_i) ratios decrease from the base of the studied succession up to a depth of 1050.26 m, from a value of 0.7092 to 0.7083. From a depth of 1026.26 m up to 916.38 m, a slight increase of initial strontium (Sr_i) ratios is encountered, with measured values of 0.7091 and 0.7093, respectively. At a depth of 899.43 m, initial strontium ratio measured a value of 0.7080.

At a depth of 879.23 m, an increase of initial strontium ratio is observed with a measured value of 0.7090. A decrease of initial $^{87}Sr/^{86}Sr$ ratios is encountered from a depth of 855.62 m up to 779.80 m, with measured values of 0.7089 and 0.7081, respectively. At a depth of 740.74 m, an increase of initial $^{87}Sr/^{86}Sr$ ratio is measured at a value of 0.7087, and suddenly a decrease in initial strontium ratio is measured at a depth of 722.50 m, with a value of 0.7082. There is a slight increase of initial strontium ratio at a depth of 697.26 m, with a measured value of 0.7091. At a depth of 678.05 m, another slight initial $^{87}Sr/^{86}Sr$ ratio decrease is observed, with a measured value of 0.7082.

An increase of initial strontium (Sr_i) ratio is again observed at depth of 659.33 m, with a measured of value of 0.7087. From a depth of 635.83 m up to 595.03 m, initial $^{87}Sr/^{86}Sr$ ratios increased, with measured values of 0.7078 and 0.7087, respectively. At depths of 572.63 m and 531.74 m, initial $^{87}Sr/^{86}Sr$ ratios slightly decreased, both with similar measured values of 0.7077.

Immediately below the Pyroxenite Marker, at a depth of 506.71 m, there is a high increase of initial strontium ratio, with a measured value of 0.7097.

From a depth of 506.71 m (lower Main Zone), across the Pyroxenite Marker, up to a depth of 426.36 m (upper Main Zone) a decrease of initial $^{87}Sr/^{86}Sr$ ratios is observed, with

measured values from 0.7097 to 0.7076, respectively. Ratios remain relatively constant over the next c. 300 m of stratigraphy, from 410.78 m up to 100.70 m, with an initial $^{87}Sr/^{86}Sr$ ratio average value of 0.708, where after an increase of initial $^{87}Sr/^{86}Sr$ ratio increased to 0.7082 at a depth of 67.84 m. The initial $^{87}Sr/^{86}Sr$ data of plagioclase of BK-2 as recalculated to 2054.4 Ma (Scoates & Friedman, 2008) is highly variable as portrayed by Figure 29 and 32, where such data compositions of individual spot analysed is plotted against depth, with error bars, as the total range in initial Sr-isotope ratio is quite small.

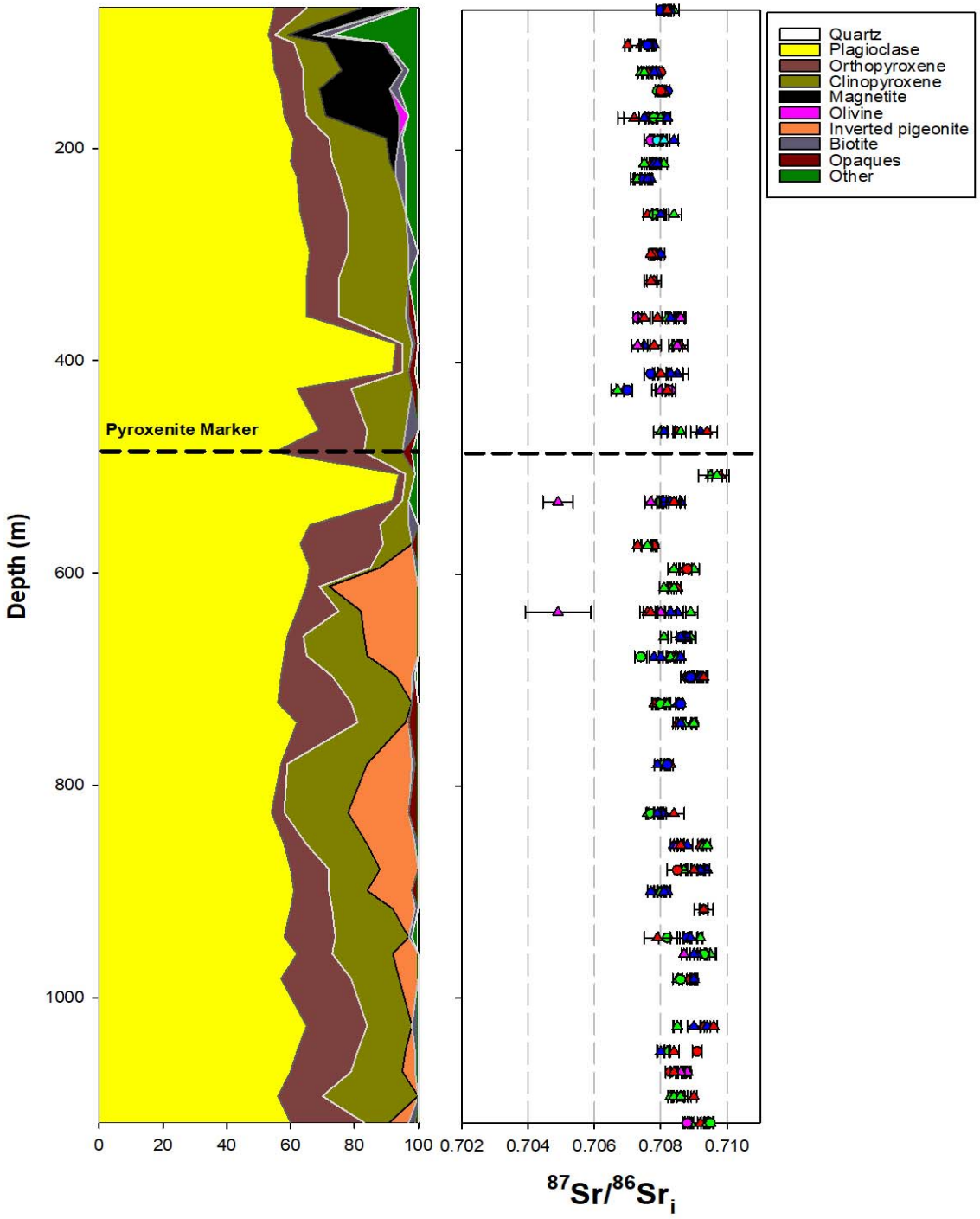

Figure 29: The initial 87Sr/86Sr composition of analysed spots plotted against depth (m) with modal mineralogy for comparison. Different colours denote coexisting plagioclase crystals per sample. Circles represent plagioclase cores and circles represent plagioclase rims, all with error bars.

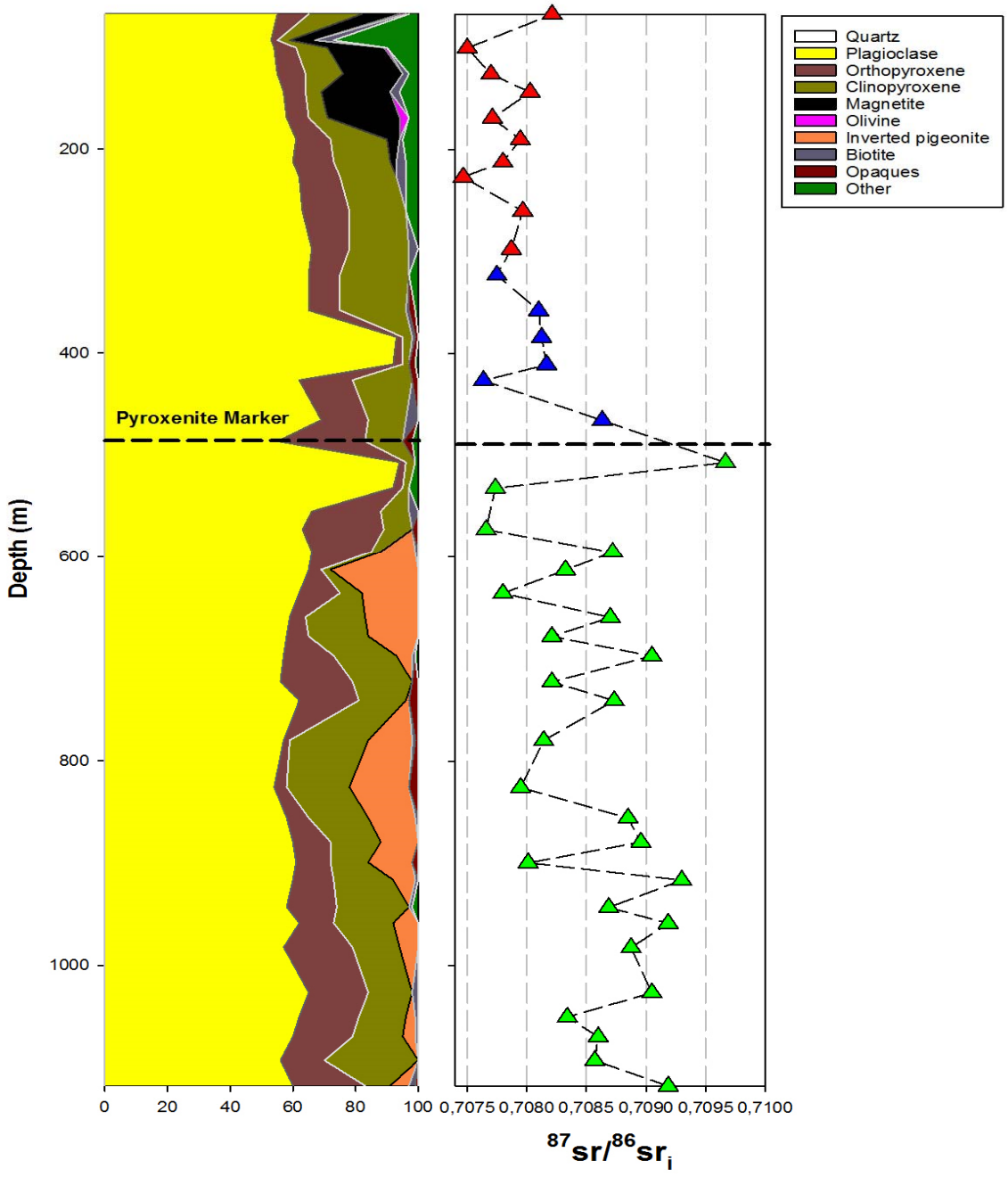

Figure 30: The initial 87Sr/86Sr average compositions of analysed samples plotted against depth (m) with modal mineralogy for comparison. (Red triangles = Upper Zone, blue triangles = upper Main Zone and green triangles = lower Main Zone).

4. Discussion

4.1 Previous work on BK-2

In the previous study of the BK-2 drill core by Cawthorn *et al.* (1991), the mineralogy as compared to this study is nearly similar (see Figure 31). The authors have placed the Pyroxenite Marker at a depth of 484 m, which is the approximate position of it in this study.

Tegner *et al.* (2006) measured whole rock Sr isotopic data for the upper Main and Upper Zones in the Bierkraal drill core of the western Bushveld Complex and showed existing and new values to be constant (0.7073 ± 0.0001), while in this study *in-situ* values for plagioclase are nominally higher at 0.7079. The difference could emanate from alteration in the whole-rock as the measurement was lower than the measurement of *in-situ* analysis, which its focus was only on selected plagioclase grains, which were less or not altered.

At approximately 100 m below the Pyroxenite Marker, inverted pigeonite disappears and in the Upper Zone, magnetite is present in both this study and that of Cawthorn *et al.* (1991).

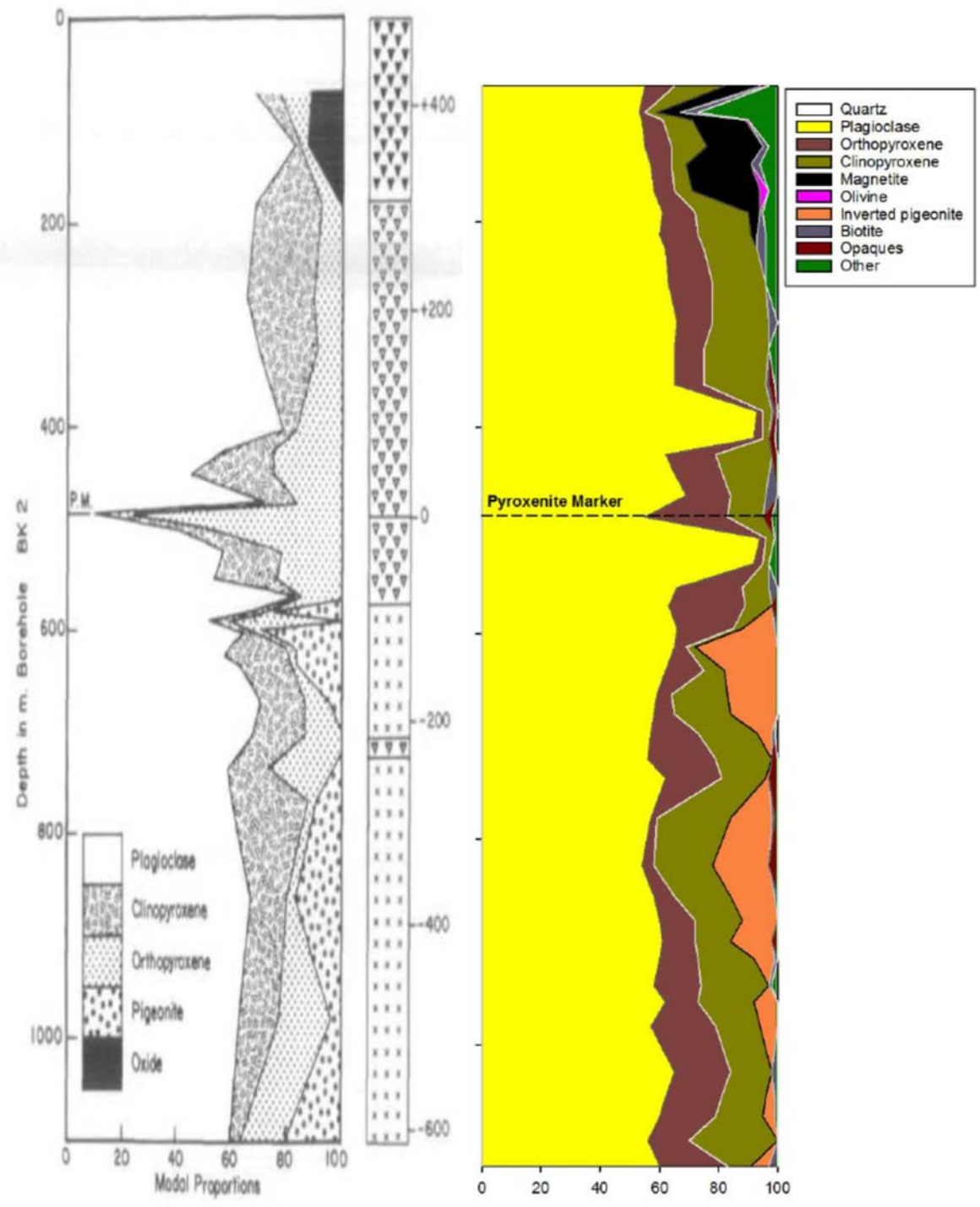

Figure 31: Comparison of modal mineralogy by Cawthorn *et al.* (1991) and this study.

4.2 Strontium isotope systematics in the western Bushveld Complex

The isotopic composition of strontium is not only a useful indicator of the ages of rocks and minerals, but it also contains information about the origin of igneous rocks and about the geologic processes that have affected their chemical composition (Faure & Powell, 1972).

The latter authors summarized the earlier findings of other researchers that Rb-Sr isochron method of dating does not only determine the age of a suite of comagmatic igneous rocks, but also indicates the initial ratios, which is the $^{87}Sr/^{86}Sr$ ratio of the magma from which the rocks crystallised.

Kruger (1994) divided the Rustenburg Layered Suite into two stages namely; 1) the integration stage, which is incorporating the Lower, Critical and lower Main zones, as manifested by an asymmetrical upward increase in the initial strontium (Sr_i) ratio from 0.7047 to 0.7091 in the Lower Zone and lower Main Zone, respectively. 2) The differentiation stage, which includes the upper Main Zone and Upper Zone, showing a nearly constant initial Sr-isotopic ratio with a value of 0.7073 (Kruger *et al*. 1987).

The isotopic heterogeneity in the integration stage, which is the lower open system, was caused by several influxes of magma of distinct composition with associated deposition of cumulates (Kruger, 1994). In contrast to the integration stage, the isotopically homogeneous differentiation stage, which is the upper closed system, was marked by magma evolution that was dominated by fractional crystallization of mega-scale, with no significant addition of new magma or *in situ* contamination (Kruger, 1994).

In support, Kruger *et al.* (1987) showed that the entire Upper Zone crystallized from a mixed magma, which underwent thorough blending before crystallization.

It is not a new phenomenon that co-existing minerals may be in isotopic disequilibrium in layered igneous intrusions, as exemplified by Yang *et al.* (2013) where they report the initial strontium (Sr_i) isotopic disequilibrium in cores and rims of plagioclase in the upper Critical Zone of the western Bushveld Complex, which is a similar case with this study. In addition, Roelofse and Ashwal (2012) reported the disequilibrium of strontium isotopes between plagioclase and co-existing orthopyroxene in the Main Zone.

Prevec *et al.* (2005) found different initial neodymium (Nd) isotope ratios of orthopyroxene and plagioclase separates from the very same sample and thus proposed Nd isotopic disequilibrium between orthopyroxene and plagioclase due to magma replenishment.

Tepley and Davidson (2003) reported strontium isotopic disequilibrium within single plagioclase grains from the Rum layered intrusion. The first *in situ* strontium isotopic analysis of the Bushveld Complex minerals that showed disequilibrium of strontium isotopes between plagioclase and co-existing orthopyroxene in the Critical Zone and between orthopyroxene from the Lower Zone were reported by Chutas *et al.* (2012), and these are suggestive of crystallization that emanates from different parental magmas.

The strontium (Sr_i) isotopic data that is presented for this study of the Western Lobe of the Bushveld Complex, exhibit a broadly similar pattern to that of Kruger (1994) (Figure 31). In this regard, it would be appropriate to divide the stratigraphic sequence into integration and differentiation stages. The suggested integration stage in this part of the Western Lobe comprises of the lower end of the lower Main Zone that is marked by

repeated reversal, which signify strontium isotopic fluctuations, and this suggests that there were repeated magma inflows during the lower Main Zone genesis. Even the An% plot against depth as shown in Figure 22, is in support of the view that the lower Main Zone was most likely constructed by repetitive, possibly crystal-laden magma influxes (Figure 32).

The suggested differentiation stage comprises of the upper Main Zone and Upper Zone. This stage shows less initial strontium isotopic ratio variations of plagioclase. This interval shows less variation in Sr-isotopic composition coupled with a broad differentiation trend towards lower temperature mineral compositions. This is indicative that magma differentiation processes played a dominant role in the formation of this sequence.

The mineralogical diversity of the Upper Zone must have been produced by fractional crystallization processes within the chamber, and not influenced by magma addition or assimilation of country rocks (Kruger *et al.* 1987), thus making it a single true magmatic series on the basis of isotopic, mineralogical and chemical constraints (Irvine, 1982).

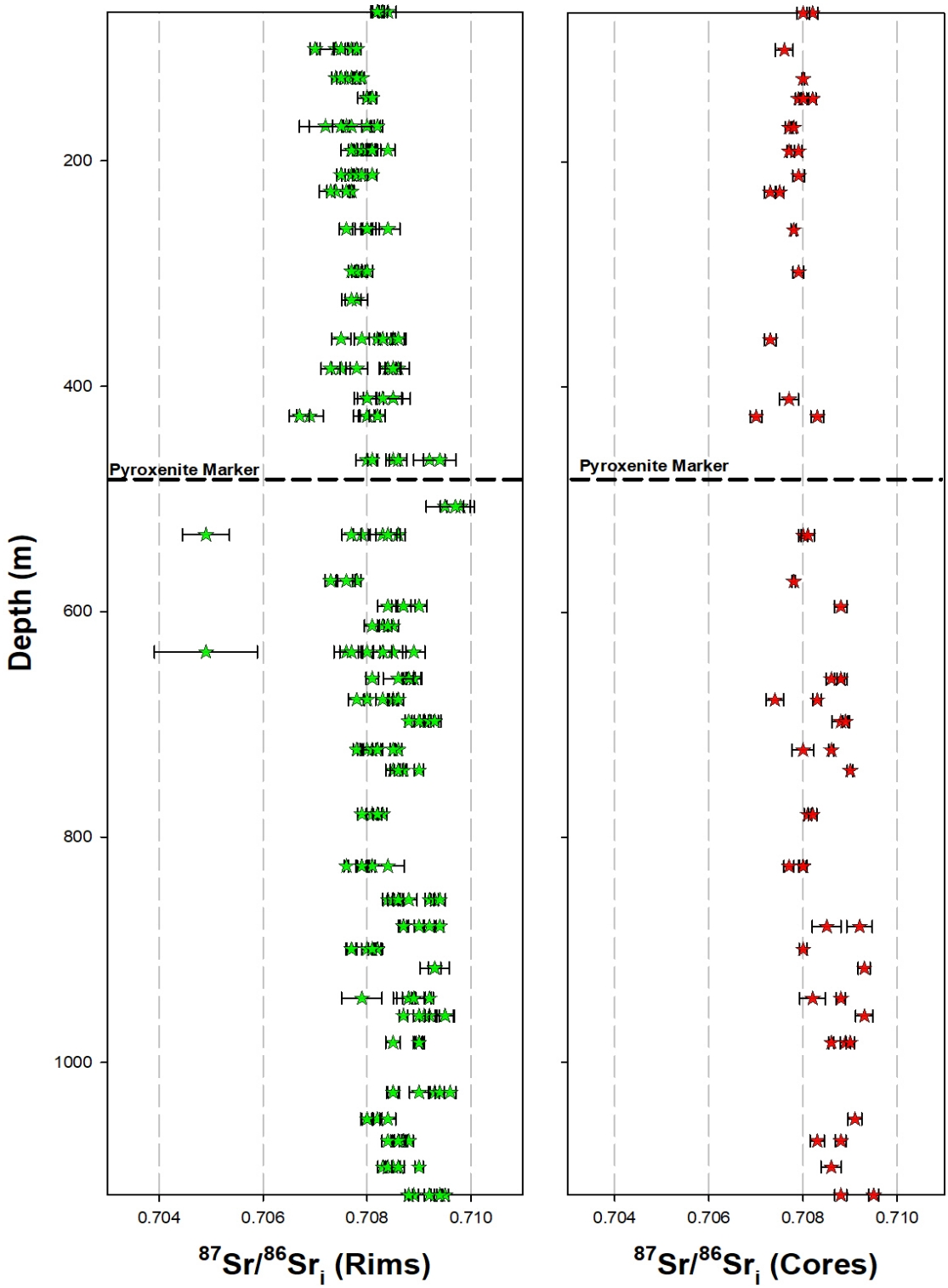

Figure 32: Plagioclase rim Sr_i isotope vs plagioclase core Sr_i isotope plots.

4.3 *In situ* major and trace element variation comparison in plagioclase of the Western and Eastern Limbs of the Bushveld Complex.

Part of the *in situ* major and trace element compositions of plagioclase from the BK-2 drill core as collected in this study is presented and compared to that of Vantongeren and Mathez (2013) (see Electronic Appendix 3). The latter authors' results were derived from surface samples collected from the eastern Bushveld Complex, from ~ 1041 m below the Pyroxenite Marker up to the Upper Zone (see Figure 33).

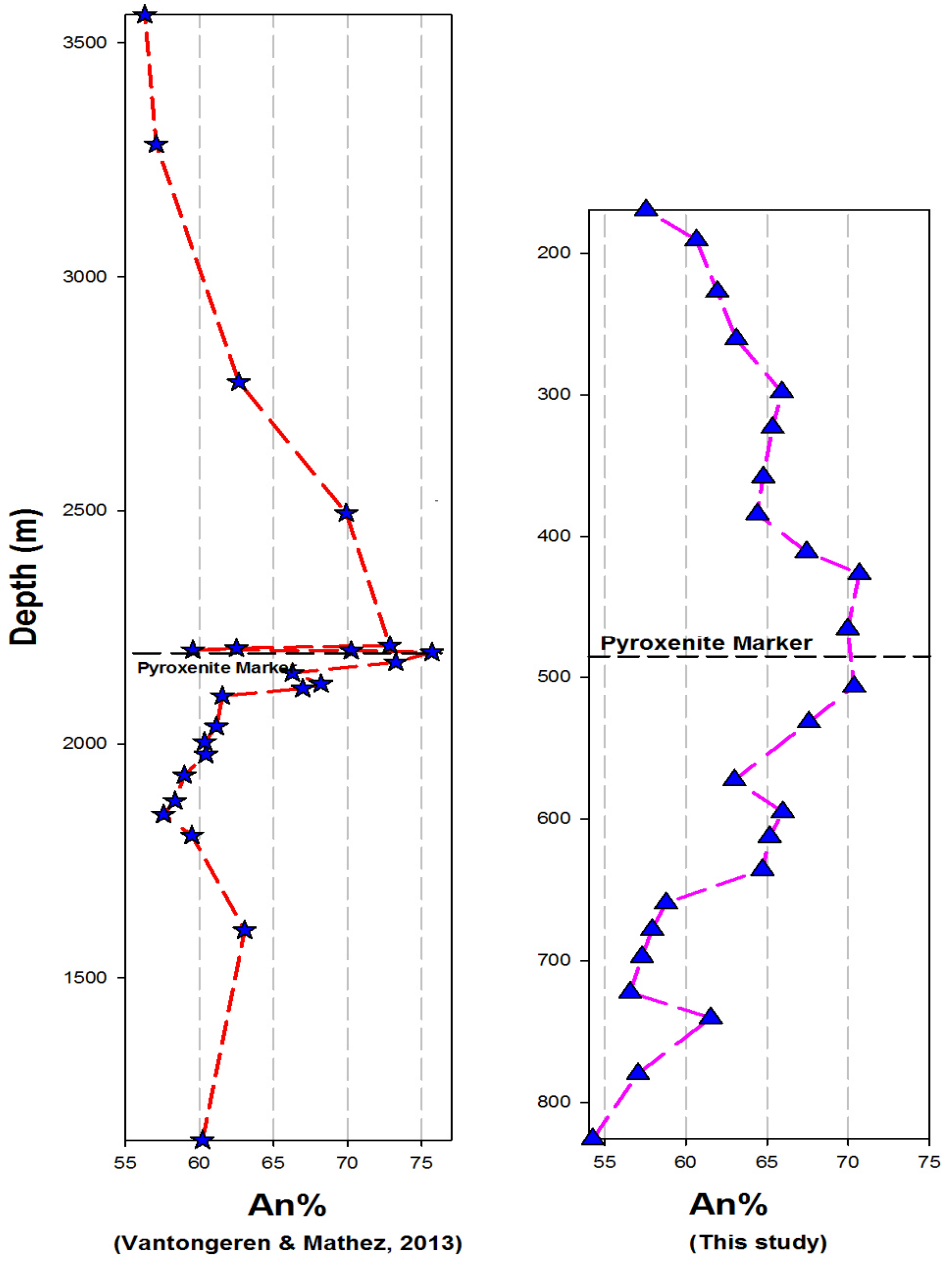

Figure 33: Comparison of anorthite (An%) content of plagioclase by Vantongeren & Mathez (2013) and this study. Red line with blue stars represents Eastern Limb and pink line with blue triangle represents Western Limb.

The eastern Bushveld Complex cumulate rocks in the ~ 350 m stratigraphic interval below the Pyroxenite Marker recorded a continuous upward trend of increasing plagioclase anorthite content, with a maximum of 75.69% (Vantongeren and Mathez, 2013), and variation of trace elements. A similar case is observed in this study, from a depth of 825.79 m (~342 m below the Pyroxenite Marker), that anorthite content recorded a continuous upward trend up to the vicinity of the Pyroxenite Marker, with a maximum value of 70.70%.

Both rare earth element compositions of the western and eastern limbs, in the Main and Upper Zones, are within a similar range (see Figure 34). The data for Gd in the eastern limb was not available.

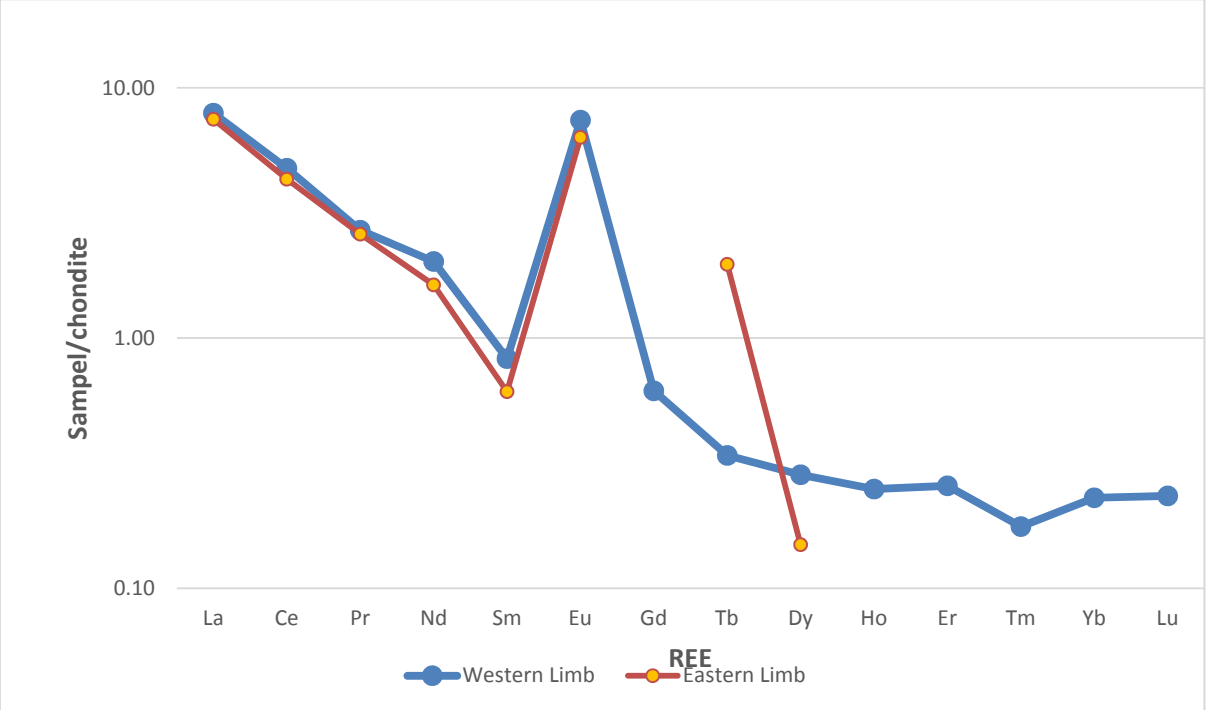

Figure 34: Comparison of the REE content from in situ analysis of plagioclase from below the Pyroxenite Marker up to the Upper Zone in the eastern (Vantongeren & Mathez, 2013) and western (this study) Bushveld Complex. Blue graph represents the Western Limb and dark red represents the Eastern Limb.

4.4 A model to explain the petrogenesis of the Pyroxenite Marker interval.

Cawthorn *et al.* (1991) documented a major, but gradual, reversal in the enigmatic variation patterns of the plagioclase and pyroxenes in the Main Zone of the western Bushveld Complex (BK-2). The Pyroxenite Marker, a distinctive orthopyroxenite layer, occurs close to the top of the reversed differentiation sequence (Cawthorn *et al.* 1991).

The Pyroxenite Marker, in the eastern Bushveld Complex, marks the termination of a prominent upward trend to more primitive major and trace element mineral compositions (Vantongeren and Mathez, 2013). The observation of the geochemical reversal ~ 350 m below the Pyroxenite Marker prompted Vantongeren and Mathez (2013) to propose the gradual recharge model. The latter model suggests that magma intruded in numerous, small, discrete batches into a thermally and chemically homogeneous magma body.

Interpretation of their observations on compositional data, Vantongeren and Mathez (2013) postulated the Pyroxenite Marker itself to have resulted from either, (i) intrusion of a large, final pulse of magma that mixed with a cooler, resident magma to force the system to orthopyroxene saturation, or (ii) intrusion of magma with an entrained pyroxene crystal load.

Based on whole-rock Sr-isotopic compositions, Sharpe (1985) proposed that at the level of the Merensky Reef, there was dense magma addition, which under-plated the resident magma and did not mix with it. He maintained that the new layer of magma partially crystallised to produce the lower Main Zone and dramatically mixed with the older, elevated magma to produce the Pyroxenite Marker and Sr-isotopic inflection.

The change in Sr_i across the Pyroxenite Marker interval indicates addition of magma (Eales & Cawthorn, 1996).

On the basis of the Sr isotopic compositional observations made in this study, I propose the following model to account for the petrogenesis of the Pyroxenite Marker interval as exposed in BK-2:

i) Influx of a hotter, less dense, less radiogenic magma (Sri = 0.7055; Cawthorn *et al.* 1991) than that present in the magma chamber took place as cumulates currently present in the BK-2 drill core at a depth of ~700 m were forming. This new influx of magma rose to the top of the magma chamber, forming a basal interface with the resident Main Zone magma. Cawthorn et al. (1991) suggested that the volume of this new magma added must have been approximately equal to that present in the magma chamber at the time.

ii) The initiation of double-diffusive convection across this interface may have led to the development of finger instabilities (resulting in the downwards percolation of pockets of newly introduced magma and the upwards percolation of pockets of resident Main Zone magma across the basal interface). The downwards percolating pockets of newly introduced magma would have mixed with the resident Main Zone magma en-route to the solidification front, initially at a depth of ~700 m in the BK-2 drill core, resulting in the onset of the reversed differentiation trend as seen in plagioclase An% and pyroxene Mg# towards the Pyroxenite Marker. The volume of newly introduced magma displaced downwards and the volume of resident magma displaced upwards across the interface should have been equal. Evidence for the involvement of downwards

percolating pockets of added magma are preserved in the core of a plagioclase crystal from a depth of 678.05 m with an initial $^{87}Sr/^{86}Sr$ ratio of 0.7074. This value is significantly lower than that recorded in plagioclase cores lower down in the succession, that have an average Sri = 0.70858.

iii) Initial $^{87}Sr/^{86}Sr$ ratios recorded in plagioclase that are higher than 0.7074 over the ensuing ~190 m towards the level of the Pyroxenite Marker are thought to be the result of varying degrees of mixing between downwards percolating pockets of newly introduced magma and resident magma below the interface between the newly introduced magma and the resident magma. As the crystallization front proceeded upwards, progressively more primitive mineral compositions would have been produced in cumulates as a result of mixing between the resident and newly introduced magmas and the volume of magma below the interface between the resident and newly introduced magma would have decreased as a result of continued crystallization and an upwards advance of the crystallization front.

iv) As the crystallization front advanced towards the level of the Pyroxenite Marker, the densities of the magmas above and below the interface between the newly introduced and resident magmas would have increased and decreased, respectively, due to continued mixing across the interface. I envisage that the densities of the magmas above and below the interface became sufficiently similar so as to allow rapid mixing of the two magmas as the crystallization front reached the approximate level of the Pyroxenite Marker, resulting in nearly

complete homogenization of the magma remaining in the magma chamber (cf. Huppert & Sparks, 1984).

v) This rapid homogenization may have resulted in a minor shift in the phase equilibria and possibly the stabilization of pyroxene at the expense of plagioclase, resulting in the accumulation of the Pyroxenite Marker. Klemm *et al*. (1985) proposed on the basis of phase relations in the system $CaAl_2Si_2O_8$-Mg_2SiO_4-SiO_2-Fe_3O_4 as reported by Osborn (1978), that a transient increase in total pressure in the system may have been responsible for preferential stabilization of pyroxene. Such an increase in pressure may potentially have been related to magmatic overturn (Manga & Brodsky, 2006).

vi) Plagioclase cores record an average Sri of ~0.7076 in the ~130 m above the Pyroxenite Marker, which is significantly different from the average value (~0.7083) for plagioclase below the onset of the reversed differentiation trend that culminated in the Pyroxenite Marker. However, over this interval, rims are generally considerably more radiogenic, possibly reflecting interaction with upwards displaced intercumulus melt derived from the compaction of the underlying crystal mush.

vii) From a depth of ~350 m in BK-2, the Sr-isotopic composition of plagioclase spots remained relatively constant at an average value of ~0.7078. This feature, coupled with the normal differentiation trend as shown in Figure 23, suggests fractionation from a well-mixed magma without additional input of magma, as has been suggested by Kruger et al. (1987). The reason for the discrepancy between the *in situ* Sr-isotopic values obtained on plagioclase in

this study and the whole-rock values of Kruger *et al*. (1987) at 0.7073 over this interval could be due to alteration products in bulk samples that would not be present in fresh zones of plagioclase grains.

5. Summary and Conclusion

5.1 Summary of results

The studied samples from the Main and Upper Zones are broadly gabbroic cumulates from the Western Limb of the Bushveld Complex. Cumulus plagioclase is the dominant mineral, associated mostly with clinopyroxene and orthopyroxene as intercumulus minerals as observed in the petrographic analysis.

Sericite, chlorite, serpentine and amphibole occur as secondary minerals resulting from localized alteration. Inverted pigeonite occurs throughout the lower Main Zone up the stratigraphy and vanishes at about 100 m below the Pyroxenite Marker. Olivine is present though hardly observed in the studied samples. The minerals biotite and quartz are minor, with little opaques in the lower Main Zone. In the Upper Zone, magnetite is abundant

The whole-rock major and trace element geochemistry of the BK-2 drill core display a high variation and magma differentiation in the Main Zone, and a normally differentiated Upper Zone.

Multiple plagioclase crystals were analysed *in situ* using electron microprobe within different samples. The major element composition of part of the Main and Upper Zones of the Western Limb of the Bushveld Complex, straddling the boundary between these

two stratigraphic groups, were determined. Individual plagioclase spot analyses of the Main Zone have an average anorthite (An%) of 62 ± 4.7%, ranging between 50.4% and 72.4%. The plagioclase anorthite content (An%) of the Upper Zone has an average of 57.9 ± 3.6%, recording values between 51.2% and 67.7%.

Plagioclase of the lower Main Zone has La concentrations covering the range of 4-10 times chondrites, Lu covers < 0.01 - 3 times chondrites and a positive Eu anomaly, with average Eu/Eu* ratio of 10.21. The Upper Main Zone has La concentrations covering the range of 5-11 times chondrites, Lu covers the range of < 0.01 – 0.3 times chondrites, and samples show positive Eu anomaly, with average Eu/Eu* ratio of 10.71. The Upper Zone has La concentrations covering the range 4 – 14 times chondrites, Lu measured below detection limit of < 0.01, and samples show a positive Eu anomaly in plagioclase, with average Eu/Eu* ratio of 10.26.

The *in situ* initial $^{87}Sr/^{86}Sr$ composition of plagioclase was also determined, and the analyses of the lower Main Zone samples yielded results that show more variation of the spots, with an initial $^{87}Sr/^{86}Sr$ average value of 0.7085, ranging from 0.7049 to 0.7098. The upper Main Zone has the variation of initial $^{87}Sr/^{86}Sr$ average of 0.7081, ranging between 0.7067 to 0.7094. In the Upper Zone, the variation of initial $^{87}Sr/^{86}Sr$ is low, as compared to the lower Main Zone, with an average value of 0.7078, ranging from 0.7079 to 0.7084.

5.2 Summary of discussion

This study has identified the similar feature as that of the previous work on BK-2 drill core by Cawthorn *et al.* (1991), the Pyroxenite Marker is at the approximate depth of 484 m, with almost identical mineralogy. *In situ* Sr isotopic data of plagioclase in this study are nominally higher in the upper Main and Upper Zones, with a recorded ratio of 0.7079 as compared to that of Tegner *et al.* (2006) on Bierkraal drill core, which showed existing and new values to be constant (0.7073 ± 0.0001). The latter is probably due to alteration products analysed from bulk samples that would not be present in fresh zones of plagioclase grains.

Like Kruger (1994), it is here suggested that the isotopic heterogeneity in the integration stage was caused by several influxes of magma of distinct composition with associated deposition of cumulates. In contrast to the integration stage, the isotopically homogeneous differentiation stage was marked by magma evolution that was dominated by fractional crystallization at a mega-scale, with no significant addition of new magma or *in situ* contamination (Kruger, 1994).

In situ major and trace element compositions from the western Bushveld Complex (this study) recorded a continuous upward trend of increasing plagioclase anorthite content, as observed from ~ 342 m below the Pyroxenite Marker. The REE concentrations of plagioclase in the Western Limb show variation as in the lower Main Zone graphs overlap (see Figure 27), which may indicate magma mixing immediately below the Pyroxenite Marker, and in the upper Main and Upper Zones, the overlaps are substantially small.

The model proposed suggest that; (i) the new influx of hot, less dense and radiogenic magma formed a basal interface with the resident magma in the Main Zone. (ii) double-diffusive convection might be suspect to magma mixing, which resulted to the onset of reversed differentiation trend (i.e. plagioclase An% & pyroxene Mg#) towards the Pyroxenite Marker. (iii) Initial $^{87}Sr/^{86}Sr$ ratios of 0.7074 above ~ 190 m towards the Pyroxenite Marker are presumed to be signifying the mixing of downwards percolating pockets and resident magmas, (iv) continued mixing across the interface would have resulted on increased and decreased magma densities above and below the interface between the new and resident magmas, respectively. (v) The Pyroxenite Marker may have formed due to stabilization of pyroxene at the expense of plagioclase after a process of rapid homogenization that may have resulted in a transient increase in pressure in the chamber.

5.3 Conclusion

The compositional (major element, trace element and Sr-isotope) results obtained in this study display a significant variation between and within plagioclase across the boundary between the Main and Upper Zones in the Western Limb of the Bushveld Complex as observed from anorthite content (An%), trace elements variation and $^{87}Sr/^{86}Sr$ isotopic disequilibria of plagioclase. The presence of the spike in anorthite content (An%) and $^{87}Sr/^{86}Sr$ at the Pyroxenite Marker represents the approximate position of the shift from the Main and Upper Zones' isotopic compositions. The latter observation is not a new phenomenon when it comes to layered intrusions.

Isotopic variations at the mineral scale are of great use in the monitoring of magma evolution, processes and timescales, together with core-rim variations that are good tracers of magma mixing. The present dataset shows the importance of *in situ* mineral compositional and isotopic determinations in the study of layered intrusions in the refinement and testing of established petrogenetic models.

Furthermore, my interpretation of the dataset has shown the importance of slow mixing of melt and crystals across a doubly diffusive interface followed by rapid homogenization of magmas of differing compositions in the petrogenesis of the Pyroxenite Marker interval of the western Bushveld Complex. A case was also made for the late-stage migration of interstitial melt from compaction of the Main Zone rocks below the Pyroxenite Marker to explain the radiogenic plagioclase rims in the rocks above the Pyroxenite Marker.

6. References

Anders, E. & Grevesse, N. (1989) Abundances of the elements: Meteoritic and solar. Geochimica et Cosmochimica Acta 53: 197-214

Ashwal, L. D., Webb, S. J., & Knoper, M. W. (2005) Magmatic stratigraphy in the Bushveld Northern Lobe: continuous geophysical and mineralogical data from the 2950 m Bellevue drillcore. *South African Journal of Geology, 108*, 199-232.

Banner, J.L. & Kaufman,J. (1994) The isotopic record of ocean chemistry and diagenesis preserved in non-luminescent brachiopods from Mississipian carbonate rocks, Illinois and Missouri. Geological Society of America Bulletin, V.106, 1074-1082.

Biesheuvel, K. (1970) An interpretation of a gravimetric survey in the area west of the Pilanesberg in the Western Transvaal in Symposium on the Bushveld Igneous Complex and other Layered Intrusions (Visser, DJL, Von Gruenewaldt, G, eds.) Geological Society of South Africa Special Publication 1, 266-282.

Bizzarro M., Simonetti A., Stevenson R.K. & Kurszlaukis S. (2003) In situ $^{87}Sr/^{86}Sr$ investigation of igneous apatites and carbonates using laser-ablation MC-ICP-MS. *Geochimica et Cosmochimica Acta*, 67(2):289-302.

Buchanan, D.L. (1975) The petrography of the Bushveld Complex intersected by boreholes in the Bethal area. Transactions of the Geological Society of South Africa 78, 335–348.

Cameron, E. N. (1980) Evolution of the lower critical zone, central sector, eastern Bushveld Complex, and its chromite deposits:Econ. Geol., v. 75, p. 845-871.

Cameron, E. N. (1982) The Upper Critical Zone of the Eastern Bushveld Complex Precursor of the Merensky Reef. *Economic Geology, 77*, 1307-1327.

Cawthorn ,R.G., Davies, G., Clubley-Armstrong, A. & McCarthy,T.S. (1981) Sills associated with the Bushveld Complex, South Africa: an estimate of the parental magma composition. Lithos 14:1–15.

Cawthorn, R. G. & McCarthy, T. S. (1985) Incompatible trace element behaviour in the Bushveld Complex. Economic Geology 80, 1016–1026.

Cawthorn, R. G. & Walsh, K. L. (1988) The use of phosphorus contents in yielding estimates of the proportion of trapped liquid in cumulates of the Upper Zone of the Bushveld Complex. Mineralogical Magazine 52, 81–89.

Cawthorn, R. G., & Walraven, F. (1998) Emplacement and crystallisation time for the Bushveld Complex. *Journal of Petrology, 39*(9), 1669-1687.

Cawthorn, R.G., Meyer, P.S. & Kruger, F.J. (1991). Major addition of magma at the Pyroxenite Marker in the Western Bushveld Complex, South Africa. Journal of Petrology, 32, 739-763.

Cawthorn, R. G., Barnes, S. J., Ballhaus, C., & Malitch, K. N. (2005) Platinum-group element, chromium and vanadium deposits in mafic and ultramafic rocks. *Economic Geology, 100th Anniversary volume*, 215-249.

Chutas, N. I., Bates, E., Prevec, S. A., Coleman, D. S., & Boudreau, A. E. (2012) Sr and Pb isotopic disequilibrium between coexisting plagioclase and orthopyroxene in the Bushveld Complex, South Africa: microdrilling and progressive leaching evidence for sub-liquidus contamination within a crystal mush. *Contributions to Mineralogy and Petrology, 163*(4), 653-668.

Davidson J., Tepley III F., Palacz Z. & Meffan-Main S. (2001) Magma recharge, contamination and residence times revealed by in situ laser ablation isotopic analysis of feldspar in volcanic rocks. Earth and Planetary Science Letters, 184:427-442.

de Waal, S. A., Maier, W. D., Armstrong, R. A., & Gauert, C. D. (2001) Parental magma and emplacement of the stratiform Uitkomst Complex, South Africa. *Canadian Mineralogist, 39*(2), 557-571.

Eales, H. V., Marsh, J. S., Mitchell, A. A., De Klerk, W. J., Kruger, F. J., & Field, M. (1986) Some geochemical constraints upon models for the crystallization of the Upper Critical Zone-Main Zone interval, northwestern Bushveld Complex. *Mineralogical Magazine, 50*, 567-582.

Eales, H. V., & Cawthorn, R. G. (1996) The Bushveld Complex. In: Cawthorn R.G (ed) *Layered Intrusions.* Elsevier, Amsterdam, pp. 181-229.

Elburg, M., Vroon, P., van der Wagt, B., & Tchalikian, A. (2005) Sr and Pb isotopic composition of five USGS glasses (BHVO-2G,BIR-1G,BCR-2G, TB-1G, NKT-1G). *Chemical Geology, 223*, 196-207.

Faure, G., & J. L. Powell. (1972) Strontium isotope Geochemistry. Springer Verlag, New York.

Faure G. (1986) Principles of Isotope Geology. J. Wiley & Sons, Chichester, pp. 1–589.

Hulbert, L.J. (1983) A petrographical investigation of the Rustenburg Layered Suite and associated mineralisation south of Potgietersrus. Unpublished D.Sc Thesis, University of Pretoria, Pretoria.

Huppert, H.E. & Sparks, R.S.J. (1984) Double-diffusive convention due to crystallization in magmas. Ann Rev Earth Planet Sci. 12:11–37

Irvine, T.N. (1982) Terminology for layered intrusions. J. Petrology, 23, 127-162.

Kinnaird,J.A. (2005) The Bushveld large igneous province. http://www.largeigneousprovinces.org.LOM.html [May 2005].

Kinnaird, J. A., Hutchinson, D., Schurmann, L., Nex, P. A. M., & De Lange, R. (2005) Petrology and mineralisation of the southern Platreef: northern limb of the Bushveld Complex, South Africa. *Mineralium Deposita, 40*, 576-597.

Klemm, D. D., Ketterer, S., Reichhardt, F., Steindl, J., & Weber-Diefenbach, K. (1985) Implication of vertical and lateral compositional variations across the Pyroxenite Marker and its associated rocks in the upper part of the Main Zone in the Eastern Bushveld Complex, Economic Geology , vol. 80 (pg. 1075-1088).

Kruger, F. J. (1990) The stratigraphy of the Bushveld Complex: a re-appraisal and the relocation of the Main Zone boundaries. *South African Journal of Geology, 93*, 376-381.

Kruger, F. J. (1994) The Sr-isotopic stratigraphy of the western Bushveld Complex. *South* African Journal of Geology, 97, 393-398.

Kruger, F. J., Cawthorn, R. G., & Walsh, K. L. (1987) Strontium isotopic evidence against magma addition in the Upper Zone of the Bushveld Complex. *Earth and Planetary Science Letters, 84*(1), 51-58.

Kruger, F. J. (2005) Filling the Bushveld Complex magma chamber: lateral expansion, roof and floor interaction, magmatic unconformities, and the formation of giant chromitite, PGE and Ti-V-magnetite deposits. Mineralium Deposita 40, 451-472.

Lee, C. A. (1996) A review of mineralisation in the Bushveld Complex and some other layered intrusions. In: Cawthorn, R.G.(ed.) *Layered Intrusions. Developments in Petrology 15,* 103-145.

Lemarchand, F., Benoit, V. & Calais, G. (1987) Trace element distribution coefficients in alkaline series. *Geochimica et Cosmochimica Acta* 51: 1,071-1,081.

Le Maitre,R.W. (editor), Bateman.P, Dudek, A.,Keller,J. *et al*. (1989) A Classification of Igneous rocks and Glossary of Term: Recommendations of the International Union of Geological Sciences Subcommission on the Systematics of Igneous Rocks. Blackwell Scientific Publications, Oxford.

Le Maitre, R.W. *et al* eds (2005) Igneous Rocks: A Classification and Glossary of Terms: Recommendations of the International Union of Geological Sciences Subcommission on the Systematics of Igneous Rocks, 2nd Edition. Cambridge University Press.

Lundgaard, K. L., Tegner, C., Cawthorn, R. G., Kruger, F. J. & Wilson, J. R. (1993). Trapped intercumulus liquid in the Main Zone of the eastern Bushveld Complex, South Africa. Contributions to Mineralogy and Petrology 151, 352–369.

Maier, W.D., Barnes, S-J. & Van der Merwe, M.J. (2001) Platinum-group elements in the Pyroxenite Marker, Bushveld Complex: implications for the formation of the Main Zone. South African Journal of Geology 104: 301-308.

Manga, M. & Brodsky, E. (2006) Seismic triggering of eruptions in the far field: volcanoes and geysers, Ann. Rev. Earth planet. Sci. , 34, 263–291.

Mangwegape, M., Roelofse, F., Mock, T., & Carlson, R. W. (2016) The Sr-isotopic stratigraphy ofthe Northern Limb of the Bushveld Complex, South Africa. *Journal of African Earth Sciences, 113*, 95-100.

Manyeruke, T.D. (2007) Compositional and lithological variation of the Platreef on the farm Nonnenwerth, northern lobe of the Bushveld Complex: Implications for the origin of Platinum-group elements (PGE) mineralization. Unpublished Ph.D Thesis, University of Pretoria, Pretoria, 248p

Mapeo, R. B., Kampuznu, A. B., Ramokate, L. V., Corfu, F., & Key, R. M. (2004) Bushveld-age magmatism in southeastern Botswana: evidence from U-Pb zircon and titanite geochronology of the Moshaneng Complex. *South African Journal of Geology, 107*, 219-232.

Merkle, R. K. W. & von Gruenewaldt, G. (1986) Compositional variation of Co-rich pentlandite: relation to the evolution of the Upper Zone of the western Bushveld Complex, South Africa. Canadian Mineralogist 24, 529–546.

Mitchell, A. A. (1990) "The stratigraphy, petrography and mineralogy of the Main Zone of the northwestern Bushveld Complex." South African Journal of Geology 93(5/6): 818-831.

Molyneux,T. G. (1974) A Geological investigation of the Bushveld Complex in Sekhukhuneland and part of the Steelport Valley. Transactions of the Geological Society of South Africa 77 329-338.

Nebel, O., Scherer, E. E., & Mezger, K. (2011) Evaluation of the ^{87}Rb decay constant by age comparison against the U-Pb system. *Earth and Planetary Science Letters,* 301, 1-8.

Nex, P.A.M., Kinnaird, J.A., Ingle, L.J., van der Vyver, B.A. & Cawthorn, R.G. (1998) A new stratigraphy for the main Zone of the Bushveld Complex, in the Rustenburg area. South African Journal of Geology, 101: 215-223.

Osborn, E . F. (1978) Changes in phase relations in response to change in pressure from 1 to 10 kbar for the system Mg_2SiO_4 - iron oxide – $CaAl_2Si;20_8$-SiO_2: Carnegie Inst. Washington Year Book 77, p. 784-790.

Paton C., Hergt J.M., Phillips D., Woodhead J.D. & Shee S.R. (2007) New insights into the genesis of Indian kimberlites from the Dharwar Craton via in situ Sr isotope analysis of groundmass perovskite. Geology, 35(11):1011-1014.

Pearce, N.J.G., Perkins, W.T., Westgate, J.A., Gorton, M.P., Jackson, S.E., Neal, C.R. & Chenery, S.P. (1997) A compilation of new and published major and trace element data for NIST SRM 610 and NIST SRM 612 glass reference materials. Geostand. Geoanal. Res. 21 (1), 115–144.

Poldervaart, A. & Hess, H.H. (1951) Pyroxenes in the crystallization of basaltic magma. Journal of Geology 59:472-489.

Prevec, S. A., Ashwal, L. D., & Mkaza, M. S. (2005) Mineral disequilibrium in the Merensky reef, western Bushveld Complex, South Africa: new Sm-Nd isotope evidence. *Contributions to Mineralogy and Petrology, 149*, 306-315.

Ramos F.C., Wolff J.A. & Tollstrup D.L. (2004) Measuring $^{87}Sr/^{86}Sr$ variations in minerals and groundmass from basalts using LA-MC-ICPMS. Chemical Geology, 211:135-158.

Reed, S. J. B. (2005) Electron Microprobe Analysis and Scanning Electron Microscopy in Geology (2nd Ed.), Cambridge University Press.

Ridley, W.I. & Lichte, F.E. (1998) Major, trace and ultratrace element analysis by Laser Ablation ICP-MS. In: McKibben, M.A., Shanks III, W.C., Ridley, W.I. (eds) Application of

mineralogical techniques in understanding mineralizing processes. Reviews in Economic Geology, 7: 199-215.

Roelofse, F. (2010) Constraints on the magmaitc evolution of the lower Main Zone and Platreef on the Northern Limb of the Bushveld Complex as inferred from the Moordkopje drill core. Ph.D. Thesis. University of the Witwatersrand.

Roelofse, F. & Ashwal, L. D. (2012) The lower Main Zone in the Northern Limb of the Bushveld Complex- a >1.3km Thick sequence of intruded and variably contaminated crystal mushes. *Journal of Petrology, 53*, 1449-1476.

Roelofse, F., Ashwal, L. D., & Romer, R. L. (2015) Multiple, isotopically, heterogeneous plagioclase populations in the Bushveld Complex suggest mush intrusion. *Chemier der Erde-Geochemistry*. 75, 465-471.

Rollinson, H. (1993) Using Geochemical Data: Evaluation, Presentation, Interpretation: John Wiley, NY.

Scoates, J. S. & Friedman, R. M. (2008) Precise age of the planitiferous Merensky Reef, Bushveld Complex, South Africa, by the U-Pb zircon chemical abrasion ID-TIMS technique. *Economic Geology, 103*, 465-471.

Sharpe, M.R. (1985) Strontium isotope evidence for preserved density stratification in the main zone of the Bushveld Complex, South Africa. Nature, 316, 119-126.

Schmidberger S.S., Simonetti A. & Francis D. 2003. Small-scale Sr isotope investigation of clinopyroxenes from peridotite xenoliths by laser ablation MC-ICP-MS — implications for mantle metasomatism. *Chemical Geology*, 199:317-329.

South African Committee of Stratigraphy (SACS) (1980) *Stratigraphy of Southern Africa Part 1: Lithostratigraphy of the Republic of South Africa, Southwest Africa/Namibia and the Republics of Bophutatswana, Transkei and Venda.(*Kent, L.E., Compiler): Handbook of the Geological survey of South Africa. Government Printer, Pretoria.

Tanner, D., Mavrogenes, J. A., Arculus, R. A., & Jenner, F. E. (2014) Trace element Stratigraphy of the Bellevue Core, Northern Bushveld: Multiple Magma Injections Obscured By Diffusive Processes. *Journal of Petrology, 55*(5), 859-882.

Tegner, C., Cawthorn, R. G. & Kruger, F. J. (2006). Cyclicity in the Main and Upper Zones of the Bushveld Complex, South Africa: Crystallization from a zoned magma sheet. Journal of Petrology 47, 2257-2279.

Tepley, F. J., & Davidson, J. P. (2003) Mineral-scale Sr-isotope constraints on magma evolution and chamber dynamics in the Rum layered intrusion, Scotland. *Contributions to Mineralogy and Petrology, 145*, 628-641.

Van der Merwe, M.J. (1978) The geology of the basic and ultramafic rocks of the Potgietersrus Limb of the Bushveld Complex. Unpublished Ph.D Thesis, University of the Witwatersrand, Johannesburg, 176p.

Vantongeren, J.A. & Mathez, E.A. (2013) Incoming magma composition and style of recharge below the pyroxenite marker, Eastern Bushveld Complex, South Africa. J Petrol 54:1585–1605.

Viljoen, M.J. & Schürmann, L.W. (1998) Platinum group metals. In: Wilson MGC, Anhaeusser CR (eds) The Mineral Resources of South Africa. Council for Geoscience, Handbook 16, 6th Edition, Pretoria, pp 532– 568.

von Gruenewaldt, G. (1970). On the phase change orthopyroxene–pigeonite and the resulting textures in the Main and Upper Zones of the Bushveld Complex in the eastern Transvaal. In: Visser, D. J. L. & von Gruenewaldt, G. (eds) Symposium on the Bushveld Igneous Complex and Other Layered Intrusions. Johannesburg: Geological Society of South Africa, pp. 67–73.

von Gruenewaldt, G. (1971). A petrological and mineralogical investigation of the rocks of the Bushveld Igneous Complex in the Tauteshoogte–Roossenekal area of the eastern Transvaal. University of Pretoria, D.Sc. thesis.

von Gruenewaldt, G. (1973) The main and upper zones of the Bushveld Complex in the Roossenekal area, Eastern Transvaal: Trans Geol Soc S Afr, v. 76, p. 207-227.

von Gruenewaldt, G. (1986) Platinum-group element-chromitite associations in the Bushveld Complex. Economic Geology **81**, A third issue devoted to platinum deposits, 1067-1079.

von Gruenewaldt, G. (1989). Contrasting platinum-group element concentration patterns in cumulates of the Bushveld Complex. Mineralium Deposita 24(3), 219-229.

von Gruenewaldt, G. (1993) Ilmenite–apatite enrichments in the Upper Zone of the Bushveld Complex: a major titanium-rock phosphate resource. International Geology Review 35, 987–1000.

Wager, L.R. & Brown, G.M. (1968). Layered Igneous Intrusions. Oliver & Boyd, Edinburgh & London, 588 pp.

Walraven, F. & Wolmarans, L. G. (1979). Stratigraphy of the upper part of the Rustenburg Layered Suite, Bushveld Complex, in the western Transvaal. Annals of the Geological Survey of South Africa 13,109–114.

Willemse, J. (1964). A brief outline of the geology of the Bushveld Igneous Complex in The Geology of some ore deposits of Southern Africa 2. Geological Society of South Africa: 91-128.

Willemse, J. (1969) The geology of the Bushveld Igneous Complex, the largest repository of magmatic ore deposits in the world. Economic Geology Monographs 4: 1-22.

Xiang, L. & Xuan, Z. (2010) "*A New EPMA Image Fusion Algorithm based on Contourlet-lifting Wavelet Transform and Regional Variance*", Journal of Software, Vol 5, No 11: 1200-1207.

Yang, S-H. Maier, W.D., Lahaye, Y., & O'Brien, H. (2013) Strontium isotope disequilibrium of plagioclase in the Upper Critical Zone of the Bushveld Complex: evidence for mixing of crystal slurries. *Contributions to Mineralogy and Petrology 166:959-974.*

Zeh, A., Ovtcharova, M., Wilson, A.H., & Schaltegger, U. (2015) The Bushveld Complex was emplaced and cooled in less than one million years – results of zirconology, and geotectonic implications. Earth and Planetary Science Letters 418: 103-11.

7. Appendices

Appendix A

Table A-1: The major element composition of plagioclase per analysed spot in weight%, and anorthite content (An%) of plagioclase. Sample depths are reported in meters (m). Calculated cation proportions in Electronic Appendix 4.

Depth	Sample	Plag	Spot	SiO_2	Al_2O_3	CaO	MgO	FeO	TiO_2	MnO	BaO	SrO	Na_2O	K_2O	Total	An%
67.84	PL-046	6	1359	55.1	27.2	10.9	n.d.	0.2	0.2	n.d.	0.1	0.1	5.1	0.3	99.0	54.4
		3	1343	54.5	27.5	11.3	n.d.	0.4	n.d.	n.d.	n.d.	0.1	4.9	0.4	99.0	56.2
		3	1341	54.2	27.2	11.3	n.d.	0.3	n.d.	n.d.	n.d.	0.1	4.8	0.4	98.2	56.6
		3	1337	55.0	27.2	10.6	n.d.	0.3	0.1	n.d.	n.d.	0.1	5.1	0.3	98.7	53.7
		2	1350	54.6	27.4	11.4	n.d.	0.3	0.1	n.d.	n.d.	0.1	4.9	0.3	99.0	56.3
		2	1348	54.8	27.6	11.1	n.d.	0.2	n.d.	n.d.	n.d.	n.d.	5.0	0.2	99.1	55.3
		2	1345	55.1	27.3	11.1	n.d.	0.2	n.d.	n.d.	n.d.	0.1	5.1	0.3	99.2	54.5
		6	1362	54.7	27.1	10.8	n.d.	0.4	n.d.	n.d.	n.d.	n.d.	5.1	0.2	98.5	54.0
100.7	PL-044	5	1317	54.8	27.3	10.9	n.d.	0.3	0.1	n.d.	n.d.	n.d.	5.2	0.2	98.8	53.6
		5	1315	55.1	27.6	11.0	n.d.	0.4	0.1	n.d.	n.d.	0.1	5.2	0.1	99.6	54.1
		2	1295	55.4	27.3	11.0	n.d.	0.3	0.1	n.d.	0.1	0.1	5.2	0.2	99.7	54.2
		2	1292	55.1	27.5	11.3	n.d.	0.2	n.d.	n.d.	n.d.	n.d.	5.0	0.2	99.5	55.8
		1	1329	55.4	27.5	10.8	n.d.	0.1	0.1	n.d.	n.d.	n.d.	5.3	0.2	99.5	53.2
		1	1326	54.9	27.5	11.1	n.d.	0.2	n.d.	n.d.	0.1	n.d.	5.0	0.1	99.0	54.9
		1	1322	55.4	27.2	10.9	n.d.	0.3	n.d.	n.d.	n.d.	0.1	5.3	0.1	99.3	53.1
126.36	PL-043	3	1291	55.2	27.3	11.1	n.d.	0.2	n.d.	n.d.	n.d.	0.1	5.0	0.3	99.3	55.2
		3	1288	55.5	27.4	11.0	n.d.	0.5	0.1	n.d.	0.1	0.1	5.0	0.4	100.0	54.8
		2	1276	55.1	27.3	10.9	n.d.	0.4	0.3	n.d.	n.d.	0.1	5.0	0.5	99.6	54.7
		2	1273	55.4	27.3	11.0	n.d.	0.2	0.1	n.d.	0.1	0.1	5.0	0.4	99.6	54.9
		1	1282	55.0	27.6	11.3	n.d.	0.4	n.d.	n.d.	n.d.	0.1	4.8	0.4	99.6	56.4
		1	1280	55.5	27.3	10.9	n.d.	0.3	n.d.	n.d.	n.d.	n.d.	4.9	0.5	99.5	55.2
		1	1278	55.3	27.1	10.7	n.d.	0.3	n.d.	n.d.	n.d.	0.1	5.0	0.4	98.9	53.9
144.04	PL-042	4	1263	54.8	27.7	11.4	n.d.	0.2	n.d.	n.d.	n.d.	0.1	4.8	0.4	99.3	56.9
		4	1262	54.5	27.8	11.3	n.d.	0.2	0.3	n.d.	n.d.	0.1	4.7	0.4	99.4	57.1
		2	1243	53.8	27.9	11.9	n.d.	0.4	n.d.	n.d.	n.d.	0.1	4.4	0.4	99.0	59.8
		2	1241	54.9	27.6	11.0	n.d.	0.4	n.d.	n.d.	n.d.	0.1	5.0	0.3	99.3	55.1
		1	1258	55.1	27.5	11.3	n.d.	0.3	n.d.	n.d.	n.d.	0.1	4.7	0.4	99.5	57.0
		1	1257	53.0	27.8	10.8	0.1	0.7	0.1	n.d.	n.d.	n.d.	4.1	0.8	97.4	59.1
		4	1265	55.3	27.7	11.1	n.d.	0.2	n.d.	n.d.	n.d.	0.1	4.9	0.4	99.7	55.6
169.37	PL-041	3	1228	54.2	27.8	11.7	n.d.	0.5	0.1	n.d.	n.d.	0.1	4.6	0.3	99.4	58.3
		3	1226	54.3	27.5	11.3	n.d.	0.2	n.d.	n.d.	n.d.	0.1	4.7	0.3	98.5	57.2
		2	1223	54.3	27.6	11.5	n.d.	0.5	0.1	n.d.	n.d.	0.1	4.6	0.3	99.2	57.9
		2	1221	53.9	28.2	11.9	n.d.	0.3	0.1	n.d.	n.d.	0.1	4.6	0.3	99.3	59.0
		2	1218	54.1	27.9	11.7	0.1	0.4	n.d.	n.d.	n.d.	0.1	4.6	0.3	99.2	58.6
		1	1237	54.5	27.3	11.1	n.d.	0.3	0.1	n.d.	n.d.	n.d.	4.8	0.4	98.4	56.2

Depth	Sample	Plag	Spot	SiO_2	Al_2O_3	CaO	MgO	FeO	TiO_2	MnO	BaO	SrO	Na_2O	K_2O	Total	An%
		1	1235	54.2	27.3	11.3	n.d.	0.3	n.d.	n.d.	n.d.	n.d.	4.7	0.3	98.2	57.0
		1	1232	54.5	27.6	11.2	n.d.	0.4	0.2	n.d.	n.d.	n.d.	4.8	0.4	99.0	56.1
190.55	PL-040	7	1169	54.4	27.8	11.4	n.d.	0.3	n.d.	n.d.	n.d.	n.d.	4.5	0.4	98.9	58.5
		7	1168	53.4	28.2	11.9	n.d.	0.4	0.1	n.d.	n.d.	n.d.	4.3	0.3	98.7	60.6
		7	1166	54.0	27.8	11.9	n.d.	0.3	n.d.	n.d.	n.d.	n.d.	4.3	0.4	98.7	60.5
		7	1164	53.4	28.3	12.1	n.d.	0.3	n.d.	n.d.	n.d.	n.d.	4.2	0.3	98.6	61.7
		5	1216	53.4	27.9	11.9	n.d.	0.3	n.d.	n.d.	0.1	0.1	4.3	0.4	98.4	60.5
		5	1214	53.3	27.7	12.0	n.d.	0.3	n.d.	n.d.	0.1	0.1	4.3	0.4	98.3	60.5
		5	1211	53.3	27.9	11.9	n.d.	0.4	0.1	n.d.	n.d.	n.d.	4.3	0.3	98.1	60.3
		3	1206	53.3	27.9	11.7	n.d.	0.2	0.1	n.d.	0.1	0.2	4.4	0.4	98.1	59.7
		3	1204	53.7	28.0	11.9	n.d.	0.4	n.d.	n.d.	n.d.	n.d.	4.3	0.4	98.6	60.7
		2	1192	53.5	27.9	11.8	n.d.	0.5	n.d.	n.d.	n.d.	0.1	4.2	0.4	98.3	60.5
		2	1189	53.8	27.8	11.6	n.d.	0.3	0.1	n.d.	n.d.	0.1	4.4	0.4	98.4	59.5
		1	1199	53.4	28.2	12.2	n.d.	0.3	0.1	n.d.	n.d.	0.1	4.2	0.3	98.9	61.9
		1	1196	53.4	28.0	12.2	n.d.	0.4	n.d.	n.d.	0.1	0.1	4.2	0.4	98.8	61.4
212.48	PL-039	4	1151	53.3	28.7	12.6	n.d.	0.4	0.1	n.d.	n.d.	n.d.	4.1	0.3	99.5	63.2
		4	1148	53.6	28.3	12.5	n.d.	0.4	0.1	n.d.	n.d.	0.1	4.3	0.4	99.6	61.8
		3	1135	53.7	28.3	12.1	n.d.	0.4	n.d.	n.d.	n.d.	n.d.	4.4	0.3	99.4	60.1
		3	1133	54.1	28.2	11.9	n.d.	0.3	0.1	n.d.	n.d.	0.1	4.4	0.4	99.5	60.1
		2	1146	54.5	28.3	11.9	n.d.	0.5	n.d.	n.d.	n.d.	0.1	4.4	0.4	100.2	59.7
		2	1145	53.9	28.2	11.7	n.d.	0.4	n.d.	n.d.	n.d.	0.1	4.3	0.4	99.0	60.0
		2	1143	54.1	28.2	12.2	n.d.	0.3	0.2	n.d.	n.d.	0.1	4.4	0.3	99.7	60.4
227	PL-038	3	1099	53.5	28.5	12.4	n.d.	0.2	n.d.	n.d.	n.d.	0.1	4.1	0.3	99.2	62.6
		3	1097	53.6	28.3	12.2	n.d.	0.3	n.d.	n.d.	n.d.	0.1	4.3	0.3	99.1	61.2
		3	1094	53.0	28.9	12.5	n.d.	0.5	n.d.	n.d.	n.d.	0.1	4.1	0.3	99.3	63.1
		2	1087	54.0	28.2	12.1	n.d.	0.3	n.d.	n.d.	n.d.	0.1	4.4	0.3	99.4	60.2
		1	1093	53.0	28.8	12.4	n.d.	0.3	0.1	n.d.	n.d.	0.1	4.2	0.3	99.3	62.3
		1	1092	53.3	28.6	12.5	n.d.	0.2	0.1	n.d.	n.d.	0.1	4.2	0.3	99.2	62.2
260.5	PL-037	6	1021	52.9	28.1	12.3	n.d.	0.4	0.1	n.d.	0.1	0.1	4.1	0.2	98.3	62.3
		4	1039	53.0	28.4	12.7	n.d.	0.3	0.1	n.d.	n.d.	n.d.	4.0	0.3	98.9	63.5
		4	1037	52.8	28.4	12.6	n.d.	0.3	n.d.	n.d.	n.d.	0.1	4.1	0.3	98.5	63.1
		4	1035	53.3	28.4	12.3	n.d.	0.2	n.d.	n.d.	n.d.	0.1	3.7	0.2	98.3	64.6
		1	1029	52.3	28.3	12.5	n.d.	0.4	0.1	n.d.	n.d.	n.d.	4.0	0.3	97.9	63.4
		1	1025	52.6	28.1	12.2	n.d.	0.2	n.d.	n.d.	n.d.	0.1	4.2	0.3	97.8	61.8
		3	993	53.3	28.7	12.7	n.d.	0.5	n.d.	n.d.	n.d.	0.1	4.0	0.3	99.6	63.9
		3	991	52.5	29.7	13.0	n.d.	0.2	0.2	n.d.	n.d.	0.1	3.6	0.3	99.7	66.6
		2	1000	52.7	28.8	12.9	n.d.	0.3	0.1	n.d.	n.d.	0.1	3.9	0.3	99.2	64.9
		2	998	51.7	29.7	13.7	n.d.	0.3	n.d.	n.d.	n.d.	0.1	3.5	0.2	99.2	68.4
		1	1009	52.2	29.0	13.3	n.d.	0.4	n.d.	n.d.	n.d.	0.1	3.8	0.2	99.1	66.1
		1	1006	52.4	29.0	13.1	n.d.	0.3	n.d.	n.d.	0.1	n.d.	3.9	0.2	99.0	65.1
		3	996	53.2	28.7	12.8	n.d.	0.4	n.d.	n.d.	n.d.	n.d.	3.9	0.3	99.5	64.4
323.16	PL-035	4	963	51.9	29.1	13.3	n.d.	0.9	0.1	n.d.	n.d.	0.1	3.7	0.2	99.2	66.5

Depth	Sample	Plag	Spot	SiO_2	Al_2O_3	CaO	MgO	FeO	TiO_2	MnO	BaO	SrO	Na_2O	K_2O	Total	An%
		4	961	52.7	28.7	13.0	n.d.	0.5	n.d.	n.d.	n.d.	n.d.	4.0	0.2	99.1	64.2
358	PL-034	7	930	52.2	29.3	13.1	n.d.	0.5	n.d.	n.d.	n.d.	n.d.	3.7	0.2	99.1	66.4
		3	923	51.5	29.3	13.5	n.d.	0.3	n.d.	n.d.	n.d.	0.1	3.5	0.2	98.5	68.1
		3	922	52.5	28.6	12.5	n.d.	0.5	0.2	n.d.	n.d.	0.1	3.9	0.3	98.7	63.7
		2	957	52.2	28.3	12.6	n.d.	0.4	n.d.	n.d.	0.1	0.1	4.0	0.3	97.8	63.7
		2	954	52.2	28.8	12.8	n.d.	0.3	0.1	n.d.	n.d.	0.1	4.0	0.3	98.5	64.1
		1	949	52.3	28.5	12.8	n.d.	0.4	n.d.	n.d.	n.d.	0.1	3.9	0.3	98.4	64.8
		1	947	52.1	28.3	12.4	n.d.	0.4	n.d.	n.d.	n.d.	0.1	3.9	0.3	97.5	63.8
		7	933	52.5	28.7	12.7	n.d.	0.2	0.1	n.d.	n.d.	0.1	4.0	0.3	98.7	63.7
384.1	PL-033	6	864	52.6	28.7	12.6	n.d.	0.4	0.1	n.d.	n.d.	n.d.	4.0	0.3	98.8	63.3
		5	875	52.7	28.6	12.7	n.d.	0.2	0.2	n.d.	n.d.	0.1	4.2	0.2	98.8	62.6
		5	871	52.0	28.9	12.6	n.d.	0.3	0.1	n.d.	n.d.	0.1	4.0	0.2	98.3	63.6
		4	898	52.0	29.1	13.0	n.d.	0.3	n.d.	n.d.	n.d.	0.1	3.8	0.3	98.6	65.7
		4	893	52.9	28.7	12.8	n.d.	0.5	n.d.	n.d.	n.d.	n.d.	4.0	0.3	99.4	63.9
		3	889	52.0	29.4	13.5	n.d.	0.6	0.2	n.d.	n.d.	0.1	3.7	0.2	99.7	66.6
		3	886	52.6	29.1	13.1	n.d.	0.4	0.1	n.d.	n.d.	0.1	3.9	0.3	99.7	65.3
		6	866	52.6	28.8	12.8	n.d.	0.4	n.d.	n.d.	n.d.	n.d.	4.0	0.3	98.9	64.0
410.78	PL-032	3	857	51.6	29.7	13.6	n.d.	0.4	0.1	n.d.	n.d.	0.1	3.6	0.2	99.2	67.9
		2	846	52.6	29.0	13.2	n.d.	0.4	n.d.	n.d.	n.d.	n.d.	3.9	0.2	99.4	65.4
		2	844	52.9	29.1	13.1	n.d.	0.6	0.3	n.d.	n.d.	n.d.	3.8	0.3	100.1	65.5
		2	843	51.7	29.8	13.9	n.d.	0.4	n.d.	n.d.	n.d.	n.d.	3.4	0.2	99.5	69.3
		1	839	52.1	29.8	13.9	n.d.	0.6	0.1	n.d.	n.d.	0.1	3.6	0.2	100.4	67.9
		3	859	51.4	29.6	13.7	n.d.	0.5	n.d.	n.d.	n.d.	0.1	3.4	0.2	99.1	68.8
		4	808	51.6	29.9	13.9	n.d.	0.2	n.d.	n.d.	n.d.	n.d.	3.3	0.3	99.2	70.0
		3	804	51.4	29.8	13.7	n.d.	0.2	n.d.	n.d.	n.d.	n.d.	3.3	0.2	98.8	69.7
		3	803	51.4	29.6	13.9	n.d.	0.4	n.d.	n.d.	n.d.	0.1	3.3	0.2	98.9	70.0
		2	826	51.2	29.7	14.0	n.d.	0.3	n.d.	n.d.	n.d.	0.1	3.3	0.3	98.9	70.3
		2	824	51.0	30.0	14.0	n.d.	0.5	0.1	n.d.	n.d.	0.1	3.2	0.3	99.1	71.1
		1	818	51.1	29.7	14.3	n.d.	0.4	0.1	n.d.	n.d.	0.1	3.2	0.2	99.1	71.3
		1	815	50.7	29.8	14.1	n.d.	0.2	0.2	n.d.	n.d.	n.d.	3.2	0.2	98.5	71.2
		4	811	50.7	30.1	14.1	n.d.	0.4	n.d.	n.d.	n.d.	n.d.	3.0	0.3	98.7	72.0
465.4	PL-030	6	790	51.6	29.8	14.0	n.d.	0.2	n.d.	n.d.	n.d.	n.d.	3.3	0.2	99.2	70.0
		5	800	51.2	30.3	13.8	n.d.	0.5	0.2	n.d.	n.d.	n.d.	3.2	0.2	99.4	70.8
		5	797	51.5	29.6	13.2	n.d.	0.2	n.d.	n.d.	n.d.	n.d.	3.4	0.2	98.2	68.2
		1	786	51.0	29.9	14.0	n.d.	0.3	n.d.	n.d.	n.d.	n.d.	3.1	0.2	98.5	71.4
		1	783	51.0	29.7	13.9	n.d.	0.3	0.2	n.d.	0.1	0.1	3.1	0.2	98.6	71.0
		6	793	51.7	29.6	13.5	n.d.	0.3	0.1	n.d.	0.1	0.1	3.5	0.3	99.1	68.4
506.71	PL-028	1	742	51.4	30.0	14.0	n.d.	0.3	n.d.	n.d.	n.d.	0.1	3.2	0.2	99.2	70.7
		1	740	51.4	30.0	14.1	n.d.	0.4	0.1	n.d.	n.d.	0.2	3.2	0.2	99.6	71.0
		2	750	50.8	29.3	13.8	n.d.	0.4	0.1	n.d.	0.1	0.1	3.4	0.2	98.1	69.5
531.74	PL-027	5	707	51.5	29.7	13.5	n.d.	0.2	n.d.	n.d.	0.1	n.d.	3.6	0.2	98.8	67.5
		4	703	51.7	29.0	13.1	n.d.	0.2	n.d.	n.d.	n.d.	n.d.	3.7	0.1	98.3	66.3

Depth	Sample	Plag	Spot	SiO_2	Al_2O_3	CaO	MgO	FeO	TiO_2	MnO	BaO	SrO	Na_2O	K_2O	Total	An%
		4	701	52.4	28.7	12.6	n.d.	0.3	n.d.	n.d.	n.d.	0.1	4.0	0.3	98.5	63.6
		2	716	51.8	29.7	13.6	n.d.	0.3	n.d.	n.d.	n.d.	n.d.	3.4	0.2	99.1	69.0
		2	715	51.4	30.1	13.8	n.d.	0.3	n.d.	n.d.	n.d.	0.1	3.3	0.2	99.2	70.1
		2	713	52.8	29.6	13.1	n.d.	0.3	n.d.	n.d.	n.d.	0.1	3.6	0.3	99.9	66.6
		1	696	51.4	30.0	14.1	n.d.	0.2	0.2	n.d.	n.d.	0.1	3.3	0.2	99.4	70.4
		5	709	52.1	29.5	13.2	n.d.	0.3	0.1	n.d.	n.d.	n.d.	3.6	0.3	99.1	67.1
572.63	PL-025	2	662	53.7	28.9	12.2	n.d.	0.2	0.1	n.d.	n.d.	0.1	4.5	0.2	99.9	59.9
		1	642	53.7	28.8	12.4	n.d.	0.3	n.d.	n.d.	n.d.	0.1	4.3	0.4	100.1	61.7
		1	641	52.8	28.9	12.8	n.d.	0.5	0.3	n.d.	n.d.	0.1	3.9	0.4	99.7	64.7
		1	640	53.0	29.4	13.1	n.d.	0.3	n.d.	n.d.	n.d.	0.1	3.8	0.4	100.1	65.6
595.03	PL-024	1	619	51.5	29.0	13.1	n.d.	0.3	0.1	n.d.	0.1	n.d.	3.8	0.2	98.1	65.8
		3	632	51.4	28.9	13.3	n.d.	0.1	0.1	n.d.	n.d.	0.1	3.7	0.2	97.9	66.4
		3	631	52.3	28.0	12.5	n.d.	0.1	n.d.	n.d.	n.d.	0.1	4.4	0.3	97.7	61.2
		2	627	52.2	29.7	13.6	n.d.	0.3	n.d.	n.d.	n.d.	n.d.	3.6	0.2	99.6	67.5
		2	625	51.2	29.3	13.4	n.d.	0.6	0.1	n.d.	n.d.	0.1	3.6	0.2	98.5	67.4
		3	634	51.0	28.9	13.3	n.d.	0.1	0.2	n.d.	n.d.	0.1	3.5	0.2	97.4	67.6
612.7	PL-023	3	607	52.9	29.3	12.8	n.d.	0.2	n.d.	n.d.	n.d.	0.1	3.8	0.3	99.2	65.2
635.83	PL-022	4	561	52.8	28.7	12.7	n.d.	0.1	n.d.	n.d.	n.d.	n.d.	3.9	0.2	98.5	64.4
		3	590	52.5	29.4	13.1	n.d.	0.4	n.d.	n.d.	n.d.	n.d.	3.6	0.3	99.3	66.7
		3	586	52.2	29.7	13.2	n.d.	0.2	0.1	n.d.	n.d.	0.1	3.7	0.2	99.5	66.7
		2	570	53.4	29.0	12.4	n.d.	0.2	n.d.	n.d.	n.d.	0.2	4.2	0.2	99.6	62.0
		2	567	53.1	28.9	12.7	n.d.	0.1	n.d.	n.d.	0.1	n.d.	4.0	0.3	99.1	63.8
		1	576	51.8	29.2	13.2	n.d.	0.1	n.d.	n.d.	n.d.	0.1	3.7	0.2	98.4	66.4
		1	574	52.4	29.5	13.1	n.d.	0.2	0.1	n.d.	n.d.	0.1	3.7	0.3	99.5	66.2
		4	563	53.6	28.8	12.5	n.d.	0.2	0.1	n.d.	n.d.	n.d.	4.3	0.3	99.7	61.8
659.33	PL-021	3	557	54.1	28.0	11.7	n.d.	0.3	0.1	n.d.	n.d.	n.d.	4.4	0.4	99.1	59.6
		3	556	53.7	28.1	12.1	n.d.	0.2	n.d.	n.d.	n.d.	0.1	4.4	0.4	99.2	60.2
		3	555	54.0	28.1	11.9	n.d.	0.2	n.d.	n.d.	n.d.	0.1	4.4	0.3	99.1	59.7
		2	545	54.5	27.7	11.7	n.d.	0.3	0.1	n.d.	n.d.	n.d.	4.6	0.4	99.5	58.2
		2	544	53.7	28.1	11.6	n.d.	0.2	n.d.	n.d.	n.d.	0.1	4.5	0.3	98.6	58.8
		2	542	54.9	27.8	11.3	n.d.	0.4	0.1	n.d.	0.1	n.d.	4.7	0.4	99.6	57.2
		1	551	54.4	27.8	11.5	n.d.	0.2	n.d.	n.d.	n.d.	0.1	4.7	0.4	99.2	57.5
		1	550	53.9	28.1	11.9	n.d.	0.1	n.d.	n.d.	n.d.	0.1	4.4	0.4	99.0	59.9
		1	549	54.5	28.2	11.5	n.d.	0.1	n.d.	n.d.	n.d.	0.1	4.6	0.4	99.5	57.9
678.05	PL-020	3	540	54.8	27.6	11.4	n.d.	0.2	n.d.	n.d.	n.d.	0.1	4.7	0.4	99.3	57.5
		3	538	54.6	27.4	11.5	n.d.	0.3	0.1	n.d.	n.d.	0.1	4.5	0.3	98.9	58.6
		3	534	54.4	27.8	11.5	n.d.	n.d.	n.d.	n.d.	0.1	0.1	4.5	0.4	98.8	58.5
		2	530	53.6	28.2	11.8	n.d.	0.1	0.1	n.d.	n.d.	0.1	4.7	0.2	98.8	57.9
		2	529	53.5	28.3	11.9	n.d.	n.d.	n.d.	n.d.	n.d.	0.1	4.5	0.2	98.5	59.2
		2	528	53.5	27.8	11.5	n.d.	0.2	n.d.	n.d.	n.d.	0.1	4.9	0.2	98.2	56.5
		1	525	54.2	27.7	11.4	n.d.	0.2	n.d.	n.d.	n.d.	0.1	4.7	0.4	98.8	57.3
		1	523	54.2	27.5	11.4	n.d.	0.1	n.d.	n.d.	0.1	0.1	4.6	0.4	98.4	57.7

Depth	Sample	Plag	Spot	SiO_2	Al_2O_3	CaO	MgO	FeO	TiO_2	MnO	BaO	SrO	Na_2O	K_2O	Total	An%
		1	520	53.6	27.5	11.5	n.d.	0.1	0.1	n.d.	n.d.	n.d.	4.6	0.4	97.7	58.1
697.26	PL-019	4	499	53.8	27.2	10.9	n.d.	0.6	n.d.	n.d.	n.d.	n.d.	4.5	0.3	97.7	57.1
		2	495	54.5	27.7	11.3	n.d.	0.2	0.1	n.d.	n.d.	n.d.	4.7	0.3	98.8	56.8
		2	494	54.2	28.0	11.5	n.d.	n.d.	0.1	n.d.	n.d.	0.1	4.6	0.3	98.8	58.3
		2	492	54.4	27.7	11.5	n.d.	n.d.	n.d.	n.d.	n.d.	0.1	4.9	0.4	99.0	56.6
		1	488	54.5	27.5	11.2	n.d.	0.2	0.1	n.d.	0.1	0.1	4.9	0.3	98.8	55.9
		1	487	54.7	27.5	11.4	n.d.	0.3	n.d.	n.d.	n.d.	0.1	4.7	0.3	99.1	57.2
		1	486	54.2	27.7	11.4	n.d.	0.2	0.2	n.d.	n.d.	0.1	4.6	0.4	98.9	57.9
		4	501	53.8	28.1	11.7	n.d.	0.1	0.2	n.d.	n.d.	n.d.	4.6	0.4	99.0	58.5
722.5	PL-018	3	478	55.0	27.3	11.2	n.d.	0.2	n.d.	n.d.	n.d.	0.2	5.0	0.4	99.2	55.4
		3	475	54.5	27.9	11.7	n.d.	0.1	n.d.	n.d.	n.d.	n.d.	4.6	0.4	99.2	58.2
		2	471	53.5	28.1	11.5	n.d.	0.1	n.d.	n.d.	n.d.	n.d.	5.0	0.2	98.3	56.3
		2	470	54.1	27.8	11.2	n.d.	0.1	0.1	n.d.	n.d.	0.1	5.1	0.2	98.7	55.0
		2	469	53.2	28.5	12.0	n.d.	0.1	n.d.	n.d.	n.d.	n.d.	4.7	0.2	98.7	58.4
		2	468	53.3	28.0	11.7	n.d.	0.1	n.d.	n.d.	0.1	0.1	4.9	0.2	98.3	57.0
		1	465	54.1	27.9	11.4	n.d.	0.2	n.d.	n.d.	n.d.	0.1	5.0	0.2	98.9	55.9
		1	464	54.4	27.9	11.3	n.d.	0.2	0.1	n.d.	n.d.	0.1	5.0	0.2	99.3	55.5
		1	462	53.6	28.2	11.7	n.d.	0.1	n.d.	n.d.	n.d.	0.1	4.9	0.2	98.8	57.2
740.74	PL-017	5	449	52.7	28.1	12.1	n.d.	0.2	n.d.	n.d.	n.d.	0.1	4.1	0.4	97.7	61.7
		2	431	54.9	27.7	11.4	n.d.	0.2	n.d.	n.d.	n.d.	n.d.	4.4	0.4	98.9	58.8
		2	430	53.5	28.5	12.2	n.d.	n.d.	0.1	n.d.	n.d.	n.d.	4.2	0.4	99.0	61.5
		2	429	53.3	28.6	12.3	n.d.	0.3	0.1	n.d.	n.d.	0.1	4.1	0.3	99.2	62.4
		1	445	53.5	28.3	12.2	n.d.	0.2	n.d.	n.d.	n.d.	0.1	4.3	0.3	98.9	61.3
		1	443	53.0	28.8	12.6	n.d.	0.2	0.3	n.d.	n.d.	n.d.	4.0	0.3	99.2	63.4
779.8	PL-015	3	428	53.0	27.6	11.5	n.d.	0.2	n.d.	n.d.	n.d.	0.1	4.5	0.3	97.3	58.4
		3	427	54.6	28.1	11.5	n.d.	0.2	0.1	0.1	0.1	n.d.	4.6	0.3	99.6	57.9
		2	421	54.6	28.1	11.3	n.d.	0.2	0.1	n.d.	n.d.	n.d.	4.9	0.3	99.5	56.0
		2	418	54.0	28.0	11.4	n.d.	0.3	0.4	n.d.	0.1	0.1	4.4	0.4	99.2	58.6
		2	416	54.9	27.8	10.9	n.d.	n.d.	0.4	n.d.	0.1	0.1	5.0	0.3	99.4	54.9
		1	425	55.1	27.5	11.1	n.d.	0.1	n.d.	n.d.	n.d.	0.1	4.9	0.4	99.2	55.4
		1	424	54.0	27.9	11.5	n.d.	0.1	n.d.	n.d.	0.1	0.1	4.6	0.4	98.8	58.0
825.79	PL-014	3	399	54.9	28.0	11.2	n.d.	0.1	n.d.	n.d.	n.d.	n.d.	5.0	0.3	99.3	55.5
		3	398	54.9	28.1	11.4	n.d.	0.1	0.2	n.d.	n.d.	0.1	4.9	0.3	100.1	56.2
		3	397	54.9	28.3	11.4	n.d.	0.1	n.d.	n.d.	0.1	0.1	5.0	0.2	100.1	55.8
		2	405	55.1	27.8	11.1	n.d.	n.d.	0.1	n.d.	n.d.	0.1	5.0	0.2	99.4	54.8
		2	404	56.2	27.2	10.3	n.d.	n.d.	n.d.	n.d.	n.d.	0.1	5.4	0.3	99.6	51.3
		2	403	55.8	27.4	10.3	n.d.	0.1	n.d.	n.d.	n.d.	n.d.	5.4	0.2	99.3	51.5
		1	412	54.9	27.3	10.9	n.d.	0.1	n.d.	n.d.	n.d.	0.1	5.2	0.3	98.9	53.9
		1	411	55.3	27.6	11.0	n.d.	0.2	n.d.	n.d.	n.d.	0.1	5.0	0.3	99.5	55.0
855.62	PL-013	4	384	53.6	29.0	12.3	n.d.	0.1	0.2	n.d.	n.d.	0.1	4.3	0.2	99.9	61.1
		3	393	53.3	29.3	12.6	n.d.	0.1	n.d.	n.d.	n.d.	0.1	4.1	0.3	99.9	63.1
		3	391	53.4	29.1	12.8	n.d.	0.1	n.d.	n.d.	n.d.	n.d.	4.1	0.3	99.9	63.3

Depth	Sample	Plag	Spot	SiO_2	Al_2O_3	CaO	MgO	FeO	TiO_2	MnO	BaO	SrO	Na_2O	K_2O	Total	An%
		2	380	53.6	28.8	12.3	n.d.	0.2	n.d.	n.d.	n.d.	n.d.	4.2	0.3	99.5	62.0
		2	378	53.9	28.6	11.9	n.d.	n.d.	n.d.	n.d.	n.d.	0.1	4.3	0.3	99.2	60.4
		1	374	53.8	28.8	12.2	n.d.	0.1	0.1	n.d.	n.d.	n.d.	4.3	0.3	99.6	61.0
		1	372	53.2	29.6	12.7	n.d.	0.3	n.d.	n.d.	n.d.	n.d.	3.9	0.2	100.0	64.1
		4	385	53.3	29.2	12.8	n.d.	n.d.	n.d.	n.d.	n.d.	n.d.	4.0	0.2	99.6	63.7
879.23	PL-012	3	364	53.7	28.2	11.9	n.d.	0.1	n.d.	n.d.	n.d.	0.1	4.5	0.4	98.8	59.5
		3	362	53.4	28.5	12.3	n.d.	0.3	n.d.	n.d.	n.d.	0.1	4.3	0.3	99.3	61.1
		2	371	51.8	28.0	12.4	n.d.	n.d.	0.1	n.d.	0.1	n.d.	4.1	0.3	96.8	62.6
		2	370	54.4	28.3	11.9	n.d.	0.2	0.1	n.d.	n.d.	0.1	4.5	0.3	99.9	59.3
		2	369	53.3	28.9	12.3	n.d.	0.1	n.d.	n.d.	n.d.	0.1	4.1	0.3	99.2	62.5
		1	355	53.8	28.7	12.1	n.d.	0.1	0.2	n.d.	0.1	0.1	4.3	0.3	99.7	61.1
		3	365	54.5	28.1	11.6	n.d.	0.1	0.1	n.d.	n.d.	0.1	4.5	0.3	99.3	59.0
899.43	PL-011	7	351	54.0	28.6	11.9	n.d.	0.2	n.d.	n.d.	n.d.	0.1	4.4	0.3	99.5	59.7
		7	349	54.8	28.5	11.7	n.d.	0.1	n.d.	n.d.	n.d.	0.1	4.6	0.3	100.2	58.3
		7	347	53.8	28.8	12.3	n.d.	0.2	n.d.	n.d.	n.d.	n.d.	4.2	0.2	99.6	61.6
		4	331	53.7	28.7	12.2	n.d.	0.2	n.d.	n.d.	n.d.	0.1	4.4	0.3	99.6	60.8
		4	328	53.4	29.0	12.9	n.d.	0.3	0.1	n.d.	n.d.	0.1	4.0	0.2	100.0	64.2
		3	326	54.3	28.5	11.8	n.d.	0.2	n.d.	n.d.	n.d.	0.1	4.6	0.2	99.6	58.8
		3	324	53.6	28.8	12.4	n.d.	0.3	n.d.	n.d.	n.d.	0.1	4.3	0.2	99.7	61.8
		3	322	53.4	28.6	12.4	n.d.	0.2	0.1	n.d.	n.d.	n.d.	4.3	0.2	99.3	61.6
916.38	PL-010	5	284	52.8	28.7	12.4	n.d.	0.4	n.d.	n.d.	n.d.	0.1	4.1	0.3	98.9	62.5
		4	290	53.2	28.3	12.1	n.d.	n.d.	0.1	n.d.	n.d.	n.d.	4.3	0.3	98.4	60.9
		5	285	53.3	28.4	12.3	n.d.	0.2	0.1	n.d.	n.d.	n.d.	4.2	0.3	98.9	61.7
943.14	PL-009	5	268	52.8	28.9	12.5	n.d.	0.2	0.1	n.d.	n.d.	0.1	4.2	0.1	99.0	62.1
		3	263	52.9	28.4	12.4	n.d.	0.2	n.d.	n.d.	n.d.	0.1	4.2	0.2	98.4	62.2
		3	261	53.6	28.2	11.7	n.d.	0.2	0.1	n.d.	n.d.	0.1	4.5	0.3	98.6	59.2
		3	259	53.8	28.1	11.9	n.d.	0.1	n.d.	n.d.	n.d.	0.1	4.4	0.3	98.8	59.8
		2	257	53.7	28.2	12.0	n.d.	n.d.	n.d.	n.d.	n.d.	n.d.	4.4	0.2	98.6	60.1
		2	255	53.1	28.5	12.2	n.d.	0.0	0.2	n.d.	n.d.	0.1	4.3	0.2	98.6	60.8
		2	253	53.1	28.3	12.1	n.d.	0.1	0.1	n.d.	n.d.	0.1	4.3	0.2	98.3	60.6
		5	275	53.2	28.4	11.9	n.d.	0.2	n.d.	n.d.	n.d.	0.1	4.6	0.2	98.5	59.1
958.64	PL-008	5	233	53.7	28.1	12.0	n.d.	0.1	n.d.	n.d.	n.d.	0.1	4.4	0.3	98.7	60.1
		4	243	53.1	28.7	12.4	n.d.	0.1	n.d.	n.d.	n.d.	0.2	4.1	0.3	98.9	62.3
		4	239	52.7	28.5	12.3	n.d.	0.1	n.d.	n.d.	n.d.	0.1	4.0	0.3	98.1	63.3
		2	215	52.6	29.1	12.8	n.d.	0.1	0.1	n.d.	0.1	n.d.	3.9	0.2	98.9	64.7
		2	212	53.2	29.0	12.4	n.d.	0.1	0.1	n.d.	n.d.	0.1	4.0	0.3	99.4	63.0
		1	208	52.9	29.0	12.7	n.d.	0.1	0.2	n.d.	n.d.	n.d.	3.8	0.3	99.0	64.8
		1	204	52.6	29.4	13.3	n.d.	0.3	n.d.	n.d.	n.d.	0.1	3.8	0.3	99.8	66.2
982.3	PL-007	4	195	54.7	28.0	11.5	n.d.	0.1	n.d.	n.d.	0.1	0.1	4.7	0.3	99.4	57.2
		4	194	55.4	27.6	11.1	n.d.	0.1	n.d.	n.d.	0.1	0.1	4.9	0.4	99.6	55.6
		3	188	54.4	28.1	11.5	n.d.	0.1	n.d.	n.d.	n.d.	0.1	4.5	0.4	99.1	58.4
		3	186	54.9	27.5	11.3	n.d.	0.2	n.d.	n.d.	n.d.	0.2	4.9	0.4	99.3	56.2

Depth	Sample	Plag	Spot	SiO_2	Al_2O_3	CaO	MgO	FeO	TiO_2	MnO	BaO	SrO	Na_2O	K_2O	Total	An%
		3	183	55.1	28.0	11.4	n.d.	0.2	0.1	n.d.	0.1	0.1	4.5	0.4	99.8	58.2
		2	181	54.9	27.6	11.0	n.d.	0.2	n.d.	n.d.	n.d.	0.1	4.8	0.4	99.1	55.8
		2	179	53.9	28.5	11.9	n.d.	0.2	0.2	n.d.	0.1	0.1	4.5	0.2	99.6	59.5
		2	174	54.5	27.7	11.4	n.d.	0.2	n.d.	n.d.	0.1	0.1	4.7	0.3	99.0	57.3
1026.6	PL-005	3	143	51.7	29.7	13.7	n.d.	n.d.	0.1	n.d.	n.d.	0.1	3.6	0.2	99.1	68.1
		2	110	49.8	30.4	14.3	n.d.	0.2	n.d.	n.d.	n.d.	0.1	3.2	0.1	98.2	71.4
		2	106	53.6	28.6	11.9	n.d.	0.2	n.d.	n.d.	n.d.	0.1	4.3	0.1	99.0	60.3
		1	138	53.0	28.4	12.2	n.d.	0.1	0.1	0.1	n.d.	0.2	4.4	0.2	98.7	60.6
		3	135	51.9	29.5	13.3	n.d.	0.1	0.1	n.d.	n.d.	0.1	3.7	0.3	99.1	66.5
		3	146	51.2	28.6	13.1	n.d.	0.2	n.d.	n.d.	n.d.	0.1	3.9	0.2	97.4	64.8
1050.26	PL-004	3	90	54.4	28.9	12.2	n.d.	n.d.	n.d.	n.d.	n.d.	n.d.	4.5	0.2	100.3	60.2
		2	100	54.0	29.0	12.4	n.d.	0.1	0.1	n.d.	n.d.	0.1	4.1	0.3	100.1	62.7
		1	85	54.2	28.4	12.1	n.d.	0.2	n.d.	n.d.	n.d.	0.1	4.4	0.3	99.9	60.5
		1	83	53.6	29.6	13.2	n.d.	0.1	n.d.	n.d.	n.d.	0.1	4.0	0.3	100.8	64.8
		3	95	54.5	29.0	12.2	n.d.	n.d.	n.d.	n.d.	n.d.	0.1	4.4	0.2	100.4	60.6
1069.65	PL-003	4	49	54.6	28.7	12.2	n.d.	0.1	0.1	n.d.	0.1	n.d.	4.3	0.4	100.5	61.1
		3	70	55.1	28.6	12.0	n.d.	n.d.	n.d.	n.d.	n.d.	0.1	4.5	0.4	100.8	59.9
		3	68	53.9	28.8	12.2	n.d.	n.d.	n.d.	n.d.	n.d.	0.1	4.3	0.4	99.8	60.9
		2	60	54.5	28.7	12.0	n.d.	0.2	0.1	n.d.	n.d.	n.d.	4.6	0.2	100.3	58.9
		2	58	54.8	28.8	12.0	n.d.	0.2	n.d.	n.d.	n.d.	0.1	4.4	0.2	100.6	60.0
		1	77	54.6	28.4	11.7	n.d.	0.3	n.d.	n.d.	n.d.	0.1	4.6	0.4	100.1	58.4
		1	74	55.2	28.6	11.7	n.d.	0.1	n.d.	n.d.	n.d.	n.d.	4.7	0.2	100.6	58.2
		4	51	54.6	28.7	12.2	n.d.	n.d.	n.d.	n.d.	0.1	0.1	4.4	0.3	100.4	60.7
1092.85	PL-002	3	39	55.3	27.9	11.3	n.d.	0.2	n.d.	n.d.	n.d.	0.1	4.6	0.5	99.9	57.3
		3	37	55.2	28.3	11.4	n.d.	0.3	n.d.	n.d.	0.1	n.d.	4.6	0.5	100.4	57.5
		3	35	55.4	28.1	11.2	n.d.	0.1	0.1	n.d.	n.d.	0.1	4.7	0.5	100.3	56.7
		3	32	55.0	28.2	11.9	n.d.	0.1	0.1	n.d.	n.d.	0.1	4.6	0.5	100.4	59.0
		1	30	55.7	27.3	10.7	n.d.	n.d.	n.d.	n.d.	0.1	0.2	5.0	0.6	99.6	54.5
		1	28	55.7	27.6	10.8	n.d.	0.2	0.1	n.d.	n.d.	0.1	5.0	0.4	99.9	54.3
		1	25	55.6	28.2	11.5	n.d.	0.3	0.2	n.d.	n.d.	n.d.	4.7	0.3	100.9	57.4
1117.68	PL-001	4	8	54.1	28.1	11.9	n.d.	0.2	0.1	n.d.	n.d.	0.1	4.5	0.3	99.3	59.6
		4	2	53.6	28.3	12.0	n.d.	0.1	n.d.	n.d.	0.1	0.1	4.4	0.2	98.8	60.2
		3	20	53.9	28.7	12.2	n.d.	0.2	n.d.	n.d.	n.d.	0.1	4.4	0.3	99.8	60.8
		3	18	54.2	28.1	11.4	n.d.	0.4	n.d.	n.d.	n.d.	n.d.	4.6	0.4	99.1	57.9
		3	17	53.9	29.2	12.5	n.d.	0.2	0.1	n.d.	n.d.	n.d.	4.3	0.3	100.5	62.0
		2	13	54.5	27.8	11.2	n.d.	0.3	0.1	n.d.	n.d.	0.1	4.9	0.3	99.2	55.8
		2	12	53.5	28.9	12.4	n.d.	0.2	0.1	n.d.	n.d.	0.1	4.1	0.3	99.5	62.8
		2	10	53.8	28.1	11.9	n.d.	n.d.	0.1	n.d.	n.d.	0.1	4.4	0.2	98.6	60.0

Appendix B

Table B-1: The trace element composition of individual spots from plagioclase analyses. This table includes the following traces elements: Rb, Sr, Y, Zr, Ba, La, Ce, Pr, Nd, Sm, and Eu. Sample depths are reported in meters (m). All concentrations are reported in parts per million (ppm).

Sample	Plag	Spot #	Depth	^{85}Rb	^{88}Sr	^{89}Y	^{90}Zr	^{137}Ba	^{139}La	^{140}Ce	^{141}Pr	^{144}Nd	^{152}Sm	^{153}Eu
PL-046	6	1359	67.84	2.99	407.20	0.20	0.01	205.00	4.49	6.82	0.60	1.95	0.21	0.97
	3	1341	67.84	4.57	428.70	0.23	0.03	185.67	4.15	6.02	0.53	1.88	0.21	0.93
	3	1337	67.84	49.27	463.27	0.28	0.01	340.95	3.31	5.11	0.47	1.63	0.22	0.73
	2	1348	67.84	3.36	410.23	0.13	0.03	176.17	4.37	6.85	0.57	1.96	0.19	0.92
	2	1345	67.84	2.95	406.07	0.12	0.01	165.13	5.56	7.37	0.53	1.99	0.17	0.94
	6	1362	67.84	2.84	413.97	0.16	0.03	196.73	4.98	7.21	0.58	1.88	0.21	0.93
PL-044	5	1317	100.7	4.17	391.70	0.23	< d.l.	158.87	3.25	5.71	0.52	1.84	0.26	0.70
	5	1315	100.7	6.81	372.70	0.15	0.01	130.07	3.02	5.43	0.49	1.78	0.22	0.66
	2	1295	100.7	5.32	429.13	0.33	0.05	161.37	2.70	4.50	0.43	1.65	0.25	0.73
	2	1292	100.7	5.22	435.43	0.30	0.02	163.97	3.60	5.94	0.54	1.96	0.24	0.75
	1	1329	100.7	5.10	469.80	0.29	0.06	118.35	3.99	6.58	0.59	2.12	0.27	0.77
	1	1326	100.7	5.11	434.03	0.37	1.43	172.03	4.29	7.11	0.65	2.35	0.30	0.77
	1	1322	100.7	20.37	420.13	0.22	0.04	207.85	3.15	5.63	0.52	1.91	0.28	0.69
PL-043	3	1291	126.36	3.21	437.83	0.38	0.01	175.67	5.16	8.88	0.82	3.01	0.42	0.76
	3	1288	126.36	3.42	445.83	0.49	0.07	183.27	5.19	8.98	0.87	3.10	0.42	0.76
	2	1276	126.36	4.15	411.50	0.35	0.01	163.73	2.49	4.23	0.43	1.53	0.24	0.75
	2	1273	126.36	4.41	422.00	0.43	0.12	147.67	2.41	4.19	0.39	1.49	0.25	0.72
	1	1282	126.36	3.53	432.75	0.41	0.02	171.40	4.51	8.15	0.77	2.77	0.39	0.71
	1	1280	126.36	4.69	395.83	0.49	0.22	138.57	3.69	6.17	0.57	2.29	0.33	0.73
	1	1278	126.36	4.19	369.73	0.32	0.07	141.43	3.13	5.85	0.55	2.05	0.30	0.66
PL-042	4	1263	144.04	2.80	441.70	0.34	0.01	160.60	4.35	7.32	0.70	2.29	0.25	0.75
	4	1262	144.04	2.90	420.33	0.29	0.02	162.77	4.17	6.78	0.63	2.27	0.27	0.73
	2	1243	144.04	2.56	410.13	0.26	0.17	154.43	4.00	6.61	0.60	2.09	0.28	0.74
	2	1241	144.04	2.77	417.77	0.36	0.04	148.63	3.75	6.06	0.59	2.10	0.26	0.70
	1	1258	144.04	3.46	421.90	0.29	0.02	151.17	2.35	3.72	0.39	1.43	0.18	0.72
	1	1257	144.04	4.48	406.83	0.36	0.40	159.50	4.00	6.81	0.60	2.33	0.27	0.71
	4	1265	144.04	3.06	393.37	0.32	0.02	159.33	4.12	6.60	0.61	2.28	0.27	0.72
PL-041	3	1228	169.37	2.84	403.00	0.53	0.02	147.87	4.96	8.67	0.80	3.21	0.44	0.72
	3	1226	169.37	3.64	385.97	0.56	0.05	138.63	4.63	8.06	0.75	2.91	0.43	0.70
	2	1223	169.37	2.59	398.90	0.54	0.01	142.37	4.24	7.62	0.76	2.74	0.45	0.68
	2	1221	169.37	2.59	394.33	0.53	0.01	136.07	4.13	7.52	0.72	2.66	0.42	0.64
	2	1218	169.37	3.46	269.87	0.45	0.01	102.59	3.25	5.78	0.57	2.15	0.31	0.54
	1	1237	169.37	3.41	437.57	0.72	0.25	150.30	4.11	7.37	0.71	2.64	0.43	0.69
	1	1235	169.37	14.62	416.40	0.65	1.00	141.35	3.13	5.93	0.54	2.19	0.38	0.71
	1	1232	169.37	3.00	413.83	0.52	0.04	147.20	4.34	7.76	0.75	2.75	0.41	0.69
PL-040	7	1166	190.55	2.97	392.73	0.15	0.01	134.13	2.97	4.86	0.43	1.38	0.18	0.66
	7	1164	190.55	2.65	374.27	0.15	< d.l.	123.50	2.76	4.54	0.41	1.35	0.19	0.65

Sample	Plag	Spot #	Depth	^{85}Rb	^{88}Sr	^{89}Y	^{90}Zr	^{137}Ba	^{139}La	^{140}Ce	^{141}Pr	^{144}Nd	^{152}Sm	^{153}Eu
	5	1216	190.55	2.29	427.73	0.18	0.02	138.20	3.24	5.23	0.46	1.64	0.18	0.71
	5	1214	190.55	2.13	436.93	0.19	0.03	143.40	3.20	5.25	0.48	1.65	0.19	0.67
	5	1211	190.55	1.85	432.20	0.16	0.02	142.47	3.79	5.77	0.48	1.68	0.21	0.68
	3	1206	190.55	1.48	423.23	0.15	< d.l.	149.70	4.36	6.38	0.54	1.72	0.17	0.67
	3	1204	190.55	1.47	416.07	0.19	0.01	142.83	4.48	6.50	0.50	1.70	0.18	0.69
	2	1192	190.55	1.50	393.47	0.19	0.02	139.43	3.68	5.65	0.49	1.68	0.20	0.71
	2	1189	190.55	1.57	408.37	0.15	0.01	143.03	3.79	5.83	0.49	1.67	0.19	0.69
	1	1199	190.55	2.72	448.70	0.18	< d.l.	133.30	2.92	4.87	0.42	1.54	0.21	0.68
	1	1196	190.55	1.72	424.83	0.17	0.01	147.53	2.73	4.67	0.42	1.58	0.19	0.71
PL-039	4	1148	212.48	6.06	411.97	0.20	0.01	147.67	3.57	5.95	0.51	1.70	0.22	0.78
	3	1135	212.48	6.19	474.17	0.19	0.11	177.83	6.34	9.03	0.71	2.20	0.24	0.89
	3	1133	212.48	6.06	458.23	0.20	0.01	184.57	5.55	8.48	0.66	1.98	0.18	0.82
	2	1145	212.48	6.80	481.37	0.25	0.02	185.73	4.62	7.26	0.61	2.04	0.24	0.94
	2	1143	212.48	12.37	454.57	0.19	0.03	195.87	6.02	8.74	0.70	2.18	0.21	0.90
PL-038	3	1099	227	14.27	477.40	0.20	0.69	140.15	7.76	10.05	0.80	2.50	0.25	0.79
	3	1097	227	4.46	489.30	0.22	0.07	160.03	5.33	7.71	0.63	2.28	0.23	0.74
	3	1094	227	5.90	485.10	0.23	0.08	171.80	4.60	7.05	0.61	2.15	0.26	0.75
	2	1087	227	4.75	443.90	0.19	< d.l.	135.23	7.04	9.04	0.65	2.22	0.20	0.72
	1	1093	227	6.77	464.17	0.18	0.02	169.23	6.52	8.93	0.69	2.37	0.21	0.75
	1	1092	227	4.80	480.67	0.20	0.07	158.63	6.08	8.64	0.70	2.36	0.23	0.77
PL-037	6	1021	260.5	1.94	375.47	0.15	0.02	72.73	4.97	6.78	0.49	1.59	0.16	0.56
	4	1039	260.5	2.95	363.37	0.18	0.04	107.63	4.21	6.45	0.54	1.74	0.16	0.58
	4	1037	260.5	3.38	345.83	0.20	0.62	99.38	4.43	6.81	0.55	1.74	0.18	0.55
	4	1035	260.5	2.64	348.77	0.14	0.03	98.19	3.08	5.23	0.46	1.50	0.15	0.54
	1	1029	260.5	2.25	392.90	0.17	0.03	124.83	3.89	5.94	0.48	1.74	0.20	0.62
	1	1025	260.5	1.85	401.83	0.16	0.01	118.87	2.61	4.28	0.39	1.40	0.16	0.57
PL-036	3	991	297.95	2.86	407.70	0.15	0.01	115.10	4.22	6.33	0.52	1.65	0.20	0.49
	2	1000	297.95	2.74	340.77	0.21	0.02	105.90	4.03	6.36	0.55	1.72	0.16	0.49
	2	998	297.95	3.26	357.47	0.15	0.01	112.87	3.82	6.12	0.48	1.63	0.17	0.47
	1	1009	297.95	3.20	353.57	0.17	0.02	98.58	3.61	5.62	0.50	1.67	0.16	0.49
	1	1006	297.95	30.62	343.25	0.15	0.36	118.10	5.27	7.33	0.54	1.73	0.18	0.45
	3	996	297.95	2.96	396.30	0.18	< d.l.	108.63	2.67	4.57	0.45	1.31	0.16	0.49
PL-035	4	963	323.16	5.21	421.77	0.12	0.01	98.82	2.70	3.95	0.34	1.13	0.12	0.49
	4	961	323.16	3.40	408.43	0.15	0.02	92.59	2.33	3.62	0.31	1.10	0.12	0.45
PL-034	7	930	358	3.50	403.07	0.18	0.02	103.97	4.12	6.02	0.52	1.72	0.19	0.51
	3	923	358	3.84	408.97	0.16	0.02	106.90	3.48	5.14	0.45	1.60	0.15	0.48
	3	922	358	2.88	391.90	0.16	0.03	101.53	2.82	4.59	0.41	1.47	0.18	0.50
	2	957	358	3.25	407.30	0.15	0.07	107.17	4.00	6.07	0.49	1.64	0.17	0.52
	2	954	358	4.53	409.63	0.17	0.32	108.33	4.28	6.31	0.53	1.71	0.13	0.49
	1	949	358	2.93	416.47	0.18	0.02	109.40	3.29	5.44	0.46	1.67	0.19	0.50
	1	947	358	3.78	405.23	0.15	< d.l.	114.93	3.71	5.65	0.47	1.60	0.20	0.50
	7	933	358	2.88	379.50	0.16	0.04	95.09	3.82	5.69	0.46	1.59	0.17	0.50

Sample	Plag	Spot #	Depth	^{85}Rb	^{88}Sr	^{89}Y	^{90}Zr	^{137}Ba	^{139}La	^{140}Ce	^{141}Pr	^{144}Nd	^{152}Sm	^{153}Eu
PL-033	6	864	384.1	3.46	338.83	0.13	0.02	100.74	3.99	5.63	0.48	1.49	0.14	0.48
	5	875	384.1	3.20	321.67	0.15	0.02	106.56	2.69	4.52	0.42	1.46	0.14	0.46
	5	871	384.1	3.19	329.77	0.18	0.03	101.67	3.64	5.57	0.44	1.75	0.18	0.49
	4	898	384.1	2.84	326.30	0.15	0.02	93.84	3.77	5.68	0.43	1.45	0.12	0.48
	4	893	384.1	3.20	321.67	0.15	0.08	98.79	3.39	5.26	0.43	1.38	0.16	0.47
	3	889	384.1	2.95	332.70	0.17	0.02	92.68	2.27	3.88	0.34	1.29	0.15	0.48
	3	886	384.1	3.17	317.37	0.14	< d.l.	100.02	2.73	4.33	0.37	1.35	0.15	0.48
	6	866	384.1	3.51	348.00	0.19	0.07	109.17	3.09	4.97	0.45	1.42	0.15	0.50
PL-032	3	857	410.78	4.68	232.43	1.44	1.08	58.62	3.60	5.97	0.51	1.92	0.25	0.44
	2	844	410.78	7.63	343.90	0.26	0.02	108.77	4.03	6.92	0.63	2.09	0.26	0.65
	2	843	410.78	9.14	318.57	0.28	0.04	133.07	4.01	6.63	0.56	1.97	0.24	0.67
	1	839	410.78	5.52	317.43	0.31	0.05	111.63	4.42	7.45	0.64	2.23	0.24	0.66
	3	859	410.78	4.20	288.47	0.44	0.39	64.22	4.23	7.14	0.58	2.01	0.23	0.53
PL-031	4	808	426.36	1.77	360.43	0.20	0.01	102.93	4.13	6.61	0.53	1.88	0.18	0.58
	3	804	426.36	1.86	338.25	0.13	0.01	110.07	4.41	6.62	0.54	1.71	0.17	0.57
	3	803	426.36	1.77	348.17	0.20	0.02	105.73	4.28	6.73	0.53	1.86	0.17	0.59
	2	826	426.36	1.53	316.37	0.14	0.01	105.47	4.49	6.80	0.58	1.78	0.17	0.57
	2	824	426.36	1.53	289.30	0.15	0.01	110.57	4.44	6.69	0.53	1.72	0.16	0.58
	1	818	426.36	2.08	276.30	0.31	0.13	102.40	3.85	6.59	0.50	1.64	0.21	0.53
	1	815	426.36	1.97	335.85	0.18	0.24	100.84	4.19	6.49	0.51	1.74	0.19	0.54
	4	811	426.36	1.73	343.07	0.13	0.01	106.90	4.39	6.76	0.55	1.89	0.20	0.56
PL-030	6	790	465.4	< d.l.	358.70	0.32	0.97	123.77	4.35	7.02	0.66	2.07	0.24	0.80
	5	800	465.4	0.20	331.17	0.11	0.01	77.40	5.70	8.27	0.60	2.04	0.19	0.76
	5	797	465.4	< d.l.	349.60	0.18	0.01	127.00	5.17	7.67	0.65	2.01	0.19	0.80
	1	786	465.4	0.17	333.50	0.20	0.01	122.93	3.74	6.28	0.54	1.81	0.19	0.81
	1	783	465.4	0.02	347.53	0.16	0.02	104.20	5.25	7.84	0.60	1.78	0.16	0.75
	6	793	465.4	< d.l.	373.23	0.19	0.01	119.83	5.19	7.79	0.63	2.19	0.20	0.83
PL-028	1	742	506.71	9.82	372.47	0.16	0.16	101.51	3.52	5.67	0.45	1.61	0.13	0.42
	1	740	506.71	4.23	272.90	1.21	1.66	63.59	2.85	4.86	0.45	1.37	0.15	0.33
	2	750	506.71	4.05	39.11	2.65	2.86	9.77	0.95	1.63	0.09	0.56	0.10	0.06
PL-027	5	707	531.74	0.87	376.70	0.11	0.03	102.09	3.83	5.89	0.46	1.45	0.14	0.54
	4	703	531.74	3.44	397.53	0.13	0.19	93.43	4.10	5.51	0.44	1.36	0.12	0.52
	4	701	531.74	2.27	373.87	0.12	0.04	72.86	4.21	5.97	0.49	1.42	0.13	0.51
	2	716	531.74	0.75	353.40	0.14	0.01	93.57	4.11	5.94	0.47	1.55	0.17	0.53
	2	715	531.74	3.07	349.87	0.13	0.01	98.34	3.59	5.48	0.48	1.45	0.15	0.54
	2	713	531.74	0.72	350.10	0.13	0.01	89.55	3.79	5.67	0.44	1.40	0.13	0.52
	1	696	531.74	2.83	359.37	0.17	0.03	90.68	4.08	6.04	0.47	1.53	0.13	0.53
	5	709	531.74	1.44	372.33	0.16	0.10	105.23	3.90	5.87	0.46	1.46	0.15	0.52
PL-025	2	662	572.63	6.91	475.17	0.14	0.02	165.63	3.22	4.96	0.41	1.35	0.19	0.97
	1	642	572.63	2.04	402.15	0.17	0.01	135.87	3.32	5.15	0.44	1.55	0.16	1.02
	1	641	572.63	2.10	473.20	0.15	0.01	139.67	3.14	4.97	0.43	1.56	0.18	1.08
	1	640	572.63	2.49	453.90	0.16	< d.l.	143.13	3.64	5.51	0.43	1.50	0.17	1.01

Sample	Plag	Spot #	Depth	^{85}Rb	^{88}Sr	^{89}Y	^{90}Zr	^{137}Ba	^{139}La	^{140}Ce	^{141}Pr	^{144}Nd	^{152}Sm	^{153}Eu
PL-024	1	619	595.03	< d.l.	108.91	17.94	51.75	28.60	2.91	8.84	1.51	8.81	2.83	0.30
	3	632	595.03	< d.l.	394.77	0.22	0.05	123.03	5.83	8.56	0.77	2.55	0.26	0.62
	3	631	595.03	2.02	385.70	0.37	0.02	140.50	4.69	8.47	0.74	2.53	0.29	0.60
	2	627	595.03	< d.l.	418.93	0.25	0.02	117.25	5.59	8.75	0.80	2.52	0.26	0.60
	2	625	595.03	0.25	442.23	0.25	0.02	130.50	5.26	8.86	0.76	2.51	0.30	0.59
	3	634	595.03	< d.l.	392.50	0.25	< d.l.	132.57	5.54	9.12	0.82	2.74	0.31	0.63
PL-023	3	607	612.7	6.44	453.73	0.06	0.01	93.36	2.11	3.00	0.19	0.74	0.08	0.58
PL-022	4	561	635.83	1.60	365.27	0.18	0.03	111.70	4.08	6.35	0.54	2.02	0.20	0.52
	3	590	635.83	1.68	387.85	0.13	0.02	116.13	3.51	5.63	0.49	1.73	0.17	0.55
	3	586	635.83	4.75	350.30	0.14	1.86	97.90	3.27	5.75	0.51	1.52	0.18	0.47
	2	570	635.83	1.59	349.55	0.17	0.02	100.20	4.12	6.53	0.56	1.93	0.19	0.53
	2	567	635.83	1.54	374.87	0.19	0.02	122.83	3.96	6.39	0.52	1.87	0.21	0.55
	1	576	635.83	1.53	361.77	0.17	0.01	98.14	3.92	6.64	0.60	1.96	0.23	0.54
	1	574	635.83	1.60	376.90	0.15	0.02	101.71	3.81	6.33	0.51	1.95	0.20	0.51
	4	563	635.83	1.70	331.45	0.14	0.01	105.37	3.23	5.99	0.54	1.53	0.20	0.47
PL-021	3	557	659.33	2.68	380.40	0.13	0.01	115.57	3.46	5.16	0.39	1.30	0.09	0.70
	3	556	659.33	2.85	399.80	0.11	0.01	106.07	3.13	4.88	0.40	1.32	0.14	0.75
	3	555	659.33	2.40	380.13	0.12	0.02	111.87	3.32	5.06	0.43	1.35	0.13	0.76
	2	545	659.33	2.10	335.13	0.12	0.01	119.23	3.72	5.46	0.39	1.30	0.13	0.75
	2	544	659.33	2.18	401.70	0.12	0.01	114.37	4.02	5.48	0.43	1.38	0.13	0.74
	2	542	659.33	3.44	386.90	0.09	0.50	128.90	3.69	5.49	0.39	1.38	0.14	0.76
	1	551	659.33	3.38	401.60	0.12	0.09	116.40	3.86	5.49	0.40	1.23	0.11	0.75
	1	550	659.33	4.80	336.20	0.12	0.01	114.87	3.50	5.10	0.44	1.25	0.13	0.71
	1	549	659.33	5.35	370.75	0.11	0.57	120.10	3.44	5.01	0.42	1.27	0.13	0.71
PL-020	3	540	678.05	4.23	406.95	0.17	0.43	144.07	3.76	5.66	0.47	1.54	0.15	0.73
	3	538	678.05	3.15	365.85	0.12	0.01	142.43	3.68	5.68	0.46	1.54	0.15	0.76
	3	534	678.05	2.16	339.05	0.10	1.42	141.73	4.25	6.26	0.48	1.50	0.15	0.76
	2	530	678.05	2.30	361.17	0.16	0.02	136.57	4.31	5.93	0.52	1.56	0.14	0.72
	2	529	678.05	3.02	381.77	0.25	0.02	125.20	4.40	6.73	0.57	1.90	0.19	0.73
	2	528	678.05	2.22	351.43	0.09	0.02	127.40	4.06	6.08	0.47	1.49	0.13	0.69
	1	525	678.05	2.22	376.80	0.15	0.01	138.30	4.43	5.93	0.45	1.48	0.15	0.75
	1	523	678.05	5.64	362.17	0.11	0.50	148.17	4.03	5.77	0.45	1.39	0.12	0.69
	1	520	678.05	2.25	366.37	0.10	0.03	136.10	3.67	5.08	0.40	1.20	0.11	0.70
PL-019	4	499	697.26	2.59	411.17	0.17	0.01	164.17	2.75	4.56	0.38	1.33	0.19	0.82
	2	494	697.26	1.81	362.23	0.19	0.01	166.20	4.82	7.37	0.57	1.86	0.19	0.84
	2	492	697.26	1.91	388.63	0.16	0.01	163.10	5.64	7.83	0.60	2.15	0.17	0.86
	1	488	697.26	1.92	375.03	0.16	0.02	168.37	4.93	7.56	0.60	1.90	0.19	0.81
	1	487	697.26	1.86	375.57	0.19	0.02	167.47	3.81	5.91	0.48	1.76	0.18	0.78
	1	486	697.26	1.93	400.60	0.13	0.04	169.53	4.85	7.08	0.54	1.78	0.15	0.80
	4	501	697.26	3.16	407.45	0.12	0.02	180.43	4.64	6.75	0.53	1.74	0.16	0.80
PL-018	3	478	722.5	2.37	437.70	0.14	0.02	161.40	2.68	4.12	0.33	1.21	0.14	1.07
	3	475	722.5	3.41	444.47	0.14	0.01	153.83	2.99	4.27	0.38	1.38	0.13	1.14

Sample	Plag	Spot #	Depth	^{85}Rb	^{88}Sr	^{89}Y	^{90}Zr	^{137}Ba	^{139}La	^{140}Ce	^{141}Pr	^{144}Nd	^{152}Sm	^{153}Eu
	2	471	722.5	2.29	441.67	0.09	< d.l.	142.77	2.53	3.89	0.33	1.24	0.12	0.98
	2	470	722.5	2.30	464.77	0.11	0.01	144.37	2.59	3.91	0.31	1.08	0.12	1.03
	2	469	722.5	2.27	483.33	0.13	0.01	171.53	2.58	3.83	0.30	1.08	0.11	1.05
	2	468	722.5	2.88	447.67	0.13	0.01	151.40	2.59	3.95	0.35	1.12	0.12	1.02
	1	465	722.5	5.53	451.60	0.17	0.02	144.40	2.40	3.85	0.32	1.14	0.13	0.98
	1	464	722.5	2.71	427.83	0.12	0.02	151.23	2.62	4.21	0.37	1.37	0.14	1.12
	1	462	722.5	2.96	462.30	0.10	0.01	160.03	2.48	4.02	0.33	1.21	0.14	1.06
PL-017	5	449	740.4	2.45	355.10	0.13	0.03	113.03	3.43	5.20	0.40	1.27	0.12	0.66
	2	431	740.4	2.85	365.10	0.14	< d.l.	122.77	3.40	5.30	0.40	1.40	0.13	0.74
	2	430	740.4	2.62	350.77	0.10	0.01	117.97	3.36	5.19	0.41	1.23	0.11	0.69
	2	429	740.4	0.03	382.83	0.11	< d.l.	131.40	3.70	5.69	0.46	1.19	0.13	0.77
	1	445	740.4	2.86	366.90	0.12	0.33	95.53	3.72	5.52	0.36	1.31	0.12	0.75
	1	443	740.4	2.46	347.70	0.11	0.02	125.50	3.42	5.30	0.41	1.33	0.13	0.74
PL-015	3	428	779.8	4.85	440.40	0.16	0.01	171.07	3.60	5.11	0.38	1.45	0.12	0.96
	3	427	779.8	5.11	435.77	0.12	0.02	166.90	2.76	4.56	0.38	1.32	0.16	0.88
	2	421	779.8	4.82	442.70	0.12	0.02	157.43	3.95	5.67	0.45	1.43	0.15	0.94
	2	418	779.8	4.86	440.93	0.11	0.02	170.60	3.63	5.08	0.37	1.16	0.11	0.87
	2	416	779.8	4.27	422.77	0.14	0.01	161.30	3.06	4.93	0.37	1.21	0.11	0.86
	1	425	779.8	5.15	406.67	0.10	0.01	139.43	3.11	4.69	0.34	1.02	0.11	0.80
	1	424	779.8	4.75	385.10	0.07	0.01	143.17	2.99	4.75	0.35	1.01	0.10	0.77
PL-014	3	399	825.79	7.84	514.03	0.10	0.01	166.23	2.19	3.26	0.27	1.03	0.12	1.38
	3	398	825.79	8.19	520.30	0.14	< d.l.	161.83	2.03	3.07	0.26	0.99	0.12	1.32
	3	397	825.79	8.71	527.63	0.11	< d.l.	160.63	2.07	3.31	0.29	1.05	0.13	1.32
	2	405	825.79	8.00	547.63	0.14	0.01	170.77	2.33	3.49	0.32	1.16	0.14	1.40
	2	404	825.79	8.52	524.33	0.12	0.01	169.33	2.33	3.43	0.31	1.05	0.13	1.41
	2	403	825.79	9.04	484.95	0.17	0.05	137.10	2.48	3.54	0.32	1.14	0.15	1.41
	1	412	825.79	7.91	520.23	0.12	0.01	159.47	2.09	3.18	0.25	0.93	0.11	1.48
	1	411	825.79	7.76	388.50	2.66	1.89	127.60	2.08	3.82	0.43	2.15	0.60	1.33
PL-013	4	384	855.62	6.18	404.30	0.07	< d.l.	94.86	1.75	2.70	0.21	0.74	0.09	0.68
	3	393	855.62	5.69	401.53	0.09	< d.l.	93.51	1.85	2.86	0.21	0.72	0.07	0.65
	3	391	855.62	5.64	409.80	0.11	< d.l.	84.68	2.00	2.99	0.24	0.81	0.06	0.69
	2	380	855.62	6.26	398.97	0.12	0.01	96.13	1.82	2.83	0.22	0.77	0.09	0.69
	2	378	855.62	5.63	403.73	0.06	0.01	101.00	1.85	2.71	0.22	0.74	0.08	0.70
	1	374	855.62	5.41	367.97	0.10	0.01	91.99	1.96	3.00	0.25	0.75	0.10	0.76
	1	372	855.62	5.49	383.10	0.06	0.01	96.25	2.12	3.01	0.22	0.82	0.08	0.75
	4	385	855.62	5.72	389.00	0.07	< d.l.	99.22	1.77	2.71	0.18	0.70	0.06	0.66
PL-012	3	364	879.23	4.67	358.13	0.07	0.12	98.78	1.97	3.22	0.23	0.96	0.08	0.64
	3	362	879.23	11.86	369.97	0.08	0.02	109.45	2.10	3.11	0.24	0.79	0.09	0.65
	2	371	879.23	3.36	376.37	0.08	0.01	97.54	1.89	3.04	0.25	0.80	0.08	0.65
	2	370	879.23	3.55	346.90	0.29	0.19	86.80	1.69	2.71	0.21	0.64	0.07	0.59
	2	369	879.23	3.68	388.97	0.08	0.02	91.96	1.93	2.94	0.20	0.78	0.08	0.58
	1	355	879.23	3.09	403.50	0.07	0.01	86.98	2.12	3.10	0.25	0.81	0.08	0.66

Sample	Plag	Spot #	Depth	^{85}Rb	^{88}Sr	^{89}Y	^{90}Zr	^{137}Ba	^{139}La	^{140}Ce	^{141}Pr	^{144}Nd	^{152}Sm	^{153}Eu
	3	365	879.23	3.94	392.43	0.10	0.01	103.93	1.98	2.93	0.24	0.71	0.08	0.64
PL-011	7	351	899.43	1.13	383.50	0.11	< d.l.	91.86	1.58	2.63	0.21	0.75	0.10	0.57
	7	349	899.43	0.99	386.93	0.10	0.01	88.50	1.60	2.74	0.21	0.80	0.07	0.59
	7	347	899.43	1.17	373.07	0.15	< d.l.	93.19	1.86	2.71	0.21	0.84	0.09	0.62
	4	331	899.43	4.86	407.30	0.09	0.02	71.08	2.13	2.92	0.26	0.88	0.07	0.60
	4	328	899.43	4.09	354.80	0.13	0.01	92.75	1.80	2.96	0.24	0.86	0.10	0.58
	3	324	899.43	8.97	435.00	0.09	0.02	162.30	1.83	2.73	0.23	0.73	0.08	0.59
	3	322	899.43	4.20	420.63	0.11	0.01	105.97	1.83	2.88	0.24	0.87	0.11	0.62
PL-010	4	290	916.38	0.80	366.10	0.11	0.01	114.20	2.67	3.98	0.33	1.11	0.12	0.80
PL-009	5	268	943.14	2.35	358.50	0.12	0.01	102.40	2.65	4.09	0.34	1.15	0.12	0.78
	3	263	943.14	2.63	324.05	0.11	0.03	103.73	2.57	3.80	0.33	1.02	0.10	0.65
	3	261	943.14	2.54	357.13	0.11	0.01	109.07	2.44	3.76	0.33	1.01	0.12	0.71
	3	259	943.14	2.76	280.80	0.15	0.03	103.93	2.24	3.58	0.29	1.02	0.12	0.62
	2	255	943.14	2.86	369.63	0.10	0.01	87.01	2.66	3.91	0.33	0.97	0.10	0.68
	2	253	943.14	3.17	358.77	0.11	0.01	105.13	2.58	3.87	0.31	1.07	0.11	0.67
	5	275	943.14	2.35	260.00	2.60	3.26	92.37	2.44	4.32	0.34	1.21	0.20	0.66
PL-008	5	233	958.64	5.85	379.45	0.10	0.04	111.75	2.52	3.63	0.28	0.87	0.09	0.71
	4	243	958.64	1.77	349.65	0.12	0.02	101.21	2.84	4.17	0.32	1.13	0.13	0.75
	4	239	958.64	1.82	355.85	0.10	0.02	98.62	2.66	3.73	0.30	0.95	0.11	0.72
	2	215	958.64	1.96	367.43	0.11	0.02	96.95	2.34	3.37	0.27	0.92	0.10	0.74
	2	212	958.64	3.08	346.65	0.11	0.01	107.77	2.32	3.42	0.28	0.93	0.14	0.72
	1	208	958.64	2.29	334.87	0.11	0.01	98.21	2.21	3.36	0.24	0.80	0.11	0.72
	1	204	958.64	1.84	338.83	0.10	0.01	101.12	2.26	3.28	0.25	0.84	0.10	0.71
PL-007	4	195	982.3	4.08	445.63	0.12	0.02	175.60	4.37	6.12	0.47	1.59	0.17	1.03
	4	194	982.3	4.20	428.27	0.12	0.01	186.13	3.96	5.89	0.44	1.46	0.17	1.00
	3	188	982.3	4.01	397.23	0.13	0.01	174.60	4.00	5.84	0.47	1.43	0.12	0.99
	3	186	982.3	4.09	404.50	0.15	0.01	181.53	4.27	6.32	0.48	1.61	0.16	1.04
	3	183	982.3	3.82	412.07	0.10	0.01	138.40	3.99	5.71	0.44	1.35	0.13	0.96
	2	181	982.3	4.29	454.40	0.12	0.02	136.30	4.85	6.71	0.53	1.97	0.15	1.05
	2	179	982.3	4.19	482.77	0.11	0.01	179.27	4.31	6.06	0.49	1.49	0.15	0.99
	2	174	982.3	3.94	452.20	0.10	0.01	169.67	4.33	6.15	0.49	1.48	0.14	0.99
PL-005	2	110	1026.6	2.43	372.17	0.13	0.04	118.40	3.43	4.86	0.36	1.20	0.13	0.95
	2	106	1026.6	2.80	331.77	0.12	0.01	100.90	3.44	4.78	0.35	1.11	0.13	0.84
	1	138	1026.6	2.60	400.27	0.13	0.03	114.80	3.56	5.16	0.36	1.28	0.13	0.85
	3	135	1026.6	2.76	430.93	0.13	0.02	118.30	3.52	4.82	0.37	1.32	0.11	0.81
	3	146	1026.6	4.10	440.70	0.16	0.02	118.75	4.24	5.96	0.49	1.42	0.13	0.91
PL-004	3	90	1050.26	3.61	420.53	0.16	0.03	113.17	3.05	4.63	0.37	1.20	0.12	1.10
	2	100	1050.26	5.17	388.53	0.14	0.00	113.93	2.94	4.45	0.40	1.23	0.16	1.16
	1	85	1050.26	4.50	384.63	0.15	0.04	105.63	2.98	4.43	0.36	1.18	0.14	1.04
	1	83	1050.26	4.90	306.75	0.11	0.32	107.27	2.65	4.26	0.36	1.16	0.12	1.02
	3	95	1050.26	3.73	392.03	0.13	0.02	102.77	3.01	4.51	0.37	1.21	0.13	1.07
PL-003	4	49	1069.65	5.93	492.10	0.17	0.02	108.37	3.84	6.36	0.52	1.65	0.16	0.62

Sample	Plag	Spot #	Depth	^{85}Rb	^{88}Sr	^{89}Y	^{90}Zr	^{137}Ba	^{139}La	^{140}Ce	^{141}Pr	^{144}Nd	^{152}Sm	^{153}Eu
	3	70	1069.65	3.37	370.60	0.19	0.01	119.80	4.09	6.59	0.56	1.86	0.19	0.64
	3	68	1069.65	3.21	403.67	0.16	0.04	108.13	4.11	6.61	0.56	2.12	0.23	0.60
	1	77	1069.65	4.56	415.70	0.18	0.04	119.27	4.09	6.08	0.52	1.74	0.19	0.61
	1	74	1069.65	3.49	396.80	0.17	0.02	121.80	3.69	6.20	0.51	1.70	0.19	0.62
	4	51	1069.65	5.01	410.53	0.23	0.03	126.63	4.27	6.95	0.57	1.85	0.18	0.66
PL-002	3	39	1092.85	3.84	345.87	0.24	0.02	178.87	4.44	7.59	0.65	2.30	0.23	1.16
	3	37	1092.85	6.43	346.00	0.13	0.01	228.90	4.65	7.13	0.55	1.86	0.16	1.17
	3	35	1092.85	8.20	356.33	0.22	0.03	179.30	4.60	7.87	0.66	2.21	0.26	1.15
	3	32	1092.85	7.22	364.73	0.24	0.05	164.10	3.94	7.24	0.63	2.24	0.25	1.10
	1	30	1092.85	3.26	383.97	0.17	0.02	221.10	4.93	6.75	0.54	1.83	0.19	1.13
	1	28	1092.85	3.77	388.00	0.19	0.03	228.70	5.06	7.40	0.62	2.06	0.21	1.13
	1	25	1092.85	3.06	370.67	0.16	0.02	202.43	4.79	6.76	0.56	1.89	0.18	1.12
PL-001	4	8	1117.68	16.75	453.20	0.14	0.01	192.00	4.01	6.54	0.53	1.79	0.20	0.95
	4	2	1117.68	8.00	439.87	0.13	0.01	192.80	4.25	6.37	0.48	4.36	0.15	0.95
	3	20	1117.68	7.18	423.43	0.14	0.01	170.17	3.98	6.24	0.51	1.83	0.20	1.18
	3	18	1117.68	7.62	428.17	0.14	0.01	170.10	4.32	6.45	0.49	1.77	0.20	1.06
	3	17	1117.68	7.27	412.60	0.15	0.01	164.47	3.37	6.13	0.45	1.59	0.13	1.07
	2	12	1117.68	7.07	441.33	0.12	< d.l.	197.13	4.44	6.42	0.51	1.61	0.19	1.09
	2	10	1117.68	6.91	397.67	0.88	1.28	170.40	4.30	6.46	0.49	1.90	0.25	1.04

Table B-2: Trace element composition of plagioclase. The following trace elements are included in this table: Tb, Gd, Dy, Ho, Er, Tm, Yb, Lu, Pb, Th, and U as continuation of table B-1. Depths are reported in meters (m). All concentrations reported in parts per million (ppm).

Sample	Plag	Spot	Depth	^{159}Tb	^{160}Gd	^{163}Dy	^{165}Ho	^{166}Er	^{169}Tm	^{174}Yb	^{175}Lu	^{208}Pb	^{232}Th	^{238}U
PL-046	6	1359	67.84	0.01	0.15	0.04	0.01	0.02	< d.l.	0.01	< d.l.	5.14	0.02	< d.l.
	3	1341	67.84	0.01	0.15	0.06	0.01	0.03	< d.l.	0.01	< d.l.	4.28	0.01	< d.l.
	3	1337	67.84	0.01	0.12	0.07	< d.l.	0.02	< d.l.	0.01	< d.l.	3.69	< d.l.	0.02
	2	1348	67.84	0.01	0.10	0.04	< d.l.	0.01	< d.l.	0.01	< d.l.	7.76	0.01	< d.l.
	2	1345	67.84	0.01	0.12	0.03	< d.l.	0.02	< d.l.	< d.l.	< d.l.	12.06	< d.l.	< d.l.
	6	1362	67.84	0.01	0.13	0.05	0.01	0.02	< d.l.	< d.l.	< d.l.	4.67	< d.l.	< d.l.
PL-044	5	1317	100.7	0.02	0.16	0.07	0.01	0.03	< d.l.	0.01	< d.l.	4.26	< d.l.	< d.l.
	5	1315	100.7	0.01	0.13	0.05	0.01	0.01	< d.l.	< d.l.	< d.l.	8.05	< d.l.	< d.l.
	2	1295	100.7	0.01	0.14	0.09	0.01	0.03	< d.l.	0.02	< d.l.	2.47	< d.l.	< d.l.
	2	1292	100.7	0.02	0.16	0.07	0.02	0.02	< d.l.	0.01	< d.l.	5.20	0.01	< d.l.
	1	1329	100.7	0.03	0.16	0.06	0.01	0.03	< d.l.	0.01	< d.l.	13.37	0.01	0.01
	1	1326	100.7	0.03	0.21	0.07	0.02	0.03	< d.l.	0.02	< d.l.	9.76	0.55	0.07
	1	1322	100.7	0.02	0.18	0.06	0.01	0.03	< d.l.	0.01	< d.l.	8.24	0.01	< d.l.
PL-043	3	1291	126.36	0.03	0.29	0.11	0.02	0.06	0.01	0.01	< d.l.	9.91	0.01	< d.l.
	3	1288	126.36	0.03	0.33	0.22	0.02	0.11	0.01	0.04	< d.l.	8.23	0.01	0.01
	2	1276	126.36	0.02	0.16	0.07	0.02	0.06	< d.l.	0.02	< d.l.	2.75	0.01	< d.l.
	2	1273	126.36	0.01	0.16	0.09	0.01	0.06	0.01	0.02	< d.l.	2.77	0.09	0.01

Sample	Plag	Spot	Depth	^{159}Tb	^{160}Gd	^{163}Dy	^{165}Ho	^{166}Er	^{169}Tm	^{174}Yb	^{175}Lu	^{208}Pb	^{232}Th	^{238}U
	1	1282	126.36	0.02	0.22	0.11	0.02	0.04	< d.l.	0.01	< d.l.	3.30	0.01	< d.l.
	1	1280	126.36	0.03	0.26	0.12	0.02	0.05	< d.l.	0.03	< d.l.	3.15	0.07	0.01
	1	1278	126.36	0.02	0.18	0.09	0.02	0.05	< d.l.	0.02	< d.l.	3.16	0.06	0.01
PL-042	4	1263	144.04	0.01	0.17	0.08	0.02	0.04	< d.l.	0.01	< d.l.	2.12	< d.l.	< d.l.
	4	1262	144.04	0.01	0.19	0.08	0.02	0.03	< d.l.	0.01	< d.l.	2.17	< d.l.	< d.l.
	2	1243	144.04	0.02	0.16	0.07	0.01	0.02	< d.l.	0.01	< d.l.	2.12	0.02	< d.l.
	2	1241	144.04	0.02	0.16	0.08	0.01	0.04	< d.l.	0.02	< d.l.	1.99	< d.l.	< d.l.
	1	1258	144.04	0.01	0.12	0.06	0.02	0.03	< d.l.	0.02	< d.l.	2.00	< d.l.	< d.l.
	1	1257	144.04	0.02	0.18	0.08	0.01	0.04	< d.l.	0.01	< d.l.	2.30	0.24	0.37
	4	1265	144.04	0.02	0.17	0.07	0.02	0.03	0.01	0.02	< d.l.	2.15	0.01	< d.l.
PL-041	3	1228	169.37	0.03	0.30	0.16	0.02	0.07	< d.l.	0.02	< d.l.	3.70	< d.l.	< d.l.
	3	1226	169.37	0.04	0.27	0.14	0.02	0.07	< d.l.	0.03	< d.l.	4.58	0.09	0.02
	2	1223	169.37	0.04	0.26	0.14	0.02	0.06	< d.l.	0.02	< d.l.	3.85	0.01	< d.l.
	2	1221	169.37	0.03	0.28	0.14	0.03	0.09	< d.l.	0.03	< d.l.	6.60	< d.l.	< d.l.
	2	1218	169.37	0.02	0.18	0.08	0.01	0.07	< d.l.	0.02	0.01	3.18	0.01	< d.l.
	1	1237	169.37	0.04	0.26	0.18	0.03	0.13	< d.l.	0.03	0.01	3.58	0.08	0.04
	1	1235	169.37	0.02	0.23	0.18	0.03	0.10	0.01	0.07	0.01	3.61	0.11	0.04
	1	1232	169.37	0.03	0.22	0.11	0.02	0.07	< d.l.	0.01	< d.l.	3.61	0.01	< d.l.
PL-040	7	1166	190.55	0.01	0.08	0.03	0.01	0.01	< d.l.	0.01	< d.l.	2.33	< d.l.	< d.l.
	7	1164	190.55	0.01	0.09	0.04	0.01	0.01	< d.l.	0.01	< d.l.	2.51	< d.l.	< d.l.
	5	1216	190.55	0.01	0.10	0.04	0.01	0.02	< d.l.	0.01	< d.l.	2.05	< d.l.	< d.l.
	5	1214	190.55	0.01	0.10	0.04	0.01	0.02	< d.l.	0.01	< d.l.	2.08	< d.l.	< d.l.
	5	1211	190.55	0.01	0.09	0.05	0.01	0.02	< d.l.	0.01	< d.l.	2.50	< d.l.	< d.l.
	3	1206	190.55	0.01	0.07	0.04	0.01	0.02	< d.l.	< d.l.	< d.l.	2.67	< d.l.	< d.l.
	3	1204	190.55	0.01	0.09	0.04	< d.l.	0.01	< d.l.	0.01	< d.l.	3.91	0.01	< d.l.
	2	1192	190.55	0.01	0.10	0.04	0.01	0.02	< d.l.	0.01	< d.l.	2.16	< d.l.	< d.l.
	2	1189	190.55	< d.l.	0.07	0.05	0.01	0.01	< d.l.	0.01	< d.l.	2.32	< d.l.	< d.l.
	1	1199	190.55	0.01	0.08	0.06	< d.l.	0.02	< d.l.	0.01	< d.l.	2.39	< d.l.	< d.l.
	1	1196	190.55	0.01	0.10	0.06	0.01	0.01	< d.l.	0.01	< d.l.	2.16	< d.l.	< d.l.
PL-039	4	1148	212.48	0.01	0.11	0.05	0.01	0.01	< d.l.	0.01	< d.l.	2.88	< d.l.	< d.l.
	3	1135	212.48	0.01	0.11	0.05	0.01	0.02	< d.l.	0.01	< d.l.	3.15	< d.l.	< d.l.
	3	1133	212.48	0.02	0.10	0.04	0.01	0.01	< d.l.	0.01	< d.l.	3.14	0.01	< d.l.
	2	1145	212.48	0.02	0.13	0.04	0.01	0.02	0.01	0.01	< d.l.	3.31	< d.l.	< d.l.
	2	1143	212.48	0.01	0.15	0.04	0.01	0.02	< d.l.	0.01	< d.l.	5.74	0.01	0.03
PL-038	3	1099	227	0.01	0.27	0.06	0.01	0.01	< d.l.	0.01	< d.l.	3.67	0.24	0.18
	3	1097	227	0.01	0.24	0.07	0.01	0.01	0.01	0.01	< d.l.	3.29	0.01	0.01
	3	1094	227	0.01	0.21	0.07	0.01	0.02	< d.l.	0.01	< d.l.	3.48	0.01	0.01
	2	1087	227	0.01	0.24	0.04	0.01	0.01	< d.l.	0.01	< d.l.	6.85	< d.l.	< d.l.
	1	1093	227	0.01	0.25	0.04	0.01	0.01	< d.l.	< d.l.	< d.l.	4.26	0.01	< d.l.
	1	1092	227	0.01	0.28	0.04	0.01	0.01	< d.l.	0.01	< d.l.	4.45	< d.l.	< d.l.
PL-037	6	1021	260.5	0.01	0.05	0.03	0.01	0.01	< d.l.	0.01	< d.l.	2.85	< d.l.	< d.l.
	4	1039	260.5	0.01	0.07	0.05	< d.l.	0.02	< d.l.	0.01	< d.l.	2.30	0.02	0.01

Sample	Plag	Spot	Depth	^{159}Tb	^{160}Gd	^{163}Dy	^{165}Ho	^{166}Er	^{169}Tm	^{174}Yb	^{175}Lu	^{208}Pb	^{232}Th	^{238}U
	4	1037	260.5	0.01	0.10	0.05	0.01	0.03	< d.l.	0.01	< d.l.	2.55	0.16	0.13
	4	1035	260.5	0.01	0.08	0.05	0.01	0.02	< d.l.	0.01	< d.l.	2.15	< d.l.	0.00
	1	1029	260.5	0.01	0.13	0.04	< d.l.	0.02	< d.l.	0.01	< d.l.	2.39	< d.l.	< d.l.
	1	1025	260.5	0.01	0.12	0.04	< d.l.	0.02	< d.l.	0.01	< d.l.	2.13	< d.l.	< d.l.
PL-036	3	991	297.95	0.01	0.10	0.04	0.01	0.02	< d.l.	< d.l.	< d.l.	2.47	< d.l.	< d.l.
	2	1000	297.95	0.01	0.14	0.05	0.01	0.02	< d.l.	0.01	< d.l.	2.23	< d.l.	< d.l.
	2	998	297.95	0.01	0.10	0.05	0.01	0.01	< d.l.	0.01	< d.l.	2.53	< d.l.	< d.l.
	1	1009	297.95	0.01	0.13	0.05	0.01	0.03	< d.l.	0.02	< d.l.	2.34	< d.l.	< d.l.
	1	1006	297.95	0.01	0.08	0.03	0.01	0.02	< d.l.	0.01	< d.l.	2.64	0.08	0.06
	3	996	297.95	0.01	0.10	0.04	0.01	0.02	< d.l.	0.01	< d.l.	1.97	< d.l.	< d.l.
PL-035	4	963	323.16	0.01	0.08	0.03	0.01	0.01	< d.l.	0.01	< d.l.	2.13	< d.l.	< d.l.
	4	961	323.16	0.01	0.07	0.03	< d.l.	0.01	< d.l.	0.01	< d.l.	1.67	< d.l.	< d.l.
PL-034	7	930	358	0.01	0.18	0.03	0.01	0.01	< d.l.	< d.l.	< d.l.	2.73	< d.l.	< d.l.
	3	923	358	0.01	0.16	0.04	0.01	0.01	< d.l.	0.01	< d.l.	2.91	0.01	< d.l.
	3	922	358	0.01	0.13	0.04	0.01	0.01	< d.l.	< d.l.	< d.l.	1.98	< d.l.	< d.l.
	2	957	358	0.01	0.13	0.03	0.01	0.01	< d.l.	0.01	< d.l.	2.75	0.01	0.01
	2	954	358	0.01	0.13	0.04	< d.l.	0.02	< d.l.	< d.l.	< d.l.	2.33	0.10	0.02
	1	949	358	0.01	0.19	0.04	0.01	0.01	< d.l.	0.01	< d.l.	2.98	< d.l.	< d.l.
	1	947	358	0.01	0.13	0.05	0.01	0.01	< d.l.	< d.l.	< d.l.	2.79	0.01	< d.l.
	7	933	358	0.01	0.17	0.04	< d.l.	0.01	< d.l.	0.01	< d.l.	1.75	< d.l.	< d.l.
PL-033	6	864	384.1	0.01	0.09	0.05	0.01	0.02	< d.l.	0.01	< d.l.	2.69	< d.l.	< d.l.
	5	875	384.1	< d.l.	0.07	0.03	0.01	0.03	< d.l.	< d.l.	< d.l.	3.29	< d.l.	< d.l.
	5	871	384.1	0.01	0.10	0.05	0.01	0.02	0.01	0.01	< d.l.	2.19	0.01	< d.l.
	4	898	384.1	0.01	0.07	0.02	< d.l.	0.01	< d.l.	< d.l.	< d.l.	2.09	0.01	< d.l.
	4	893	384.1	0.01	0.06	0.03	0.01	0.02	< d.l.	0.01	< d.l.	1.96	0.01	< d.l.
	3	889	384.1	0.01	0.10	0.06	0.01	0.01	< d.l.	0.01	< d.l.	2.00	0.01	< d.l.
	3	886	384.1	0.01	0.08	0.04	0.01	0.01	< d.l.	0.01	< d.l.	2.32	< d.l.	< d.l.
	6	866	384.1	0.01	0.09	0.03	0.01	0.03	< d.l.	0.01	< d.l.	2.38	< d.l.	0.01
PL-032	3	857	410.78	0.02	0.16	0.23	0.05	0.24	0.03	0.36	0.04	2.13	0.07	0.03
	2	844	410.78	0.01	0.12	0.06	0.02	0.03	< d.l.	0.01	< d.l.	2.03	< d.l.	< d.l.
	2	843	410.78	0.02	0.13	0.06	0.01	0.02	< d.l.	0.02	< d.l.	2.35	< d.l.	< d.l.
	1	839	410.78	0.02	0.12	0.07	0.01	0.03	0.01	0.02	< d.l.	2.64	0.01	< d.l.
	3	859	410.78	0.02	0.12	0.09	0.02	0.07	0.01	0.10	0.01	2.48	0.01	0.02
PL-031	4	808	426.36	0.01	0.10	0.06	0.01	0.03	< d.l.	0.01	< d.l.	2.04	< d.l.	< d.l.
	3	804	426.36	0.01	0.07	0.03	< d.l.	0.01	< d.l.	< d.l.	< d.l.	2.13	< d.l.	< d.l.
	3	803	426.36	0.02	0.08	0.05	0.01	0.02	< d.l.	0.01	< d.l.	2.03	< d.l.	< d.l.
	2	826	426.36	0.01	0.08	0.04	0.01	0.01	< d.l.	0.01	< d.l.	2.03	< d.l.	< d.l.
	2	824	426.36	0.01	0.08	0.02	< d.l.	0.01	< d.l.	< d.l.	< d.l.	1.96	< d.l.	< d.l.
	1	818	426.36	0.01	0.10	0.07	0.01	0.06	0.01	0.04	< d.l.	1.95	0.01	0.01
	1	815	426.36	< d.l.	0.08	0.05	< d.l.	0.02	< d.l.	0.01	0.01	2.15	< d.l.	0.01
	4	811	426.36	0.01	0.11	0.04	0.01	0.02	< d.l.	0.01	< d.l.	2.00	< d.l.	< d.l.
PL-030	6	790	465.4	0.02	0.13	0.06	0.01	0.03	< d.l.	0.02	0.01	2.83	0.12	0.05

Sample	Plag	Spot	Depth	^{159}Tb	^{160}Gd	^{163}Dy	^{165}Ho	^{166}Er	^{169}Tm	^{174}Yb	^{175}Lu	^{208}Pb	^{232}Th	^{238}U
	5	800	465.4	0.01	0.08	0.04	< d.l.	0.02	< d.l.	< d.l.	< d.l.	2.90	< d.l.	< d.l.
	5	797	465.4	0.02	0.12	0.05	0.01	0.02	< d.l.	0.01	< d.l.	2.67	0.01	< d.l.
	1	786	465.4	0.01	0.10	0.06	0.01	0.02	< d.l.	0.01	< d.l.	2.66	< d.l.	< d.l.
	1	783	465.4	0.01	0.09	0.05	0.01	0.01	< d.l.	0.01	< d.l.	2.64	< d.l.	< d.l.
	6	793	465.4	0.02	0.13	0.05	0.01	0.02	< d.l.	0.01	< d.l.	2.60	0.01	< d.l.
PL-028	1	742	506.71	< d.l.	0.16	0.04	< d.l.	0.01	< d.l.	0.01	< d.l.	1.80	< d.l.	< d.l.
	1	740	506.71	0.04	0.37	0.26	0.02	0.15	0.01	0.18	0.03	1.52	0.02	0.01
	2	750	506.71	0.05	0.30	0.41	0.11	0.41	0.07	0.59	0.09	0.25	0.04	0.02
PL-027	5	707	531.74	0.01	0.09	0.03	< d.l.	0.02	< d.l.	< d.l.	< d.l.	2.26	0.01	< d.l.
	4	703	531.74	0.01	0.06	0.03	< d.l.	0.01	< d.l.	0.01	< d.l.	2.50	0.01	< d.l.
	4	701	531.74	< d.l.	0.08	0.03	< d.l.	0.01	< d.l.	0.01	< d.l.	2.23	0.02	< d.l.
	2	716	531.74	0.01	0.07	0.04	< d.l.	0.01	< d.l.	< d.l.	< d.l.	2.02	< d.l.	< d.l.
	2	715	531.74	0.01	0.10	0.03	< d.l.	0.01	< d.l.	< d.l.	< d.l.	2.06	0.01	< d.l.
	2	713	531.74	0.01	0.05	0.03	0.01	0.01	< d.l.	0.01	< d.l.	1.91	0.01	< d.l.
	1	696	531.74	0.01	0.08	0.03	0.01	0.01	< d.l.	0.01	< d.l.	2.05	< d.l.	0.01
	5	709	531.74	0.01	0.09	0.04	0.01	0.02	< d.l.	< d.l.	< d.l.	2.35	0.01	< d.l.
PL-025	2	662	572.63	0.01	0.10	0.04	0.01	0.01	< d.l.	0.01	< d.l.	3.39	< d.l.	< d.l.
	1	642	572.63	0.01	0.08	0.05	0.01	0.01	< d.l.	0.01	< d.l.	2.29	< d.l.	< d.l.
	1	641	572.63	0.01	0.12	0.04	0.01	0.01	< d.l.	0.01	< d.l.	2.24	< d.l.	< d.l.
	1	640	572.63	0.01	0.07	0.04	0.01	0.01	< d.l.	< d.l.	< d.l.	2.29	0.01	< d.l.
PL-024	1	619	595.03	0.57	5.97	3.74	0.71	1.97	0.27	1.91	0.27	0.63	0.09	0.02
	3	632	595.03	0.01	0.28	0.11	0.01	0.02	< d.l.	0.01	< d.l.	2.42	0.02	0.01
	3	631	595.03	0.01	0.30	0.09	0.02	0.03	< d.l.	0.01	< d.l.	2.53	0.04	0.11
	2	627	595.03	0.01	0.29	0.07	0.01	0.01	< d.l.	< d.l.	< d.l.	2.26	< d.l.	< d.l.
	2	625	595.03	0.01	0.27	0.06	< d.l.	0.02	< d.l.	0.01	< d.l.	2.15	< d.l.	< d.l.
	3	634	595.03	0.02	0.22	0.06	0.01	0.02	< d.l.	0.01	< d.l.	2.33	< d.l.	< d.l.
PL-023	3	607	612.7	< d.l.	0.04	0.02	0.01	0.01	< d.l.	< d.l.	< d.l.	1.19	< d.l.	< d.l.
PL-022	4	561	635.83	0.01	0.12	0.04	0.01	0.02	< d.l.	0.01	< d.l.	1.84	< d.l.	< d.l.
	3	590	635.83	0.01	0.07	0.04	0.01	0.01	< d.l.	0.01	< d.l.	1.72	< d.l.	< d.l.
	3	586	635.83	0.01	0.11	0.04	< d.l.	0.01	< d.l.	0.01	< d.l.	1.73	0.28	0.08
	2	570	635.83	0.01	0.11	0.03	0.01	0.01	< d.l.	0.01	< d.l.	1.84	< d.l.	< d.l.
	2	567	635.83	0.01	0.11	0.04	0.01	0.01	< d.l.	0.01	< d.l.	1.88	< d.l.	< d.l.
	1	576	635.83	0.01	0.10	0.05	< d.l.	0.02	< d.l.	< d.l.	< d.l.	1.75	< d.l.	< d.l.
	1	574	635.83	0.01	0.10	0.03	0.01	0.02	< d.l.	< d.l.	< d.l.	1.75	< d.l.	< d.l.
	4	563	635.83	0.01	0.11	0.04	0.02	0.02	0.01	0.04	< d.l.	1.72	< d.l.	0.01
PL-021	3	557	659.33	0.00	0.06	0.03	< d.l.	0.01	< d.l.	< d.l.	< d.l.	1.57	< d.l.	< d.l.
	3	556	659.33	0.01	0.07	0.03	0.01	0.01	< d.l.	0.01	< d.l.	1.64	< d.l.	< d.l.
	3	555	659.33	0.01	0.07	0.03	< d.l.	0.02	< d.l.	0.01	< d.l.	1.50	0.01	< d.l.
	2	545	659.33	0.01	0.07	0.03	< d.l.	0.02	< d.l.	0.01	< d.l.	1.55	< d.l.	< d.l.
	2	544	659.33	0.01	0.08	0.03	< d.l.	0.01	< d.l.	< d.l.	< d.l.	1.68	< d.l.	< d.l.
	2	542	659.33	< d.l.	0.06	0.03	0.01	0.01	< d.l.	< d.l.	< d.l.	1.79	0.05	0.01
	1	551	659.33	0.01	0.05	0.03	< d.l.	0.01	< d.l.	0.01	< d.l.	1.91	0.01	< d.l.

Sample	Plag	Spot	Depth	^{159}Tb	^{160}Gd	^{163}Dy	^{165}Ho	^{166}Er	^{169}Tm	^{174}Yb	^{175}Lu	^{208}Pb	^{232}Th	^{238}U
	1	550	659.33	0.01	0.07	0.03	< d.l.	0.01	< d.l.	< d.l.	< d.l.	1.68	< d.l.	< d.l.
	1	549	659.33	0.01	0.06	0.03	< d.l.	0.02	< d.l.	0.01	< d.l.	1.59	0.05	0.02
PL-020	3	540	678.05	0.01	0.09	0.05	< d.l.	0.01	< d.l.	0.01	< d.l.	2.28	0.02	0.01
	3	538	678.05	0.01	0.09	0.04	0.01	0.01	< d.l.	0.01	< d.l.	2.28	< d.l.	< d.l.
	3	534	678.05	0.01	0.06	0.03	0.01	0.01	< d.l.	0.01	< d.l.	2.11	< d.l.	< d.l.
	2	530	678.05	0.01	0.07	0.04	< d.l.	0.01	< d.l.	0.01	< d.l.	2.16	< d.l.	0.01
	2	529	678.05	0.01	0.07	0.05	0.01	0.03	< d.l.	0.01	< d.l.	2.03	0.01	< d.l.
	2	528	678.05	< d.l.	0.09	0.02	< d.l.	0.02	< d.l.	< d.l.	< d.l.	2.03	< d.l.	< d.l.
	1	525	678.05	0.01	0.08	0.04	0.01	0.02	< d.l.	0.01	< d.l.	2.21	< d.l.	< d.l.
	1	523	678.05	< d.l.	0.06	0.02	0.01	0.02	< d.l.	0.01	< d.l.	2.24	0.06	0.09
	1	520	678.05	< d.l.	0.05	0.02	0.01	0.01	< d.l.	0.01	< d.l.	1.98	< d.l.	< d.l.
PL-019	4	499	697.26	0.01	0.11	0.05	0.01	0.02	< d.l.	0.01	< d.l.	2.61	< d.l.	< d.l.
	2	494	697.26	0.01	0.11	0.05	0.01	0.02	< d.l.	< d.l.	< d.l.	2.77	< d.l.	< d.l.
	2	492	697.26	0.01	0.10	0.05	< d.l.	0.02	< d.l.	0.01	< d.l.	2.81	< d.l.	< d.l.
	1	488	697.26	0.01	0.09	0.03	0.01	0.02	< d.l.	< d.l.	< d.l.	2.85	0.01	< d.l.
	1	487	697.26	0.02	0.09	0.03	0.01	0.01	< d.l.	0.01	< d.l.	2.53	0.01	< d.l.
	1	486	697.26	0.01	0.09	0.04	0.01	0.02	< d.l.	< d.l.	< d.l.	2.61	< d.l.	< d.l.
	4	501	697.26	0.01	0.08	0.05	0.01	0.03	< d.l.	0.01	< d.l.	2.65	< d.l.	< d.l.
PL-018	3	478	722.5	0.01	0.11	0.04	< d.l.	0.02	< d.l.	< d.l.	< d.l.	1.72	< d.l.	< d.l.
	3	475	722.5	0.01	0.10	0.02	< d.l.	0.01	< d.l.	0.01	< d.l.	1.67	< d.l.	0.01
	2	471	722.5	0.01	0.08	0.03	< d.l.	0.01	< d.l.	< d.l.	< d.l.	1.62	< d.l.	< d.l.
	2	470	722.5	< d.l.	0.08	0.02	< d.l.	0.02	< d.l.	< d.l.	< d.l.	1.69	< d.l.	< d.l.
	2	469	722.5	0.01	0.06	0.03	< d.l.	0.02	< d.l.	< d.l.	< d.l.	1.74	< d.l.	< d.l.
	2	468	722.5	0.01	0.07	0.02	< d.l.	0.01	< d.l.	0.01	< d.l.	1.58	< d.l.	< d.l.
	1	465	722.5	< d.l.	0.09	0.03	< d.l.	0.02	< d.l.	< d.l.	< d.l.	1.53	< d.l.	< d.l.
	1	464	722.5	0.01	0.09	0.03	0.01	0.01	< d.l.	< d.l.	< d.l.	1.74	< d.l.	< d.l.
	1	462	722.5	< d.l.	0.06	0.03	< d.l.	0.01	< d.l.	< d.l.	< d.l.	1.65	< d.l.	< d.l.
PL-017	5	449	740.4	< d.l.	0.12	0.03	< d.l.	0.01	< d.l.	< d.l.	< d.l.	2.04	< d.l.	< d.l.
	2	431	740.4	< d.l.	0.16	0.04	0.01	0.01	< d.l.	0.01	< d.l.	2.30	< d.l.	< d.l.
	2	430	740.4	0.01	0.16	0.02	< d.l.	0.01	0.01	< d.l.	< d.l.	2.10	< d.l.	< d.l.
	2	429	740.4	0.01	0.12	0.02	< d.l.	0.01	< d.l.	< d.l.	< d.l.	2.48	< d.l.	< d.l.
	1	445	740.4	0.01	0.13	0.03	0.01	0.01	< d.l.	0.01	< d.l.	2.13	0.11	0.03
	1	443	740.4	0.01	0.16	0.04	< d.l.	0.01	< d.l.	< d.l.	< d.l.	2.04	< d.l.	< d.l.
PL-015	3	428	779.8	< d.l.	0.10	0.04	< d.l.	< d.l.	< d.l.	< d.l.	< d.l.	1.78	< d.l.	< d.l.
	3	427	779.8	0.01	0.06	0.02	0.01	0.01	< d.l.	0.01	< d.l.	1.92	< d.l.	< d.l.
	2	421	779.8	0.01	0.07	0.04	< d.l.	0.01	< d.l.	0.01	< d.l.	1.71	< d.l.	< d.l.
	2	418	779.8	0.01	0.08	0.03	< d.l.	0.01	< d.l.	< d.l.	< d.l.	1.83	< d.l.	< d.l.
	2	416	779.8	0.01	0.07	0.02	0.01	0.01	< d.l.	0.01	< d.l.	1.60	< d.l.	< d.l.
	1	425	779.8	< d.l.	0.05	0.02	< d.l.	0.01	< d.l.	< d.l.	< d.l.	1.58	< d.l.	< d.l.
	1	424	779.8	0.01	0.07	0.02	< d.l.	0.01	< d.l.	< d.l.	< d.l.	1.57	< d.l.	< d.l.
PL-014	3	399	825.79	< d.l.	0.09	0.03	< d.l.	0.01	< d.l.	0.01	< d.l.	2.60	< d.l.	< d.l.
	3	398	825.79	0.01	0.08	0.04	< d.l.	0.01	< d.l.	< d.l.	< d.l.	1.92	< d.l.	< d.l.

Sample	Plag	Spot	Depth	^{159}Tb	^{160}Gd	^{163}Dy	^{165}Ho	^{166}Er	^{169}Tm	^{174}Yb	^{175}Lu	^{208}Pb	^{232}Th	^{238}U
	3	397	825.79	0.01	0.09	0.03	0.01	0.01	< d.l.	0.01	< d.l.	1.91	< d.l.	< d.l.
	2	405	825.79	< d.l.	0.09	0.02	< d.l.	0.02	< d.l.	< d.l.	< d.l.	2.81	< d.l.	< d.l.
	2	404	825.79	0.01	0.06	0.04	< d.l.	0.01	< d.l.	< d.l.	< d.l.	3.03	< d.l.	< d.l.
	2	403	825.79	0.01	0.07	0.07	0.01	0.02	< d.l.	0.02	< d.l.	3.12	0.01	< d.l.
	1	412	825.79	< d.l.	0.07	0.02	0.01	0.01	< d.l.	0.01	< d.l.	2.84	< d.l.	< d.l.
	1	411	825.79	0.08	0.63	0.60	0.14	0.37	0.04	0.34	0.04	2.59	0.03	< d.l.
PL-013	4	384	855.62	< d.l.	0.04	0.02	0.01	0.01	< d.l.	< d.l.	< d.l.	1.13	< d.l.	< d.l.
	3	393	855.62	< d.l.	0.05	0.02	0.01	0.01	< d.l.	0.01	< d.l.	1.13	< d.l.	< d.l.
	3	391	855.62	0.01	0.04	0.02	0.01	0.01	< d.l.	< d.l.	< d.l.	1.12	< d.l.	< d.l.
	2	380	855.62	0.01	0.05	0.02	< d.l.	0.01	< d.l.	< d.l.	< d.l.	1.13	< d.l.	< d.l.
	2	378	855.62	0.01	0.04	0.02	< d.l.	< d.l.	< d.l.	< d.l.	< d.l.	1.20	< d.l.	< d.l.
	1	374	855.62	0.01	0.05	0.03	< d.l.	0.01	< d.l.	0.01	< d.l.	1.18	< d.l.	< d.l.
	1	372	855.62	< d.l.	0.07	0.03	< d.l.	0.01	< d.l.	0.01	< d.l.	1.22	< d.l.	< d.l.
	4	385	855.62	0.01	0.04	0.01	< d.l.	< d.l.	< d.l.	< d.l.	< d.l.	1.14	< d.l.	< d.l.
PL-012	3	364	879.23	< d.l.	0.04	0.03	< d.l.	0.01	0.01	0.01	< d.l.	1.20	0.01	0.01
	3	362	879.23	0.01	0.05	0.03	0.01	0.01	< d.l.	0.01	< d.l.	1.26	0.01	< d.l.
	2	371	879.23	0.01	0.04	0.03	0.01	0.01	< d.l.	0.01	< d.l.	1.15	< d.l.	< d.l.
	2	370	879.23	0.01	0.05	0.05	0.02	0.07	0.01	0.10	0.02	1.18	< d.l.	< d.l.
	2	369	879.23	0.01	0.03	0.01	< d.l.	0.01	< d.l.	0.01	< d.l.	1.09	< d.l.	< d.l.
	1	355	879.23	< d.l.	0.05	0.02	< d.l.	0.01	< d.l.	< d.l.	< d.l.	1.11	< d.l.	< d.l.
	3	365	879.23	< d.l.	0.04	0.02	< d.l.	0.01	< d.l.	0.01	< d.l.	1.21	< d.l.	< d.l.
PL-011	7	351	899.43	0.01	0.05	0.02	< d.l.	< d.l.	< d.l.	< d.l.	< d.l.	1.05	< d.l.	< d.l.
	7	349	899.43	0.01	0.05	0.02	< d.l.	0.01	< d.l.	0.01	< d.l.	0.98	< d.l.	< d.l.
	7	347	899.43	< d.l.	0.05	0.04	< d.l.	< d.l.	< d.l.	< d.l.	< d.l.	1.19	< d.l.	< d.l.
	4	331	899.43	< d.l.	0.08	0.02	< d.l.	0.01	< d.l.	< d.l.	< d.l.	1.16	< d.l.	< d.l.
	4	328	899.43	0.01	0.09	0.03	0.01	0.01	< d.l.	< d.l.	< d.l.	1.15	0.01	0.01
	3	324	899.43	< d.l.	0.05	0.02	0.01	< d.l.	< d.l.	0.01	< d.l.	1.23	< d.l.	< d.l.
	3	322	899.43	< d.l.	0.06	0.02	< d.l.	0.01	< d.l.	0.01	< d.l.	1.16	< d.l.	< d.l.
PL-010	4	290	916.38	0.01	0.07	0.04	< d.l.	0.01	< d.l.	0.01	< d.l.	1.48	0.01	< d.l.
PL-009	5	268	943.14	0.01	0.05	0.02	0.01	0.02	< d.l.	< d.l.	< d.l.	1.58	< d.l.	< d.l.
	3	263	943.14	0.01	0.08	0.03	0.01	0.02	< d.l.	0.01	< d.l.	1.55	< d.l.	< d.l.
	3	261	943.14	0.01	0.05	0.03	< d.l.	0.02	< d.l.	0.01	< d.l.	1.57	< d.l.	< d.l.
	3	259	943.14	0.01	0.07	0.03	< d.l.	0.02	< d.l.	< d.l.	< d.l.	1.57	< d.l.	< d.l.
	2	255	943.14	< d.l.	0.05	0.02	0.01	0.02	< d.l.	< d.l.	< d.l.	1.61	< d.l.	< d.l.
	2	253	943.14	0.01	0.08	0.02	0.01	0.01	< d.l.	< d.l.	< d.l.	1.61	< d.l.	< d.l.
	5	275	943.14	0.09	0.53	0.58	0.10	0.55	0.05	0.33	0.05	1.47	0.09	0.01
PL-008	5	233	958.64	0.01	0.04	0.03	< d.l.	0.01	< d.l.	0.01	< d.l.	1.63	< d.l.	< d.l.
	4	243	958.64	0.01	0.06	0.04	< d.l.	0.01	< d.l.	0.01	< d.l.	1.14	< d.l.	< d.l.
	4	239	958.64	0.01	0.06	0.02	< d.l.	0.01	< d.l.	0.01	< d.l.	1.23	0.01	< d.l.
	2	215	958.64	0.01	0.08	0.02	< d.l.	0.01	< d.l.	0.01	< d.l.	1.45	< d.l.	< d.l.
	2	212	958.64	0.01	0.05	0.03	< d.l.	0.01	< d.l.	0.01	< d.l.	1.21	< d.l.	< d.l.
	1	208	958.64	< d.l.	0.05	0.02	< d.l.	0.01	< d.l.	0.01	< d.l.	1.04	< d.l.	< d.l.

Sample	Plag	Spot	Depth	^{159}Tb	^{160}Gd	^{163}Dy	^{165}Ho	^{166}Er	^{169}Tm	^{174}Yb	^{175}Lu	^{208}Pb	^{232}Th	^{238}U
	1	204	958.64	0.01	0.05	0.02	0.01	0.01	< d.l.	0.01	< d.l.	1.00	< d.l.	< d.l.
PL-007	4	195	982.3	0.01	0.10	0.04	0.01	0.02	< d.l.	< d.l.	< d.l.	1.90	< d.l.	0.01
	4	194	982.3	0.01	0.07	0.04	< d.l.	0.01	< d.l.	0.01	< d.l.	1.92	< d.l.	< d.l.
	3	188	982.3	0.01	0.07	0.02	0.01	0.01	< d.l.	0.01	< d.l.	2.05	< d.l.	< d.l.
	3	186	982.3	0.01	0.07	0.04	< d.l.	0.01	< d.l.	0.01	< d.l.	1.97	< d.l.	< d.l.
	3	183	982.3	< d.l.	0.06	0.03	0.01	0.01	< d.l.	0.01	< d.l.	1.93	< d.l.	< d.l.
	2	181	982.3	0.01	0.08	0.03	0.01	0.01	< d.l.	0.01	< d.l.	1.93	< d.l.	< d.l.
	2	179	982.3	0.01	0.07	0.03	0.01	0.01	< d.l.	0.01	< d.l.	2.00	< d.l.	< d.l.
	2	174	982.3	0.01	0.07	0.02	< d.l.	0.01	< d.l.	0.01	< d.l.	1.84	< d.l.	< d.l.
PL-005	2	110	1026.6	0.01	0.06	0.04	< d.l.	0.02	< d.l.	< d.l.	< d.l.	2.66	< d.l.	< d.l.
	2	106	1026.6	0.01	0.09	0.03	< d.l.	0.01	< d.l.	0.01	< d.l.	2.46	< d.l.	< d.l.
	1	138	1026.6	0.01	0.06	0.04	0.01	0.01	< d.l.	0.01	< d.l.	1.88	0.01	< d.l.
	3	135	1026.6	0.01	0.06	0.03	< d.l.	0.01	< d.l.	0.00	< d.l.	2.22	< d.l.	< d.l.
	3	146	1026.6	0.01	0.06	0.03	0.01	0.02	< d.l.	0.01	< d.l.	2.17	< d.l.	< d.l.
PL-004	3	90	1050.26	0.01	0.11	0.03	0.01	0.01	< d.l.	0.01	< d.l.	1.55	< d.l.	< d.l.
	2	100	1050.26	0.01	0.12	0.05	0.01	0.01	< d.l.	0.01	< d.l.	2.02	< d.l.	< d.l.
	1	85	1050.26	0.01	0.09	0.03	0.01	0.01	< d.l.	< d.l.	< d.l.	1.43	< d.l.	< d.l.
	1	83	1050.26	0.01	0.10	0.03	< d.l.	0.01	< d.l.	0.01	< d.l.	1.52	0.02	0.01
	3	95	1050.26	0.01	0.11	0.04	< d.l.	0.01	< d.l.	0.01	< d.l.	1.51	0.01	0.01
PL-003	4	49	1069.65	0.01	0.13	0.05	0.01	0.01	< d.l.	0.01	< d.l.	2.02	0.03	< d.l.
	3	70	1069.65	0.02	0.15	0.06	0.01	0.01	< d.l.	0.01	< d.l.	2.07	< d.l.	< d.l.
	3	68	1069.65	0.01	0.14	0.04	0.01	0.01	< d.l.	0.01	< d.l.	1.96	0.01	< d.l.
	1	77	1069.65	0.02	0.12	0.04	0.01	0.01	< d.l.	0.01	< d.l.	1.96	0.01	< d.l.
	1	74	1069.65	0.01	0.13	0.04	0.01	0.01	< d.l.	0.01	< d.l.	1.91	< d.l.	< d.l.
	4	51	1069.65	0.01	0.19	0.05	0.01	0.01	< d.l.	0.01	< d.l.	2.15	0.02	< d.l.
PL-002	3	39	1092.85	0.02	0.14	0.06	0.01	0.03	< d.l.	0.01	< d.l.	2.60	< d.l.	< d.l.
	3	37	1092.85	0.01	0.07	0.04	0.01	0.02	< d.l.	< d.l.	< d.l.	2.71	0.01	< d.l.
	3	35	1092.85	0.01	0.16	0.05	0.01	0.02	< d.l.	0.01	< d.l.	2.77	< d.l.	0.01
	3	32	1092.85	0.01	0.18	0.07	0.01	0.02	< d.l.	0.01	< d.l.	2.60	0.03	0.01
	1	30	1092.85	0.01	0.10	0.04	0.01	0.02	< d.l.	0.01	< d.l.	2.52	< d.l.	< d.l.
	1	28	1092.85	0.02	0.10	0.05	0.01	0.02	< d.l.	0.01	< d.l.	2.62	0.01	< d.l.
	1	25	1092.85	0.01	0.10	0.04	< d.l.	0.02	< d.l.	0.01	< d.l.	2.41	< d.l.	< d.l.
PL-001	4	8	1117.68	0.01	0.16	0.03	0.01	0.01	< d.l.	0.01	< d.l.	2.29	0.01	< d.l.
	4	2	1117.68	0.01	0.10	0.03	< d.l.	0.01	< d.l.	0.01	< d.l.	2.10	0.01	< d.l.
	3	20	1117.68	0.01	0.12	0.03	< d.l.	0.01	< d.l.	0.01	< d.l.	2.48	< d.l.	< d.l.
	3	18	1117.68	0.01	0.13	0.05	0.01	0.01	< d.l.	< d.l.	< d.l.	2.45	< d.l.	< d.l.
	3	17	1117.68	0.01	0.10	0.06	0.01	0.01	< d.l.	< d.l.	< d.l.	2.39	< d.l.	< d.l.
	2	12	1117.68	0.01	0.11	0.03	0.01	0.01	< d.l.	0.01	< d.l.	2.38	< d.l.	< d.l.
	2	10	1117.68	0.04	0.25	0.20	0.04	0.06	0.01	0.09	0.02	2.07	0.01	< d.l.

Appendix C

Table C-1: The Sr-isotopic composition of plagioclase per analysed spot. Depths are reported in meters (m). Initial $^{87}Sr/^{86}Sr$ ratios calculated using the decay constant of Nebel *et al*. (2011) at an age 2054.4 Ma (Scoates & Friedman, 2008).

Depth	Sample	Plag #	Spot #	Texture	Zone	$^{87}Sr/^{86}Sr$	$^{87}Rb/^{86}Sr$	$^{87}Sr/^{86}Sr_i$	2SE	Rim/Core
67.84	46	6	1359	Eu	UZ	0.7085	0.0077	0.7082	1.29E-04	Rim
	46	3	1343	Eu	UZ	0.7083	0.0114	0.7080	1.34E-04	Core
	46	3	1341	Eu	UZ	0.7083	0.0031	0.7083	9.08E-05	Rim
	46	3	1337	Eu	UZ	0.7083	0.0037	0.7082	8.69E-05	Rim
	46	2	1350	S-eu	UZ	0.7083	0.0019	0.7082	1.22E-04	Core
	46	2	1348	S-eu	UZ	0.7082	0.0009	0.7082	1.21E-04	Rim
	46	2	1345	S-eu	UZ	0.7084	0.0002	0.7084	1.61E-04	Rim
	46	6	1362	Eu	UZ	0.7083	0.0043	0.7082	1.09E-04	Rim
100.70	44	5	1317	Eu	UZ	0.7081	0.0189	0.7076	1.89E-04	Core
	44	5	1315	Eu	UZ	0.7078	0.0008	0.7078	7.45E-05	Rim
	44	2	1295	Eu	UZ	0.7081	0.0121	0.7077	1.15E-04	Rim
	44	2	1292	Eu	UZ	0.7081	0.0220	0.7075	1.49E-04	Rim
	44	1	1329	S-eu	UZ	0.7083	0.0456	0.7070	9.51E-05	Rim
	44	1	1326	S-eu	UZ	0.7078	0.0105	0.7075	1.25E-04	Rim
	44	1	1322	S-eu	UZ	0.7086	0.0387	0.7074	3.65E-04	Rim
126.36	43	3	1291	Eu	UZ	0.7081	0.0092	0.7078	6.68E-05	Rim
	43	3	1288	Eu	UZ	0.7082	0.0086	0.7079	5.03E-05	Rim
	43	2	1276	Eu	UZ	0.7080	0.0162	0.7075	7.55E-05	Rim
	43	2	1273	Eu	UZ	0.7077	0.0122	0.7074	7.85E-05	Rim
	43	1	1282	S-eu	UZ	0.7081	0.0182	0.7076	1.19E-04	Rim
	43	1	1280	S-eu	UZ	0.7083	0.0114	0.7080	3.00E-05	Core
	43	1	1278	S-eu	UZ	0.7079	0.0078	0.7077	7.01E-05	Rim
144.04	42	4	1263	S-eu	UZ	0.7083	0.0089	0.7080	8.22E-05	Core
	42	4	1262	S-eu	UZ	0.7082	0.0055	0.7081	8.09E-05	Rim
	42	2	1243	S-eu	UZ	0.7084	0.0140	0.7080	6.34E-05	Rim
	42	2	1241	S-eu	UZ	0.7084	0.0084	0.7082	7.62E-05	Core
	42	1	1258	Eu	UZ	0.7082	0.0081	0.7080	7.19E-05	Rim
	42	1	1257	Eu	UZ	0.7082	0.0123	0.7079	5.85E-05	Core
	42	4	1265	S-eu	UZ	0.7083	0.0098	0.7080	1.75E-04	Rim
169.37	41	3	1228	Eu	UZ	0.7085	0.0109	0.7082	5.95E-05	Rim
	41	3	1226	Eu	UZ	0.7103	0.0977	0.7075	8.00E-04	Rim
	41	2	1223	Eu	UZ	0.7082	0.0075	0.7080	9.85E-05	Rim
	41	2	1221	Eu	UZ	0.7081	0.0106	0.7078	6.14E-05	Core
	41	2	1218	Eu	UZ	0.7082	0.0167	0.7077	3.62E-04	Rim
	41	1	1237	S-eu	UZ	0.7081	0.0151	0.7077	7.57E-05	Core
	41	1	1235	S-eu	UZ	0.7082	0.0208	0.7076	5.72E-05	Rim
	41	1	1232	S-eu	UZ	0.7090	0.0631	0.7072	3.16E-04	Rim

Depth	Sample	Plag #	Spot #	Texture	Zone	$^{87}Sr/^{86}Sr$	$^{87}Rb/^{86}Sr$	$^{87}Sr/^{86}Sr_i$	2SE	Rim/Core
190.55	40	7	1169	Eu	UZ	0.7083	0.0061	0.7081	9.92E-05	Rim
	40	7	1168	Eu	UZ	0.7083	0.0051	0.7081	7.59E-05	Rim
	40	7	1166	Eu	UZ	0.7081	0.0061	0.7079	8.44E-05	Core
	40	7	1164	Eu	UZ	0.7081	0.0040	0.7080	7.19E-05	Rim
	40	5	1216	Eu	UZ	0.7078	0.0054	0.7077	4.14E-05	Core
	40	5	1214	Eu	UZ	0.7080	0.0054	0.7079	7.97E-05	Rim
	40	5	1211	Eu	UZ	0.7079	0.0056	0.7077	5.22E-05	Rim
	40	3	1206	Eu	UZ	0.7082	0.0030	0.7081	5.75E-05	Rim
	40	3	1204	Eu	UZ	0.7087	0.0095	0.7084	1.35E-04	Rim
	40	2	1192	Eu	UZ	0.7080	0.0053	0.7079	8.76E-05	Rim
	40	2	1189	Eu	UZ	0.7082	0.0151	0.7078	8.08E-05	Rim
	40	1	1199	Eu	UZ	0.7081	0.0042	0.7080	7.87E-05	Rim
	40	1	1196	Eu	UZ	0.7078	0.0061	0.7077	2.00E-04	Rim
212.48	39	4	1151	S-eu	UZ	0.7085	0.0182	0.7079	6.03E-05	Rim
	39	4	1148	S-eu	UZ	0.7079	0.0044	0.7078	8.06E-05	Rim
	39	3	1135	Eu	UZ	0.7082	0.0056	0.7081	9.53E-05	Rim
	39	3	1133	Eu	UZ	0.7076	0.0037	0.7075	7.82E-05	Rim
	39	2	1146	Eu	UZ	0.7079	0.0052	0.7077	5.05E-05	Rim
	39	2	1145	Eu	UZ	0.7080	0.0038	0.7079	1.26E-04	Core
	39	2	1143	Eu	UZ	0.7084	0.0215	0.7077	1.87E-04	Rim
227.00	38	3	1099	Eu	UZ	0.7079	0.0119	0.7076	7.32E-05	Rim
	38	3	1097	Eu	UZ	0.7079	0.0128	0.7075	9.51E-05	Core
	38	3	1094	Eu	UZ	0.7078	0.0029	0.7077	5.19E-05	Rim
	38	2	1087	Eu	UZ	0.7074	0.0047	0.7073	7.46E-05	Rim
	38	1	1093	Eu	UZ	0.7096	0.0743	0.7074	3.19E-04	Rim
	38	1	1092	Eu	UZ	0.7074	0.0046	0.7073	1.25E-04	Core
260.50	37	6	1021	S-eu	UZ	0.7081	0.0051	0.7080	2.32E-04	Rim
	37	4	1039	Eu	UZ	0.7085	0.0043	0.7084	2.29E-04	Rim
	37	4	1037	Eu	UZ	0.7079	0.0059	0.7078	5.73E-05	Core
	37	4	1035	Eu	UZ	0.7082	0.0080	0.7080	1.10E-04	Rim
	37	1	1029	Eu	UZ	0.7081	0.0030	0.7080	8.20E-05	Rim
	37	1	1025	Eu	UZ	0.7080	0.0120	0.7076	1.29E-04	Rim
297.95	36	3	993	S-eu	UZ	0.7079	0.0062	0.7077	5.87E-05	Rim
	36	3	991	S-eu	UZ	0.7079	0.0042	0.7078	9.49E-05	Rim
	36	2	1000	S-eu	UZ	0.7084	0.0144	0.7080	1.05E-04	Rim
	36	2	998	S-eu	UZ	0.7081	0.0065	0.7079	6.76E-05	Rim
	36	1	1009	Eu	UZ	0.7084	0.0187	0.7079	1.12E-04	Rim
	36	1	1006	Eu	UZ	0.7082	0.0107	0.7079	1.08E-04	Rim
	36	3	996	S-eu	UZ	0.7082	0.0086	0.7079	1.13E-04	Core
323.16	35	4	963	Eu	MZu	0.7085	0.0285	0.7077	1.89E-04	Rim
	35	4	961	Eu	MZu	0.7080	0.0053	0.7078	2.16E-04	Rim

Depth	Sample	Plag #	Spot #	Texture	Zone	$^{87}Sr/^{86}Sr$	$^{87}Rb/^{86}Sr$	$^{87}Sr/^{86}Sr_i$	2SE	Rim/Core
358.00	34	7	930	Eu	MZu	0.7077	0.0068	0.7075	1.86E-04	Rim
	34	3	923	S-eu	MZu	0.7084	0.0379	0.7073	1.27E-04	Core
	34	3	922	S-eu	MZu	0.7087	0.0023	0.7086	1.15E-04	Rim
	34	2	957	Eu	MZu	0.7085	0.0095	0.7083	8.60E-05	Rim
	34	2	954	Eu	MZu	0.7087	0.0088	0.7085	2.46E-04	Rim
	34	1	949	Eu	MZu	0.7084	0.0069	0.7082	5.41E-05	Rim
	34	1	947	Eu	MZu	0.7086	0.0032	0.7085	4.33E-05	Rim
	34	7	933	Eu	MZu	0.7080	0.0024	0.7079	1.46E-04	Rim
384.10	33	6	864	S-eu	MZu	0.7079	0.0061	0.7078	2.08E-04	Rim
	33	5	875	Eu	MZu	0.7074	0.0029	0.7073	1.82E-04	Rim
	33	5	871	Eu	MZu	0.7087	0.0052	0.7085	1.53E-04	Rim
	33	4	898	Eu	MZu	0.7090	0.0544	0.7075	1.78E-04	Rim
	33	4	893	Eu	MZu	0.7086	0.0050	0.7085	1.43E-04	Rim
	33	3	889	Eu	MZu	0.7090	0.0226	0.7084	1.68E-04	Rim
	33	3	886	Eu	MZu	0.7085	0.0038	0.7084	1.54E-04	Rim
	33	6	866	S-eu	MZu	0.7088	0.0060	0.7086	2.11E-04	Rim
410.78	32	3	857	Eu	MZu	0.7082	0.0066	0.7080	1.86E-04	Rim
	32	2	846	Eu	MZu	0.7098	0.0518	0.7083	3.70E-04	Rim
	32	2	844	Eu	MZu	0.7087	0.0356	0.7077	2.00E-04	Core
	32	2	843	Eu	MZu	0.7090	0.0162	0.7085	1.80E-04	Rim
	32	1	839	Eu	MZu	0.7089	0.0131	0.7085	3.35E-04	Rim
	32	3	859	Eu	MZu	0.7084	0.0154	0.7080	2.44E-04	Rim
426.36	31	4	808	Eu	MZu	0.7083	0.0056	0.7082	1.50E-04	Rim
	31	3	804	S-eu	MZu	0.7081	0.0036	0.7080	1.62E-04	Rim
	31	3	803	S-eu	MZu	0.7084	0.0020	0.7083	1.37E-04	Core
	31	2	826	S-eu	MZu	0.7081	0.0032	0.7080	2.58E-04	Rim
	31	2	824	S-eu	MZu	0.7073	0.0091	0.7070	1.25E-04	Core
	31	1	818	Eu	MZu	0.7077	0.0365	0.7067	1.90E-04	Rim
	31	1	815	Eu	MZu	0.7075	0.0188	0.7069	2.54E-04	Rim
	31	4	811	Eu	MZu	0.7081	0.0043	0.7080	1.35E-04	Rim
465.40	30	6	790	S-eu	MZu	0.7100	0.0207	0.7094	3.11E-04	Rim
	30	5	800	S-eu	MZu	0.7082	0.0038	0.7081	8.23E-05	Rim
	30	5	797	S-eu	MZu	0.7094	0.0074	0.7092	2.98E-04	Rim
	30	1	786	S-eu	MZu	0.7088	0.0053	0.7086	1.67E-04	Rim
	30	1	783	S-eu	MZu	0.7083	0.0085	0.7080	2.08E-04	Rim
	30	6	793	S-eu	MZu	0.7086	0.0029	0.7085	1.37E-04	Rim
506.71	28	1	742	Eu	LMZ	0.7098	0.0018	0.7097	2.85E-04	Rim
	28	1	740	Eu	LMZ	0.7096	0.0016	0.7095	3.59E-04	Rim
	28	2	750	Eu	LMZ	0.7099	0.0024	0.7098	2.58E-04	Rim
531.74	27	5	707	Eu	LMZ	0.7088	0.0131	0.7084	2.32E-04	Rim
	27	4	703	S-eu	LMZ	0.7086	0.0312	0.7077	1.80E-04	Rim

Depth	Sample	Plag #	Spot #	Texture	Zone	$^{87}Sr/^{86}Sr$	$^{87}Rb/^{86}Sr$	$^{87}Sr/^{86}Sr_i$	2SE	Rim/Core
	27	4	701	S-eu	LMZ	0.7088	0.1353	0.7049	4.53E-04	Rim
	27	2	716	Eu	LMZ	0.7090	0.0217	0.7083	2.79E-04	Rim
	27	2	715	Eu	LMZ	0.7086	0.0185	0.7081	1.39E-04	Core
	27	2	713	Eu	LMZ	0.7087	0.0051	0.7086	1.36E-04	Rim
	27	1	696	Eu	LMZ	0.7084	0.0125	0.7080	9.63E-05	Core
	27	5	709	Eu	LMZ	0.7085	0.0205	0.7079	1.66E-04	Rim
572.63	25	2	662	Eu	LMZ	0.7086	0.0343	0.7076	1.70E-04	Rim
	25	1	642	Eu	LMZ	0.7082	0.0154	0.7078	7.41E-05	Rim
	25	1	641	Eu	LMZ	0.7082	0.0114	0.7078	8.34E-05	Rim
	25	1	640	Eu	LMZ	0.7082	0.0113	0.7078	3.48E-05	Core
	25	1	619	Eu	LMZ	0.7081	0.0278	0.7073	1.08E-04	Rim
595.03	24	3	632	S-eu	LMZ	0.7090	0.0071	0.7088	1.31E-04	Core
	24	3	631	S-eu	LMZ	0.7089	0.0057	0.7087	1.47E-04	Rim
	24	2	627	Eu	LMZ	0.7091	0.0049	0.7090	1.55E-04	Rim
	24	2	625	Eu	LMZ	0.7090	0.0210	0.7084	1.91E-04	Rim
	24	3	634	S-eu	LMZ	0.7089	0.0061	0.7087	2.25E-04	Rim
612.70	23	3	Z	S-eu	LMZ	0.7087	0.0082	0.7084	7.32E-05	Rim
	23	3	607	S-eu	LMZ	0.7088	0.0226	0.7081	1.44E-04	Rim
	23	1	Y	S-eu	LMZ	0.7087	0.0116	0.7083	9.75E-05	Rim
	23	1	X	S-eu	LMZ	0.7089	0.0144	0.7085	1.08E-04	Rim
635.83	22	4	561	Eu	LMZ	0.7079	0.0080	0.7077	2.19E-04	Rim
	22	3	590	Eu	LMZ	0.7081	0.0047	0.7080	1.09E-04	Rim
	22	3	586	Eu	LMZ	0.7147	0.3374	0.7049	9.92E-04	Rim
	22	2	570	S-eu	LMZ	0.7083	0.0009	0.7083	1.70E-04	Rim
	22	2	567	S-eu	LMZ	0.7086	0.0011	0.7085	2.49E-04	Rim
	22	1	576	S-eu	LMZ	0.7090	0.0055	0.7089	2.18E-04	Rim
	22	1	574	S-eu	LMZ	0.7086	0.0011	0.7085	1.88E-04	Rim
	22	4	563	Eu	LMZ	0.7083	0.0238	0.7076	2.33E-04	Rim
659.33	21	3	557	Eu	LMZ	0.7097	0.0349	0.7086	2.89E-04	Rim
	21	3	556	Eu	LMZ	0.7089	0.0115	0.7086	1.16E-04	Core
	21	3	555	Eu	LMZ	0.7092	0.0134	0.7088	9.53E-05	Rim
	21	2	545	Eu	LMZ	0.7092	0.0088	0.7089	1.38E-04	Rim
	21	2	544	Eu	LMZ	0.7090	0.0046	0.7088	8.65E-05	Core
	21	2	542	Eu	LMZ	0.7094	0.0461	0.7081	1.18E-04	Rim
	21	1	551	S-eu	LMZ	0.7091	0.0132	0.7088	1.24E-04	Rim
	21	1	550	S-eu	LMZ	0.7092	0.0138	0.7088	1.41E-04	Core
	21	1	549	S-eu	LMZ	0.7091	0.0067	0.7089	1.55E-04	Rim
678.05	20	3	540	Eu	LMZ	0.7083	0.0093	0.7080	6.30E-05	Rim
	20	3	538	Eu	LMZ	0.7082	0.0118	0.7078	1.55E-04	Rim
	20	3	534	Eu	LMZ	0.7087	0.0058	0.7086	1.05E-04	Rim
	20	2	530	S-eu	LMZ	0.7088	0.0128	0.7085	6.60E-05	Rim

Depth	Sample	Plag #	Spot #	Texture	Zone	$^{87}Sr/^{86}Sr$	$^{87}Rb/^{86}Sr$	$^{87}Sr/^{86}Sr_i$	2SE	Rim/Core
	20	2	529	S-eu	LMZ	0.7094	0.0676	0.7074	1.87E-04	Core
	20	2	528	S-eu	LMZ	0.7089	0.0219	0.7083	1.32E-04	Rim
	20	1	525	Eu	LMZ	0.7087	0.0122	0.7083	9.24E-05	Core
	20	1	523	Eu	LMZ	0.7088	0.0110	0.7085	6.94E-05	Rim
	20	1	520	Eu	LMZ	0.7087	0.0060	0.7085	1.07E-04	Rim
697.26	19	4	499	S-eu	LMZ	0.7094	0.0053	0.7093	6.73E-05	Rim
	19	2	495	Eu	LMZ	0.7093	0.0040	0.7092	8.60E-05	Rim
	19	2	494	Eu	LMZ	0.7090	0.0040	0.7089	5.85E-05	Core
	19	2	492	Eu	LMZ	0.7089	0.0035	0.7088	6.58E-05	Rim
	19	1	488	Eu	LMZ	0.7093	0.0030	0.7093	1.21E-04	Rim
	19	1	487	Eu	LMZ	0.7101	0.0444	0.7088	1.87E-04	Core
	19	1	486	Eu	LMZ	0.7093	0.0090	0.7090	8.29E-05	Rim
	19	4	501	S-eu	LMZ	0.7093	0.0070	0.7091	7.60E-05	Rim
722.50	18	3	478	Eu	LMZ	0.7089	0.0103	0.7086	5.27E-05	Core
	18	3	475	Eu	LMZ	0.7088	0.0108	0.7085	5.42E-05	Rim
	18	2	471	S-eu	LMZ	0.7088	0.0225	0.7082	8.98E-05	Rim
	18	2	470	S-eu	LMZ	0.7095	0.0508	0.7080	2.33E-04	Core
	18	2	469	S-eu	LMZ	0.7088	0.0076	0.7086	6.96E-05	Rim
	18	2	468	S-eu	LMZ	0.7088	0.0244	0.7081	1.62E-04	Rim
	18	1	465	Eu	LMZ	0.7089	0.0278	0.7081	1.99E-04	Rim
	18	1	464	Eu	LMZ	0.7089	0.0354	0.7078	6.92E-05	Rim
	18	1	462	Eu	LMZ	0.7088	0.0272	0.7080	1.74E-04	Rim
740.74	17	5	449	S-eu	LMZ	0.7088	0.0054	0.7086	8.14E-05	Rim
	17	2	431	S-eu	LMZ	0.7092	0.0087	0.7090	8.55E-05	Rim
	17	2	430	S-eu	LMZ	0.7092	0.0066	0.7090	5.82E-05	Core
	17	2	429	S-eu	LMZ	0.7090	0.0094	0.7087	6.53E-05	Rim
	17	1	445	Eu	LMZ	0.7088	0.0066	0.7086	1.51E-04	Rim
	17	1	443	Eu	LMZ	0.7095	0.0331	0.7085	1.38E-04	Rim
779.80	15	3	428	Eu	LMZ	0.7085	0.0179	0.7079	8.48E-05	Rim
	15	3	427	Eu	LMZ	0.7085	0.0107	0.7082	8.94E-05	Core
	15	2	421	S-eu	LMZ	0.7084	0.0080	0.7081	7.68E-05	Core
	15	2	418	S-eu	LMZ	0.7084	0.0067	0.7082	8.49E-05	Rim
	15	2	416	S-eu	LMZ	0.7085	0.0091	0.7082	8.08E-05	Rim
	15	1	425	Eu	LMZ	0.7087	0.0140	0.7083	7.76E-05	Rim
	15	1	424	Eu	LMZ	0.7087	0.0206	0.7081	1.08E-04	Rim
825.79	14	3	399	S-eu	LMZ	0.7081	0.0045	0.7079	1.13E-04	Rim
	14	3	398	S-eu	LMZ	0.7082	0.0052	0.7080	7.19E-05	Core
	14	3	397	S-eu	LMZ	0.7082	0.0048	0.7081	5.93E-05	Rim
	14	2	405	S-eu	LMZ	0.7080	0.0027	0.7079	8.66E-05	Rim
	14	2	404	S-eu	LMZ	0.7079	0.0070	0.7077	1.07E-04	Core
	14	2	403	S-eu	LMZ	0.7079	0.0078	0.7076	4.27E-05	Rim

Depth	Sample	Plag #	Spot #	Texture	Zone	$^{87}Sr/^{86}Sr$	$^{87}Rb/^{86}Sr$	$^{87}Sr/^{86}Sr_i$	2SE	Rim/Core
	14	1	412	S-eu	LMZ	0.7089	0.0153	0.7084	3.14E-04	Rim
	14	1	411	S-eu	LMZ	0.7081	0.0025	0.7080	9.27E-05	Core
855.62	13	4	384	S-eu	LMZ	0.7088	0.0041	0.7086	1.06E-04	Rim
	13	3	393	S-eu	LMZ	0.7088	0.0095	0.7085	9.87E-05	Rim
	13	3	391	S-eu	LMZ	0.7088	0.0065	0.7086	8.02E-05	Rim
	13	2	380	S-eu	LMZ	0.7088	0.0112	0.7084	9.82E-05	Rim
	13	2	378	S-eu	LMZ	0.7097	0.0314	0.7088	1.63E-04	Rim
	13	1	374	S-eu	LMZ	0.7095	0.0047	0.7094	1.07E-04	Rim
	13	1	372	S-eu	LMZ	0.7094	0.0026	0.7093	7.28E-05	Rim
	13	4	385	S-eu	LMZ	0.7093	0.0056	0.7092	8.17E-05	Rim
879.23	12	3	364	Eu	LMZ	0.7097	0.0410	0.7085	3.06E-04	Core
	12	3	362	Eu	LMZ	0.7092	0.0043	0.7090	9.07E-05	Rim
	12	2	371	Eu	LMZ	0.7094	0.0074	0.7092	9.14E-05	Rim
	12	2	370	Eu	LMZ	0.7094	0.0066	0.7092	2.70E-04	Core
	12	2	369	Eu	LMZ	0.7095	0.0037	0.7094	6.47E-05	Rim
	12	1	355	S-eu	LMZ	0.7089	0.0057	0.7087	5.98E-05	Rim
	12	3	365	Eu	LMZ	0.7093	0.0195	0.7087	9.59E-05	Rim
899.43	11	7	351	S-eu	LMZ	0.7081	0.0137	0.7077	8.90E-05	Rim
	11	7	349	S-eu	LMZ	0.7082	0.0041	0.7081	7.41E-05	Rim
	11	7	347	S-eu	LMZ	0.7082	0.0010	0.7082	9.39E-05	Rim
	11	4	331	S-eu	LMZ	0.7083	0.0035	0.7082	7.16E-05	Rim
	11	4	328	S-eu	LMZ	0.7082	0.0050	0.7080	1.09E-04	Rim
	11	3	326	Eu	LMZ	0.7083	0.0093	0.7080	8.04E-05	Core
	11	3	324	Eu	LMZ	0.7084	0.0253	0.7077	1.03E-04	Rim
	11	3	322	Eu	LMZ	0.7084	0.0058	0.7082	6.34E-05	Rim
916.38	10	5	284	Eu	LMZ	0.7094	0.0032	0.7093	1.19E-04	Rim
	10	4	290	Eu	LMZ	0.7103	0.0332	0.7093	2.83E-04	Rim
	10	5	285	Eu	LMZ	0.7094	0.0031	0.7093	1.28E-04	Core
943.14	9	5	268	S-eu	LMZ	0.7116	0.1267	0.7079	3.87E-04	Rim
	9	3	263	S-eu	LMZ	0.7090	0.0038	0.7089	4.08E-05	Rim
	9	3	261	S-eu	LMZ	0.7090	0.0046	0.7088	9.53E-05	Core
	9	3	259	S-eu	LMZ	0.7090	0.0074	0.7088	2.98E-04	Rim
	9	2	257	S-eu	LMZ	0.7093	0.0354	0.7082	2.72E-04	Core
	9	2	255	S-eu	LMZ	0.7093	0.0168	0.7088	1.22E-04	Rim
	9	2	253	S-eu	LMZ	0.7093	0.0034	0.7092	7.43E-05	Rim
	9	5	275	S-eu	LMZ	0.7101	0.0417	0.7089	3.34E-04	Rim
958.64	8	5	233	S-eu	LMZ	0.7094	0.0225	0.7087	8.41E-05	Rim
	8	4	243	S-eu	LMZ	0.7091	0.0048	0.7090	1.12E-04	Rim
	8	4	239	S-eu	LMZ	0.7092	0.0041	0.7091	9.22E-05	Rim
	8	2	215	S-eu	LMZ	0.7095	0.0098	0.7093	1.81E-04	Core
	8	2	212	S-eu	LMZ	0.7097	0.0092	0.7095	1.58E-04	Rim

Depth	Sample	Plag #	Spot #	Texture	Zone	$^{87}Sr/^{86}Sr$	$^{87}Rb/^{86}Sr$	$^{87}Sr/^{86}Sr_i$	2SE	Rim/Core
	8	1	208	S-eu	LMZ	0.7096	0.0123	0.7092	1.86E-04	Rim
	8	1	204	S-eu	LMZ	0.7099	0.0123	0.7095	1.82E-04	Rim
982.30	7	4	195	S-eu	LMZ	0.7091	0.0038	0.7090	7.59E-05	Rim
	7	4	194	S-eu	LMZ	0.7092	0.0052	0.7090	8.52E-05	Core
	7	3	188	Eu	LMZ	0.7088	0.0044	0.7086	5.75E-05	Core
	7	3	186	Eu	LMZ	0.7092	0.0234	0.7085	1.41E-04	Rim
	7	3	183	Eu	LMZ	0.7091	0.0049	0.7090	5.73E-05	Rim
	7	2	181	Eu	LMZ	0.7091	0.0066	0.7089	1.07E-04	Core
	7	2	179	Eu	LMZ	0.7091	0.0038	0.7090	8.38E-05	Rim
	7	2	174	Eu	LMZ	0.7092	0.0078	0.7090	1.10E-04	Rim
1026.60	5	3	143	S-eu	LMZ	0.7099	0.0109	0.7096	1.12E-04	Rim
	5	2	110	Eu	LMZ	0.7098	0.0139	0.7094	8.90E-05	Rim
	5	2	106	Eu	LMZ	0.7097	0.0236	0.7090	1.83E-04	Rim
	5	1	138	Eu	LMZ	0.7087	0.0066	0.7085	9.95E-05	Rim
	5	3	135	S-eu	LMZ	0.7092	0.0213	0.7085	1.27E-04	Rim
	5	3	146	S-eu	LMZ	0.7094	0.0050	0.7093	9.06E-05	Rim
1050.26	4	3	90	Eu	LMZ	0.7091	0.0231	0.7084	1.51E-04	Rim
	4	2	100	Eu	LMZ	0.7084	0.0157	0.7080	9.32E-05	Rim
	4	1	85	Eu	LMZ	0.7086	0.0196	0.7080	1.20E-04	Rim
	4	1	83	Eu	LMZ	0.7088	0.0196	0.7082	9.05E-05	Rim
	4	3	95	Eu	LMZ	0.7094	0.0123	0.7091	1.47E-04	Core
1069.65	3	4	49	Eu	LMZ	0.7092	0.0252	0.7084	1.13E-04	Rim
	3	3	70	Eu	LMZ	0.7091	0.0188	0.7086	1.44E-04	Rim
	3	3	68	Eu	LMZ	0.7089	0.0061	0.7088	8.65E-05	Rim
	3	2	60	Eu	LMZ	0.7091	0.0134	0.7088	1.13E-04	Core
	3	2	58	Eu	LMZ	0.7089	0.0096	0.7087	7.83E-05	Rim
	3	1	77	S-eu	LMZ	0.7091	0.0192	0.7086	7.03E-05	Rim
	3	1	74	S-eu	LMZ	0.7090	0.0108	0.7086	1.14E-04	Rim
	3	4	51	Eu	LMZ	0.7085	0.0094	0.7083	1.50E-04	Core
1092.85	2	3	39	Eu	LMZ	0.7093	0.0268	0.7086	1.19E-04	Rim
	2	3	37	Eu	LMZ	0.7087	0.0109	0.7084	7.42E-05	Rim
	2	3	35	Eu	LMZ	0.7086	0.0095	0.7083	8.74E-05	Rim
	2	3	32	Eu	LMZ	0.7086	0.0058	0.7085	1.45E-04	Rim
	2	1	30	Eu	LMZ	0.7092	0.0197	0.7086	2.17E-04	Core
	2	1	28	Eu	LMZ	0.7093	0.0232	0.7086	1.09E-04	Rim
	2	1	25	Eu	LMZ	0.7093	0.0100	0.7090	7.99E-05	Rim
1117.68	1	4	8	Eu	LMZ	0.7090	0.0084	0.7088	1.25E-04	Core
	1	4	2	Eu	LMZ	0.7091	0.0076	0.7088	7.26E-05	Rim
	1	3	20	S-eu	LMZ	0.7090	0.0021	0.7089	9.45E-05	Rim
	1	3	18	S-eu	LMZ	0.7095	0.0013	0.7095	1.02E-04	Core
	1	3	17	S-eu	LMZ	0.7095	0.0015	0.7094	6.14E-05	Rim

Depth	Sample	Plag #	Spot #	Texture	Zone	$^{87}Sr/^{86}Sr$	$^{87}Rb/^{86}Sr$	$^{87}Sr/^{86}Sr_i$	2SE	Rim/Core
	1	2	13	Eu	LMZ	0.7095	0.0129	0.7092	9.51E-05	Rim
	1	2	12	Eu	LMZ	0.7096	0.0058	0.7095	6.41E-05	Rim
	1	2	10	Eu	LMZ	0.7095	0.0056	0.7094	1.73E-04	Rim